ISSN 2663-0419 (Online)
ISSN 2218-8754 (Print)

AZERBAIJAN NATIONAL ACADEMY OF SCIENCES

ANAS TRANSACTIONS

EARTH SCIENCES



www.journalesgia.com

2025
№2

We are Crossref Member

ELSEVIER Scopus

Crossref
This journal is included and indexed in the GeoRef database

REDAKSİYA HEYƏTI

Əlizadə Ak.A. – baş redaktor (Azərbaycan), Qədirov F.Ə. – baş redaktorun müavini (Azərbaycan), Quliyev İ.S. – baş redaktorun müavini (Azərbaycan), Babayev Q.R. – baş redaktorun müavini) (Azərbaycan), Süleymanov B.Ə. – baş redaktorun müavini (Azərbaycan), Babazadə V.M. (Azərbaycan), Calalov Q.İ. (Azərbaycan), Abbasov O.R. (Azərbaycan), Əfəndiyev Q.M. (Azərbaycan), Hüseynov D.A. (Azərbaycan), Feyzulayev Ə.Ə. (Azərbaycan), Kəngərli T.N. (Azərbaycan), Rəsulov M.Ə. (Azərbaycan), Yetirmişli Q.C. (Azərbaycan), Qardaşov R.H. (Azərbaycan), Səfərov S.H. (Azərbaycan), Səfərov R.T. (Azərbaycan).

İsmail-zadə Ə.T. (Almaniya), Eppelbaum L.V. (İsrail), Sobiseviç A.L. (Rusiya), Boqoyavlenski V. (Rusiya), Şuanqqen C. (Çin), Vernant F. (Fransa), Teleska L. (İtaliya), Ali A. (Türkiyə), Maden N. (Türkiyə), Karslı H. (Türkiyə), Çelidze T.L. (Gürcüstan), Kərimov V.Y. (Rusiya), Qliko A.O. (Rusiya), Lavruşin V.Y (Rusiya), Çifci G. (Türkiyə), Kostyanoy A. (Rusiya), Reylinger R. (ABŞ), Saqiya T. (Yaponiya), Tibaldi Alessandro (İtaliya), Zavyalov A.D. (Rusiya), Qupta S.P. (Hindistan), Nilfuruşan F. (İsveç), Erqintav S. (Türkiyə).

EDITORIAL BOARD

Alizadeh Ak.A. – Editor-in-Chief (Azerbaijan), Kadirov F.A. – Deputy Editor-in-Chief (Azerbaijan), Suleimanov B.A. – Deputy Editor-in-Chief (Azerbaijan), Guliyev I.S. – Deputy Editor-in-Chief (Azerbaijan), Babayev G.R. – Deputy Editor-in-Chief (Azerbaijan), Suleimanov B.A. – Deputy Editor-in-Chief (Azerbaijan), Babazade V.M. (Azerbaijan), Jalalov G.I. (Azerbaijan), Abbasov O.R. (Azerbaijan), Afandiyev G.M. (Azerbaijan), Huseynov D.A. (Azerbaijan), Feyzullayev A.A.(Azerbaijan), Jalalov G.I. (Azerbaijan), Kangarli T.N. (Azerbaijan), Rasulov M.A. (Azerbaijan), Yetirmishli G.J. (Azerbaijan), Gardashov R.H. (Azerbajan), Safarov S.H. (Azerbaijan), Safarov R.T. (Azerbaijan).

Ismail-zadeh A.T. (Germany), Eppelbaum L.V. (Israel), Sobisevich A.L. (Russia), Bogoyavlenski V. (Russia), Shuanggen J. (China), Vernant Ph. (France), Telesca L. (Italy), Ali A. (Türkiye), Maden N. (Türkiye), Karslı H. (Türkiye), Ghelidze T.L. (Gürcüstan), Kerimov V.Y. (Russia), Gliko A.O. ((Russia), Lavrushin V.Y (Russia), Çifci G. (Türkiye), Kostyanoy A. (Russia), Reilinger R. (USA), Sagiya T. (Japan), Tibaldi A. (Italy), Zavyalov A.D. (Russia), Gupta S.P. (India), Nilfouroushan F. (Sweden), Ergintav S. (Türkiye).

РЕДАКЦИОННАЯ КОЛЛЕГИЯ

Ализаде Ак.А. – главный редактор (Азербайджан), Кадиров Ф.А. – зам.главного редактора (Азербайджан), Гулиев И.С. – зам.главного редактора (Азербайджан), Бабаев Г.Р. – зам.главного редактора (Азербайджан), Сулейманов Б.А. – зам.главного редактора (Азербайджан), Бабазаде В.М. (Азербайджан), Джалалов Г.И. (Азербайджан), Аббасов О.Р. (Азербайджан), Эфендиев Г.М. (Азербайджан), Гусейнов Д.А. (Азербайджан), Фейзуллаев А.А. (Азербайджан), Кенгерли Т.Н. (Азербайджан), Расулов М.А. (Азербайджан), Етирмишли Г.Дж. (Азербайджан), Гардашов Р.Г. (Азербайджан), Сафаров С.Г. (Азербайджан), Сафаров Р.Т. (Азербайджан).

Исмаил-заде А.Т. (Германия), Эппельбаум Л.В. (Израиль), Собисевич А.Л. (Россия), Богоявленский В.И. (Россия), Шуангген Ж. (Китай), Вернант Ф. (Франция), Телеска Л. (Италия), Айдын Али (Турция), Маден Н. (Турция), Карслы Х. (Турция), Челидзе Т.Л. (Грузия), Керимов В.Ю. (Россия), Глико А.О. (Россия), Лаврушин В.Ю. (Россия), Чифджи Г. (Турция), Костяной А.Г. (Россия), Рейлингер Р. (США), Сагия Т. (Япония), Завялов А.Д. (Россия), Гупта С.П. (Индия), Нилфурушан Ф. (Швеция), Ергинтав С. (Турция).

Buraxılışına məsul: **Qabil Abıyev**

Dizayn/Qrafika: **Kərim Nəbiyev**
Xəlil Nəbiyev

Veb-redaktor: **Tofiq Rəşidov**

Jurnal Geologiya və Geofizika İnstitutunda yığılmış və səhifələnmişdir

* * *

Responsible for the issue: **Gabil Abiyev**

Design/Graphycs: **Karim Nabiyev**
Khalil Nabiyev

Web-editor: **Tofig Rashidov**

The journal has been compiled and paginated at the Geology and Geophysics Institute

* * *

Ответственный за выпуск: **Габил Абиев**

Дизайн/графика: **Керим Набиев**
Халил Набиев

Веб-редактор: **Тофиг Рашидов**

Журнал набран и сверстан в Институте геологии и геофизики

* * *

Ünvan: AZ1001, Bakı şəhəri, İstiqlaliyyət küçəsi 30, "ANAS Transactions, Earth Sciences"

Address: "ANAS Transactions, Earth Sciences" 30, Istiglaliyyat str., Baku, Azerbaijan, AZ1001

Адрес: AZ1001, г. Баку, Истиглалият, 30. Редакция "ANAS Transactions, Earth Sciences"

* * *

İcraçı redaktorlar: **A.A.İsrafilova, C.S.Qurbanova**
Executive Editors: **A.A.Israfilova, J.S.Gurbanova**
Исполнительные редакторы: **А.А.Исрафилова**
Дж.С.Курбанова

ELM NƏŞRİYYATI

Formatı: 60x84 1/8. Həcmi: 15,25 ç.v.
Tirajı: 300 nüsxə

© "Elm" nəşriyyatı, 2025

ANAS Transactions Earth Sciences 2 / 2025

http://www.journalesgia.com

REGIONAL STRUCTURAL CONTROL ON ORE DEPOSITS LOCATION IN THE CENTRAL CAUCASUS SEGMENT OF AZERBAIJAN: AN INVESTIGATION OF THE ROLE OF TECTONIC DISLOCATIONS

Babazadeh V.M.[1], Abdullayeva Sh.F.[1*], Novruzova S.R.[1], Valiyev A.A.[2], Ibrahimov J.R.[2]

[1]Baku State University, Azerbaijan

23, Academician Zahid Khalilov str., Baku AZ 1148

[2]Azerbaijan International Mining Company Limited, Azerbaijan

2, Izmir Str., Hyatt Tower 2, floor 3, Baku, AZ1065

Corresponding author: *shakhla.a@gmail.com*

Keywords: *ore-concentrating structures, ore deposit, gold, hydrothermal alteration, Central Caucasus Segment of Azerbaijan, the Lesser Caucasus*

Summary. The most important distinctive feature of the central part of the Central Caucasus Segment of Azerbaijan (the Lesser Caucasus) is the connection of mineralisation with ore-concentrating dislocation systems. These systems are characterized by extensive northwestern trending fault zones. Major ore deposits (Zod, Tutkhun, etc.) are located at their intersections with meridional strike zones. An important part of the local structure is the Zod tectonic node, which has a significant influence on the localisation of gold mineralisation. One of the main factors determining the position of the area is its confinedness with the gabbroic massif occupying the tectonic centre, as well as the linearly extended contact strip of ultramafic igneous rocks and gabbro plates. Gold mineralisation in the Tutkhun area is localized in narrow and prolonged zones of intensely altered rocks of the granitoid complex and its exocontact halos. There are many dikes that are the most recent members of the intrusive formations. The distinct geological and structural characteristics of mineralisation identified at the Agduzdag deposit suggest a complex stockwork-style ore body, which integrates multiple structural elements. The Zod-Tutkhun-Agduzdag block represents a triune system of dislocations forming a geologically significant structural framework. The intersection of these dislocations has given rise to a complex tectonic center with a heterogeneous structural composition serving as the focal point for a multi-stage ore-forming process. These findings provide new insights into the potential for gold mineralisation within the Central Caucasus Segment of Azerbaijan and the southeastern part of the region, where similar geological conditions prevail.

© 2025 Earth Science Division, Azerbaijan National Academy of Sciences. All rights reserved.

Introduction

The authors' work has established that the occurrence of dissimilar gold-quartz-sulphide, gold-quartz and gold-quartz-tellurium mineralisations of the Central Caucasus Segment of Azerbaijan are different types of ore-magmatic systems with different types of sections.

Information on the geological settings of these fields and partially on the structural conditions of gold mineralisation localisation are given in the works by M.A.Kashkay, I.G.Magakyan, G.A.Tvalchrelidze, V.M.Babazadeh, V.I.Aliyev, T.N.Nasibov, Sh.D.Musayev, M.M.Konstantinov, E.S.Suleymanov, R.K.Hasanov, etc.

The most important peculiarity of the field under study is the connection of mineralisation with through ore-concentrating dislocations (Thomson, 1988; Favorskaya et al., 1974), which was first established by M.A.Kashkay (Kashkay, Tamrazyan, 1967). Later, V.M.Babazadeh (Babazadeh, 1975; Babazadeh et al., 2003) revealed that gold ore fields are located at the intersection of latitudinal and meridional faults representing a complex network of deep structures. Their certain independence and duration of development is emphasized by the presence of specific igneous and sedimentary formations. In this regard, the author developed a concept of them as zones of deep-laid permeability, repeated revival causing the basic divisibility of the lithosphere into systems of blocks of different dimensions. The deep penetration of ore-concentrating structures is also supported by such peculiarities as the extent, magma saturation, significant facies alterations of rocks, sharp gradients of sediment thickness, the presence of mineral formations of different ages, etc.

The triune complex system of faults developed within the Zod-Tutkhun-Agduzdag block is of great interest among the fractures (Babazadeh, 1975; Babazadeh et al., 2003; Konstantinov, 1984; Konstantinov, Bochek, 1984; Kostenko et al., 2001). The block turned out to be the most optimal for the localisation of mineralisation, where a complex tectonic centre of heterogeneous structure was formed leading to a multi-stage ore-forming process.

The system is characterized by straightness and subvertical position of fault planes; the orientation and density of dislocations in different parts are not the same. All other directions are suppressed by a system of sublatitudinal strikes in the central part of the block. It is quite possible that the existing network of differently oriented dislocations is a reflection of the primary heterogeneity of the Earth's crust. At the same time, having a deep nature, they do not penetrate to depths below the lithosphere judging by the granitoid composition of igneous melts.

Geodynamic settings and conditions of field formation

The history of the geodynamic development of the Caucasian folded mountain structure including the gold ore strip of the central part of the Lesser Caucasus was determined by the interaction of microcontinents – "fragments" of the Afro-Arabian and Eurasian lithospheric plates. According to reconstructions (Baba-zadeh et al.., 2020; Gugushvili, 2017), early pre-collisional heterogenization of the Earth's crust, which was provoked by the spreading of microplates occurred during the formation of the ocean floor (The Lesser Caucasus branch of the Neotethys) and rift depressions on the margins of microplates (Early Bajocian volcanics of the South Caucasus and subalkaline volcanites of the North Caucasus), and later heterogenization (subduction period – Late Bajocian-Early Cretaceous) in the formation of a volcanic island arc (Abdullayeva, 2018; Kostenko et al., 2001) on the southern margin of the South Caucasus microcontinent, and on the northern margin of the marked continent occurred in the formation of flysch troughs, rift structures (Late Jurassic Colchian alkaline basalts) with the simultaneous growth of neighbouring blocks.

Tectonic processing of previously formed geomorphostructures continued at the collision stage. This age boundary should be associated with collisional compression accompanied by a first-order dislocation, volcanic depressions became isolated along transverse structures, the process of rafted flyschoid sediments of marginal marine origin began, as well as the obduction of oceanic sediments onto the margins of contacting microplates, which later led to the formation of collisional structures of suture zones (Baba-zadeh et al., 2020; Gordienko et al., 2019). One of them is the Goycha-Hakari zone (it is called a trace of the closed Lesser Caucasus branch of the Neotethys) – composed of the early and late Cretaceous deformed volcanogenic-sedimentary deposits consisting of siliceous shales, sodium basalts with tectonic ultrabasic melange. Glaucophane schists are found in the western part of the latter development.

Intensive convergence of microplates predetermined the modern appearance of the folded mountain structure, which is perceived as a pile of heterogeneous blocks in allochthonous relationships (Baba-zadeh et al., 2020). Fields occupy clear spatial and temporal positions in the folded mountain structure. For example, sulphide-rich hydrothermal-sedimentary deposits of the Eastern Caucasus (Filizchay, etc.) are associated with complexes of the basins of the paleo-marginal sea. The time of their ore genesis is limited by the Early Jurassic – Early Middle Jurassic, and the space – by local depressions of the paleo-marginal sea. Significant accumulations of volcanogenic epigenetic ores of precious and non-ferrous metals are associated with complexes that mark a fundamental restructuring of tectonic regimes (the beginning of subduction and collisional stage) (Abdullayeva, 2018). Research conducted in recent years in the central part of the Lesser Caucasus showed that lithogeodynamic complexes are specialized in magmatic chromite (Heydar, etc.), plutonogenic and volcanogenic gold ore (Tutkhun, Zod, Soyudlu, Agduzdag, etc.) and amagmatic mercury, mercury-antimony-arsenic (Shorbulag, Agyatag, Lev) fields.

Peculiarities of the geological framework and genetic types of gold ore fields

The Tutkhun ore field covers the upper reaches of the river of the same name, a large right inflow of the Terter River (Abdullayeva, Novruzova, 2023; Babazadeh и др., 2024; Suleimanov, 1982). The ore field within the area under consideration occupies a central place with an area of about 20 km^2. The geological settings of the ore field include mainly post-Upper Eocene subvolcanic and hypabyssal granitoid bodies of the Gazikhanli-Zergulu (Gazikhanli-Zergulu) intrusive complex (absolute age is 43-44 million years – middle Eocene) and comagmatic volcanites (Eocene andesites and their tuffs) developed within adjacent synclinal structures. Apparently (Baba-zadeh, 1975; Baba-zadeh и др., 2024; Svirko, 1973), they represent a single volcano-plutonic association. The intrusion is mapped from the surface as a large fractured pluton elongated in the northwest direction (300-310º) along the Tutkhun River valley, with a strike length of more than 10 km, a dip of at least 300 m, and a thickness of 0.2-2 km.

Probably, the massif fixes one of the Early Paleogene faults accompanied by regional structures of the region, in particular, with the axis of the Gazıkhanli anticlinal fold stretching more than 20 km in the north-west direction across the entire area of the ore field (Fig. 1). The wingspan of the fold reaches 4 km.

The bodies are stock-shaped up to 3 km^2 in size and up to 1 km in diameter. Contacts with host rocks are sharp, cross-cutting, sometimes subconformable and tectonic in places. Contact alterations are expressed in hornfels formation, scarn mineralisation, epidositisation. The massifs are characterized by banding and the occurrence of xenoliths of host rocks. The width of the band of altered rocks is 250-300 m. Low-temperature alterations are represented by silicification, sericitisation and carbonatisation.

This is followed by the formation of vein facies of rocks, as well as subvolcanic rocks of the same complex, at the final stage of which occurrences of gold, silver, molybdenum are localized including the Tutkhun ore field. The dykes are predominantly pre-ore concentrated in the apical and marginal parts of the intrusive massifs, usually in the host rocks.

The largest fractured structure within the ore field is the Zod-Tutkhun fault (or a series of subparallel upthrusts, upthrust-shifts) of north-west strike, which coincides with the general orientation of the folded structures and can be observed for tens of kilometres (Baba-zadeh, 1975; Konstantinov et al., 1984). The dislocation was activated in Eocene to Pliocene, which led to the intrusion of intrusive masses of the Gazikhanli-Zergulu complex. The fault is accompanied by intersecting ore-bearing fractures bearing traces of active hydrothermal alterations, which are reminiscent of listvenites (zones closest to the fracture cavity) in the body of the intrusion and in the host volcanogenic-sedimentary rocks. They usually contain ore bodies.

Large dislocations, folded forms and smaller fracturing, which are observed in the ore field are characterized by a close relationship causing a wide occurrence of general fracturing.

The industrial ore bodies of the field are represented mainly by hydrothermally altered gold-bearing zones demonstrating many variations depending on the types of host rocks, the composition of ore fluids, spatial position, fluid/rock ratio, etc. (Li et al., 2022). Active deformation and high fluid pressure promote interaction of the fluid with the rock and formation of quartz veins (Phillips, 2022). The main part of the metal is contained in quartz veins in the contours of ore zones. According to the author, gold is deposited mainly by reduction and sulfidation of the host rocks. Most often, these veins are confined to shear cracks in the bodies of granitoid massifs. Their length is 100-200 m, rarely up to 400-500 m, thickness 15-20 cm and more. Rich accumulations of pyrite, molybdenite, fahlore, etc. have been observed in separate quartz veins. The occurrence (Gizilitan) is also associated with a volcanic pipe (Babazadeh et al., 2003), gold-bearing throughout the entire cross-section, containing Ag, Mo, Cu, Pb and Zn. The pipe was observed to a depth of 340 m.

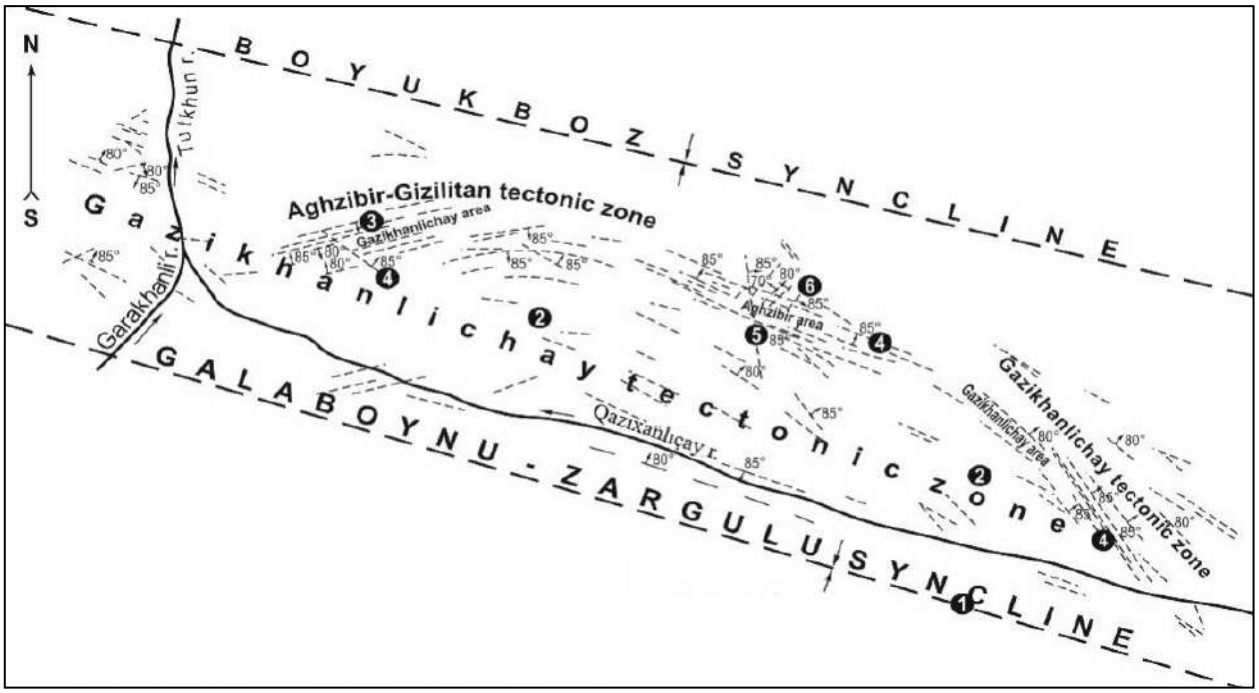


Fig. 1. 1 – Syncline axes; 2 – Gazikhanlichay tectonic zone; 3 – gold-bearing zones of north-eastern strike; 4 – gold-bearing zones of north-eastern strike (near latitude); 5 – gold-bearing zones of north-eastern strike (near meridional); post-mineral fault planes of northeast strike

There are about 10 gold-bearing areas (Gazikhanli, Aghzibir, etc.) from east to west differing in the nature of mineralisation and localized in rocks of different stratigraphic levels. Gold occurs in 3 forms: native, finely dispersed in quartz and isomorphic impurity in sulphides and sulfosalts. The largest amount of gold is finely dispersed in quartz, as well as isomorphic impurity in sulphides (Babazadeh, 1975; Babazadeh et al., 2003; Volkov et al., 2011; Volkov et al., 2018).

The field belongs to the class of sulphidic epithermal gold ore quartz-gold-sulphide formation. The span of mineralisation is approximately 300-400 m to 500 m from the daylight surface at a depth.

The Tutkhun field like the Zod has a similar tectonic setting and geological characteristics with typical orogenic gold fields of the North-East of Russia (Shkolnoye), Eastern Transbaykal (Talatuy), Eastern Kunlun (China), Mergui (Myanmar), Canadian Appalachians of the Baie Verte Peninsula (Canada), etc. (Volkov et al., 2011; Piercey et al., 2021; Gong et al., 2023; Hlaing et al., 2021).

The Zod ore field is located on the watershed of the Zangezur Range along the border of Armenia and the Kalbajar region of Azerbaijan covering the spurs and summit of Mount Misgainakh. The total area occupied by the ore field is 30-35 km^2. In accordance with the boundary line, a major part of the field (about 73%) is located in the territory of Azerbaijan. The ore field is located in the obducted basite-ultramafic complex of the Lesser Caucasus suture zone activated in the Neogene. As a result, crystalline schists of the Precambrian basement and rhythmically early Senonian layered volcanogenic-sedimentary deposits are raised to the surface (Fig. 2). The allochthonous block composed of serpentinised ultrabasic rocks and gabbroids is intensively fragmented and complicated by granodiorite porphyry dykes intruding into it (Baba-zadeh et al., 2020).

The field is also located in a distinctive block limited on all sides by faults and, in turn, dissected into a number of tectonic blocks – sections limited by faults (Amiryan, 1984; Babazadeh, 1975; Babazadeh et al., 2003; Baba-zadeh et al., 2020; Konstantinov et al., 1984; Melikyan, 1977).

The most significant is the raised Central block. This area is almost entirely located on the territory of Azerbaijan.

The main ore-concentrating structure is the Zod sublatitudinal fault along which tectonic displacements occurred repeatedly. The latter led to strong processing of ultrabasic rocks, gabbroids and other rocks, which indicates that this structure is continuous.

The Ketidag and Zod-Tutkhun tectonic sutures are associated with the Zod fault accompanied by crushing zones and metasomatic new formations with gold ore mineralisation.

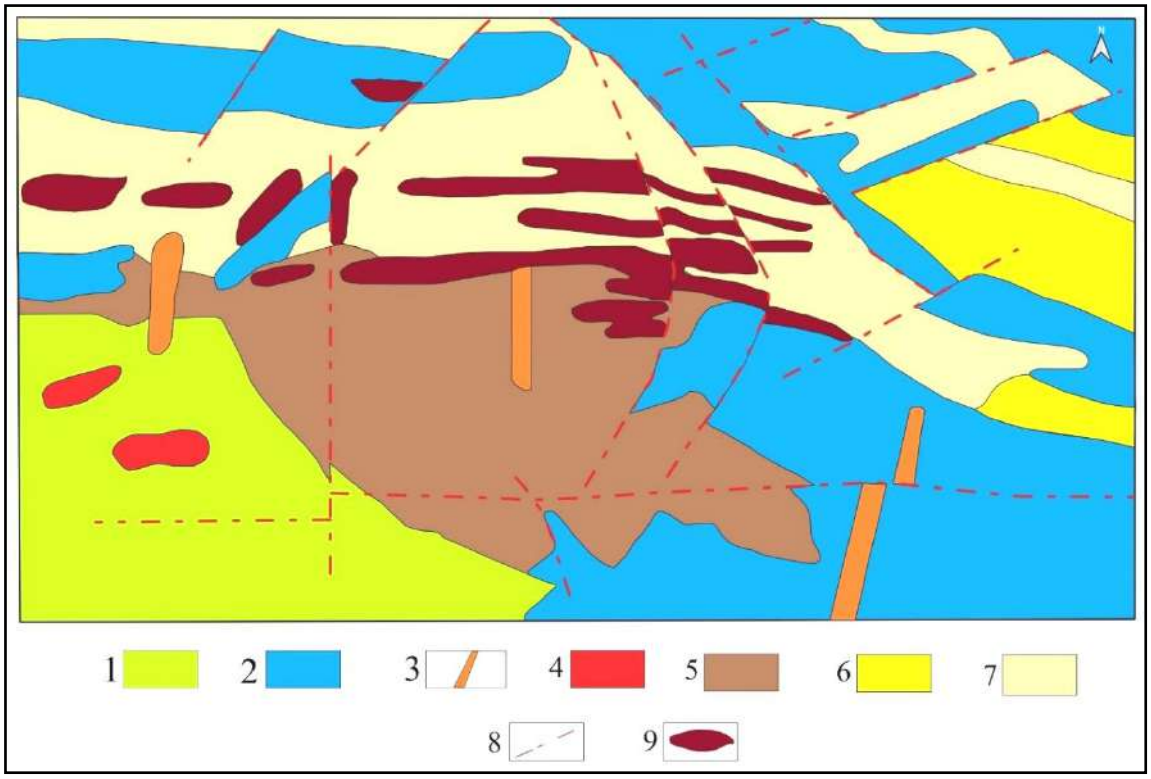


Fig. 2. Geological map (in part schematic) of the Zod ore field (according to data of the Zod geological party). 1 – Coniacian-Maastrichtian limestones and marls; 2 – basalts, their lava breccias and tuffite; 3 – dykes of granodiorite porphyry; 4 – quartz diorite; 5 – gabbro; 6 – amphibolite; 7 – serpentinized peridotite; 8 – fractures; 9 – ore-bearing zones

The Zod gabbroic massif (Martirosyan, 1990), which occupies the central axial position in the tectonic wedge and occupies more than 50% of its total area also plays a significant role in ore formation. The confinement of industrial mineralisation (Melikyan, 1977; Baba-zadeh и др., 2024) to linearly elongated plates of ultrabasic rocks enclosed between contacts of gabbroids is quite characteristic here. The persistent contact band is represented by sublatitudinal extended zone of pre-ore quartz-carbonate metasomatites-listvenites and listvenite-like rocks with gold ore mineralisation marking the Zod fault. It is associated with the veinlet-impregnated type of mineralisation (mineralised gabbro).

Gold mineralisation ore bodies are consistent along the strike and dip and are represented by vein zones, lens veins and veins of quartz with sulphide mineralisation. Stockwork bodies of impregnated and veinlet ores in metasomatite, sometimes beyond them are no less important. The gold content in them is high – from 1.5-2 to 4-5 g/t and more. The development of ore column is typical in the most intensively tectonically processed areas characterised by the greatest thickness of ore bodies and high metal content in them (bonanzas).

Ores are characterised by a complex, multicomponent composition (Amiryan, 1984). Useful components of ores are gold, silver, tellurium, bismuth, copper and zinc; harmful impurities are arsenic. Gold and silver are of industrial importance. The overwhelming amount of gold (95.98%) occurs in free form, in intergrowths and compounds with tellurium. Dispersed gold is concentrated in pyrite, and large native gold is associated with sulphides, tellurides and vein minerals.

The deposit contains zones of exceptionally high-grade gold mineralisation (ranging from 840 to 953 g/t), with an average gold content of 9.24 g/t, silver at 15.67 g/t, and tellurium at 30.9 g/t. The Au\Ag ratio is approximately 1:7. Tellurium represents a significant accessory element within the ore, occurring predominantly as discrete telluride minerals, which suggests a notable geochemical enrichment and potential genetic linkage to a telluride-bearing epithermal system. The ores belong to the gold-quartz-tellurium formation type (Amiryan, 1984). Post-Lower Oligocene-Lower Miocene age of mineralisation is allowed (Babazadeh et al., 2020).

The vertical extent of mineralisation is determined at 500 m from the daylight surface taking into account the values of ore-bearing intensity by the hanging wall and footwall of ore bodies. The basic-ultrabasic complex has undergone irregular greenstone alteration (amphibole-quartz-albite-epidote association). The Zod shows some similarities to ancient fields in greenstone belts, such as Kirkland Lake and Hollinger in Canada or Nosquil in California (Nekrasov, 1988).

The Soyudlu ore field lies to the east and southeast of the Zod field covering the basin of the river of the same name in the upper reaches of the Levchay River (left tributary of the Terter River) and the Sarıyal-Heydari watershed between that river and the Terter River.

More than 20 gold-bearing zones of hydrothermally altered rocks have been observed here representing a set of lenses and lens-veins of listvenites and controlling by northwestern-oriented dislocations. Their sizes fluctuate from the first hundred meters to several kilometres reaching 5-6 km and more with thickness from 2-15 to 40-50 m.

Unlike the Zod ore field, the development intensity of ore-concentrating faults of submeridional strike decreases within the Soyudluchay area and a system of echeloned low-amplitude fractures (Eastern-Poludlu, Gunashli, etc.) of north-eastern direction occurs. According to geological explorations, the Zod gold-localizing structure passes to the left slope of the Soyudluchay River and can be observed with representative parameters of gold mineralisation at a distance of more than 1 km.

The data, mainly geological and structural, as well as distinctive linear geophysical anomalies in combination with points of primary gold content and placer signs of gold suggest that the gold-concentrating zone, which is not quite clearly expressed on the surface can be observed at least 2 km to the west.

This is confirmed by the intersection of gold-bearing intervals that exposed ore zones (Au – 2.5-11.0 g/t). Further, this zone called Zod-Soyudlu (Babazadeh et al., 2003) is intersected by borehole No. 14 with a shaft length of 12.3 m (in the interval of 129-141.3 m) and an average gold content of 3.2 g/t in the eastern direction. A straight shaft of a driven adit at a depth of 558.0-585.8 m intersected a gold-bearing interval with a thickness of 27.8 m and a gold content of 10-42 g/t in the same area.

According to the set of facts, mainly geological and structural, the possible eastern continuation of the Zod gold-bearing zones passes along the left slope of the Soyudluchay River (Baba-zadeh, 1975; Baba-zadeh et al., 2003).

A somewhat hidden connection (through quartz-sulphides of the vein-veinlet zone in siliceous shale rocks and serpentine schists) between the Damirchidam gold-bearing zone and the Gonur zone is also suggested. This means that against the background of the general dispersion of gold with the formation of local concentrations in gold occurrences, it is very likely that we are dealing with a large Zod-Damirchidam gold-concentrating structure characterised by almost ubiquitous gold mineralisation with localisation of significant concentrations in separate areas.

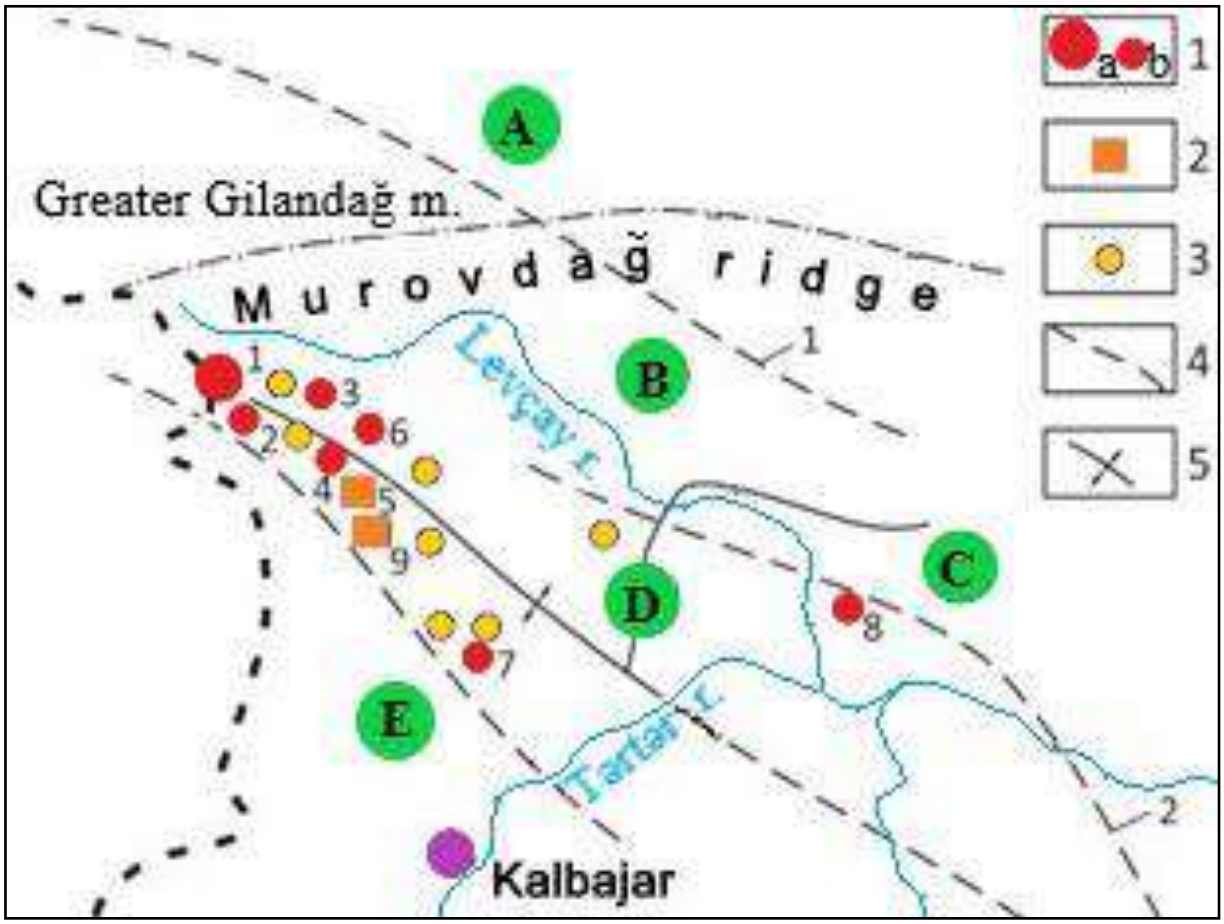


Fig. 3. The arrangement of the Soyudluchay group of gold ore objects. 1 – gold ore fields (a), occurrences (b) (red dots): 1 – Zod (field), 2 – Zod (occurrence), 3 – Gonur, 4 – Soyudluchay; 5 – Heydari, 6 – Damirchidam, 7 – Istibulag, 8 – Gamishli; 2 – chromite field (Heydari) (rectangle dots); 3 – placer gold aureoles; 4 – tectonic faults (the main ones: 1 – Murovdagh and 2 – Karabakh); 5 – axis line of the Almalı-Heydari anticlinal fold. A – Murovdagh uplift; B – Toraghachay trough; C –Karabakh uplift; D – Sarıbaba trough; E – Kalbajar superimposed trough

The Agduzdag field of gold-quartz formation was formed in a different geodynamic regime. It is located in the middle and upper reaches of the Zerchay and Zaylikchay rivers (left tributaries of the Terter River) on the border of Azerbaijan and Armenia (Fig. 3). The geological and tectonic position of the ore field determined its block structure (Babazadeh, 1975; Baba-zadeh et al., 2003; Ali-zadeh, 2003; Kostenko et al., 2001, Prokofiev et al., 2007), which are enclosed between the deep Lachın-Bashlıbel fault of the northwestern direction and its southern branch – the Delidag fault of the same strike. The block is bounded by the Terter submeridional fault from the east, which is a system of extension fracture-rupture. Stretching along the valley of the Terter River, the fault zone covers a strip about 2.0-2.5 km wide and is represented by multiple mineralised vein formations, densely intersecting the Middle Eocene volcanogenes along the southern border of the Agduzdag ore field. These rocks are dislocated in a series of crushed folds, complicated along the limbs and in the axial parts by reverse dislocations extending in a near-meridional direction (Fig. 4).

The structural bar of the ore field is the Ketidag and Shirvan deep faults of meridional direction with steep dip angles (70-85°), which are slightly inferior in prevalence to the zones of latitudinal and diagonal (mainly northwestern) strikes. There is a complex junction of the Shirvan, Ketidag and Agduzdag tectonic sutures to the east of the Terter orocline.

The zones of the mentioned faults are obviously observed in geophysical fields. The results of geophysical data suggest that the system of meridional dislocations exposing the ore-concentrating structure affects subcrustal depths. Meridional dislocations are partially deciphered in space images.

Another, no less significant Ketidag fault stretches along the Zangezur ridge starting from the Agduzdag field in the south to the Zod field in the north. The surface of its fault dips either to the southeast or to the northwest at steep angles of 60-80°. The dislocation forms three smooth foldings on the surface from which a number of small feathering fractures of south-eastern strike extend (Fig. 4).

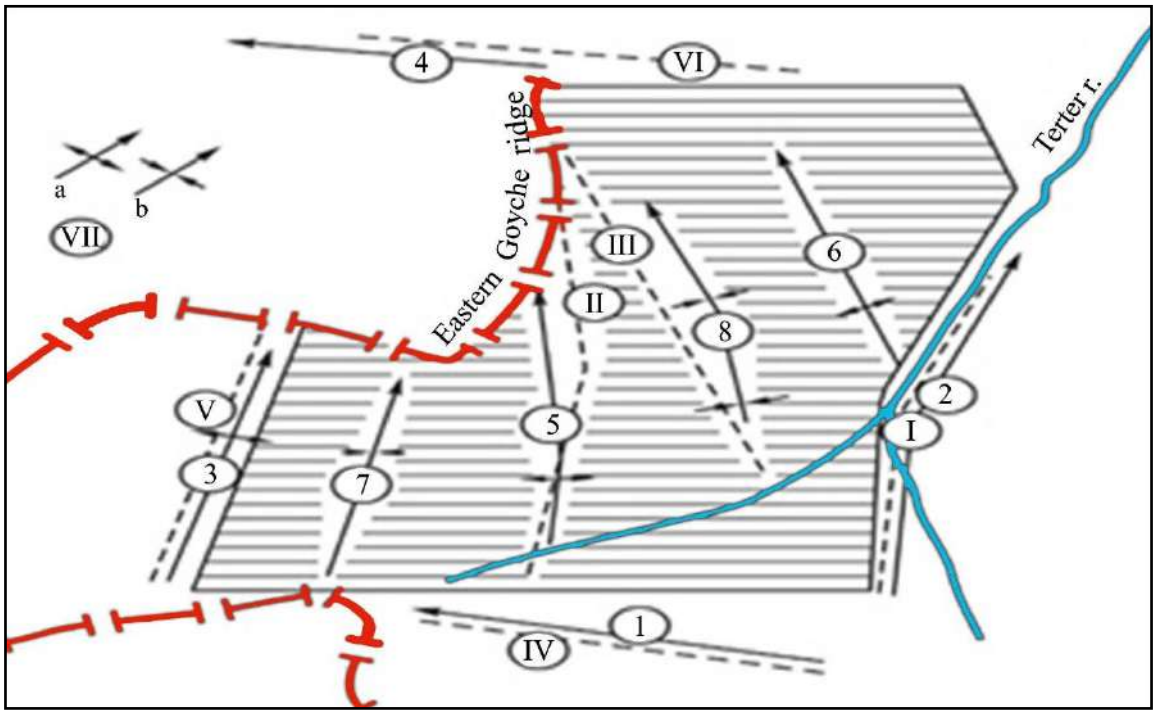


Fig. 4. Scheme of the tectonic structure of the Agduzdag ore field. The ore field is hatched. 1 – Garanlyg-Baghirsag - Garaaghaj anticline; 2 – Terter transverse anticline; 3 – Gurbaghalichay anticline; 4 – Goshabulag anticline; 5 – Zeylik anticline; 6 – Khanurli anticline; 7 – Ketidag syncline; 8 – Komurdag syncline; I – Terter fault; II – Shirvan reverse fault; III – Zeylik reverse fault; IV – Garaaghaj fracture; V – Gurbaghalichay fracture; VI – Goshabulag fracture; VII – axis and direction of plunge of anticlinal (a) and syncline (b)

The Agduzdag fracture (zone No. 3) is located 250-300 m west of the elevation point of 3335.6 m and can be observed at a distance of 1.3 km almost along the watershed ridge. The fracture is confined to a gold-bearing quartz vein accompanied by later quartz and quartz-carbonate veinlets (Fig. 5).

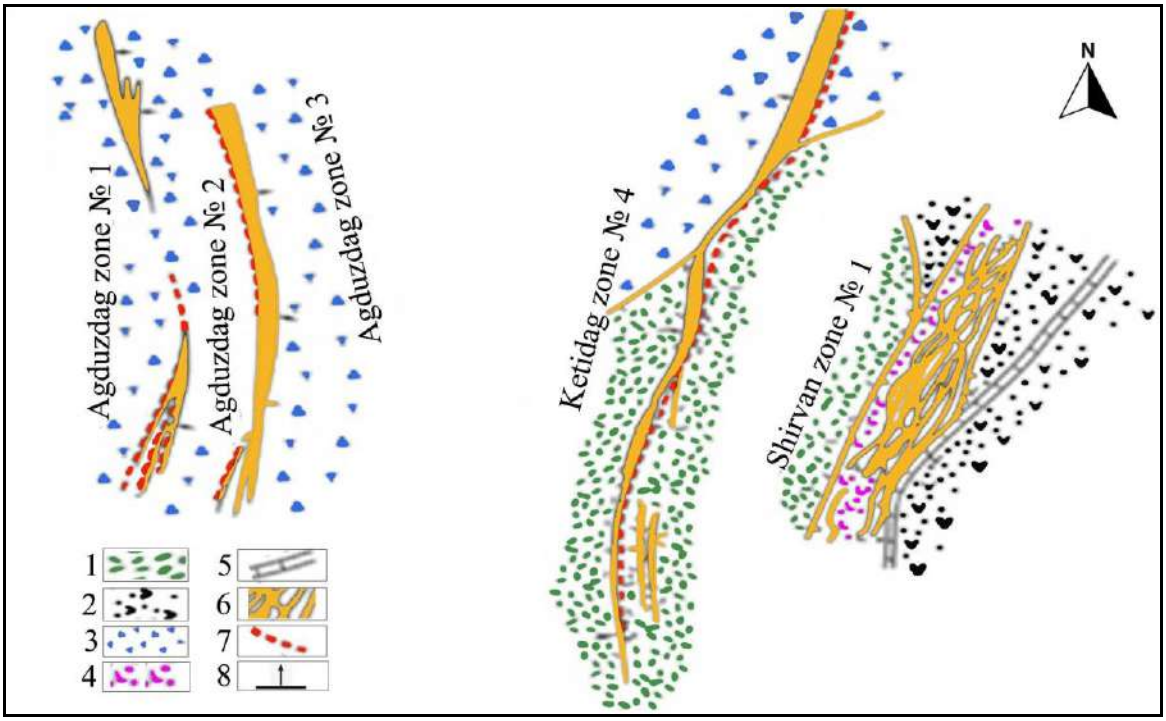


Fig. 5. Morphology of quartz-ore bodies of the Aghduzdagh gold ore field
1 – rhyolites and rhyolite-dacites (Mio-Pliocene); 2 – kaolinized and silicified andesite (Middle Eocene); 3 – andesite and andesite-dacite tuff-breccias, 4 – rhyolite dyke; 5 – syenite-porphyry dyke; 6 – ore bodies; 7 – fault-type tectonic fractures; 8 – dip angle

Exploration and prospecting works have identified more than one hundred silicified, kaolinized, and sometimes ferruginous-sulphide zones, usually healed by subvolcanic bodies (rhyolite dikes and lenses). The degree of hydrothermal alteration and gold ore mineralisation decreases gradually with distance from the selvedge part of the dykes.

Gold is not observed macroscopically, gold particles of 0.1-0.3 mm in size and light yellow in colour are rarely observed (Babazadeh et al., 2003; Volkov et al., 2018; Alizadeh, 2003).

The main mineral of the veins is inequigranular, predominantly fine-grained quartz up to chalcedony (95-98%) saturated with fluid inclusions. The share of ore minerals represented by pyrite, chalcopyrite, sphalerite, galena, magnetite, native gold, altaite, actinolite, rutile, etc. accounts for 2-3% of the total mass of ore.

Ore mineralisation is often confined to areas of quartz saturated with fluid inclusions. Inclusions, which are trapped in minerals, are classified as primary, primary-secondary and secondary. Microinclusions from minerals are represented by essentially liquid phase with an insignificant content of gas. Homogenization of these inclusions occurred in the liquid phase, which shows the hydrothermal nature of ore formation. The abundance of gas-liquid inclusions in minerals characterised by insignificant sizes provide to some extent additional data on the near-surface conditions of their formation at low and medium temperatures (340-180°C) with insignificant lithostatic pressure up to 200 atm.

The study provides insights into the genesis of orogenic gold ore fields in the Lesser Caucasus, with a particular focus on the Tutkhun ore field, emphasizing its structural controls, metallogenic evolution, and tectono-magmatic setting within the broader regional geodynamic context. Most researchers point to a close connection between gold ore mineralisation and the complex of volcanic-plutonic rocks of the Gazikhanli-Zergulu massif. First of all, such a connection is evidenced by the analysis of the distribution of impurity elements in the composition of rocks at all stages of massif formation in different facies of altered rocks and within the zones of gold ore mineralisation. All the above-mentioned rocks are characterized by a certain complex of through impurity elements among which Be, Se, Mo, Cu, Ag, Co, Au, Te and others occur constantly in above Clarke contents from 2 to 5-10 times. Moreover, each of the above-mentioned elements experiences a certain tendency in concentration or dispersion during the process of evolution of the massif rocks, their post-magmatic alterations and during the formation of mineralised zones. Comparative data on the content of the dispersed gold in rocks of the Gazikhanli-Zergulu massif of different formation times show that it accumulates gradually in rocks of later intrusive phases along with an increase in the content of volatile compounds in the same rocks. A close temporal connection between the dykes and ore zones formed under the preserved deformation plan is also observed. The close connection between them is also indicated by the similar complex of superimposed minerals in the composition of the dykes and the hydrothermal-metasomatic complex of minerals in the composition of the ore zones excluding the late complex of sulphides of the ore stage and the gold mineralisation.

A similar tectonic setting is also observed in the Zod and Soyudlu gold ore fields located 50-60 km to the north in the same tectonic zone of the Sarıbaba trough.

Besides the above, it should be stated that most genetic on orogenic gold fields that are associated with near-surface or magmatic-hydrothermal fluids are currently refuted from the point of view of the global mineral system model (Groves et al., 2020). The model of orogenic gold system supports a source of metal and fluid in the geological conditions in which mineralisation occurred and is applicable only to three of the twelve fields studied (Meyer, 2023). All other fields were formed most likely from a crustal source, which supports the crustal metamorphic model (Meyer, 2023).

Conclusion

The fault network of the region exhibits a well-organized structural framework characterised by distinct sublatitudinal, northwestern, and submeridional dislocation systems. The primary ore-controlling structures include the Agduzdag-Zod, Zod-Tutkhun, and Ketidag systems, each displaying key diagnostic features typical of this class of structures:

a) Association with long-lived linear fault systems, which have undergone multiple episodes of tectono-magmatic reactivation;

b) Anomalous landscape and structural-material heterogeneity resulting from intensive block fracturing, high-strain fault tectonics, the accumulation of nodes of long-term endogenous activity, and an increased concentration of igneous complexes of varying ages;

c) A diverse range of lithological formations and a broad temporal spectrum of mineralisation marking the most structurally stressed zones within ore-bearing fault systems.

Several key characteristics define the gold ore fields in the region:

1. Hypogene gold mineralisation is spatially controlled occurring in specific structural settings either in dome-shaped exposures or, conversely, in depressions within subvolcanic and hypabyssal granitoid bodies of the Late-Middle Eocene intrusive complex.

2. Significant occurrences of both ore and non-metallic mineralisation are localized within the exo-contact and endocontact zones of intrusive bodies. Due to the highly developed fractured nature of the host rocks, mineralisation is preferentially concentrated within spatially persistent northeast-trending fractures.

3. The ores are compositionally complex and exhibit a multi-stage formation history.

4. Ore bodies are classified into distinct structural types:

a) Those developed along steeply dipping thrust-shift faults and low-amplitude strike-slip faults oriented parallel to the axial plane of a major anticline and the longitudinal weld of a deep-seated fault (Zod, Soyudlu type);

b) Those controlled by steeply dipping intersecting fractures within host rocksoccurring primarily along fractures without significant displacement (Tutkhun type);

c) Those forming as an interconnected network of veins and veinlets developed along echeloned minor fractures with diagonal, longitudinal, and transverse orientations (Agduzdag type).

A key exploration criterion of gold mineralisation in adjacent areas of the Central Caucasus Segment of Azerbaijan is the close structural relationship between gold-bearing veins and dyke intrusions associated with granitoid intrusive complexes. These magmatic and post-magmatic features, which are formed within similar temporal and structural frameworks, tend to utilize the same ore-controlling fault systems.

The most promising areas of gold mineralisation are those hosting Paleogene-Neogene intrusive formations petrochemically related to the gabbro-monzonite-granodiorite series. These favorable zones are typically located at the margins of intrusive rock outcrops, where they dip beneath porphyritic volcanic rocks, argillites, and limestones of the Upper Cretaceous stratigraphic sequence. In most cases, these prospective areas are closely associated with subvolcanic facies rocks (monzonite-porphyrites) suggesting a strong spatial control of ore-bearing zones by the highest (near-surface) levels of intrusive massifs.

REFERENCES

Abdullayeva ShF (2018) Volcanogenic gold-bearing sulphide fields of island-arc zones, conditions of their geodynamic development, patterns of arrangement and forecasting criteria (Lesser Caucasus). Abstract of dissertation… Doctor of Geological and Mineral Sciences. Baku p 58 (in Russian)

Abdullayeva ShF, Novruzova SR (2023) Gold-bearing epithermal Tutkhun ore field (central part of the Lesser Caucasus): geological framework, structure, mineralogical and geochemical features, conditions of ore formation. Proceedings of the Republican Scientific Conference, Baku, pp 84–89 (in Russian)

Ali-zadeh AkA (ed) (2003) Geology of Azerbaijan. Vol. VI. Mineral Resources. Gold Deposits in the North-West and Central Parts of the Lesser Caucasus. Nafta-Press, Baku, pp 236–272 (in Russian)

Ali-zadeh AkA (ed) (2005) Geology of Azerbaijan. Tectonics, vol IV. Nafta-Press, Baku, p 506 (in Russian)

Amiryan ShO (1984) Gold ore formations of the Armenian SSR. Publishing House of the Academy of Sciences of the Arm.SSR, Yerevan, p 303 (in Russian)

Babazadeh VM (1975) Endogenous ore formations of the Sevan-Karabakh zone. Abstract of dissertation… Doctor of Geological and Mineral Sciences. Baku, p 47 (in Russian)

Baba-zadeh VM, Abdullayeva ShF, Novruzova SR (2024) Structural conditions for the localisation of gold mineralization within the Tutkhun ore field (the central part of the Lesser Caucasus). ANAS Transactions earth sciences 1:104–118. https://doi.org/10.33677/ggianas20240100112

Baba-zadeh VM, Kekeliya SA, Abdullayeva ShF et al (2020) The main peculiarities of the metallogeny of the Caucasus. Nedra, Moscow, p 187 (in Russian)

Babazadeh VM, Musayev ShD, Nasibov TN et al (2003) Gold of Azerbaijan. Publishing and Printing Association "Azerbaijan Milli Ensiklopediyası", Baku, p 424 (in Russian)

Favorskaya MA, Thomson IN, Baskina VI et al (1974) Global patterns of distribution of large ore fields. Nedra, Moscow (in Russian)

Gong D et al (2023) Genesis of the Heihaibei gold deposits in the East Kunlun Orogenic Belt, China: Evidence from in situ trace elements of gold-bearing sulphides and stable isotopes. Ore Geology Reviews 157(4):105431. https://doi.org/10.1016/j.oregeorev. 2023.105431

Gordiyenko IV, Badmatsyrenova RA, Lantseva VS et al (2019) Selenga ore district in Western Transbaikalia: structural and minerageneticzoning, genetic types of deposits and geodynamic settings of ore localization. Geology of ore fields 61(5):3–36. https://doi.org/10.31857/S0016-77706153-36 (in Russian)

Groves DI, Santosh M, Zhang LA (2020) Scale-Integrated exploration model for orogenic gold deposits based on a mineral system approach. Geoscience Frontiers 11(3):719–738. https://doi.org/10.1016/j.gsf.2019.12.007

Gugushvili VI (2017) Precollisional and post-collisional geodynamics of the Tethys Ocean in relation to regional metamorphism, volcanism and metallogeny, on the example of the Eurasian active margin. Proceedings of the A.Janelidze Institute of Geology. New series 129:109–180, Tbilisi (in Russian)

Hlaing MK et al (2021) Origin and characteristics of the Shwetagun Deposit, Modi Taung-Nankwe Gold District and the Kinzeik and Zibyaung Deposits, Kyaikhto Gold District in Mergui Belt Myanmar: Implications for Fluid source and Orogenic Gold Minirali-zation, Frontiers in Earth science 9(772083):1–24. https://doi.org/10.3389/feart.2021.772083

Kashkay MA, Tamrazyan GP (1967) Transverse (anti-Caucasian) dislocations of the Crimean-Caucasian region. Nedra, Moscow, p 74 (in Russian)

Konstantinov MM (1984) Gold and silver mineralization of volcanogenic belts of the world. Nedra, Moscow, p 138 (in Russian)

Konstantinov MM, Bochek LI (1984) Zod field. Geology of gold ore fields of the European part of the USSR (Urals, Carpathians, Caucasus). Ministry of Geology of the USSR, Moscow, pp 206–228 (in Russian)
Kostenko NP, Panina LV, Bryantseva GV (2001) Late orogenic structure of the Lesser Caucasus. Bulletin of Moscow University, Series 4 Geology 4:20–27 (in Russian)
Li H, Qingfei W, Yang L et al (2022) Alteration and mineralization patterns in orogenic gold deposits: Constraints from deposit observation and thermodynamic modeling. Chemical Geology 607(4):121012. http://dx.doi.org/10.1016/j.chemgeo.2022.121012
Martirosyan AM (1990) Factors of localization of industrial gold mineralization at the Zod field. Abstract of dissertation… Cand. of Geological and Mineral Sciences. Tbilisi, p 25 (in Russian)
Melikyan LS (1977) Geology and structural localisation conditions of mineralization of the Zod field. Abstract of dissertation … Cand. of Geological and Mineral Sciences. Yerevan, p 25 (in Russian)
Meyer FM (2023) Case histories of orogenic gold deposits. Minerals 13(3):369. https://doi.org/10.3390/min13030369
Nekrasov YM (1988) Foreign endogenous gold fields. Nedra, Moscow, p 288 (in Russian)
Phillips N (2022) Formation of gold deposits. Springer, Verlag, Singapore, p 291
Piercey SJ et al (2021) Contrasting gold-bearing, volcanogenic massive sulphide (VMS) and orogenic gold deposits in the Baie Verte Peninsula, Newfoundland Appalachian orogeny. Atlantic Geology 57:103–135. https://doi.org/10.4138/atlgeol.2021.00
Prokofiyev VYu, Zorina LD, Kovalenker VA et al (2007) Composition, conditions of ore formation and genesis of the Talatui gold field (Eastern Transbaikalia, Russia). Geology of ore fields, 49(1):37–76. https://doi.org/10.1134/S1075701507010023 (in Russian)
Suleimanov ES (1982) Gold ore formations of the Lesser Caucasus. Elm, Baku, p 280 (in Russian)
Svirko VN (1973) Peculiarities of Tertiary intrusive formations of the Zod-Tutkhun and Mehri-Ordubad Regions of the Lesser Caucasus. Abstract of dissertation … Cand. of Geological and Mineral Sciences. Moscow, p 25 (in Russian)
Thomson IN (1988) Metallogeny of ore regions. Nedra, Moscow, p 215 (in Russian)
Volkov AV, Savva NE, Kolova EE et al (2018) Dvoinoe Au-Ag epithermal field (Chukotka Peninsula, Russia). Geology of ore fields 60(6):590–609 (in Russian)
Volkov AV, Savva NE, Sidorov AA et al (2011) Shkolnoye gold ore field (North-East of Russia). Geology of ore fields 53(1):3–31 (in Russian)

РЕГИОНАЛЬНЫЙ СТРУКТУРНЫЙ КОНТРОЛЬ РАЗМЕЩЕНИЯ РУДНЫХ МЕСТОРОЖДЕНИЙ В АЗЕРБАЙДЖАНСКОМ СЕГМЕНТЕ ЦЕНТРАЛЬНОГО КАВКАЗА: ИССЛЕДОВАНИЕ РОЛИ ДЛИТЕЛЬНО РАЗВИВАЮЩИХСЯ ТЕКТОНИЧЕСКИХ ДИСЛОКАЦИЙ

Баба-заде В.М.[1], Абдуллаева Ш.Ф.[1*], Новрузова С.Р.[1], Велиев А.А.[2], Ибрагимов Д.Р.[2]
[1]Бакинский Государственной Университет, Азербайджан
AZ1148, Баку, ул. акад. Захида Халилова, 33
[2]Азербайджанская международная горнодобывающая компания, Азербайджан
AZ1065, Баку, ул. Измир,2, Hyatt башня 2, этаж 3
Автор, отвечающий за переписку: shakhla.a@gmail.com

Резюме. Важнейшей особенностью центральной части Малого Кавказа является связь оруденения с рудоконцентрирующими системами нарушений. Они представлены широкими северо-западного простирания зонами разломов. В их пересечении с зонами меридионального простирания локализуются крупные рудные поля (Зодское, Тутхунское и др.). Выделяются также широтные и северо-восточные зоны региональной трещиноватости, которые оказывают влияние на позицию рудных полей. В строении последних важная роль принадлежит локальным концетрическим структурам Зодского рудного поля, сыгравшим важную роль в локализации золотого оруденения. Среди главных факторов, определяющих позицию месторождения – приуроченность его к габбровому массиву, занимающему центральную позицию в тектоническом узле, а также к линейно вытянутой контактовой полосе пластин гипербазитов и габброидов. В Соютлинском рудном поле интенсивность развития рудоконцентрирующих разломов близмеридионального простирания обусловлена системой эшелонированных малоамплитудных разрывов с резко обогащенными участками оруденения с наибольшими мощностями рудных тел и высокими содержаниями в них металла, образующих бонанцы. В Тутхунском рудном поле золотая минерализация локализуется в узких и протяженных зонах интенсивно измененных пород гранитоидного комплекса и его экзоконтактовых ореолов, куда проникают обильные дайки, наиболее поздние члены интрузивных образований. Своеобразие выявленных геолого-структурных особенностей оруденения на Агдуздагском месторождении, четкое и характерное их проявление позволили выделить сложную штокверковую форму рудного тела, комбинированную и сочетающую в себе отдельные структурные элементы. Весьма интересной структурой представляется триединая сложная система нарушений, слагающая Зод-Тутхун-Агдуздагский блок, в результате сочленения которых образовался сложный тектонический узел гетерогенного строения, оказавшийся ареной развития полиэтапного рудообразующего процесса. Выдвинутые положения открывают новые возможности для прогноза золотого оруденения как в пределах центральной части Малого Кавказа, так и в юго-восточной части региона, отличающихся сходным геологическим строением.

Ключевые слова: *Малый Кавказ, рудоконцентрирующие структуры, рудное поле, глубинный разлом, золото, дайка, гидротермальное изменение*

MƏRKƏZİ QAFQAZIN AZƏRBAYCAN SEQMENTİNDƏ FİLİZ YATAQLARININ YERLƏŞMƏSİNDƏKİ REGİONAL STRUKTUR NƏZARƏT: UZUN MÜDDƏT İNKİŞAF EDƏN DİSLOKASİYALARIN TƏDQİQİ ROLU

Babazadə V.M.[1], Abdullayeva Ş.F.[1*], Novruzova S.R.[1], Vəliyev A.Ə.[2], İbrahimov C.R.[2]
[1]Bakı Dövlət Universiteti, Azərbaycan
AZ1148, Bakı şəh., akad.Zahid Xəlilov küç., 33
[2]Azərbaycan Beynəlxalq Mədən Şirkəti
AZ1065, Bakı şəh., İzmir küç., 2, Hyatt güllə 2, mərtəbə 3
**Yazışmalara məsul: shakhla.a@gmail.com*

Xülasə. Kiçik Qafqazın mərkəzi hissəsinin mühüm xüsusiyyəti filizləşmənin filizi konsentrasiya edən pozulma sistemləri ilə bağlılığıdır. Onlar şimali-qərb istiqamətli qırılma zonaları ilə təmsil olunmuşlar. Bu sistemlərin meridional istiqamətli zonalarla kəsişməsi iri filiz sahələrinin (Zod, Tutxun və s.) lokallaşmasına səbəb olmuşdur. Enlik və şimali-şərq istiqamətli regional çat zonaları da ayrılır. Qızıl filizləşməsinin lokallaşmasında Zod tektonik qovşağı mühüm rol oynayır. Yatağın mövqeyini təyin edən əsas faktorlar: filiz qovşağında başlıca yer tutan qabbro massivi, habelə kontakt zolaqda hiperbazitlərlə qabbroidlərin xətti uzanmış plastinləridir. Söyüdlü filiz sahəsində konsentrasiya edən parçalanmaların inkişafının intensivliyi şimali-şərq istiqamətli kiçik amplitudalı eşolonlaşmış pozulma sistemlərilə təyin edilir; pozulmaların filizləşmə ilə zənginləşmiş məntəqələrində böyük qalınlıqlı filiz kütlələri əmələ gəlmişdir; onlarda metalın miqdarı yüksəkdir, bir sıra hallarda bonantslar yaranmışdır. Tutxun filiz sahəsində diqqəti cəlb edən xüsusiyyət qranitoid kompleksinin və onun ekzokontakt oreolunda hidrotermal dəyişmiş süxurlarda ensiz və böyük məsafəyə uzanan qızıldaşıyan minerallaşma zonalarının aşkar edilməsidir. İntruziv əmələgəlmələrin ən gec üzvü olan daykalar bu zonalara nüfuz etmişdir. Ağduzdaq yatağının da özünəməxsus geoloji-struktur xüsusiyyəti vardır; mürəkkəb, bir növ ayrı-ayrı struktur elementlərin vəhdəti, ştokverk formalı filiz kütləsinin əmələ gəlməsinə də imkan yaratmışdır. Zod-Tutxun-Ağduzdaq blokunun əmələ gətirdiyi mürəkkəb pozulma sistemləri və onların üzvləşməsi nəticəsində heterogen mənşəli tektonik qovşaq yaranmışdır; o, cox mərhələli filiz əmələgəlmə prosesinin inkişaf arenası olmuşdur. İrəli sürülən iddialar istər Kiçik Qafqazın mərkəzi hissəsində, istərsə də bu ərazinin geoloji quruluşu ilə fərqlənən cənubi-şərqində, qızıl filizləşməsinin proqnozlaşdırmasına geniş imkanlar yaradır.

Açar sözlər: *Kiçik Qafqaz, filizə nəzarət edən strukturlar, filiz sahəsi, dərinlik qırılması, qızıl, dayka, hidrotermal dəyişmə*

ANAS Transactions Earth Sciences 2 / 2025

http://www.journalesgia.com

WHERE DID THE INITIAL SOURCES OF THE ALLOCHTHONOUS OCEANIC CRUST IN THE SOUTHERN EASTERNMOST MEDITERRANEAN ORIGINATE?

Eppelbaum L.[1,2*], Katz Y.[3], Kadirov F.[4,5,6], Ben-Avraham Z.[1]

[1]Department of Geophysics, Faculty of Exact Sciences, Tel Aviv University, Israel
Ramat Aviv 6997801, Tel Aviv
[2]Azerbaijan State Oil and Industry University, Azerbaijan
20 Azadlig ave., Baku, AZ1010
[3]Steinhardt Museum of Natural History & National Research Center,
Faculty of Life Sciences, Tel Aviv University, Israel
Ramat Aviv 6997801, Tel Aviv
[4]Ministry of Science and Education of the Republic of Azerbaijan,
Institute of Geology and Geophysics, Azerbaijan
119 H. Javid Ave., Baku, AZ1073
[5]Baku State University, Azerbaijan
33, Acad. Zahid Khalilov str., Baku AZ 1148
[6]Ministry of Science and Education of the Republic of Azerbaijan,
Institute of Oil and Gas, Azerbaijan
9, F.Amirov str., Baku, AZ1000
**Corresponding author: levap@tauex.tau.ac.il*

Keywords: *Easternmost Mediterranean, oceanic crust structure, allochthonous nature, Kiama paleomagnetic hyperzone, integrated analysis*

Summary. For a long time, it was believed that tectonic movements in the southernmost Eastern Mediterranean (EMM), located south of the Aegean-Anatolian Plate, were linked to the transcontinental shears originating from the Atlantic Ocean. However, an integrated analysis of numerous geological and geophysical data has led us to conclude that the primary structures in the EMM are not associated with these shears but instead with the spreading and collision processes of the Neotethys Ocean. Over the Neoproterozoic orogenic belt, a Mesozoic terrane belt (MTB) has been identified within the Arabian and Sinai lithospheric plates. The westernmost part of this belt contains allochthonous oceanic crust. We propose that the characteristics of total collision processes are influenced by the presence of a large, deep, counterclockwise-rotating structure. A significant finding in this context is the identification of an ancient block of oceanic crust in the western portion of the MTB, which corresponds to the reversely magnetized Kiama hyperzone (Early Permian). This block has moved along transform faults originating from the Neotethys region, which is roughly aligned with the current location of Eastern Arabia. The movement of the MTB terranes has, for example, contributed to the formation of the Mt. Carmel ophiolites in northern Israel. Therefore, we conclude that a comprehensive geophysical-geological assessment – which includes 3D magnetic-gravity modeling and transformations, thermal field analysis, GPS vector behavior, seismotomographic data, and analyses of paleomagnetism, paleobiogeography, petrology, and tectonic structure – clearly indicates the allochthonous nature of the MTB and the oceanic crust of the EMM. These findings necessitate a reevaluation of the tectono-geodynamic evolution of the Easternmost Mediterranean and suggest a reassessment of hydrocarbon exploration prospects in this region.

© 2025 Earth Science Division, Azerbaijan National Academy of Sciences. All rights reserved.

1. Introduction

The Easternmost Mediterranean (EMM) is a region situated in the transition zone between the two most prominent tectonic structures of the Earth: Eurasia and Gondwana (McKenzie, 1972; Ben-Avraham et al., 2002; Stern and Johnson, 2010). In

the Cenozoic, four lithospheric plates were formed in this region: the Nubian, Arabian, Aegean-Anatolian, and Sinai plates. The area is characterized by unique geodynamics that simultaneously express the elements of the geodynamic collision associated with the Tethys Ocean evolution (Le Pichon and Kreemer, 2010; Stampfli et al., 2013) and the initial spreading of the Red Sea rift system (Bosworth et al., 2005). However, to date, the EMM's paleogeodynamics remain poorly understood. One of the main problems is the origin of the EMM's oceanic crust. The tectonic processes in the southern Easternmost Mediterranean (EMM), situated south of the Aegean–Anatolian Plate, have long been attributed to transcontinental shear propagation from the Atlantic Ocean (e.g., Neev, 1975).

The geodynamic–geophysical models developed in this study are primarily grounded in the integrated geophysical identification of the giant, counterclockwise-rotating mantle structure (CRMS) in the Eastern Mediterranean (Eppelbaum et al., 2021). Independently, the counterclockwise rotation of the Levant Basin and the Arabian Plate, inferred solely from geological evidence, was previously demonstrated by Le Pichon and Gaulier (1988). We propose that the primary mechanism of the rotational influence is thermal convection. The essential role of thermal convection in deep geodynamics is underlined by many authors (e.g., Anderson, 2007).

Addressing such complex geodynamic phenomena, however, requires an integrated multidisciplinary approach that combines geological and geophysical analyses. The present result corroborate our earlier hypothesis (e.g., Eppelbaum and Katz, 2015) that the southern sector of the Easternmost Mediterranean (EMM) crust is allochthonous in nature and was transported into the studied region from the northeast.

2. Combined gravity, magnetic, and GPS data analysis

The oceanic crust block relating to the Kiama paleomagnetic hyperzone has been detected in the EMM (Ben-Avraham et al., 2002; Eppelbaum and Katz, 2015; Eppelbaum et al., 2014). We suggested that this oceanic block was formed in the region near the present position of the Persian Gulf (Eppelbaum et al., 2014). Nevertheless, how did this block get there? Figure 1 shows a combination of the residual satellite-derived gravity anomaly (Eppelbaum et al., 2021, 2024a), GPS vector behavior (Eppelbaum et al., 2021, 2025), and the smoothly averaged ΔZ magnetic map compiled for the 2.5 km over the mean sea level (msl) (Eppelbaum et al., 2024a, 2025). The revised quantitative analysis of the residual gravity anomaly yields a center mass location at a depth of approximately 1450 km. On average, a comprehensive analysis of seismotomographic data (Li et al., 2008; Trifonov and Sokolov, 2018; Eppelbaum et al., 2025) indicates that depths are underestimated by approximately 4-5%. These data, combined with the detailed paleomagnetic analysis (Eppelbaum et al., 2021, 2025) and other geological-geophysical data, enabled the unambiguous determination that the deep mantle experienced counterclockwise rotation (Eppelbaum et al., 2021, 2024a, 2025). Without hesitation, this deep structure rotation affects the layers and slabs above. The onset of mantle structure rotation, inferred from numerous geological and geophysical factors, was estimated to be 160-180 million years ago (Ma) (Eppelbaum et al., 2024b).

Satellite-derived gravity data enabled delineation of the deep mantle oval and identification of local structures within the Mesozoic terrane belt (MTB) and other components of the tectonosphere (Eppelbaum et al., 2024a). Mainly by magnetic and paleomagnetic data analysis, in the central zone of the deep structure projection, the block of ancient oceanic crust of the Kiama hyperzone was discovered (Eppelbaum et al., 2014), and active geodynamics to the north of it, in the Cyprus region, was outlined (Eppelbaum et al., 2021). The constructed smooth map of the magnetic field $\Delta\mathbf{Z}$ (Figure 1) was first presented by Eppelbaum et al. (2024a) to illustrate the reality of apical center rotation in the axial zone of the deep mantle structure in the Eastern Mediterranean.

Here, regions of magnetic field behavior coincide with gravity isolines of the deep-mantle structure oval (Figure 1). It is easy to see that the residual satellite-gravity anomaly, GPS vector behavior, and the magnetic field pattern create a joint ensemble.

3. Development of the biopaleogeographical map

Examining paleobiogeographic data confirms deep structure rotation and its relationship with near-surface structures. The region under consideration is crucial for analyzing the Neotethys Ocean's development stage (mainly Mesozoic) and its adjacent parts of Gondwana and Laurasia. Special attention is drawn to anomalous biogeographic indicators, particularly shell remains of the giant Ethiopian brachiopods Septirhynchia–Somalirhynchia and Mediterranean brachiopods *Pygope* (Eppelbaum and Katz, 2015; Eppelbaum et al., 2021). Based on the analysis of numerous sources, three paleobiogeographic provinces were selected (Figure 2): Boreal (Eurasian shelf), (2) Mediterranean (Mediterranean Basin), and (3) Ethiopian (Eastern Africa and South Arabia).

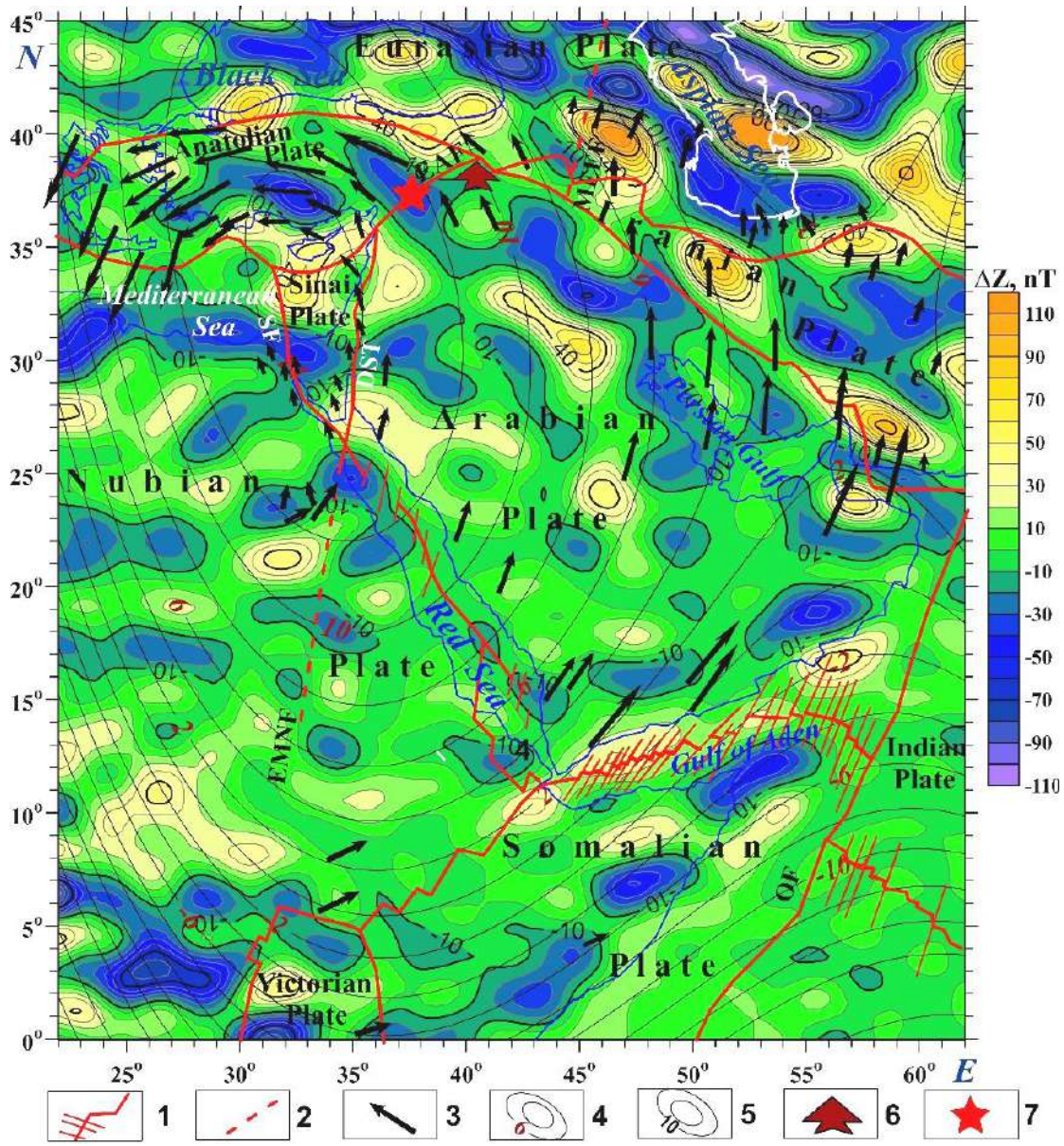


Fig. 1. Smoothly averaged magnetic ΔZ map recalculated to one common level of 2.5 km over the msl (initial data from https://geomag.colorado.edu/magnetic-field-model-mf7.html) for the African-Arabian region with the main tectonic elements, the behavior of the GPS vectors, and overlaid residual gravity anomaly.
(1) intraplate faults, (2) interplate faults, (3) GPS vectors (after Reilinger et al. (2006), Khorrami et al., 2019; Kadirov et al. (2024), (4) residual gravity field isolines (after Eppelbaum et al. (2021)), (5) magnetic field isolines (after Eppelbaum et al. (2025)), (6) distal part of the MTB, (7) epicenters of two main catastrophic earthquakes in eastern Turkey (February 06, 2023) ((6) after (Karabulut et al. (2023)). SF, Sinai Fault, DST, Dead Sea Fault, EMNF, Eastern Mediterranean-Nubian Fault, MEEF, Main Eastern European Fault, EAF, Eastern Anatolian Fault

The constructed map (Figure 2) illustrates the phenomenon (indicated by the red arrow rotating counterclockwise) of the geodynamic transfer of tectonic blocks, including remnants of Ethiopian fauna, from the present position of the Persian Gulf to the Levant, and ultimately to the Egyptian Eastern Desert. This fact demonstrates the counterclockwise movement of the eastern and central parts of near-surface projections of the anomalous deep structure in the Jurassic and Early Cretaceous periods.

Thus, the foreland sediments of Northern Arabia and Eastern Nubia are tectonically discordantly attached to the allochthonous Mesozoic terrane belt, which rotated counterclockwise toward the Gondwana paleocontinent. This geodynamic feature enables, for the first time, an explanation for the uniqueness of the biogeographically anomalous zone of terrane block attachment to the Gondwana paleocontinent during the Levantine phase of tectonic activity (Eppelbaum and Katz, 2015). To the north of this belt, within the marginal oceanic zone (along with the transform arc faults), an allochthonous block with the Kiama paleomagnetic hyperzone moved to the west to the current Levantine basin (Figure 2).

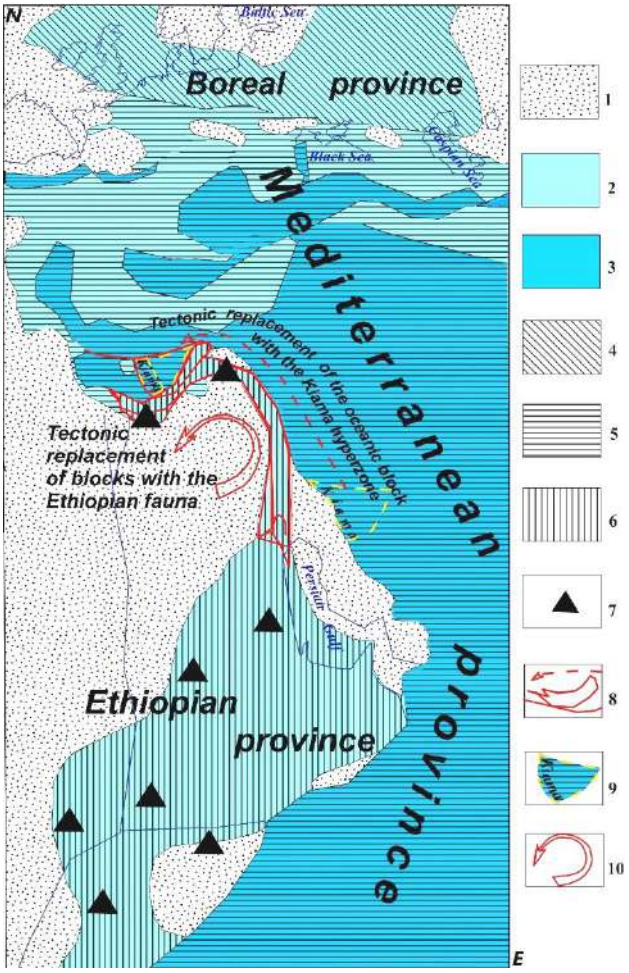


Fig. 2. The **s**chematic Late Jurassic paleobiogeographic map of the transitional region of Eurasia and Gondwana with elements of the subsequent Early Cretaceous geodynamics of the MTB. The blue lines show the boundaries between the seas and land. The following paleobiogeographic data were used (Arkell, 1956; Makridin et al., 1968; Feldman, 1987; Hirsch, 1988; Hirsch and Picard, 1988; Cooper, 1989; Lapkin and Katz, 1990). The tectonic-geodynamic data were reconstructed from (Scotese, 1991; Hall et al., 2005; Stampfli and Kozur, 2006; Eppelbaum and Katz, 2015; Alizadeh et al., 2016).
(1) land, (2) continental shields and arcs, (3) oceanic plateaus and rifts, (4) Boreal paleobiogeographic province, (5) Mediterranean paleobiogeographic province, (6) Ethiopian paleobiogeographic province, (7) points with the revealed Ethiopian brachiopods *Septirhynchia-Somalirhynchia*, (8) tectonic lines of the discordant paleobiogeographic replacements, (9) block of the oceanic crust with the Kiama hyperzone, (10) counterclockwise rotated tectonic blocks

4. Development of the tectonic-paleomagnetic map of the Easternmost Mediterranean

The developed map (Figure 3A) and paleomagnetic scale (Figure 3B) reflect the stages of formation of autochthonous and allochthonous structures in the EMM. This map was developed based on the most suitable paleomagnetic classification presented in Pechersky et al. (2010). Particularly distinct at the level of paleomagnetic analysis is the Mesozoic terrane belt with the Cretaceous and more ancient traps and ophiolites (Eppelbaum et al., 2023) and a block of anomalous ancient oceanic crust (relating to the Kiama paleomagnetic hyperzone of inverse polarity) in the Levant basin (Ben-Avraham et al., 2002; Eppelbaum et al., 2014; Eppelbaum and Katz, 2015). This block is discordantly attached to the younger (mainly Middle Cretaceous) crust of the Nubian and Aegean-Anatolian plates, as well as the north-western part of the Sinai Plate (Eppelbaum et al., 2023). This map will undoubtedly be refined and detailed as new paleomagnetic data are obtained.

5. Influence of the rotating mantle structure on the asymmetry of the sedimentary basins

Figure 3 presents a comparison between the residual satellite gravity-GPS map and the tectonic background of the region under study, revised after Eppelbaum et al. (2025). It includes a map of earthquake epicenters along the Dead Sea Transform (DST) and surrounding areas for the years 1983-2017, reconstructed from Sharon et al. (2020). The arc-shaped arrangement of the DST, along with the locations of numerous earthquake epicenters (Fig. 3B), closely aligns with the combined tectonic-geophysical map (Fig. 3A). This suggests that the bending of the DST, and consequently the epicenter locations of earthquakes, can be logically explained by the counterclockwise rotation of deep geological structures, which subsequently affects the overlying lithospheric blocks. Here, we observe a combination of shear and rotational movements.

Let us delve into the rotational effect on the asymmetry of sedimentary basins. In the Dead Sea region, as well as in the Eilat (Israel–Jordan) graben system, the axial part of the graben is confined to the east, while the flattened portion of the structure extends to the west (Ben-Avraham, 1985, 1992; Garfunkel and Ben-Avraham, 1996). The tectonic–geomorphological and magmatic asymmetry between the eastern and western coasts of the Dead Sea basin is well-documented, with the east side exhibiting higher amplitude and greater activity (Garfunkel and Ben-Avraham, 1996). Based on the generally gently arcuate structure of the DST (Smit et al., 2010), we propose a new geodynamic concept to explain the asymmetry of tectonic types associated with the deep displacement of graben-like structures. This concept posits that the regional development involves not only shear displacements but also rotational displacements of crustal blocks, which we consider fundamental to understanding the asymmetry of the regional basins.

The Sea of Galilee (also known as Lake Kinneret) is situated in northern Israel, along the northern extension of the DST. It has long been recognized that the axis of the deep-water basin of Lake Kinneret is shifted towards its eastern shore, while the axis

of its shallow-water basin is displaced towards the western coast (Eppelbaum et al., 2007). In earlier studies, a model of tectonic shear along a line or system of transform fault lines was proposed (Ben-Avraham, 1992). However, an analysis of paleomagnetic data (Eppelbaum et al., 2023) collected from areas adjacent to the Galilee region, along with structural mapping data, has identified widespread arcuate faults within the shear zone (Smit et al., 2010). This data helps clarify the dominant geodynamic processes in the region. These processes are associated with the counterclockwise axial rotation of continental crustal blocks in the Arabian-Nubian region, which aligns well with GPS monitoring data.

The asymmetry of local sedimentary basins in relation to the deep rotating structure is highlighted by the geomorphological features of the Arabian–Nubian zone of Gondwana during the Late Cenozoic. In the western part, corresponding to the junction of the Nubian Plate and the Red Sea rift zone, the elevation of the plateau and the Nile River valley generally does not exceed 500 meters. In contrast, the eastern part (the Arabian–Sinai zone), where these lithospheric plates meet the Red Sea rift zone system and the Dead Sea shear zone, exhibits elevations that clearly exceed 500 to 1000 meters (Eppelbaum et al., 2021). Along the marginal zones of the Arabian and Sinai plates, mountain ranges with heights exceeding 2000 to 3000 meters have formed. We suggest that this regional geomorphological asymmetry on either side of the Red Sea rift zone is geodynamically influenced by the counterclockwise rotation of the region.

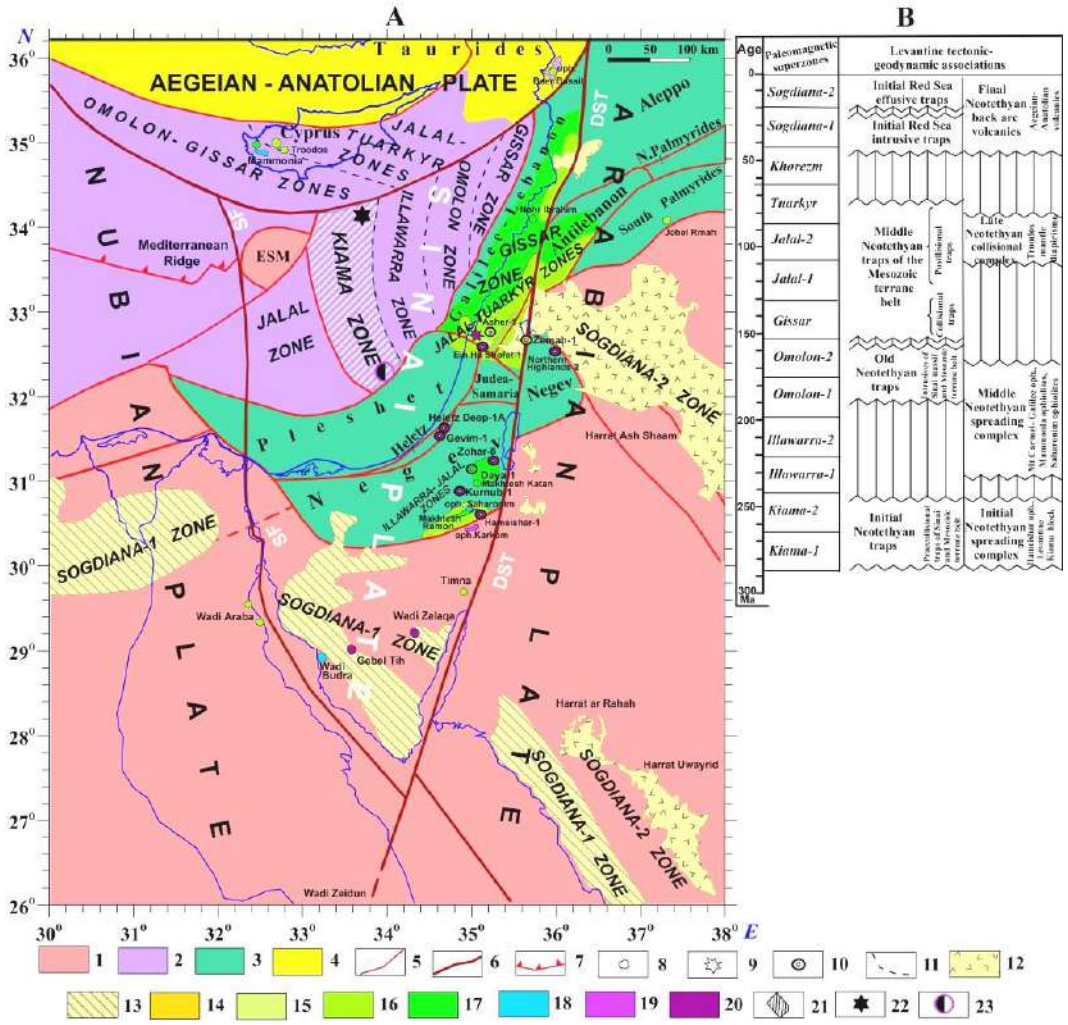


Fig. 3. Tectonic-paleomagnetic map of the Eastern Mediterranean and Near East (**A**) and its paleomagnetic scale (**B**).
(1) Neoproterozoic belt of the Eastern Gondwana, (2) oceanic crust of the relict Neotethyan depression, (3) Mesozoic terrane belt (MTB), (4) Alpine-Himalayan fold belt, (5) intraplate faults, (6) interplate faults, (7) Mediterranean accretionary ridge, (8) outcrops of magmatic bodies, (9) xenoliths in the Cretaceous volcanics, (10) magmatic bodies in the boreholes, (11) suggested boundaries between the paleomagnetic hyperzones, (12) effusive traps of the Sogdiana-2 superzone, (13) intrusive traps of the Sogdiana-1 superzone, super- and hyperzones detected by radiometric data (14-20): (14) Khorezm, (15) Tuarkyr, (16) Jalal-1 and Jalal-2, (17) Gissar, (18) Omolon, (19) Illawarra, (20) Kiama, (21) contour of the Kiama paleomagnetic hyperzone revealed in the EMM by geophysical data, (22) point of the extremely low heat flow measurements: 13.9±2.9 mW/m^2 (after Eckstein, 1978, corrected for the sedimentation rate), (23) zone of the low-temperature anomaly (after Kahn, 2025). The paleomagnetic scale (**B**) was constructed based on the classification presented in Pechersky et al. (2010). SF, Sinai Fault, DST, Dead Sea Transform, ESM, Eratosthenes Sea Mount

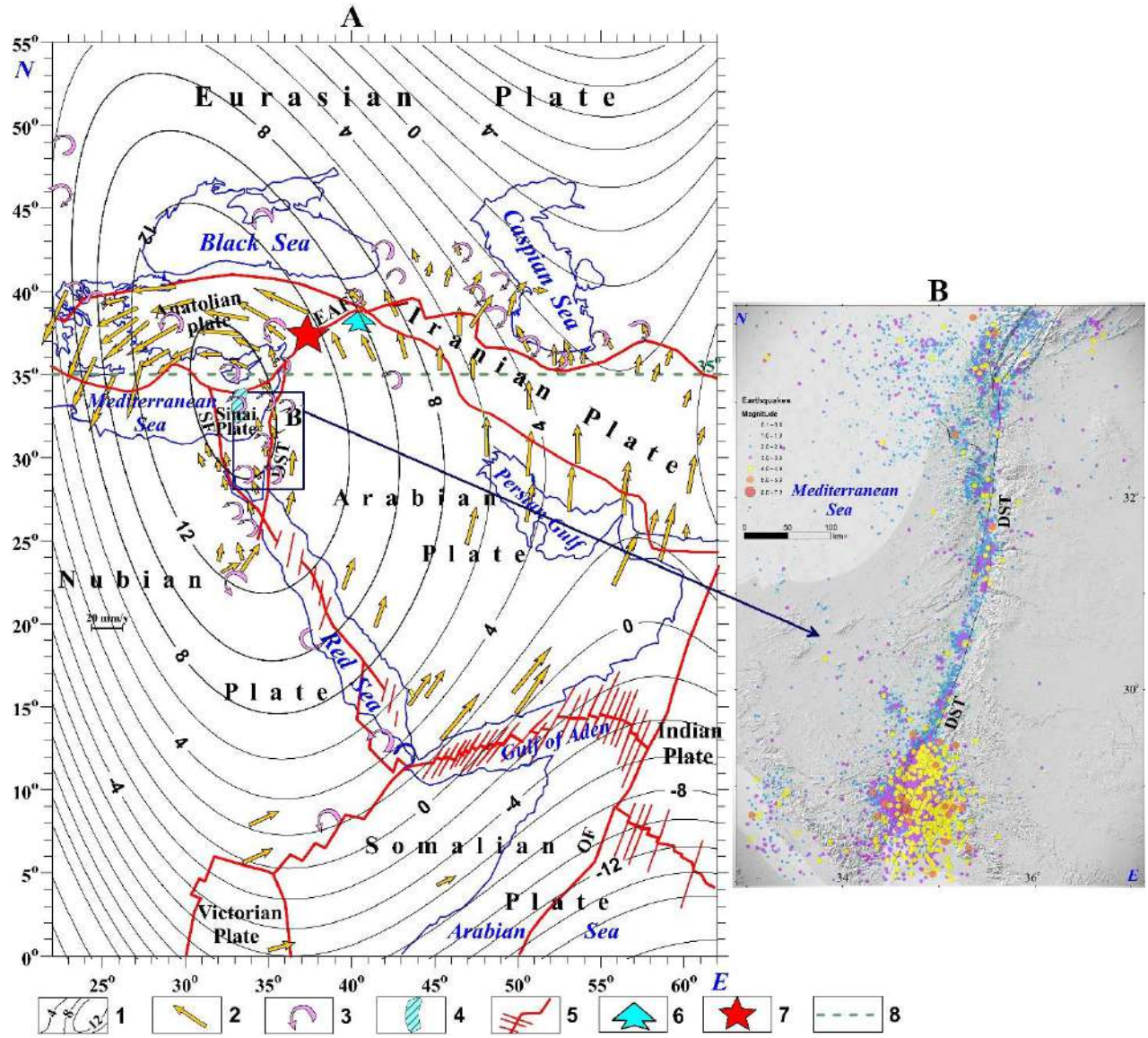


Fig. 4. Comparison of the combined tectonic-geophysical map (A) (revised and supplemented after Eppelbaum et al., 2025) and map of the earthquake epicenters along the Dead Sea Transform and surrounding areas for 1983-2017 years (B) (modified after Sharon et al., 2020).
(1) isolines of the residual satellite gravity anomaly (after Eppelbaum et al., 2021), (2) GPS velocity vectors (after Reilinger et al. (2006), Khorrami et al. (2019), Kadirov et al. (2024)), (3) rotation geodynamic elements (obtained mainly from the paleomagnetic data) indicating clockwise and counterclockwise rotations (see detailed explanations in Eppelbaum et al., 2025); (4) contour of the oceanic crust block relating to the Kiama paleomagnetic hyperzone (after Eppelbaum et al., 2014), (5) main intraplate faults, (6) distal part of the Mesozoic terrane belt, (5) center of the high magnitude seismogenic zone in the Eastern Turkey (*February 06, 2023*; Hancilar et al. (2023)), (8) critical latitude of the Earth (after Véronnet (1912)). OF, Owen Fault, DST, Dead Sea Transform, EAF, Eastern Anatolian Fault

6. Discussion

The region was previously geodynamically associated with latitudinal and diagonal movements from the Atlantic rifts in the transcontinental direction (Neev, 1975). The Aegean-Anatolian part of the EMM was identified with the collisional geodynamics of the final stages of the Neotethys Ocean development Le Pichon and Kreemer, 2010). On the other hand, concerning the southern part of the Eastern Mediterranean, data from paleobiogeographical (Figure 2), structural-sedimentological (e.g., Hall et al., 2025; Eppelbaum and Katz, 2015), and geophysical studies (e.g., Ben-Avraham et al., 2006; Eppelbaum et al., 2023), we suggested the allochthonous nature of the continental and oceanic crust located here (Eppelbaum and Katz, 2015; Eppelbaum et al., 2014, 2021, 2025). The allochthonous structure was referred to as the Mesozoic terrane belt (MTB), and the stage of its discordant attachment to the Gondwanaland foreland along deep-seated shears was termed the Levantine phase of tectonic activity (Eppelbaum et al., 2015; Eppelbaum et al., 2023).

The critical latitude of 35° on the Earth (Véronnet, 1912) is of great importance, as it nearly

coincides with the projection of the center of the identified mantle structure (Eppelbaum et al., 2021). The interplay between mid-latitudes, rotation factors, and global geodynamics has been discussed by Khain (2001) and Anderson (2007). Additionally, Levin et al. (2017) explored the specific characteristics of critical latitudes within the context of the Earth's rotating ellipsoid. They established a connection between a body's degree of compression and its angular velocity of rotation, suggesting that geodynamic activity increases at and near the critical latitudes. The instability of the Earth's mantle and lithosphere, especially below and near the Earth's critical latitude, along with the rotation of geological structures, may have contributed to the movement of crustal blocks from their origination in the eastern Arabia to the current location in the southern part of the Eastern Mediterranean.

The determined oceanic crust block with the Kiama hyperzone (Eppelbaum et al., 2014) was formed over more than 1,000 km northeast (Eppelbaum and Katz, 2015), near the current position of the Persian Gulf. Let us examine this issue in more detail to ensure everything is clear between the modern and paleo-coordinates. It is well known that the Neo-Tethys began to form in the Early Permian near eastern Arabia (Hall et al., 2005) at the border with the MTB (Eppelbaum et al., 2021). This belt developed here until the Jurassic-Cretaceous boundary. After that, it moved counterclockwise along the arc transform faults until the middle of the Early Cretaceous (133 Ma), pending consolidation with the northern ledge of the Arabian part of Gondwana. After this, a similar movement occurred along the arc-transform faults of the terrane, composed of the primary (mainly Permian-Triassic) oceanic crust. It formed north of the MTB. The terrane block was located 150-200 km north of the north-western edge of the Persian Gulf, at 32° northern latitude, i.e., almost at the same latitude as in the modern allochthonous position. Considering the arcuate movement within the Arabian salient, this block descended into the Eastern Mediterranean trough from the northeast, from latitude of 38°–39° to 32° in modern coordinates.

A combined analysis of geological and geophysical materials suggested that this movement began approximately 160-180 million years ago. The determined age and direction of the movement coincided with the recently determined great breakup in Pangea (Le Pichon et al., 2023) and the tectonic constructions presented in Stampfli et al. (2013).

The anomalous joining of oceanic block crust with reversely magnetized basalts to the Eratosthenes Sea Mount (ESM), a continental block of thinned continental crust, is reliably contoured through a thorough analysis of seismic, gravity, and magnetic data (Ben-Avraham et al., 2002). The Eratosthenes block belonged to the marginal zone of the Neoproterozoic belt and was torn off during the movement of the Anatolian belt massifs to the north. After that, the ESM was geodynamically assembled along a deep thrust system with the Kiama oceanic block, which moved from the east (Eppelbaum and Katz, 2015).

The oceanic block of the Levant with an anomalously ancient crust – up to the late Paleozoic (Kiama paleomagnetic hyperzone) (Figure 3B) was studied by geophysical method integration (Eppelbaum et al., 2014, 2021; Eppelbaum and Katz, 2015) and by correlation with the extensive field of the Carmel–Lower Galilee ophiolites (Eppelbaum et al., 2023). Geologically, radiometric, facial, and petrological methods were comprehensively applied to study this area (e.g., Segev, 2000, 2009; Fleischer and Varshavsky, 2012). A series of four ophiolite nappes with a total thickness of up to 4,000 m and a length of up to 40 km has developed here. At the same time, the youngest nappe, containing mélange and ophiolites (with an age of up to 164.3 Ma), is created at the base of the sequence. The most ancient nappe of the olivine-basalt mélange (up to 222.4 Ma old) occupies the top part of the section (Dvorkin and Kohn, 1989; Eppelbaum et al., 2023). This phenomenon indicates that the attachment of the marginal part of the ophiolite belt near the Galilee-Lebanon terrane was carried out not by linear shifts but by rotation of the oceanic plate in a counterclockwise direction (Figure 5).

Moreover, its oldest part (relating to the paleomagnetic Kiama hyperzone) forms the marginal western boundary of the Levantine oceanic terrane and, according to seismic data (Ben-Avraham et al., 2002), is thrust over the younger autochthonous Levantine crust (Figures 3A, B).

The data of the paleogeography of the Jurassic seas of Central Gondwana (Arkell, 1956), along with extensive studies in the field of paleobiogeographic zoning of the Jurassic basins of Eurasia and Gondwana (Makridin et al., 1968) showed a paradoxical discrepancy in the position of brachiopod localities in the Eastern Mediterranean (Figures 2 and 5), sharply isolated from the central area of the Ethiopian Basin and separated from the Eastern Mediterranean by a vast land mass. The allochthonous nature of the *Septirhynchia–Somalirhynchia* brachiopod fauna in the Levant, several thousand kilometers from the main East Arabian-Ethiopian area, has not been adequately explained.

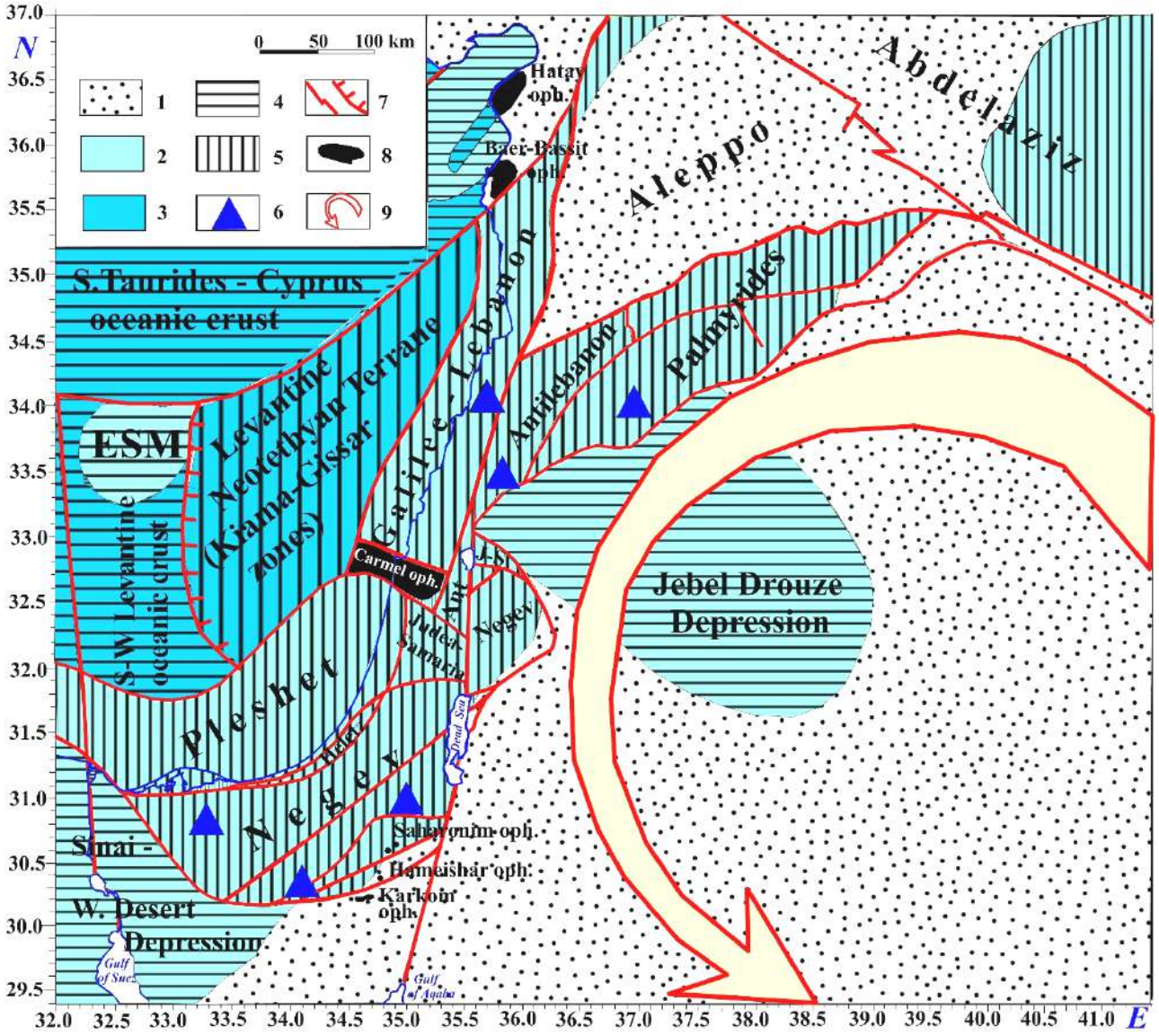


Fig. 5. Structural and geodynamic scheme of the relationship between autochthonous and allochthonous biogeographic systems of the Easternmost Mediterranean.
(1) Nubian-Arabian shield, (2) oceanic crust blocks, (3) continental crust terranes, (4) west of the Neotethyan autochthonic block system, (5) Ethiopian allochthonous block systems, (6) points with *Septirhynchia–Somalirhynchia* Ethiopian Jurassic brachiopods, (7) tectonic faults, (8) ophiolites, (9) direction of the regional counterclockwise rotation of tectonic blocks with the Ethiopian fauna. ESM, Eratosthenes Sea Mount, Ant, Antilebanon, J-S, Judea-Samaria

At that time, plate tectonics had not yet found a sufficient theoretical basis for setting up work in the field of geodynamic cartography. One way or another, the revealed paradox of the allochthonous nature of the Jurassic fauna in the Levant was the first evidence in the field of the complexity of the Levantine geodynamic processes, and it showed the need for extensive geological-geophysical studies to identify geodynamic processes in the complex zone of interaction between Eurasia and Gondwana. Over the past decades, these studies have mainly been implemented due to the progress of innovative geological and geophysical research by teams from many countries of the world (e.g., Ben-Avraham et al., 2002, 2006; Hall et al., 2005; Jimenez-Munt et al., 2006; Reilinger et al., 2006; Muttoni et al., 2009; Stern and Johnson, 2010; Burov, 2011; Stampfli et al., 2013; Faccenna et al., 2014; Eppelbaum et al., 2021, 2025; Le Pichon et al., 2023; Bosworth, 2024).

Historical-planetological analysis indicates that the final phase of the Paleozoic represents the most extreme period of the Phanerozoic in terms of tectono-thermal, paleomagnetic, hydrospheric, and climate-sedimentation activity (Lapkin and Katz, 1990; Eide and Torsvik, 1996). During this period, a stable geomagnetic regime characterized mainly by reverse polarity coexisted with significant thermal and geodynamic activity in the lithosphere and upper mantle. This activity reflects the convective

geodynamics related to the plate tectonic interactions of the Pangea and Panthalassa structures (Eide and Torsvik, 1996). Recent paleomagnetic reconstructions (Muttoni et al., 2009; Domeier et al., 2012) analyze the geodynamic situation within models of Late Permian Pangea A and Early Permian Pangea B. The Pangea B reconstruction, which includes the authors' supplements, is illustrated in Figure 6. This reconstruction clearly shows that the oceanic crust of Neotethys, along with surrounding terrane belts, was located to the east of the present-day area of the Easternmost Mediterranean (EMM). A key geodynamic feature of Pangea B is the triple plate junction boundary, which corresponds to zones of spreading, subduction, and deep displacement (intra-Pangea dextral shear). Notably, displacements of oceanic and continental crust blocks, as well as the mantle lithosphere, have occurred over significant distances during various stages of the Neotethys Ocean evolution in the Late Mesozoic and Cenozoic eras (Jimenez-Munt et al., 2006; Burov, 2011; Yamasaki and Stephenson, 2011; Stampfli et al., 2013).

According to the plate tectonic concepts and sequence of opening of the Neo-Tethys rift system, the Kiama hyperzone extended in a SE-NW direction immediately adjacent to the terrane belt, and the younger Illawarra and Omolon hyperzones adjoined in the form of strips to the northeast of it. Moving along the transform fault in the northwest, the uplift of the Arabian Shield of Gondwana (Figure 2) rotated this terrane 180° counterclockwise. It encountered the Galilee-Lebanon terrane, which is characterized by the youngest strip zone of the oceanic crust. Then, as the terrane rotated and moved into the Levantine basin, pressure from the surrounding masses of the autochthonous oceanic crust and the Taurid structures caused more ancient band anomalies of the allochthonous terrane complex to collide. After a counterclockwise rotation of almost 360°, the Kiama block assumed an orientation close to its adopted orientation, which is now in place (Figures 2 and 3). The features of such movements are identified using various multiscale techniques and methods of geological-geophysical mapping, with careful consideration of the diverse geological and geophysical data.

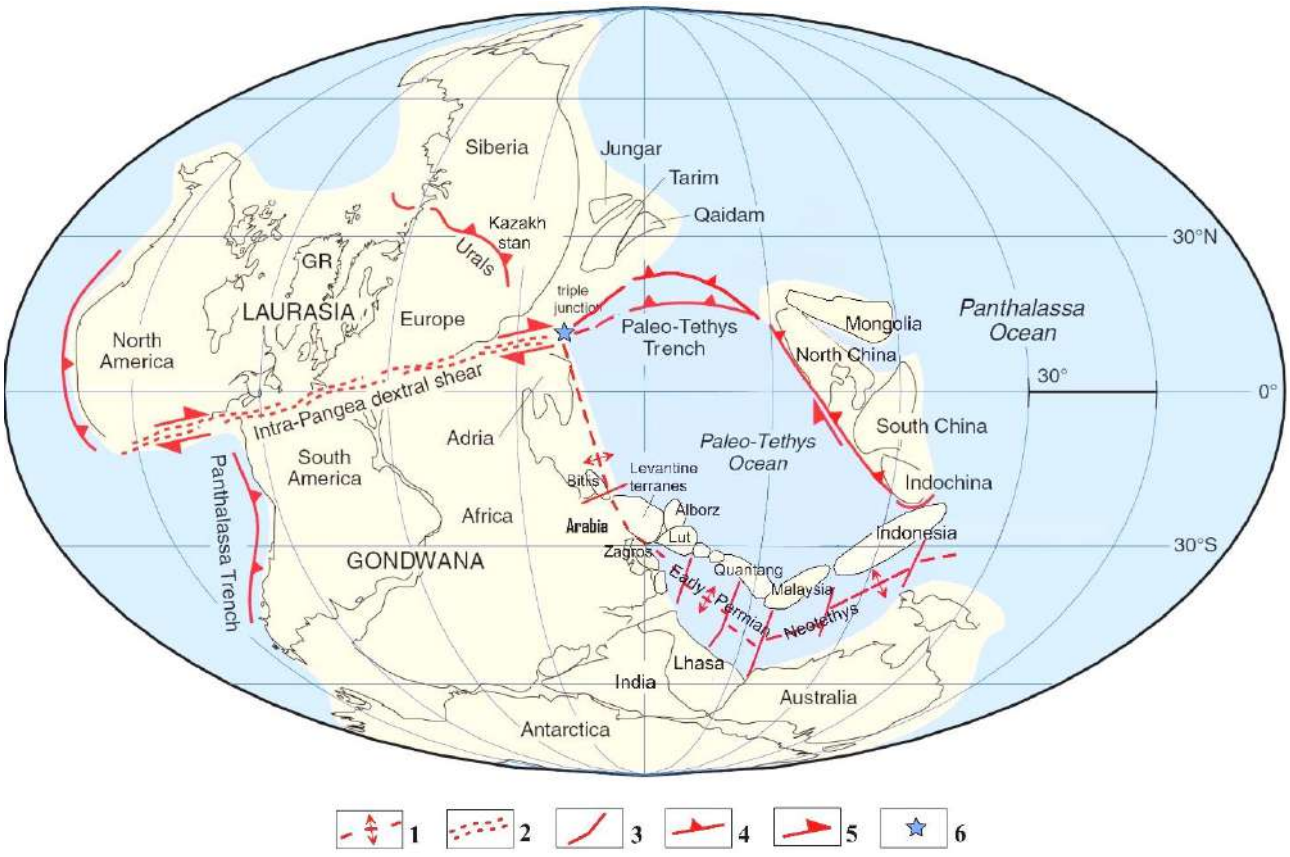


Fig. 6. Early Permian Neotethys position within the Pangea B–Panthalassa reconstruction (after Muttoni et al. (2009), with supplements from Stampfli et al. (2013), Golonka and Ford (2000), and some authors' supplements).
(1) Neotethyan ocean spreading center, (2) intra-Pangea dextral shear, (3) transform oceanic faults, (4) subduction zones, (5) direction of the strike-slip motion, (6) triple junction

Discovery of the mantle counterclockwise rotating mantle structure (Eppelbaum et al., 2021, 2025), influencing the above lithospheric blocks and geological layers, supported the assumption that the oceanic crust of the present southern EMM was displaced from the northeast (apparently, along the transform faults). Among twelve independent geophysical-geological factors confirming this counterclockwise rotation, we can note here the GPS counterclockwise rotation (Figure 1) (Reilinger et al., 2006; Khorrami et al., 2019; Karabulut et al., 2023; Kadirov et al., 2024), a combination of the residual satellite-derived (Figure 1) and land/sea gravity anomalies (Eppelbaum et al., 2021), smoothly averaged magnetic $\Delta\mathbf{Z}$ map (Eppelbaum et al., 2025) (Figure 1), Late Jurassic paleobiogeographical map (Figure 2), numerous paleomagnetic-geodynamic data (e.g., Morris et al., 2002; Borradaile et al., 2010; van Hinsbergen et al., 2010; Uzel et al., 2015; Kaymakci et al., 2018; Çabuk and Cengiz, 2021; Eppelbaum et al., 2021, Lazos et al., 2022; Cengiz and Karabulut, 2023; Eppelbaum et al., 2025), tectonic-paleomagnetic map (Figure 3), geoid isolines map (Eppelbaum et al., 2024a), seismotomographic data (Li et al., 2008; Trifonov and Sokolov, 2018; Eppelbaum et al., 2025), analysis of last seismological data (Karabulut, 2023; KeAi, 2023), and diverse tectonic-geodynamical and mineralogical-petrological data (Eppelbaum et al., 2014, 2024a; Eppelbaum and Katz, 2015).

It is assumed that the significant impact of the deep-rotating structure prevented the Kiama oceanic crust block (possibly including other oceanic crust blocks) from subducting and preserving its current location. The average thermal flow in the eastern Mediterranean: from 11.5 to 40 mW/m^2 (Erickson et al., 1977; Eckstein, 1978; Cermak, 1980; Verzhbitsky, 1996; Elgabry et al., 2013) is several times less than average values in the central and western Mediterranean, likely to reflect the older crust (e.g., Sclater et al., 1980). The minimum observed value (11.5 mW/m^2; uncorrected for the sedimentation rate) is in the northern part of the reversely magnetized Kiama zone (corresponding to the most ancient block of the oceanic crust adjacent to the Aegean-Anatolian Plate). The recent temperature field analysis enabled us to recognize a circular low-temperature anomaly at different depths in the EMM (4, 6, 8, and 10 km) (Kahn, 2025) corresponding to the southern end of the ancient oceanic crust block with the Kiama paleomagnetic hyperzone (Figure 3A).

The prolonged counterclockwise rotation of the deep structural elements has significantly influenced the asymmetry of sedimentary basins (see Figure 4). Additionally, the anomalous en-echelon Late Cretaceous troughs of the Antilebanon and Galilea-Lebanon terranes (Figure 5) exhibit a similar asymmetrical pattern. In this region, the sedimentary deposits have varying thicknesses: (i) a maximum thickness of up to 1453 m and 1550 m in the eastern part of the zone, and (ii) a minimum thickness ranging from 300 to 449 m in the western part of the zone.

Finally, our previous investigation of the beginning of this mantle structure rotation was expected to be 160-180 Ma (Eppelbaum et al., 2024b). This period was reasonably sufficient for the Earth's crust displacement from the region north of the present position of the Persian Gulf to the Easternmost Mediterranean. Based on paleomagnetic data analysis, the velocity of the counterclockwise rotation of the Cyprus Island over the last 70 million years has been calculated (Eppelbaum et al., 2025). The velocity was estimated to be 18 mm per year, which is consistent with modern GPS velocity data (e.g., Reilinger et al., 2006). If we extrapolate this rotation velocity to the period of 180 Ma, we obtain the total displacement of tectonic blocks as approximately 3200 km. This value is in good agreement with other independent estimates, such as those performed by Khalafly (2006) for the Lesser Caucasus (most of whose structure is influenced by the deep structure rotating counterclockwise).

The geodynamic features of the block structures in the continental and oceanic crust of the Eastern Mediterranean are revealed in the analysis of trap and ophiolitic complexes (Figures 3 and 5), which were studied using radiometric and paleomagnetic methods (Eppelbaum and Katz, 2015).

This was especially evident when comparing the ages of the oceanic crust of the Aegean-Anatolian and Levantine segments. Within the Aegean-Anatolian Plate are young ophiolites, which mark young oceanic crust (corresponding to the upper parts of the Jalal and Tuarkyr paleomagnetic zones). There are ophiolitic complexes of Baer-Bassit (Jalal zone), Hatay, and Troodos (Jalal-Tuarkyr zones) (Figures 3 and 5).

The age of the Levant ophiolites (Saharonim basalts, Hameishar basaltic boudinites) and the paleomagnetic age of the Karkom ophiolites exceed 200 million years. These data are consistent with the average radiometric ages of the Carmel ophiolites (Eppelbaum et al., 2025).

Thus, according to the presented analysis, the oceanic crust of the Levant has a more ancient, Permian-Triassic age, compared to the oceanic crust of the southern part of the Aegean-Anatolian lithospheric plate, whose age on average corresponds to the Late Mesozoic – mainly the end of the Cretaceous period.

Let us especially note the geodynamic consequences of the two strongest earthquakes in eastern Turkey (06.02.2023), when the combination of counterclockwise rotation of the Earth's crust blocks and accumulated stress in the Earth's crust resulted in a shift of sections of the Aegean-Anatolian Plate more than eleven m to the southwest (Hancilar et al. 2023; Karabulut et al., 2023) (i.e., counterclockwise). The probability of all the above data being a random coincidence of all the mentioned factors is very low.

6. Conclusions

The main conclusions of the studies are the following:

1) Previously, the direction of the dominant geodynamic stresses in Central Gondwana was traced from the West (Atlantic Ocean). However, innovative geological and geophysical analyses have revealed a wide range of geodynamic connections in the Arabian-Nubian segment of Gondwana, pointing towards the East,

2) The allochthonous oceanic crust in the southern part of the Eastern Mediterranean formed more than 1,000 km to the northeast, near the current position of the Persian Gulf,

3) The deep rotating structure exerted a significant influence that hindered the subduction of ancient oceanic crust blocks. The interaction between collisional and spreading processes, combined with the effects of the counterclockwise-rotating deep structure, created a unique tectono-geodynamic environment,

4) The above facts necessitate a reevaluation of the geodynamic evolution of the region under study.

Acknowledgments

The authors would like to thank two anonymous reviewers for their thorough review of the manuscript; their critical comments and valuable suggestions were very helpful in preparing this paper.

REFERENCES

Alizadeh AA, Guliyev IS, Kadirov FA, Eppelbaum LV (2016) Geosciences in Azerbaijan. vol 1. Geology. Springer, Heidelberg, NY, p 239

Anderson DL (2007) New theory of the Earth. Cambridge University Press, Cambridge, https://doi.org/10.1017/CBO9781139167291

Arkell WJ (1956) Jurassic geology of the world. Olivier and Boyd, London, p 808

Ben-Avraham Z (1985) Structural framework of the Gulf of Elat (Aqaba), northern Red Sea. J Geophys Res, Solid Earth Planets 90:703–726. https://doi.org/10.1029/JB090iB01p00703

Ben-Avraham Z (1992) Development of asymmetric basins along continental transform faults. Tectonophysics 215:209–220. https://doi.org/10.1016/0040-1951(92)90082-H

Ben-Avraham Z, Ginzburg A, Makris J, Eppelbaum L (2002) Crustal structure of the Levant basin, Eastern Mediterranean. Tectonophysics 346:23–43. https://doi.org/10.1016/S0040-1951(01)00226-8

Ben-Avraham Z, Schattner U, Lazar M et al (2006) Segmentation of the Levant continental margin, eastern Mediterranean. Tectonics 25:1–17. https://doi.org/10.1029/2005TC001824

Borradaile GJ, Lagroix F, Hamilton TD et al (2010) Ophiolite tectonics, rock magnetism and paleomagnetism, Cyprus. Surv Geophys 31:285–359. https://doi.org/10.1007/s10712-009-9090-2

Bosworth W (2024) Continental rift asymmetry and segmentation – contributions from the African plate. J African Earth Sci 210(105128):1–15

Bosworth W, Huchon P, McClay K (2005) The Red Sea and Gulf of Aden basins. J of African Earth Sci 43:334–378. https://doi.org/10.1016/j.jafrearsci.2005.07.020

Burov EB (2011) Rheology and strength of the lithosphere. Marine and Petroleum Geology 28(8):1402–1433. https://doi.org/10.1016/j.marpetgeo.2011.05.008

Çabuk BS, Cengiz M (2021) Paleomagnetic rotations in the circum-Marmara region, northwestern Turkey since the Late Cretaceous. J of Asian Earth Sci 213(104748):1–15. https://doi.org/10.1016/j.jseaes.2021.104748

Sclater JG, Jaupart C, Galson D (1980) The heat flow through oceanic and continental crust and the heat loss of the Earth. Rev Geophys Space Phys, 18(1): 269–311. https://doi.org/10.1029/RG018i001p00269

Cermak V (1980) Heat flow in the Eastern Mediterranean and the Black Sea. EGS Program and Abstracts, Budapest, p. 121

Cengiz M, Karabulut S (2023) A two-stage deformation of the Anatolian Plate deduced from Paleomagnetic signals: The initial age of the Anatolian's escape. Turkish J of Earth Sciences 33(3):243–259. https://doi.org/10.55730/1300-0985.1910

Cooper GA (1989) Jurassic Brachiopods of Saudi Arabia. Smithsonian Contributions to Paleobiology 65:1–213.

Domeier M, Van der Voo R, Torsvik T (2012) Paleomagnetism and Pangea: The road to reconciliation. Tectonophysics 514(3). https://doi.org/10.1016/j.tecto.2011.10.021

Dvorkin A, Kohn BP (1989) The Asher volcanics, northern Israel: Petrography, mineralogy, and alteration. Isr. J Earth Sci, 38:105–123

Eckstein Y (1978) Review of heat flow data from the Eastern Mediterranean region. Pageoph, 117:150–159. https://doi.org/10.1007/BF00879742

Eide AE, Torsvik TH (1996) Paleozoic supercontinental assembly, mantle flushing, and genesis of the Kiaman Superchron. Earth Planet Sci Lett 144:389–402.

Elgabry MN, Panza GF, Badawy AA et al (2013) Imaging a relic of complex tectonics: the lithosphere asthenosphere structure in the Eastern Mediterranean. Terra Nova 25(2):102–109. https://doi.org/10.1111/ter.12011

Eppelbaum LV, Ben-Avraham Z, Katz Y (2007) Structure of the Sea of Galilee and Kinarot Valley derived from combined geological-geophysical analysis. First Break 25(1):21–28. https://doi.org/10.3997/1365–2397.2007001

Eppelbaum LV, Ben-Avraham Z, Katz Y, Cloetingh S, Kaban M (2021) Giant quasi-ring mantle structure in the African-Arabian junction: Results derived from the geological-geophysical data integration. Geotectonics (Springer) 55(1):67–93. https://doi.org/10.1134/S0016852121010052

Eppelbaum LV, Katz YuI (2015) Eastern Mediterranean: Combined geological-geophysical zonation and paleogeodynamics of the Mesozoic and Cenozoic structural-sedimentation stages. Marine and Petrol Geology 65:198–216. https://doi.org/10.1016/j.marpetgeo.2015.04.008

Eppelbaum LV, Katz YI, Ben-Avraham Z (2023) Geodynamic aspects of magnetic data analysis and tectonic-paleomagnetic mapping in the Easternmost Mediterranean: A review. Applied Sciences, Spec. Issue "Ground-Based Geomagnetic Observations: Techniques, Instruments and Scientific Outcomes" 13(18):1–44. https://doi.org/10.3390/app131810541

Eppelbaum LV, Katz YI, Ben-Avraham Z (2024a) The reasons for the enormous accumulation of the geodynamic tension in Eastern Turkey: a multidisciplinary study. Geology, Geophysics, Earth Sciences 2(2):1–28. https://doi.org/10.58396/gges020202

Eppelbaum LV, Katz YI, Kadirov FA (2024b) The relationship between the paleobiogeography of the northern and southern sides of the Neotethys and the deep geodynamic processes. ANAS Transactions, Earth Sciences 1:57–76. https://doi.org/10.33677/ggianas20240100109

Eppelbaum LV, Katz YI, Ben-Avraham Z (2025) A giant quasi-ring mantle structure beneath the Eastern Mediterranean: Interpretation of new magnetic, paleobiogeographic, and seismic tomography data. Geotectonics 59(2):101–126. https://doi.org/10.1134/S001685212570013X

Eppelbaum LV, Nikolaev AV, Katz YI (2014) Space location of the Kiama paleomagnetic hyperzone of inverse polarity in the crust of the eastern Mediterranean. Doklady Earth Sciences (Springer) 457(6):710–714. https://doi.org/10.1134/S1028334X14080212

Erickson AJ, Simmons G, Ryan WBF (1976) Review of Heat Flow Data from the Mediterranean and Aegean Seas. In: Biju-Duval B, Montadert L (eds), Proceed. of the Intern. Symposium on the Structural History of the Mediterranean Basins, Split, Yugoslavia, 25-29 Oct. 1976, pp 263–280

Faccenna C, Becker TW, Auer L, Billi A et al (2014) Mantle dynamics in the Mediterranean. Reviews of Geophysics 52:283–332. https://doi.org/10.1002/2013RG000444

Feldman HR (1987) A new species of the Jurassic (Callovian) Brachiopod *Septirhynchia* from the Northern Sinai. Journal of Paleontology 61(6):1156–1172. https://doi.org/10.1017/S002233600002953X

Fleischer L, Varshavsky AA (2012) Lithostratigraphic database of oil and gas wells drilled in Israel. Rep. OG/9/02, Ministry of National Infrastructures of Israel, Jerusalem, Israel.

Garfunkel Z, Ben-Avraham Z (1996) The structure of the Dead Sea basin. Tectonophysics 266:155–176. https://doi.org/10.1016/S0040-1951(96)00188-6

Golonka J Ford D (2000) Pangean (Late Carboniferous–Middle Jurassic) paleoenvironment and lithofacies. Palaeogeography, Paleoclimatology, Paleoecology 161:1–34. https://doi.org/10.1016/S0031-0182(00)00115-2

Hall JK, Krasheninnikov VA, Hirsch F, Benjamini C, Flexer A (2005) Geological Framework of the Levant. The Levantine Basin and Israel, vol 2. Historical Productions-Hall, Jerusalem, Israel, p 836

Hancilar U et al (2023) Kahramanmaraş - Gaziantep Türkiye M7.7 Earthquake, 6 February 2023. Strong ground motion and building damage estimations. Preliminary Report. Dept. of Earthquake Engineering, Bogazici University, Turkey

Hirsch F (1988) Jurassic biofacies versus sea level changes in the Middle eastern Levant (Ethiopian province). Trans of the 2nd Intern Symp of Jurassic Stratigraphy, Lisbon, pp. 963–981

Hirsch F, Picard L (1988) The Jurassic facies in the Levant. Jour of Petroleum Geology 11(3): 277–308. https://doi.org/10.1111/j.1747-5457.1988.tb00819.x

Jimenez-Munt I, Sabadini R, Gardi A (2006) Active deformation in the Mediterranean from Gibraltar to Anatolia inferred from numerical modeling and geodetic and seismological data. Jour of Geophys Research 108(B1):1–24, https://doi.org/10.1029/2001JB001544

Khorrami F, Vernant P, Masson F, Nilfouroushan F, Mousavi Z, Nankali H et al. (2019) An up-to-date crustal deformation map of Iran using integrated campaign-mode and permanent GPS velocities. Geophys Jour Intern 217:832–843. https://doi.org/10.1093/gji/ggz045

Kadirov F, Yetirmishli G, Safarov R, Mammadov S, Kazimov I, Floyd M, Reilinger R, King R (2024) Results from 25 years (1998–2022) of crustal deformation monitoring in Azerbaijan and adjacent territory using GPS. ANAS Transactions, Earth Sciences 1:28–43. https://doi.org/10.33677/ggianas20240100107

Kahn A (2025) Geothermal evaluation of deep boreholes throughout Israel. MSc Thesis, Haifa University, Israel, p 1-115

Karabulut H, Güvercin SE, Hollingsworth J, Konca1 AÖ (2023) Long silence on the East Anatolian Fault Zone (Southern Turkey) ends with devastating double earthquakes (6 February 2023) over a seismic gap: implications for the seismic potential in the Eastern Mediterranean region. Jour of the Geological Society, London 180:1–10. https://doi.org/10.1144/jgs2023-021

Kaymakci N, Langereis C, Özkaptan M, Özacar AA, Gülyüz E, Uzel B, Sözbilir H (2018) Paleomagnetic evidence for upper plate response to a STEP fault, SW Anatolia. Earth and Planet Sci Lett 498:101–115. https://doi.org/10.1016/j.epsl.2018.06.022

KeAi (2023) The magnitude of the 2023 Turkish earthquake matches the largest in the country's history, according to new study (11 April 2023). Phys.org. Retrieved 18 July 2023. phys.org/news/2023-04-magnitude-turkish-earthquake-largest-country.html (last visited on 25.08.2025)

Khain VE (2001) Tectonics of continents and oceans. Nauchniy mir, Moscow, Russia, p 606 (in Russian)

Khalafly AA (2006) Paleomagnetism of the Lesser Caucasus. Takhsil, Baku, p 1–112 (in Russian)

Lapkin IY, Katz YI. (1990) Geological events at the boundary of the Carboniferous and Permian. Izvestiya, USSR Acad of Sci, Ser: Geol 8: 45–58. https://www.tandfonline.com/doi/pdf/10.1080/ 00206819009465817

Lazos I, Sboras S, Chousianitis K, Kondopoulou D, Pikridas C, Bitharis S, Pavlides S (2022) Temporal evolution of crustal rotation in the Aegean region based on primary geodetically-derived results and palaeomagnetism. Acta Geodaetica et Geophysica 57:317–334. https://doi.org/10.1007/s40328-022-00379-3

Le Pichon X, Gaulier J-M (1988) The rotation of Arabia and the Levant fault system. Tectonophysics 153:271–294. https://doi.org/10.1016/0040-1951(88)90020-0

Le Pichon X, Kreemer C (2010) The Miocene-to-present kinematic evolution of the Eastern Mediterranean and Middle East and its implications for dynamics. Annu Rev Earth Planet Sci 38:323–351. https://doi.org/10.1146/annurev-earth-040809-152419

Le Pichon X, Şengör AMC, Jellinek M, Lenardic A, İmren C (2023) Breakup of Pangea and the Cretaceous Revolution. Tectonics 42(e2022TC007489):1–30. https://doi.org/10.1029/2022TC007489

Li C, van der Hilst RD, Engdahl ER, Burdick S (2008) A new global model for P wave speed variations in Earth's mantle. Geochemistry, Geophysics, Geosystems 9(5):1–21. https://doi.org/10.1029/2007GC001806

Levin BW, Sasorova EV, Steblov GM, Domanski GM, Prytkov AS, Tsyba EN (2017) Variations of the Earth's rotation rate and cyclic processes in geodynamics. Geodes Geodynam 8:206–212. https://doi.org/10.1016/j.geog.2017.03.007

McKenzie D (1972) Active tectonics of the Mediterranean region. Geoph J of the Royal Ast Soc 30(2):109–185. https://doi.org/10.1111/j.1365-246X.1972.tb02351.x

Makridin VP, Katz YI, Kuzmicheva EI (1968) Principles, methodology, and significance of fauna of coral constructions for zoogeographic zonation of Jurassic and Cretaceous seas of Europe, Middle Asia, and adjacent countries. In: Smirnov GA, Kluzhina ML (eds) Fossil organogenic constructions and methods of their studying. Ural Branch of the USSR Acad of Sci, pp 184–195 (in Russian)

Morris A, Erson MW, Robertson AH, Al-Riyami K (2002) Extreme tectonic rotations within an eastern Mediterranean ophiolite (Baer–Bassit, Syria). Earth Planet Sci Lett 202:247–261. https://doi.org/10.1016/S0012-821X(02)00782-3

Muttoni G, Gaetani M, Kent DV, Sciunnach D, Angiolini L, Berra F et al (2009) Opening of the Neo-Tethys Ocean and the Pangea B to Pangea A transformation during the Permian. GeoArabia 14(4):17–48. https://doi.org/10.2113/geoarabia140417

Neev D (1975) Tectonic evolution of the Middle East and the Levantine Basin (easternmost Mediterranean). Geology 3:683–686. https://doi.org/10.1130/0091-7613(1975)3<683:TEOTME>2.0.CO;2

Pechersky DM, Lyubushin AA, Sharonova ZV (2010) On the synchronism in the events within the core and on the surface of the earth: the changes in the organic world and the polarity of the geomagnetic field in the Phanerozoic. Izvestiya, Physics of the Solid Earth 46:613–623. https://doi.org/10.1134/s1069351310070050

Reilinger RE, McClusky S, Vernant P et al (2006) GPS constraints on continental deformation in the Africa-Arabia-Eurasia continental collision zone and implications for the dynamics of plate interactions. Jour of Geophysical Research BO5411:1–26. https://doi.org/10.1029/2005JB004051

Sclater JG, Jaupart C, Galson D (1980) The heat flow through oceanic and continental crust and the heat loss of the Earth. Reviews of Geophysics 18:269–311. https://doi.org/10.1029/RG018i001p00269

Scotese CR (1991) Jurassic and Cretaceous plate tectonic reconstructions. Palaeogeography, Palaeoclimatology, Palaeoecology 87:493–501. https://doi.org/10.1016/0031-0182(91)90145-H

Segev A (2000) Synchronous magmatic cycles during the fragmentation of Gondwana: Radiometric ages from the Levant and other provinces. Tectonophysics 325:257–277. https://doi.org/10.1016/S0040-1951(00)00122-0

Segev A (2009) $^{40}Ar/^{39}Ar$ and K-Ar geochronology of Berriasian-Hauteririan and Cenomanian tectomagmatic events in northern Israel: Implications for regional stratigraphy. Cretaceous Res 30:818–828. https://doi.org/10.1016/j.cretres.2009.01.003

Sharon M, Sagy A, Kurzon I, Marco S, Rosensaft M (2020) Assessment of seismic sources and capable faults through hierarchic tectonic criteria: implications for seismic hazard in the Levant. Nat Hazards Earth Syst Sci 20:125–148. https://doi.org/10.5194/nhess-20-125-2020

Smit J, Brun J-P, Cloetingh S, Ben-Avraham Z (2010) The rift-like structure and asymmetry of the Dead Sea Fault. Earth Planet Sci. Lett 290:74–82. https://doi.org/10.1016/j.epsl.2009.11.060

Stampfli GM, Hochard C, Vérard C et al. (2013) The formation of Pangea. Tectonophysics 593:1–19. https://doi.org/10.1016/j.tecto.2013.02.037

Stampfli GM, Kozur HW (2006) Europe from the Variscan to the Alpine cycles. Geological Society London Memoirs 32:57–82. https://doi.org/10.1144/GSL.MEM.2006.032.01.04

Stern RJ, Johnson P (2010) Continental lithosphere of the Arabian Plate: A geologic, petrologic, and geophysical synthesis. Earth-Science Reviews 101:29–67. https://doi.org/10.1016/j.earscirev.2010.01.002

Trifonov VG, Sokolov YuS (2018) Mantle structure and tectonic zonality of the central part of the Alpine-Himalayan belt. Geodynamics & Tectonophysics 9(4):1127–1145. https://doi.org/10.5800/GT-2018-9-4-0386 (in Russian)

Uzel B, Langereis CG, Kaymakci N, Sozbilir H, Ozkaymak C, Ozkaptan M (2015) Paleomagnetic evidence for an inverse rotation history of Western Anatolia during the exhumation of Menderes Core Complex. Earth and Planet Sci Lett 414:108–125. https://doi.org/10.1016/j.epsl.2015.01.008

van Hinsbergen DJJ, Dekkers MJ, Bozkurt E, Koopman M (2010) Exhumation with a twist: Paleomagnetic constraints on the evolution of the Menderes metamorphic core complex, western Turkey. Tectonics 29(3), TC3009:1–33. https://doi.org/10.1029/2009TC002596

Véronnet A (1912) Rotation of the Heterogeneous Ellipsoid and Exact Shape of the Earth. J Math Pures et Appl 8(6):331–463 (in French)

Verzhbitsky EV (1996) Geothermal regime and tectonics of marine areas bottom along the Alpine-Himalayan Belt. Nauka, Moscow, p 131 (in Russian)

Yamasaki T, Stephenson R (2011) Back-arc rifting initiated with a hot and wet continental lithosphere. Earth Planet Sci Lett 302**(**1-2):172–184. https://doi.org/10.1016/j.epsl.2010.12.009

ГДЕ БЫЛИ СФОРМИРОВАНЫ ИСТОЧНИКИ АЛЛОХТОННОЙ ОКЕАНИЧЕСКОЙ КОРЫ ЮЖНОЙ ЧАСТИ ВОСТОЧНОГО СРЕДИЗЕМНОМОРЬЯ?

Эппельбаум Л.[1,2*], Кац Ю.[3], Кадиров Ф.[4,5,6], Бен-Аврахам Ц.[1]
[1]Кафедра геофизики, факультет точных наук, Тель-Авивский университет, Израиль
Рамат Авив 6997801, Тель-Авив
[2]Азербайджанский государственный университет нефти и промышленности, Азербайджан
AZ1010, Баку, просп. Азадлыг, 20
[3]Музей естественной истории им. Штейнгарда и Национальный исследовательский центр
Факультет наук о жизни, Тель-Авивский Университет, Израиль
Рамат Авив 6997801, Тель-Авив
[4]Министерство науки и образования Республики Азербайджан, Институт геологии и геофизики, Азербайджан
AZ1073, Баку, просп. Г.Джавида, 119
[5]Бакинский государственный университет, Азербайджан
г. Баку, ул. акад. Захида Халилова, 33, Az1148
[6]Министерство науки и образования Республики Азербайджан, Институт нефти и газа, Азербайджан
AZ1000, Баку, ул. Ф.Амирова, 9
**Автор, отвечающий за переписку: levap@tauex.tau.ac.il*

Резюме. Долгое время считалось, что тектонические движения в южной части Восточного Средиземноморья (ВС), расположенного к югу от Эгейско-Анатолийской плиты, связаны с трансконтинентальными сдвигами, исходящими из Атлантического океана. Однако комплексный анализ многочисленных геолого-геофизических данных привёл нас к выводу, что первичные структуры ВС связаны не с этими сдвигами, а со спрединговыми и коллизионными процессами океана Неотетис. Над Неопротерозойским орогенным поясом в пределах Аравийской и Синайской литосферных плит выявлен мезозойский террейновый пояс (МТБ). Западная часть этого пояса представлена аллохтонной океанической корой. Мы предполагаем, что характеристики процессов коллизии в данном регионе в основном определяются влиянием крупной глубинной структуры, вращающейся против часовой стрелки. Значимым открытием в этом контексте является выявление древнего блока океанической коры в западной части МТВ, соответствующего обратно намагниченной падеомагнитной гипер зоне Киама (относящейся к ранней перми). Этот океанический блок был перемещен вдоль трансформных разломов из региона, примерно совпадающего с современным положением Восточной Аравии. Движение террейнов МТВ способствовало, например, формированию офиолитов горы Кармель на севере Израиля. Таким образом, мы приходим к выводу, что комплексная геофизико-геологическая оценка, включающая трехмерное магнито-гравитационное моделирование, анализ теплового поля, трансформации потенциальных полей, поведение векторов GPS, сейсмотомографические данные, анализ палеомагнетитных, палеобиогеографических и петрологических данных, а также характерных тектонических особенностей, ясно указывает на аллохтонную природу МТВ и океанической коры ВС. Эти результаты требуют пересмотра тектоно-геодинамического развития Восточного Средиземноморья и предполагают необходимость переоценки перспектив разведки углеводородов в этом регионе.

Ключевые слова*: Восточное Средиземноморье, структура океанической коры, аллохтонная происхождение, палеомагнитная гипер зона Киама, комплексный анализ*

ARALIQ DƏNİZİNİN CƏNUB-ŞƏRQİNİN ALLOKTON OKEAN QABIĞININ MƏNBƏLƏRİ HARADA ƏMƏLƏ GƏLMİŞDİR?

Eppelbaum L.[1,2], Katz Yu.[3], Qədirov F.[4,5,6], Ben-Avraham Z.[1]
[1]Geofizika Departamenti, Dəqiq Elmlər Fakültəsi, Tel-Əviv Universiteti, İsrail
Ramat-Əviv 6997801, Tel-Əviv, (E-mail: levap@tauex.tau.ac.il)
[2]Azərbaycan Dövlət Neft və Sənaye Universiteti, Azərbaycan
AZ1010, Bakı, Azadlıq prospekti, 20
[3]Şteynhardt adına Təbiət Tarixi Muzeyi və Milli Tədqiqat Mərkəzi, Həyat Elmləri Fakültəsi, Tel-Əviv Universiteti, İsrail
Ramat-Əviv 6997801, Tel-Əviv
[4]Azərbaycan Respublikasının Elm və Təhsil Nazirliyi, Geologiya və Geofizika İnstitutu, Azərbaycan
AZ1073, Bakı, H.Cavid prosp., 119
[5]Bakı Dövlət Universiteti, Azərbaycan
AZ1148, Bakı, akad. Zahid Xəlilov küç., 33
[6]Azərbaycan Respublikasının Elm və Təhsil Nazirliyi, Neft və Qaz İnstitutu, Azərbaycan
AZ1000, Bakı, F.Əmirov, 9
**Yazışmalara məsul: levap@tauex.tau.ac.il*

Xülasə. Egey-Anadolu plitəsinin cənubunda yerləşən Şərqi Aralıq dənizinin (ŞAD) cənub hissəsindəki tektonik hərəkətlərin Atlantik okeanından qaynaqlanan transkontinental qırılmalarla əlaqəli olduğu çox əvvəllər qəbul edilirdi. Bununla belə, çoxsaylı geoloji və geofiziki məlumatların hərtərəfli təhlili bizi belə nəticəyə gətirdi ki, Şərqi Aralıq Dənizinin ilkin strukturları bu qırılmalarla deyil, Neotetis okeanının həm spredinq, həm də kolliziya prosesləri ilə əlaqəlidir. Mezozoy Terran Qurşağı (MTQ) Ərəbistan və Sinay litosfer plitələri üzərindəki Neoproterozoy orogenik qurşağının üstündə müəyyən edilmişdir. Bu qurşağın qərb hissəsi allokton okean qabığı ilə təmsil olunur. Biz təklif edirik ki, bu regionda toqquşma proseslərinin xüsusiyyətləri əsasən saat əqrəbinin əksinə fırlanan böyük dərin strukturun təsiri ilə müəyyən edilir. Struktur-geodinamik analiz, əsas geoloji-geofiziki amillərlə yanaşı, Efiopiya əyalətinin allokton yura faunasının ŞAD-də geniş yayılmasını göstərən paleobiocoğrafi məlumatlar ilə də dəstəklənir. Bu kontekstdə əhəmiyyətli kəşf MTQ-nın qərb hissəsində əks maqnitləşmiş paleomaqnit Kiama hiperzonasına (erkən Perm dövrünə aid) uyğun

gələn qədim okean qabığı blokunun müəyyən edilməsidir. Bu okean bloku Şərqi Ərəbistanın müasir mövqeyi ilə təxminən üst-üstə düşən bölgədən transformasiya qırılması boyunca yerini dəyişmişdir. MTQ terranlarının hərəkəti nəticəsində İsrailin şimalında Karmel dağında ofiyolitlərinin meydana gəlməsinə kömək etmişdir. Beləliklə, belə qənaətə gəlirik ki, 3D maqnit-qravitasiya modelləşdirməsi, istilik sahəsinin təhlili, potensial sahə transformasiyaları, GPS vektorlarının davranışı, seysmik tomoqrafik məlumatlar, paleomaqnit, paleobiocoğrafi və petroloji məlumatlar, o cümlədən xarakterik tektonik xüsusiyyətlər, o cümlədən, inteqrasiya olunmuş geofiziki-geoloji qiymətləndirmə MTQ-nin və ŞAD yer qabığının alloxton xarakterini aydın göstərir. Bu nəticələr Şərqi Aralıq dənizinin tektono-geodinamik inkişafının yenidən nəzərdən keçirilməsini tələb edir və bu regionda karbohidrogen kəşfiyyatı perspektivlərinin yenidən qiymətləndirilməsinin zəruriliyini irəli sürür.

***Açar sözlər**: Şərqi Aralıq dənizi, okean qabığının quruluşu, allokton mənşəli, Kiama paleomaqnit hiperzonası, inteqrasiya olunmuş analiz*

ANAS Transactions Earth Sciences 2 / 2025

http://www.journalesgia.com

ГЕОЛОГИЧЕСКОЕ СТРОЕНИЕ И ПЕТРОФИЗИЧЕСКИЕ ОСОБЕННОСТИ ПОРОД-КОЛЛЕКТОРОВ КАРБОНАТНОЙ ФОРМАЦИИ ЮРЫ В СЕВЕРО-ЗАПАДНОЙ ЧАСТИ ЧАРДЖОУСКОЙ СТУПЕНИ

Каршиев О.А.[1*], Евсеева Г.Б.[1], Токарева К.М.[1], Кудашева Л.Р.[1], Раббимкулов С.А.[1,2]

[1]Институт геологии и разведки нефтяных и газовых месторождений, Республика Узбекистан

100164, Ташкент, Мирзо-Улугбекский район, ул. Олимлар, 64

[2]Ташкентский государственный технический университет имени Ислама Каримова, Республика Узбекистан

100100, г. Ташкент, ул. Университетская, 2

**Автор, отвечающий за переписку: odashkarshiev@gmail.com*

GEOLOGICAL STRUCTURE AND PETROPHYSICAL FEATURES OF COLLECTOR ROCKS OF THE JURASSIC CARBONATE FORMATION IN THE NORTHWESTERN PART OF THE CHARDZHOU STEP

Karshiyev O.A.[1*], Evseeva G.B.[1], Tokareva K.M.[1], Kudasheva L.R.[1], Rabbimkulov S.A.[1,2]

[1]Institute of Geology and Exploration of Oil and Gas Fields, Republic of Uzbekistan
64, Olimlar str., Mirzo-Ulugbek district, Tashkent, 100164
[2]Tashkent State Technical University named after Islam Karimov, Republic of Uzbekistan
2, Universitetskaya str., Tashkent, 100100
**Corresponding author: odashkarshiev@gmail.com*

Keywords: *Jurassic, carbonate formation, lithology, tectonics, reservoir, stratigraphy, porosity, permeability, boundary values*

Summary. The paper investigates the geological structure of the Middle–Upper Jurassic carbonate formation in the northwestern part of the Chardzhou Step, with the Birgutlin and Karakul troughs and the Kulbeshkak–Pitnyak swell taken as key examples. The study presents comprehensive results on the tectonic setting, lithological–stratigraphic characteristics, and facies composition of the carbonate sequence, as well as the petrophysical properties of reservoir rocks derived from deep-well core analyses. Based on these data, the main reservoir parameters and threshold values of productive intervals were determined. The findings indicate that the lagoonal zone developed in the study area is composed mainly of carbonate and carbonate–sulfate chemogenic deposits, rich in evaporites, dolomites, and terrigenous materials of open shallow-water origin. It was revealed that a reliable understanding of porous and permeable rock distribution within the carbonate formation requires identifying the relationships between the genetic types of carbonate rocks and their reservoir properties, which depend on structural and textural features. Petrophysical analysis and the determination of threshold values for open porosity and permeability were performed using graphical–analytical methods, producing cumulative reservoir–non-reservoir curves. The reservoir rocks of lagoonal deposits were found to be porous–fractured and highly heterogeneous, as reflected by a wide range of porosity and permeability variations. A schematic map showing the predicted spatial trends of reservoir properties within the Jurassic carbonate formation was developed. The results demonstrate that the distribution of reservoir properties is consistent and reveal zones with favorable parameters for further oil and gas exploration.

© 2025 Earth Science Division, Azerbaijan National Academy of Sciences. All rights reserved.

Введение

Изучение геологического строения, литолого-стратиграфических, петрофизических, геохимических характеристик пород-коллекторов в нефтегазоносных провинциях и регионах, направленных на определение перспектив нефтегазоносности, вызывает большой интерес геологов-нефтяников во всем мире.

В работе (Mohamed et al., 2025) рассматривается Южная часть Суэцкого залива, которая является перспективной нефтегазоносной провинцией, где возможно выявление значительных

скоплений углеводородов (УВ). Авторами проведён детальный геохимический анализ и 2D бассейновое моделирование нефтяного месторождения Рас Гара и оценены качество нефтематеринской породы, термическая зрелость и процессы миграции углеводородов.

В статье (Aliyeva, Guliyev, 2025) приводятся данные изучения тектонической обстановки, происхождения осадочных пород, палеовыветривания, палеоклимата и гидротермальных влияний на формирование пород верхнемеловых отложений Лок-Карабахской зоны, что позволяет оценить геодинамическую эволюцию территории и потенциал резервуара.

Исследования (Sidorov, Rizvanova, 2023) посвящены разработке методики определения граничных значений открытой пористости (Кп.г.) и газопроницаемости (Кпр.гр) карбонатных пород-коллекторов порового типа на примере турнейских отложений нефтяного месторождения Республики Татарстан, что дает возможность существенно повлиять на подсчёт запасов УВ, технологические расчёты и планирование разработки месторождений.

Коллективом авторов (Krasovskiy et al., 2016) проведён анализ разработки массивных газовых залежей и установлено, что при учёте эффекта динамических фазовых проницаемостей можно определить достоверную расчетную динамику пластового давления по скважинам и повысить достоверность прогнозных технологических показателей разработки залежи.

В (Ponomarev et al., 2021) изучены возможности применения компьютерной рентгеновской микротомографии (микро-КТ) в нефтепромысловой геологии и обосновывается возможность применения этого метода для совершенствования направления «Цифровая петрофизика».

В статье (Gerke et al., 2021) приведены результаты применения технологии «цифрового» керна для создания цифровой модели внутреннего строения керна и моделирования в такой модели многофазных потоков в масштабе пор. Это даст возможность повысить уровень петрофизических исследований и достоверность построения гидродинамических моделей.

Статья (Postnikova et al., 2025) посвящена литологическим исследованиям пород-коллекторов терригенных отложений нижнего мела Красноленинского свода Западной Сибири, сложенных различными литотипами пород, что влияет на характер их нефтенасыщения. Авторами на основе оценки суммарного количества нефтенасыщенных пород-коллекторов и степени их расслоенности разработаны модели распределения нефтенасыщенных пород-коллекторов в разных фациальных комплексах для количественной оценки неоднородности распределения нефтенасыщения.

В работе (Matthew et al., 2025) отмечается, что в петрофизических исследованиях трещиноватых горных пород редко используются временные ограничения, что затрудняет процесс исследования трещиноватых пород. Для установления этих параметров авторами предложен концептуальный подход, использующий стохастический метод, (учитывающий) абсолютный возраст и создание дискретных моделей сети трещин.

В северо-западной части Чарджоуской ступени и, в частности, на территории Биргутлинского, Каракульского прогибов и Кульбешкак-Питнякского вала (рис.1), нефтегазоносные отложения связаны в основном с карбонатной формацией средне-верхнеюрского возраста и в меньшей степени с отложениями терригенной формации нижней-средней юры. Изучением геологического строения территории занимались такие исследователи, как А.М.Акрамходжаев, М.Х.Арифджанов, В.П.Алексеев, Г.С.Абдуллаев, П.У.Ахмедов, А.А.Абидов, А.Г.Бабаев, Ш.Д.Давлятов, З.С.Ибрагимов, О.А.Каршиев, Х.Х.Миркамалов, Б.Б.Таль-Вирский, Б.И.Хожиев, М.Э.Эгамбердыев и многие другие.

Коротко остановимся на результатах изучения геологического строения, геохимических особенностей и фильтрационно-емкостных свойств пород, полученных в последние годы.

Евсеевой (Evseeva, 2015) проанализированы литолого-фациальные особенности разрезов терригенной формации юры нижне-среднеюрского возраста и определены закономерности изменения значений фильтрационно-ёмкостных свойств пород-коллекторов, накопившихся в определенных палеогеографических условиях.

Работа (Ismagulova et al., 2016) посвящена результатам моделирования нефтегазовых систем бассейна Амударьи, включающих Бухарскую и Чарджоускую тектонические ступени. В процессе исследований установлена история созревания нефтематеринских пород и возможных маршрутов миграции углеводородов, а также даны рекомендации по проведению дальнейших исследований на перспективных участках.

В 2023 году вышла работа (Karshiev, Akramova, 2023) «Геолого-геохимические предпосылки нефтегазоносности юрских терригенных отложений Чарджоуской ступени», где приводятся характеристики рассеянного органического вещества, битумоидов и газов отложений терригенной формации нижне-среднеюрского возраста. Установлено, что изучаемые отложения, а также сте-

пень катагенетической трансформации органического вещества позволяют предположить возможность открытия новых скоплений нефти и газа и наличие пород-коллекторов, что позволяет обосновать перспективы нефтегазоносности рассматриваемых отложений.

Bogdanov et al. (2024) отмечают, что на сегодняшний день в Бухаро-Хивинском регионе выявлено 514 залежей нефти и газа, которые сконцентрированы в приуроченных в стратиграфическом отношении отложениях от нижней-средней юры до верхнего мела включительно, где основными продуктивными комплексами являются отложения карбонатной формации средней-верхней юры, на долю которых приходится до 82.4% начальных запасов и 78.5% накопленной добычи региона.

В работе (Bogdanov et al., 2024) обнаруживается, что для увеличения углеводородной базы Республики Узбекистан необходимо кратно увеличить объемы добычи нефти и газа, а в геологоразведочные работы вовлекать не только уже изученные нефтегазоносные регионы и стратиграфические комплексы, но и новые перспективные площади на слабо изученных территориях, а также глубоко погруженные стратиграфические комплексы.

Геологическое строение и петрофизические характеристики карбонатной формации территории исследования.

В тектоническом отношении Кульбешкак-Питнякский вал**,** размеры которого составляют 200х15 км, с северо-востока ограничивается Биргутлинским прогибом, который граничит с Учбаш-Каршинской флексурно-разрывной зоной (УКФРЗ) (Khozhiev, 2022). Максимальная глубина залегания доюрского комплекса пород составляет 3.2 км. В пределах вала установлена серия крупных локальных структур: Даяхатын, Кульбешкак, Жанубий Кульбешкак и др., где открыты месторождения углеводородного сырья.

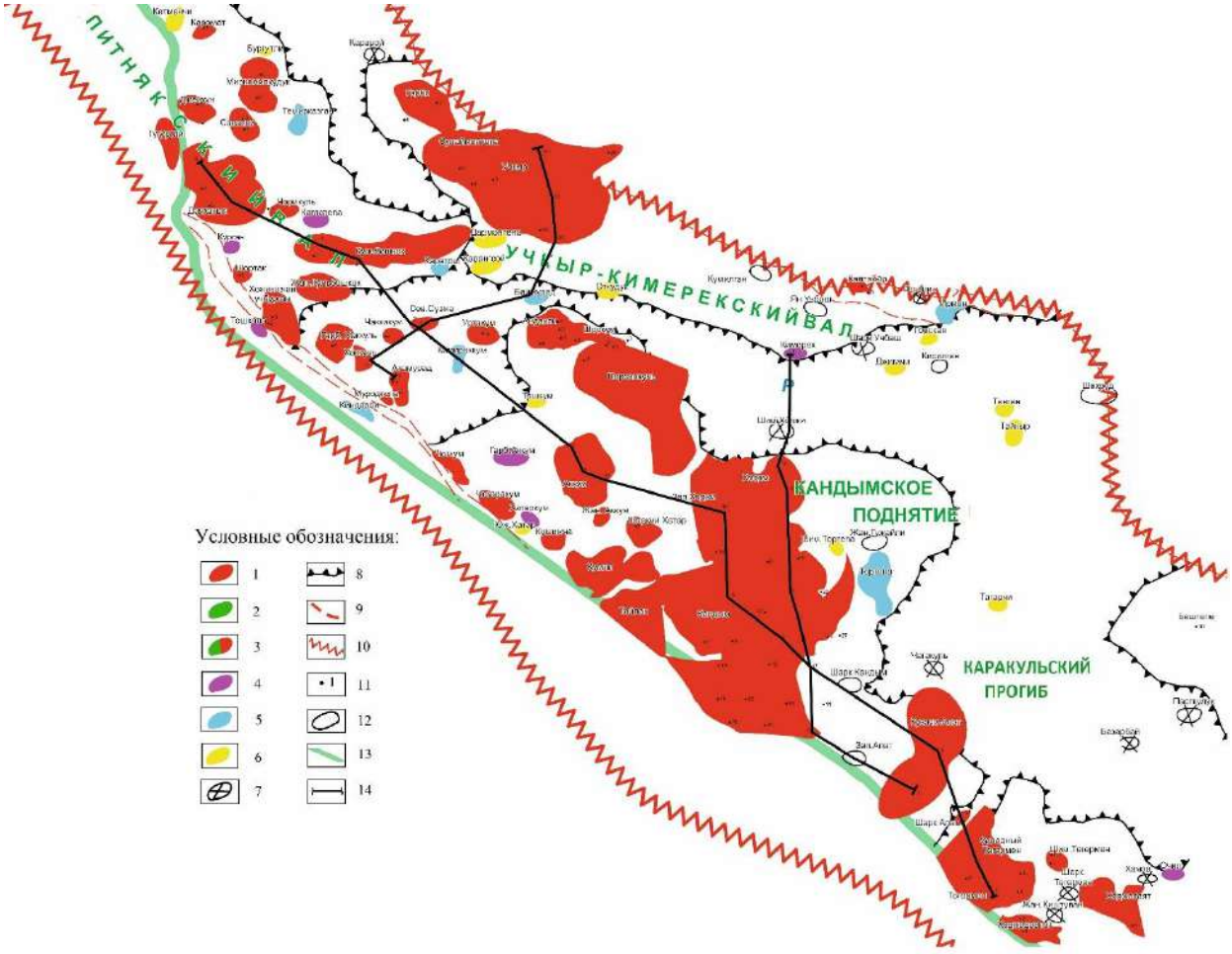


Рис. 1. Обзорная карта района работ (по материалам ГУ «ИГИРНИГМ»).
Условные обозначения: 1 – газовые месторождения, 2 – нефтяные месторождения, 3 – нефтегазовые месторождения, 4 – находящиеся в бурении, 5 – подготовленные структуры, 6 – выявленные структуры, 7 – выведенные из бурения, 8 – границы тектонических элементов, 9 – локальные разломы, 10 – региональный разлом, 11 – скважина, 12 – зона локальных поднятий, 13 – государственная граница, 14 – линии профилей

Каракульский прогиб полосой протягивается с северо-запада на юго-восток вдоль Учбаш-Каршинской флексурно-разрывной зоны протяженностью 100 км и шириной 30 км. Согласно Давлятову (Davlyatov, 1971), залегание поверхности доюрских отложений отмечается на глубине 4000 м. Прогиб имеет асимметричное строение (северо-восточная часть более крутая и ограничена Учбаш-Каршинской флексурно-разрывной зоной).

Вдоль Учбаш-Каршинской зоны протягивается узкий (5-15 км) Кимирекский грабен, где мощность юрских терригенных и карбонатных отложений может достигать 2 км (Abidov, 2004).

Анализ геолого-геофизических материалов по разрезам глубоких скважин на изучаемой территории позволил установить литолого-фациальные особенности отложений карбонатной формации (КФ) средне-верхнеюрского возраста, а также проследить взаимоотношения сопряженных осадочных фаций.

На территории Биргутлинского, Каракульского прогибов и Кульбешкак-Питнякского вала выделяется Кандымский подтип лагунного разреза (Abdullaev, 2004; Evseeva, 2015; Egamberdyev, 1981).

Далее приведем литолого-стратиграфические особенности и фациальную характеристику этих образований с сопоставлением с опорными разрезами Юго-Западных отрогов Гиссарского хребта (ЮЗОГ). Описание разреза приводится снизу вверх.

Кандымская свита (XVI промысловый горизонт): верхи нижнего – средний келловей.

На рассматриваемой территории свита сложена известняками серыми, темно-серыми, микрозернистыми, пелитоморфными, нередко глинистыми и песчанистыми (Тумарис, скважина №1, Курган, скважина №2, Каромат, скважина №1).

Породы в различной степени пиритизированные, доломитизированные, окремненные, битуминозные. В подчиненном значении встречаются прослои водорослево-детритовых, органогенно-обломочных, онколитовых, оолитовых разностей известняков, а также песчаников и алевролитов. Из этих отложений определены двустворки *Entolium ivanovi* Pčel (месторождения Кульбешкак, Ходжи), которые встречаются в отложениях верхней части нижнего и низах среднего келловея Кугитанга, соответствующих зоне *Macrocephalites macrocephalus* и *Kosmoceras jason* (верхи нижнего – средний келловей) (Abdullaev, 2004; Evseeva, 2015). Общая мощность свиты – 60-80 м.

Мубарекская свита (XV2, XV3, XVa промысловые горизонты): верхний келловей–нижний-средний оксфорд.

Отложения мубарекской свиты на территории Биргутлинского, Каракульского прогибов и Кульбешкак-Питнякского вала вскрыты многими скважинами (Тумарис, скважина №2; Даяхатын, скважина №10; Саватли, скважина №2, 4, Миркомилкудук, скважина №1, Жанубий Кульбешкак, скважина № 1 и др.) (рис.2).

Нижняя часть разреза (XV_3, XV_a промысловые горизонты) в основном сложена микрозернистыми известняками – серыми, темно-серыми, глинистыми с редкими прослоями водорослевых известняков, доломитизированных и кальцитизированных, с примесью алевритового материала. Отложения, сформировавшиеся на этом этапе карбонатонакопления, выделяются как нижняя пачка мубарекской свиты.

В верхней части разреза (XV_2 промысловый горизонт) преимущественное развитие получили оолитовые, комковато-обломочные и водорослево-комковатые разности. Отложения верхней толщи отличаются меньшей глинистостью, особенно в верхней части.

На месторождении Даяхатын, скв.2 В.В.Курбатовым приводятся органические остатки: двустворки – *Camptonectes lens* Sow., *Entolium ivanovi* Pčel, *Posidonia cf. buchi* Roem., фораминиферы – *Epistomina sp.*, *Trocholina ex gr. transversarii* Paalzow, возраст которых не противоречит нижнему-среднему оксфорду (Abdullaev, 2004; Evseeva, 2015).

Из этих же отложений на площадях Кульбешкак, Даяхатын, Ходжи определены брахиоподы *Zeilleria cf. bucharensis* Moiss, *Terebratula vandobensis* Moiss. и др., которые Е.А.Репман также относит к верхнему келловею – нижнему-среднему оксфорду (Abdullaev, 2004; Evseeva, 2015). Поэтому возраст описываемых отложений можно определить как верхний келловей – нижний-средний оксфорд. Общая мощность свиты – 150-160 м.

Аналоги гардаринской свиты (XV_1промысловый горизонт). **Верхний оксфорд-киммеридж.**

На территории Биргутлинского, Каракульского прогибов и Кульбешкак-Питнякского вала эта секция разреза вскрывается всеми скважинами, изучена на площадях и месторождениях Каромат, скважина №1, Курган, скважина №1, Каттатепа, скважина №2, Саватли, скважина №2 и др. Разрез сложен толщей переслаивания известняков, ангидритов, песчаников, алевролитов, глин, которые являются фациальным и возрастным аналогом гардаринской свиты, развитой в Бешкентском прогибе и на территории Юго-Западных отрогов Гиссара (ЮЗОГ).

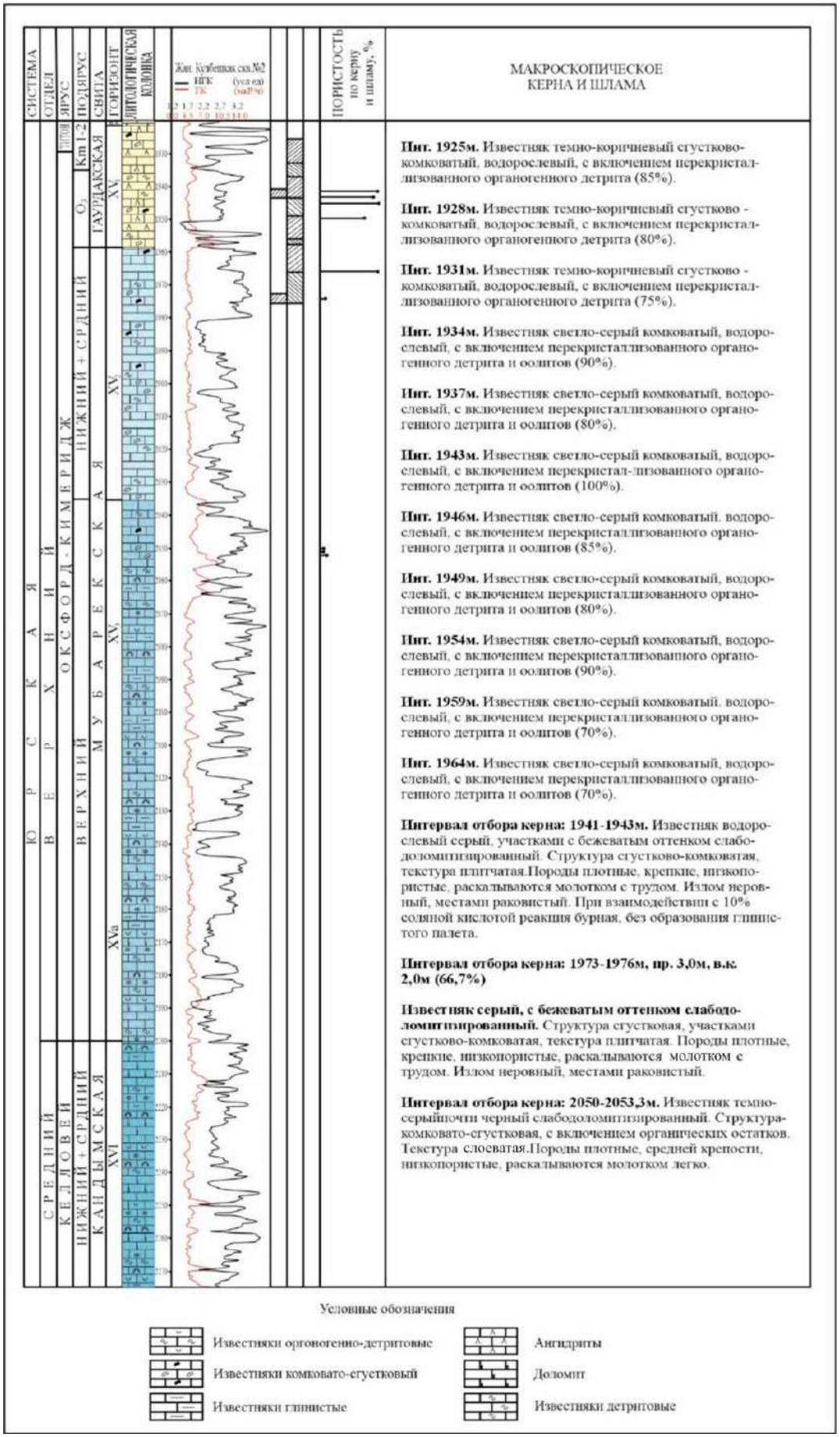


Рис. 2. Литологический разрез площади Жанубий Кульбешкак-скв. 2 (Составила Л.Р.Кудашева)

Из этих отложений на площадях и месторождениях Ходжи, Кульбешкак, Даяхатын были определены двустворчатые моллюски *Astarte sp. ind.*, *Modiolus cf. hannoverana* Str., *Cypricardia sp. ind.*, *Camptonectes cf. normalicus* Rep. и др. По мнению Е.А.Репман, возраст отложений можно определить как верхнеоксфордский (Abdullaev, 2004; Evseeva, 2015).

Фациальные особенности разреза карбонатной формации на исследуемой территории

Ранний-средний келловей. Интервал разреза, выделяемый в объёме кандымской свиты (XVI промысловый горизонт), отражает смену накопления терригенно-карбонатных осадков байсунской свиты карбонатными образованиями кандымской свиты. Тонкослоистая текстура и микрозернистая структура осадков, наличие тонких прослоев черных глинисто-алевритистых, пиритизированных и битуминозных известняков, развитие стеногалинной фауны свидетельствуют о том, что осадконакопление происходило на дне умеренно глубоководного моря с нормальной соленостью вод (Evseeva, 2017; Egamberdyev, 1981; Babaev, 1983).

Необходимо отметить, что в отложениях свиты отмечаются прослои детритовых, оолитовых и комковато-водорослевых разностей известняков, что дает возможность говорить о периодической смене глубоководных условий мелководными.

Поздний келловей – ранний-средний оксфорд. Выделяется в объёме мубарекской свиты – нижняя (XVa, XV_3 промысловые горизонты) и верхняя толщи (XV_2 промысловый горизонт).

Нижняя толща (поздний келловей) накапливалась в обстановке продолжающегося погружения бассейна седиментации в относительно спокойных тектонических условиях, почти в таком же темпе, что и в кандымское время (Abdullaev, 2004; Evseeva, 2015). Фациальные особенности разреза указывают на то, что осадконакопление большей частью происходило на мелководьях с увеличением доли детритовых (по сравнению с кандымской свитой) и водорослевых известняков, часто пористых. В меньшем количестве наблюдаются плотные, мелкозернистые пелитоморфные известняки, накопление которых проходило в относительно глубоководных условиях.

Верхняя толща (ранний-средний оксфорд) формировалась в условиях некоторого оживления тектонических движений и дифференциации дна палеобассейна, что обусловило фациальную неоднородность отложений и накопление различных генетических типов пород. В это время на территории северо – западной части Чарджоуской ступени накопление карбонатных осадков происходило в аридных условиях, что способствовало осолонению седиментационного бассейна. Это подтверждается и бедными комплексами органических остатков, получивших развитие на изучаемой территории, в том числе рифостроящих, с преобладанием эвригалинных водорослей (Evseeva et al., 2021).

В разрезах верхней толщи мубарекской свиты, накопление которой проходило в раннем-среднем оксфорде наблюдается широкое развитие пластообразных тел, сложенных органогенно-обломочными и водорослевыми образованиями. Эти толщи формировались в основном на мелководьях, с частыми сменами на умеренно глубоководные условия. Таким образом, формирование карбонатных отложений проходило на мелководном шельфе с ограниченным водообменом, где процессы ангидритизации и доломитизации иногда достигали 30% (Evseeva, 2017).

Поздний оксфорд-кимеридж. В позднем оксфорде формирование отложений лагунной фациальной зоны на территории Биргутлинского, Каракульского прогибов и Кульбешкак-Питнякского вала связано с экранированием шельфа барьерно-рифовой системой. Осадконакопление происходило в приливно-отливных условиях в режиме периодической, часто длительной изоляции от основного бассейна. Отложения представлены пачкой переслаивания известняков, ангидритов и пестроцветных терригенных пород – песчаников, алевролитов и глин (Abdullaev, 2004; Evseeva, 2015). Часто наблюдаются прослои доломитов и доломитизированных известняков. Наличие прослоев песчаников, алевролитов, глин, а также маленькая мощность (50-60 м) лагунных отложений позволяет говорить о том, что зона развития лагунного разреза совпала с завершающей стадией карбонатонакопления.

Методы исследования

Для изучения петрофизических свойств и определения граничных значений карбонатных пород были использованы данные петрофизических исследований, отобранные со следующих скважин – Тумарис №1,2,3,4; Даяхатын №10; Саватли №2,4; Джейхун №1; Миркомилкудук №4; Темирказган №1; Каттатепа №1,2; Курган №1,2; Каромат №1; Чорикуль №1,3; Шортак №4; Сулаймонтепа №1.

Так как для определения граничных значений необходима выборка по каждому месторождению в количестве не менее 30 образцов, а в данном случае такой выборки по горизонтам не собралось ни на одном из представленных объ-

ектов, было принято решение объединить данные всех горизонтов карбонатных отложений и провести исследования для КФ в целом.

На рис. 3 представлена гистограмма распределения открытой пористости. Всего было исследовано 234 образца из разреза КФ. Большую часть коллекции представляют образцы с очень низкой пористостью в диапазоне 0-5 %. Средневзвешенное значение пористости равно 5.12 %, минимальное значение составляет 0.14 % и максимальное – 22.43 %. В целом был сделан вывод о том, что из всех исследованных тектонических элементов на рассматриваемой территории количество низкопористых и низкопроницаемых образцов преобладает, что свидетельствует о низком качестве ФЕС.

На рис. 4 представлена гистограмма распределения проницаемости. Из рисунка видно, что большая часть образцов является либо непроницаемой, либо обладает очень низкой проницаемостью (более 70% коллекции), т.к. большую часть пород с низкой проницаемостью представляют твердые, плотные известняки и доломиты.

Для определения граничного значения открытой пористости были построены кумулятивные кривые коллектор-неколлектор по значениям открытой пористости (рис. 5). Само значение определено по графоаналитическому методу. По результатам проведенных исследований наиболее вероятностное граничное значение открытой пористости: Кп.гр = 5 %.

Результаты рассмотренных ранее гистограмм пористости и проницаемости подтверждаются и сходятся с построенными кумулятивными кривыми коллектор-неколлектор. Можно заключить, что юрские отложения КФ на данной территории в основном сложены плотными непроницаемыми известняками и доломитами. И для увеличения дебитов скважин необходимо организовывать мероприятия по вторичному воздействию на призабойную зону (соляно-кислотная обработка).

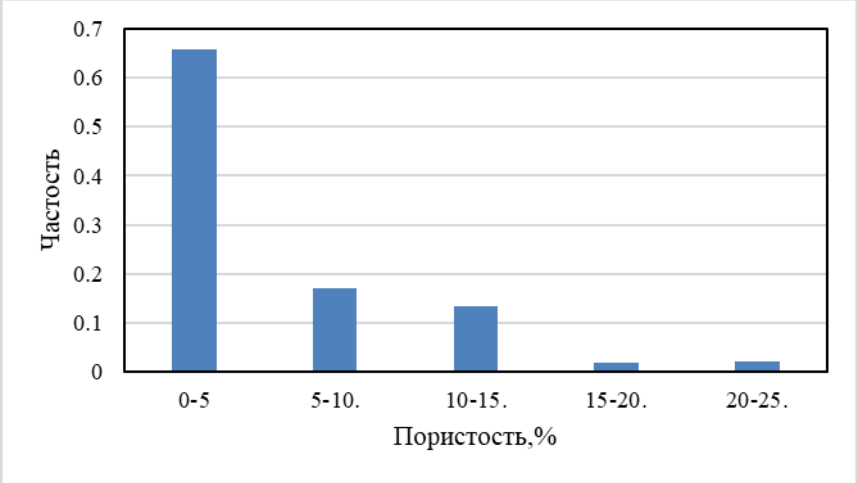


Рис. 3. Гистограмма распределения открытой пористости

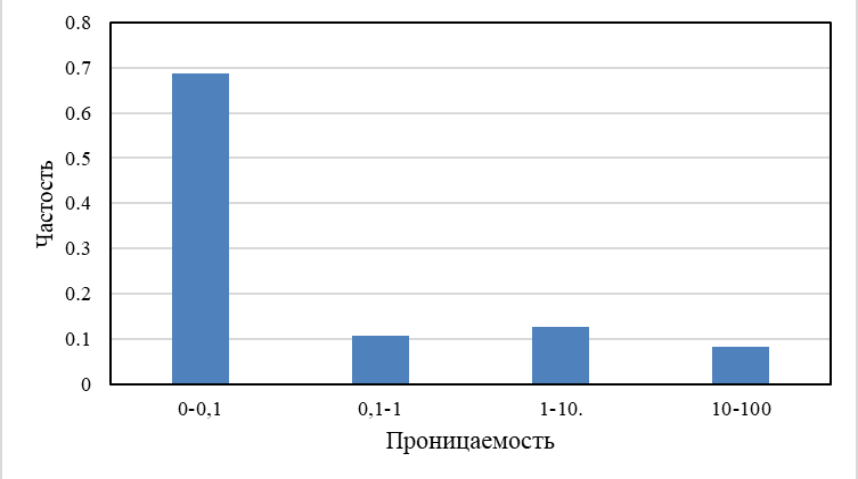


Рис. 4. Гистограмма распределения проницаемости

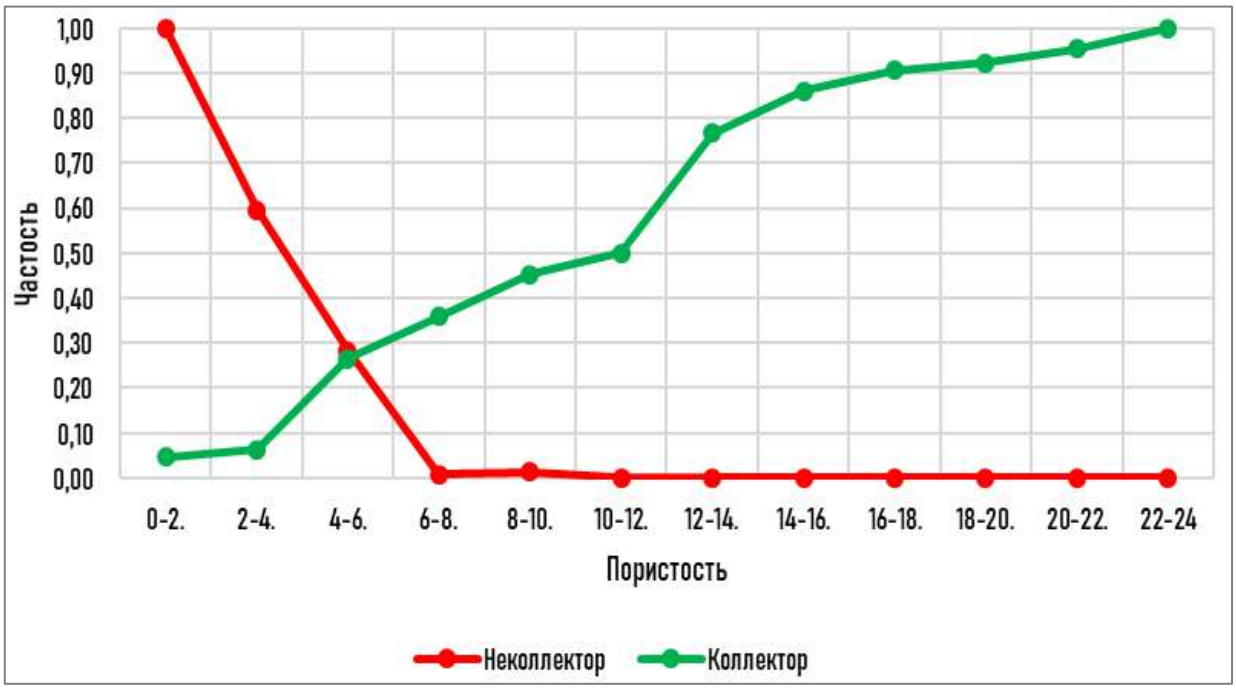


Рис. 5. Кумулятивные кривые распределения коллектор-неколлектор по значениям открытой пористости

На рис. 6 представлена зависимость проницаемости от коэффициента открытой пористости. Как видно из рисунка, корреляционной зависимости выявить не удалось вследствие того, что есть точки, которые однозначно выбиваются из тренда. Это может происходить по причине того, что в коллекции представлены образцы с трещинной и кавернозной проницаемостью. Это обычно точки с самыми высокими значениями проницаемости. Из построенной зависимости также видно, что вплоть до пористости 10% большая часть образцов обладает проницаемостью, меньше граничной (Кпр.гр = 0.1 мД), установленной для данного тектонического элемента.

Также не удалось чётко определить тенденцию возрастания проницаемости с возрастанием открытой пористости. Как видно из рисунка, образцы с пористостью более 20% имеют проницаемость ниже, чем образцы с пористостью от 10 до 15%. Это свидетельствует о неоднородности распределения фильтрационно-емкостных свойств (ФЭС) внутри юрских отложений среди представленной коллекции образцов керна.

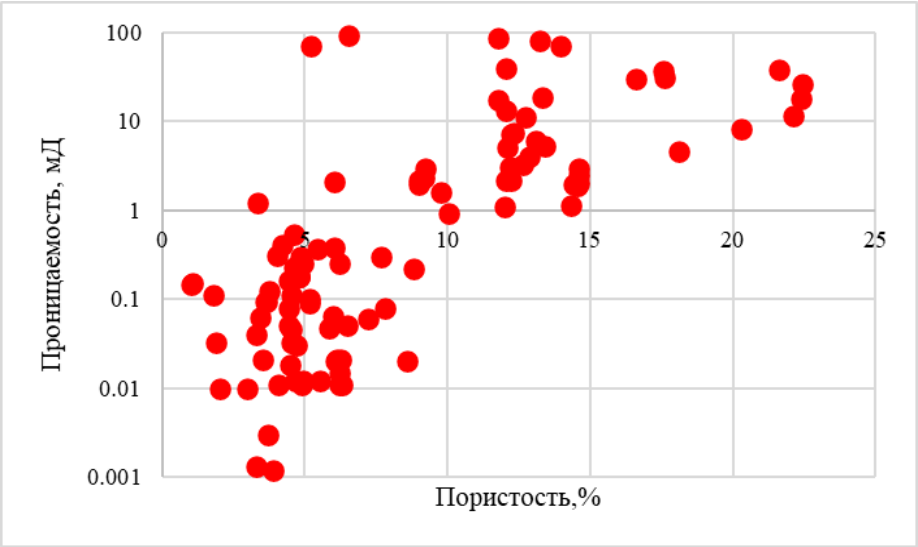


Рис. 6. Зависимость коэффициента проницаемости от коэффициента открытой пористости

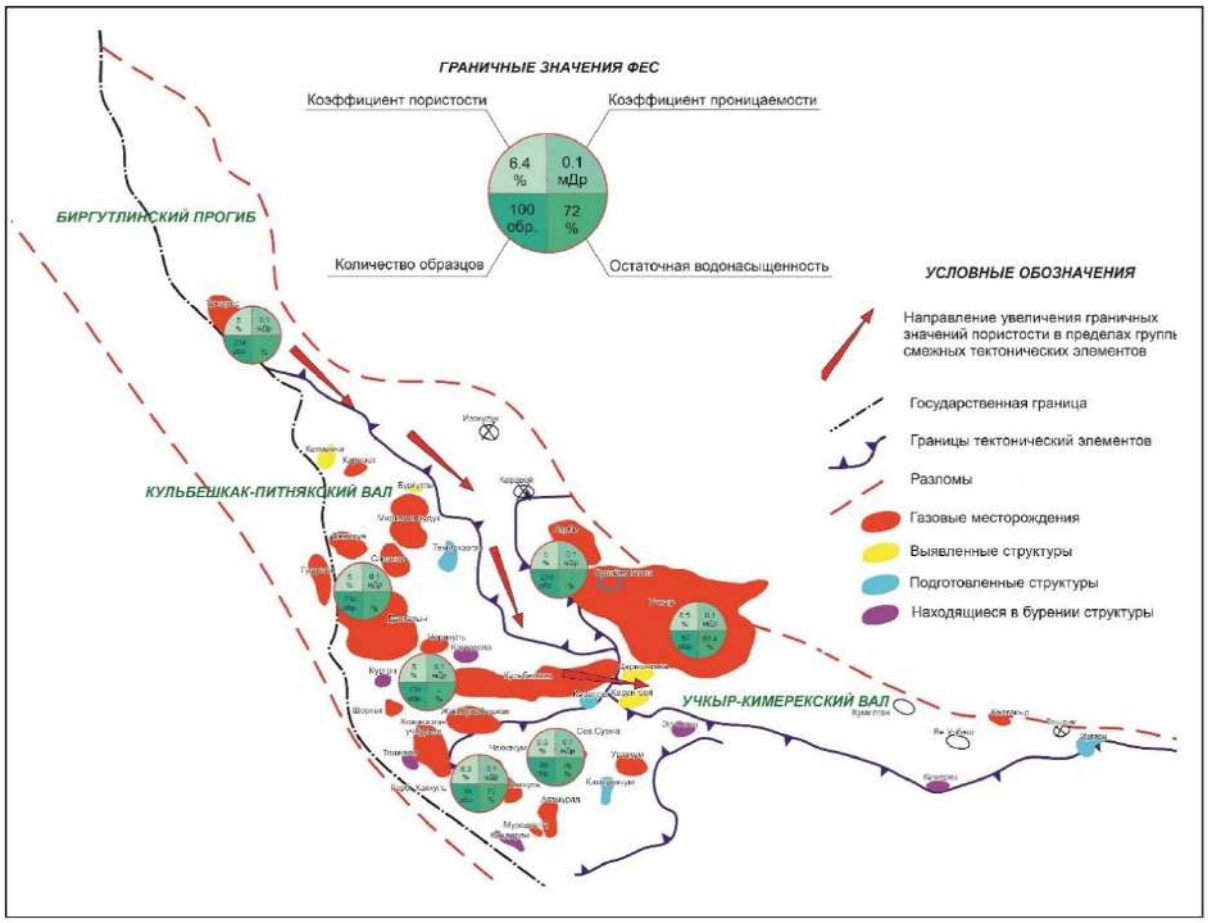


Рис. 7. Карта-схема прогнозных направлений изменения граничных значений фильтрационно-ёмкостных свойств карбонатных отложений XV-1, XV-2, XV-3 горизонтов Биргутлинского прогиба и Кульбешкак-Питнякского вала. (Составила: К.М.Токарева)

На основе установленных петрофизических характеристик была построена карта-схема прогнозных направлений изменения граничных значений ФЕС для юрских карбонатных отложений XV_1, XV_2, XV_3 горизонтов (рис.7), по которой определено, что в целом ФЕС по данной территории распространены равномерно. Небольшое увеличение граничных значений пористости наблюдается в направлении месторождений Тумарис → Кульбешкак → Гарбий Хаккуль → Чаккакум.

В заключение необходимо отметить, что в лагунной зоне на рассматриваемой территории широко развиты карбонатные и карбонатно-сульфатные хемогенные отложения, подтверждённые большим количеством эвапоритов, также встречаются доломиты и терригенные образования открытого мелководья. В известняках имеется незначительная примесь органогенного детрита, часто присутствуют целые и перекристаллизованные скелетные обломки водорослей и кораллов, что является продуктом разрушения рифа. Некоторые разрезы представлены криптокристаллическими известняками с комковато-сгустковым материалом.

Породы, представленные плотными сгустковыми, оолитово-сгустковыми известняками, микрозернистыми разностями хемогенного и биохемогенного происхождения, характеризуются низкими значениями ФЕС. Структура пород тонкопористая. Породы в различной степени трещиноватые. Тип пористости в этих образованиях межкристаллический, тип коллектора – трещинный, порово-трещинный.

Высокими ёмкостными свойствами характеризуются известняки, накопившиеся в условиях высокой гидродинамической активности – оолитовые, обломочно-детритовые, комковатые разности с хорошо развитой системой межзерновых поровых каналов, что в конечном итоге обеспечивает хорошие коллекторские свойства пород. На формирование пустотного пространства этих пород большое влияние оказывали процессы выщелачивания, поэтому они характеризуются высокими значениями ФЕС коллекторов порового или кавернозно-порового типов с межзерновым типом пористости.

Заключение

На территории Биргутлинского, Каракульского прогибов и Кульбешкак-Питнякского вала разрезы карбонатной формации характеризуется строгим слоистым строением. Отдельные пласты выдержаны и прослеживаются на значительном расстоянии (площади и месторождения Учкыр, Кульбешкак, Даяхатын и др.). С карбонатными образованиями прибрежной зоны связаны залежи газа месторождений Ходжикаган, Кульбешкак, Даяхатын и др.

Литолого-петрографическими исследованиями установлено, что коллекторы XV_1, XV_2 горизонтов сложены оолитовыми и мелкокомковатыми известняками с мелкозерновой пористостью, переслаивающимися с плотными пелитоморфными, органогенно-обломочными известняками, а в верхней части – маломощными прослоями алевролита и ангидрита. В нижней части XV_2 горизонта коллекторами служат преимущественно строматолитовые водорослевые известняки со вторичной пористостью (кавернозностью) и трещиноватостью.

XV_3 горизонт представлен главным образом плотными органогенно-обломочными известняками с прослоями оолитовых, криптокристаллических и глинистых разностей, обладающих невысокими коллекторскими свойствами. Породы данного горизонта от таковых подстилающих и перекрывающих отличаются интенсивной трещиноватостью, причём в случае пористых слоев – чем плотнее их разности, тем менее они трещиноваты.

Правильное решение вопроса закономерности распределения пористых пород в разрезе карбонатной формации немыслимо без выяснения связи между генетическими типами карбонатных пород и их ёмкостными свойствами, которые главным образом зависят от структурно-текстурных особенностей пород, а последние – от генетических разновидностей осадков.

Породы-коллекторы Кандымского подтипа лагунных отложений на изучаемой территории относятся к порово-трещинным. Исходя из выявленной характеристики их фильтрационно-ёмкостных свойств, определено, что породы обладают существенной неоднородностью, что нашло свое отражение в широком диапазоне изменения коэффициентов пористости и проницаемости.

REFERENCES

Abdullaev GS (2004) Biostratigraphy, lithophages and prospects of oil and gas content of the carbonate Jurassic of the northern side of the Amudarya depression. Abstract of the dissertation for the degree of Doctor of Geological Sciences, Tashkent, p 198 (in Russian)

Abidov AA (ed) Abidov AA, Talbirsky BB, Babajanov TL et al (2004) Map of the tectonic zoning of the Bukhara-Khiva oil and gas region, 1:500 000. Uzbekgeofizika, Tashkent

Aliyeva E, Guliyev EKh (2025) Geochemical and mineralogical characteristics of Upper Cretaceous sediments in the Lok-Karabakh zone (Azerbaijan): Implications for provenance, paleo weathering, paleoclimate and reservoir prediction. SOCAR Proceedings 1:3–8

Babaev AG (1983) The Jurassic age carbonate formation of the platform region of Uzbekistan and its oil and gas potential. Publisher FAN, Tashkent, p 160

Bogdanov AN, Karshiev OA, Khmyrov PV (2023) The role of the Bukhara-Khiva region in the state of the hydrocarbon potential of the Republic of Uzbekistan. ANAS Transactions, Earth Sciences, Special issue:168–172. https://doi.org/10.33677 / ggianas-conf20230300041 (in Russian)

Bogdanov AN, Qarshiyev OA, Gaffarov MA et al (2024) Evolution of oil and gas prospecting in the Tajikistan region. SOCAR Proceedings 4:12–19

Davlyatov ShD (1971) Tectonics of oil and gas-bearing regions of Western Uzbekistan. Institute of Geology and Development of Oil and Gas Fields.Tashkent (in Russian)

Egamberdyev ME (1981) Oil and gas bearing facies of the Mesozoic and Paleogene. Publisher FAN, Tashkent, p 158

Evseeva GB (2015) Bukhara-Khiva oil and gas region - depositional environment of the Jurassic carbonate deposits and reservoir rock properties. Oil and gas geology. Theory and practice 10(2):1–17. St. Petersburg. https://doi.org/10.17353/2070-5379/15_2015

Evseeva GB (2015) Lithological and facies features and filtration–capacitance properties of Jurassic terrigenous deposits of the Bukhara-Khiva oil and gas region. SOCAR Proceedings 2:4–9. https://doi.org/10.5510/OGP20150200237 (in Russian)

Evseeva GB (2017) Evolution and facies differentiation of foraminifera complexes and their role in detailing biostratigraphic schemes of the Jurassic sedimentation basin of the Bukhara–Khiva oil and gas region. Abstract of the dissertation for the degree of Doctor of Geological Sciences, Tashkent, p 198 (in Russian)

Gerke KM, Korost DV, Karsanina MV et al (2021) Study and analysis of modern approaches to the construction of digital core models and methods of modeling multiphase filtration on the scale of pore space. Георесурсы/Georesources 23(2):197–213. https://doi.org/10.18599/grs.2021.2.20

Hodge MS, Cottrell M, Knies J et al (2025) Discrete fracture network modeling reconstructs fracture array evolution and related petrophysical properties over geological time. Communications Earth and Environment 6(183): 1–12

Ismagulova S, Abbasova S, Karshiyev O (2016) Petroleum Systems Modeling in Amudarya Basin. Paper presented at the SPE Annual Caspian Technical Conference and Exhibition, Astana, Kazakhstan, November. Paper Number: SPE-182543-MS. https://doi.org/10.2118/182543-MS

Karshiev AO, Akramova NM (2023) Geological and geochemical prerequisites for the oil and gas potential of the Jurassic terrigenous deposits of the Chardzhou stage. ANAS Transactions, Earth Sciences, Special issue:137–141. https://doi.10.33677/ggianasconf20230300033 (in Russian)

Khozhiev BI (2022) Productivity and oil and gas potential of Mesozoic deposits of the western part of the Bukhara-Khiva region. Thesis for the degree of Doctor of Geological and Mineralogical Sciences, Tashkent p. 209 (in Russian)

Krasovskiy AV, Golofast SL, Raudanen EV (2016) Influence of dynamic phase permeability on reduction of drained gas reserves of Cenomanian deposits. SOCAR Proceedings 4:48–54 (in Russian)

Ponomarev AA, Zavatsky MD, Nurullina TS et al (2021) Application of X-ray microtomography of the core in oilfield geology. Георесурсы/Georesources 23(4):34–43. https://doi.org/10.18599/grs.2021.4.4

Postnikov AV, Postnikova OV, Yzyurova ES et al (2025) A method for quantifying the heterogeneity of oil saturation distribution in terrigenous reservoir rocks. Георесурсы/Georesources 27(1):51–62. https://doi.org/10.18599/grs.2025.1.8

Reda M, Salem T, Abdel-Fattah MI et al (2025) Petroleum system analysis of the Ras Ghara oil Field: Geochemical evaluation and 2D basin modelling of pre-rift and syn-rift formations in the southern Gulf of Suez, Egypt. Marine and Petroleum Geology 180(107464)

Sidorov SV, Rizvanova ZM (2023) Substantiation boundary values of open porosity and gas permeability using data from flow studies for pore-type carbonate reservoirs. Георесурсы / Georesources 25(4):115–120. https://doi.org/18599/grs.2023.4.8

ГЕОЛОГИЧЕСКОЕ СТРОЕНИЕ И ПЕТРОФИЗИЧЕСКИЕ ОСОБЕННОСТИ ПОРОД-КОЛЛЕКТОРОВ КАРБОНАТНОЙ ФОРМАЦИИ ЮРЫ В СЕВЕРО–ЗАПАДНОЙ ЧАСТИ ЧАРДЖОУСКОЙ СТУПЕНИ

Каршиев О.А.[1*], Евсеева Г.Б.[1], Токарева К.М.[1], Кудашева Л.Р.[1], Раббимкулов С.А.[1,2]

[1]Институт геологии и разведки нефтяных и газовых месторождений,
Республика Узбекистан
100164, Ташкент, Мирзо-Улугбекский район, ул. Олимлар, 64
[2]Ташкентский государственный технический университет имени Ислама Каримова, Республика Узбекистан
100100, г. Ташкент, ул. Университетская, 2
**Автор, ответственный за переписку: odashkarshiev@gmail.com*

Резюме. В статье рассматривается геологическое строение карбонатной формации средне-верхнеюрского возраста в северо-западной части Чарджоуской ступени на примере Биргутлинского, Каракульского прогибов и Кульбешкак-Питнякского вала. Приведены результаты комплексных исследований тектонических, литолого-стратиграфических и фациальных особенностей карбонатных отложений и петрофизическая характеристика карбонатных пород-коллекторов, изученная по керновым материалам глубоких скважин. На этой базе установлены фильтрационно-ёмкостные свойства пород, обоснованы граничные значения коллекторов продуктивных отложений. На основе полученных результатов доказано, что в лагунной зоне, получившей развитие на рассматриваемой территории, распространены карбонатные и карбонатно-сульфатные хемогенные отложения с большим количеством эвапоритов, а также встречаются доломиты и терригенные образования открытого мелководья. Установлено, что для достоверного представления о закономерности распределения пористых и проницаемых пород в разрезе карбонатной формации необходимо определить связи между генетическими типами карбонатных пород и их коллекторскими свойствами, которые главным образом зависят от структурно-текстурных особенностей пород, а последние – от генетических разновидностей осадков. При проведении петрофизических исследований и установлении граничного значения открытой пористости и проницаемости на основе графоаналитического метода были составлены кумулятивные кривые коллектор-неколлектор. Установлено, что породы-коллекторы лагунных отложений на изучаемой территории относятся к порово-трещинным. Из выявленной характеристики их фильтрационно-ёмкостных свойств определено, что породы обладают существенной неоднородностью, что нашло свое отражение в широком диапазоне изменения коэффициентов пористости и проницаемости. На этой основе построена карта-схема прогнозных направлений изменения граничных значений фильтрационно-емкостных свойств для продуктивных нефтегазоносных отложений, приуроченных к юрской карбонатной формации. Исходя из проведенных исследований определено, что фильтрационно-емкостные свойства пород-коллекторов на изучаемой территории распространены равномерно, также выявлены закономерности их распространения, что позволило определить участки с хорошими коллекторскими свойствами для определения дальнейших направлений геологоразведочных работ на нефть и газ.

Ключевые слова: *юра, карбонатная формация, литология, тектоника, коллектор, стратиграфия, пористость, проницаемость, граничные значения.*

ÇARCOU MƏRHƏLƏSİNİN ŞİMAL-QƏRB HİSSƏSİNDƏKİ YURA KARBONAT FORMASİYASININ KOLLEKTOR SÜXURLARININ GEOLOJİ QURULUŞU VƏ PETROFİZİKİ XÜSUSİYYƏTLƏRİ

Karşiyev O.A.[1*], Evseeva G.B.[1], Tokareva K.M.[1], Kudaşeva L.R.[1], Rabbimkulov S.A.[1,2]

[1]Neft və Qaz yataqlarının Geologiyası və Kəşfiyyatı İnstitutu, Özbəkistan Respublikası,
100164, Daşkənd, Mirzo-Uluqbek rayonu, Olimlar küç., 64
[2]İslam Kərimov adına Daşkənd Dövlət Texniki Universiteti, Özbəkistan Respublikası,
100100, Daşkənd şəh., Universitet küç., 2
**Yazışmalara məsul:odashkarshiev@gmail.com*

Xülasə. Məqalə Çarcou pilləsinin şimal-qərb hissəsində yerləşən Orta–Yuxarı Yura karbonat formasiyasının geoloji quruluşunu tədqiq edir və bu məqsədlə Birqutlin və Karakul çökəklikləri, həmçinin Kulbeshkak–Pitnyak qabarması nümunə kimi götürülmüşdür. Tədqiqatda karbonat çöküntülərinin tektonik, litoloji-stratiqrafik və fasiya xüsusiyyətləri, eləcə də dərin quyulardan alınmış nüvələr

əsasında öyrənilmiş lay süxurlarının petrofiziki göstəriciləri üzrə kompleks nəticələr təqdim olunur. Bu məlumatlar əsasında süxurların kollektor xüsusiyyətləri və məhsuldar layların sərhəd qiymətləri müəyyən edilmişdir. Nəticələr göstərir ki, tədqiq olunan ərazidə formalaşmış laqun zonası karbonat və karbonat–sulfat mənşəli kimyəvi çöküntülərlə, çoxlu buxarlanma məhsulları, dolomitlər və açıq dayaz suların terrigen süxurları ilə xarakterizə olunur. Müəyyən edilmişdir ki, karbonat formasiyasında məsaməli və keçirici süxurların paylanma qanunauyğunluqlarını anlamaq üçün onların genetik tipləri ilə kollektor xüsusiyyətləri arasındakı əlaqə əsas rol oynayır və bu xüsusiyyətlər süxurların struktur-faktura göstəricilərindən asılıdır. Petrofiziki tədqiqatlar zamanı qrafik-analitik üsulla məsaməlilik və keçiricilik üçün sərhəd qiymətləri müəyyən edilmiş və məcmu rezervuar–qeyri-rezervuar əyriləri qurulmuşdur. Nəticələr göstərir ki, laqonal çöküntülərin lay süxurları məsaməli-qırıqlıdır və güclü heterogenlik nümayiş etdirir. Bu əsasda Yura karbonat formasiyasına aid məhsuldar neft-qaz yataqları üçün kollektor xassələrinin sərhəd meyllərini əks etdirən sxematik xəritə tərtib edilmişdir.

Açar sözlər: *Yura, karbonat formasiyası, litologiya, tektonika, kollektor, stratiqrafiya, məsaməlik, keçiricilik, sərhəd dəyərləri*

ANAS Transactions Earth Sciences 2 / 2025

http://www.journalesgia.com

DISTRIBUTION OF CALCITE CEMENTS AND THEIR INFLUENCE ON RESERVOIRS IN THE PRODUCTIVE SERIES OF THE SOUTH CASPIAN AND KUR BASINS

Zeynalov G.A.

Baku Higher Oil School, Azerbaijan

New Salyan highway, 3rd km, 25, Sabail district, Baku: gasham.zeynalov@bhos.edu.az

Keywords: *calcite cement, South Caspian basin, Kur basin, diagenesis, fluid flow, Productive Series*

Summary. The quality of the reservoirs in the Productive Series in the South Caspian and Kur Basins is directly influenced by calcite cementation and compaction. Studying these processes provides an opportunity to analyze diagenetic patterns in sandstones and especially the influence of carbonate cementation on fluvial deltaic sandstones. Precipitation of calcite cement during compaction in clastic rocks significantly affects the permeability of reservoirs and fluid flow during oil and gas production. From this point of view, the distribution characteristics of calcite cement concretions in the reservoirs of the Upper Productive Series in the South Caspian and Kur Basins, and their impact on porosity, permeability and fluid flow have been studied. The distribution of calcite concretions was mapped in outcrops of the Upper Productive Series sandstones in the Yasamal (Shubany) anticline in the western flank of the South Caspian Basin. Large, tabular calcite concretions in this fluvial-deltaic sandstone generally follow basinward-inclined bedding. Based on the XRD and SEM data, a large amount of calcite cement precipitation in the sandstones of the Upper Productive Series (Bal VIII and Bal VI horizons) in the Yasamal (Shubany) anticline has reduced the porosity and permeability for fluid flow. Understanding the depositional environment of calcite cement precipitation observed in the sandstones of the Productive Series in the South Caspian Basin is crucial in evaluating the quality of the analogue reservoirs in the Kur Basin. The presence of large volumes of calcite cement significantly affects the petrophysical properties of reservoirs, which makes studying their origin important.

© 2025 Earth Science Division, Azerbaijan National Academy of Sciences. All rights reserved.

Introduction

The porosity and permeability of reservoir rock can be controlled by various geological and sedimentological processes. Primary porosity is the direct consequence of lithology, fabric, and texture of clastic rocks, while secondary porosity is generated afterward, through diagenetic processes caused by alteration of the original sediments. Carbonate cement strongly affects fluid flow in sandstone reservoirs, as it is usually distributed unevenly with stratification and concretions, which commonly create barriers to fluid transmission and pressure compartments. These concretions, as one of the features of diagenetic processes such as compaction or the formation of cement can reduce the initial porosity during burial and create a diagenetic fingerprint to the permeability distribution as well, which should be incorporated into reservoir models for simulation fluid flow. Considerable research works have been attracted on impact of calcite cement diagenesis to reservoir quality in sandstones (e.g., Kantorowicz et al., 1987; Saigal, Bjørlykke, 1987; Walderhang et al., 1989; Bjorkum, Walderhang, 1990; Sulivan, McBride, 1991; Ortoleva,1994; McBride et al., 1995; Mozley, Davis, 1996; Crossey et al., 1996; Milliken et al., 1998; Morad, 1998; Walderhang, Bjorkum, 1998; Worden, Matray, 1998; Klein et al.,1999; Dutton et al., 2000; Taylor et al., 2000; Dutton et al., 2002; Boles, Ramseyer, 2002; Dutton, 2008; Delu Xie et al., 2020; Zeynalov, 2024).

However, calcite cements generally occur as irregularly distributed concretions in sandstones, and quantifying the effect of concretionary carbonate cement on fluid flow in sandstone reservoirs is not easy. This makes it challenging to forecast diagenetic permeability modifications in the subsurface from spaced wells. Therefore, an outcrop study can help to observe a continuous image of the spread of cement in analogues reservoirs.

In this paper, we studied distribution of calcite cement concretions in the exposed Upper Productive Series (Balakhany suite) of the Absheron peninsula, South Caspian Basin, and their impact on porosity and permeability properties of sandstone reservoirs

of the Balakhany VIII (Bal VIII) and Balakhany VI (Bal VI) horizons.

In our study, calcite concretions were mapped in a well-exposed outcrop of the Balakhany Suite sandstones (Bal VIII and Bal VI horizons) of the Upper Productive Series fluvial-deltaic sandstones in the Yasamal Valley of Absheron peninsula in the western flank of the South Caspian Basin.

Our goals were to (1) quantify the volume and spatial distribution of calcite concretions, (2) analyze the effect of the cement on fluid flow, and (3) provide comparison of petrophysical properties of calcite-rich consolidated and unconsolidated sandstones data that can be used to condition models of concretionary calcite-cement distribution in the subsurface. Our study demonstrates the importance of diagenesis-modified permeability distribution in consolidated tight sandstones for reservoir models.

Geological settings

The South Caspian and Kur Basins are the main geostructural elements in the Caspian and Caucasus regions of the Alpine-Himalayan folded belt. The South Caspian Basin encompasses the territory of the south part of the Caspian Sea. It is bordered by the Kur Basin in the east, which covers the intermontane area of Azerbaijan and SE Georgia (Fig.1).

The South Caspian Basin's basement surface lies at a depth of 22–25 km, making it one of the deepest basins in the world. The sedimentary fill of the South Caspian Basin has been significantly deformed and folded. The folded succession is unconformably overlain by the Lower Pliocene–Quaternary sediments (Zonenshain, Le Pichon, 1986; Granath, Baganz, 1996; Jackson et al., 2002; Allen et al., 2002; Allen et al., 2003; Brunet et al., 2003; Abdullayev et al., 2018).

Compared to the South Caspian Basin, the Kur Basin has more complicated geological history with multi-phase active tectonic processes accompanied by the collision, accretion, and rotation of the plates of the Eastern European Platform and Arabian plate during the Eocene-Pliocene period which were accompanied by different types of volcanogenic processes, abrupt changes in facies and facies associations, and stratigraphically irregular oil and gas accumulations in volcanic, carbonate and siliciclastic rocks. The Kur intermountain basin is a large structural element separating the Greater and Lesser Caucasus Mountain systems and is represented by the Lower Kur and Middle Kur (Yevlakh-Agjabedi trough, interfluve of the Kur and Gabyrry, Ajinohur trough) and Upper Kur (Kartly) sub-basins.

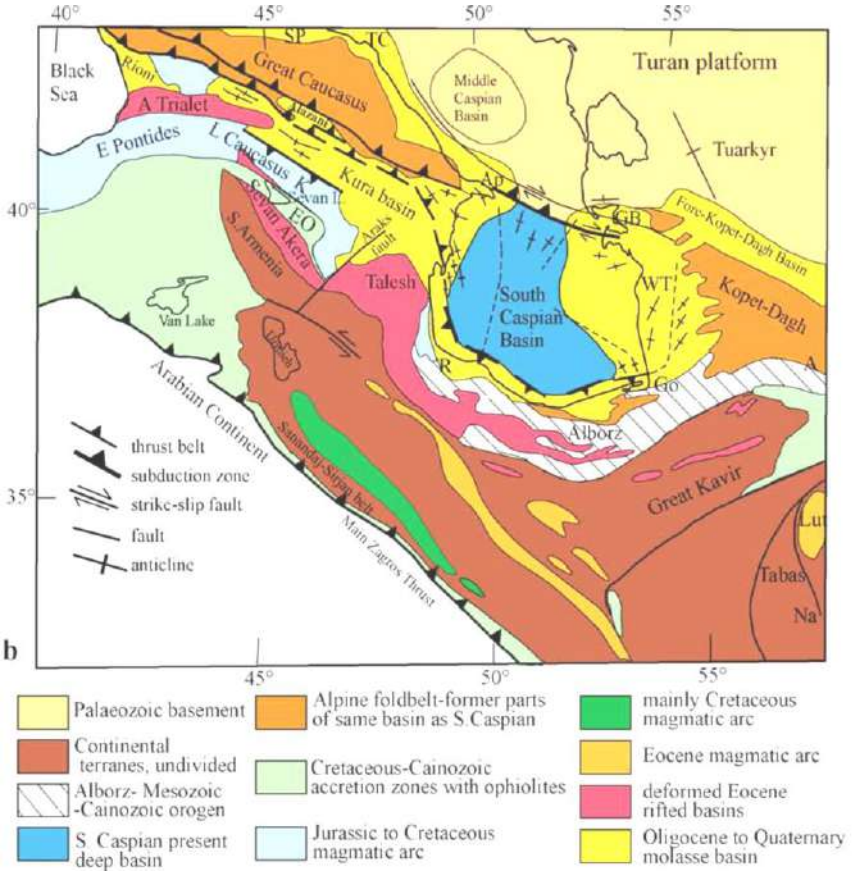


Fig. 1. Regional geological map of Caspian region main tectonic units (from Brunet et al., 2003)

The eastern part of the basin called the Lower Kur sub-basin is close in its deep structure and geological development to the South Caspian Basin, which in relatively recent Pliocene-Quaternary period was characterized by high rates of sedimentation. Tectonically, the Lower Kur is a deep buried sub-basin (the depth of the crystalline basement is 20-22 km) extending towards the General Caucasus. Although the Lower Kur sub-basin is the eastern part of the Kur intermountain basin, in general this indicates that it is a northeastern extension and the bay of the South Caspian Basin. The latter idea is confirmed by the mutual similarity of the elements of the geological structure and the history of geological development both in the Southern Caspian Basin and in the Lower Kur Basin (Khain, Shardanov, 1952; Zonenshain, Le Pichon, 1986; Granath, Baganz, 1996; Devlin et al., 1999; Jackson et al., 2002; Allen et al., 2002; Allen et al., 2003; Brunet et al., 2003; Guliyev et al., 2003; Golonka, 2004; Kadirov, 2004; Artyushkov, 2007; Nemcok et al., 2011; Forte et al., 2012; Kadirov and Safarov, 2014; Javanshir et al., 2015; Alizadeh et al., 2016; Abdullayev et al., 2018).

In the South Caspian and Kur Basins, oil and gas reservoirs are associated with a wider stratigraphic interval from the Upper Cretaceous to the Lower Pliocene rocks. The majority of the reservoirs are located in the Lower Pliocene Productive Series sandstones (Ushkin, 1916; Gorin, 1939; Aliev, 1960; Alizadeh et al., 1966; Guliyev et al., 2003; Aliyeva, 2005; Alizadeh et al., 2018).

The Productive Series considered being the main reservoir facies in the South Caspian and nearby Lower Kur Basins (the eastern part of the Kur Basin) were transported and deposited by the Paleo-Volga, Paleo-Amu Darya, Paleo-Kur and Paleo-Pirsagat rivers after the isolation of the Caspian Lake from the world ocean in the Late Miocene. The giant Paleo-Volga River played a significant role in bringing a large quantity of sand-rich sediments of the Productive Series, which caused the creation of quartz-rich, high-quality reservoirs of sandstones distributed toward Absheron and the NW part of the Baku archipelago in the South Caspian and Lower Kur sub-basins. (Jones, Simmons, 1996; Granath, Baganz, 1996; Reynolds et al., 1998; Devlin et al., 1999; Morton et al., 2003; Hinds et al., 2004; Aliyeva, 2005; Hinds et al., 2007; Green et al., 2009; Abdullayev et al., 2018; Zeynalov, Alkhasli, 2018; Zeynalov, 2022).

Facies of the Productive Series have a very wide distribution and mainly are represented by the alternation of sand, sandstone, shales and sometimes with coarse grained rock fragments with thickness of more than 3500 meters. Thick strata of conglomerates and breccia of the Productive Series appeared in the peripheral parts of the Lower Kur Basin. The most productive reservoirs of the Productive Series in the South Caspian Basin are associated with the Fasila and the Balakhany suits in its upper section, and their analogues in the Lower Kur sub-basin are XIV–XX horizons.

Calcite cementation and diagenesis are one of the important control elements of the quality of these fluvial deltaic reservoirs. In some cases, cementation and compaction can reduce porosity, and in other instances, cemented sediment can create dissolution resulting in increasing pore spaces and permeability of reservoirs.

Such calcite cement occurrence is observed in the outcrops of the Balakhany suite's fluvial-deltaic sandstones in the Lower Pliocene Productive Series in the Absheron Peninsula and which is considered a good analogue of the major reservoirs of the Azeri-Chirag-Azeri (ACG) field in the South Caspian Basin and the Lesser Harami, Greater Harami, Pirsagat, etc. fields in the Lower Kur sub-basin (Zeynalov et al., 2017; Zeynalov, Alkhasli, 2018; Alkhasli et al., 2022; Zeynalov, 2022).

Sharp facies changes characterised by fluvial-deltaic and lacustrine depositional environments in the geological section of the Productive Series indicate its heterogeneity of reservoir properties. The Balakhany, Sabunchu, and Surakhany suites of the upper section of the Productive series are exposed at the Yasamal (Shubany) anticline in the Absheron peninsula, specifically in the area of the SE and NNE plunging of the Shubany anticline. In this regard, it is very important to pay attention to the study of controlling factors affecting the quality of reservoirs including the calcite cement diagenesis of rocks, both in the South Caspian Basin and in the neighbouring Kur Basin.

The Shubany anticline is situated in the Absheron peninsula of the western flank of the South Caspian Basin. On the limbs and periclinal ends of the anticline fold, sandy and shaly sediments of the Balakhany, Sabunchu, and Surakhany suits of the Productive Series are widely exposed. The anticline structure is sharply asymmetrical. At the same time on the western limb, dipping angles of the layers varies within $45\text{-}65^0$, and on the eastern limb the layers are placed on their heads and in places overturned. As the fold submerges, dipping angles gradually decrease. The anticline has plunging structure and was complicated by three longitudinal faults and one of which has thrust character formed as a result of thrusting the west limb and dome of the anticline to the east limb (Fig. 2). The thrust merges at depth with another longitudinal fault. A number of small transverse faults were also revealed (Alizadeh et al., 1966).

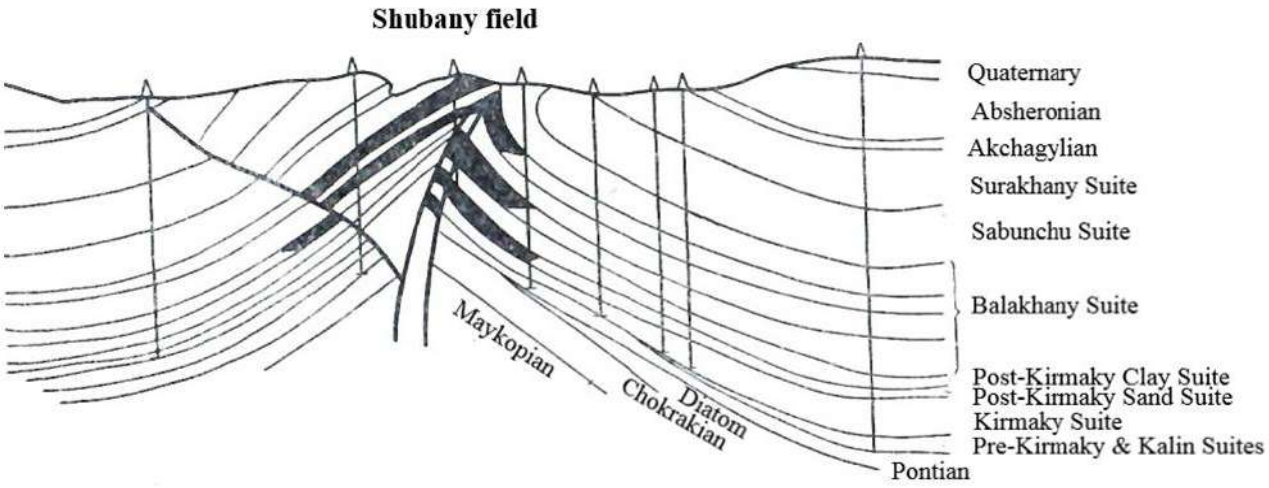


Fig. 2. Schematic cross sections through the Shubany oil field illustrating outcropping and the presence of oil accumulations in the Upper Productive Series (Balakhany, Post-Kirmaky Sand Suits) (From Alizadeh et al., 1966)

The Shubany anticline has the most favourable conditions for studying calcite cement concretions on the well-outcropping Upper Productive Series, which was chosen as the main area of investigation of the study of the mentioned problem (Fig.3).

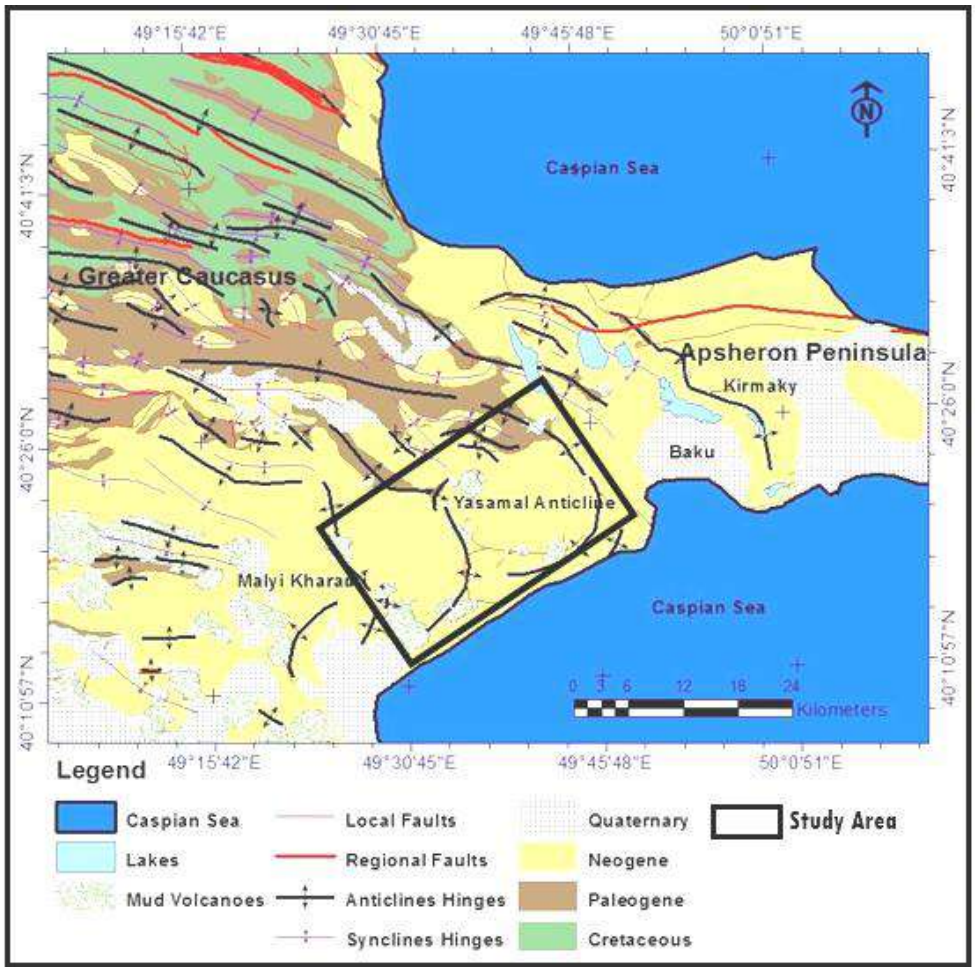


Fig. 3. Geological map of the Absheron peninsula and surrounded area showing location of the study area (from Allen et al., 2003)

Methodology

Field measurements using a Gamma Ray Spectrometer and laboratory study of the XRD, SEM, Thin Section Petrography, porosity, and permeability measurements were used to map the distribution of calcite cement concretions in the outcrop, quantify the volume and spatial distribution of calcite concretions, analyse the cement's effect on fluid flow, and provide a comparison of petrophysical properties.

The fieldwork survey was conducted in the Shubany anticline, where calcite cement precipitation was observed in outcrops of sandstones of the Balakhany Suite with fluvial-deltaic depositional environment. For these purposes, field measurements were performed across the sand-dominated Balakhany VI and Balakhany VIII horizons using the Gamma Ray Spectrometer (MGS-150).

Measurements were conducted in two locations: in the southern (log1) and northern (log 2) parts of the outcrop of the east limb with a length of 5.1 km (Fig.4), where calcite cement concretions are widely distributed in amalgamated broad, shallow channels of coarse-to-medium grained sandstone of the Balakhany VIII horizon and proximal floodplain and major channel sands with planar based, sheet-like medium-fine-grained sandstone of the Balakhany VI horizon of the Balakhany suite. These sand-dominated horizons were deposited during increased fluvial-deltaic discharge and coarse to medium-fine-grained sediment input to the South Caspian Basin.

Measurements show that calcite-rich sandstones are distributed along the east limb of the anticline starting from the north end of the structure and extending around two km towards the south. Calcite cement is precipitated mostly in channel-fill fluvial sandstones in the form of tabular concretions (Fig.5). These concretions generally follow basin ward-inclined bedding but in rare cases terminate within a bed across facies.

In some surveillances, calcite concretions have eroded, since being exposed as an outcrop, and hematite has precipitated in the resulting pores giving the concretions a reddish-dominated colour, easily distinguished from unconsolidated sandstones around them. However, field measurements alone are not sufficient for a full evaluation of the properties of the revealed calcite cement-rich rock units. Properties of calcite cement diagenesis were also studied on the micro-scale to look for their dependency on intrinsic rock properties based on merged analysis of thin section petrography and laboratory measurements such as the XRD and SEM on samples acquired from the outcrops of the mentioned sandstone horizons in the Shubany anticline.

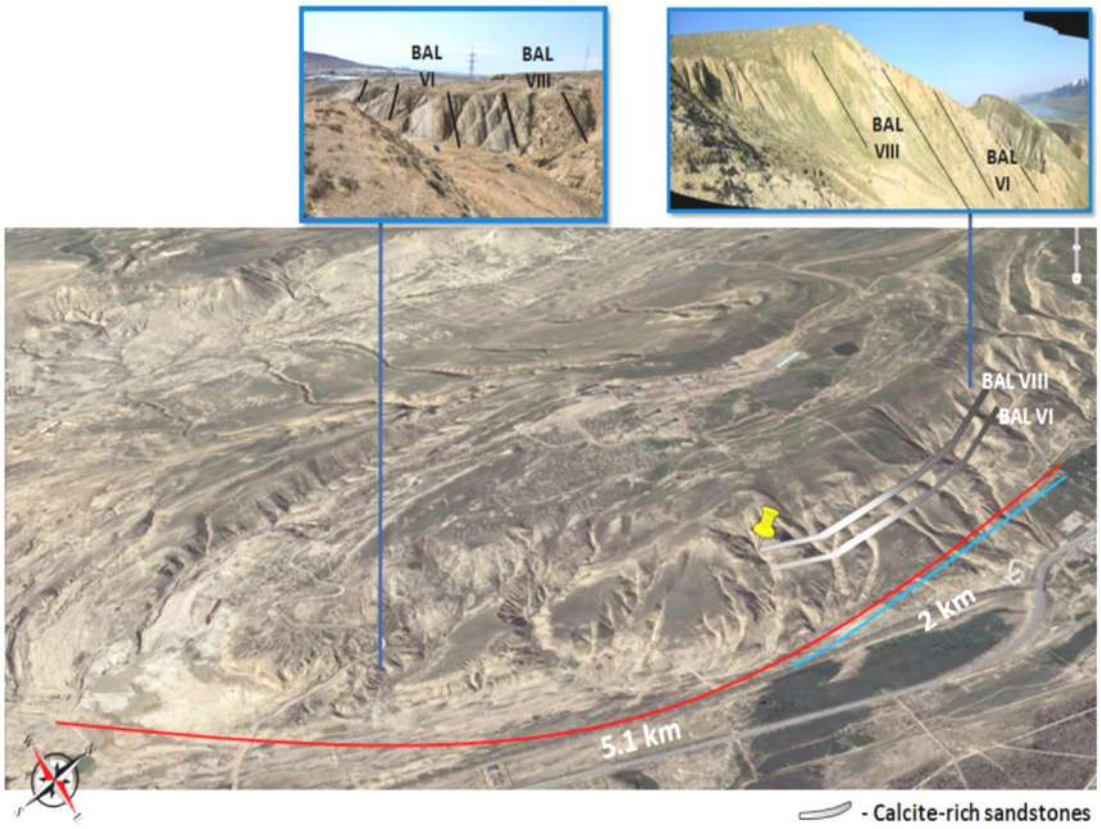


Fig. 4. Calcite cement concretions in Balakhany VIII and Balakhany VI horizons' sandstones observed at NE limb, Shubany anticline (Zeynalov et al., 2017)

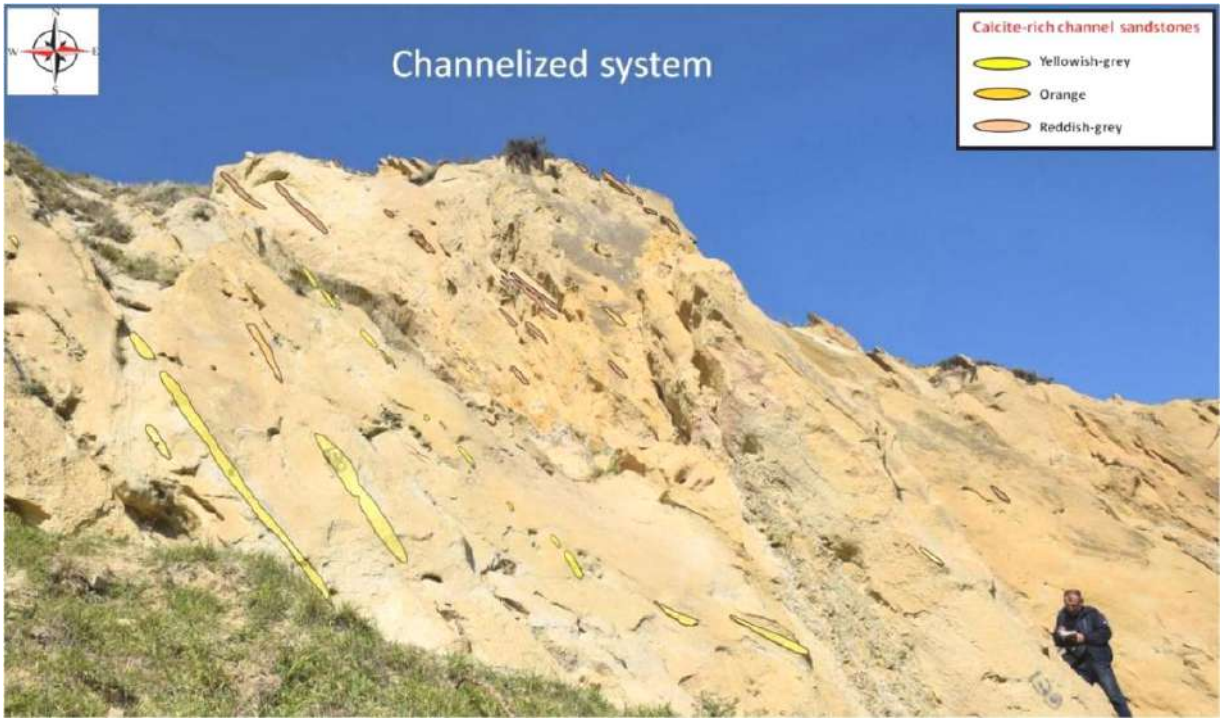


Fig. 5. Distribution of the calcite concretions in Bal VIII horizon sandstones in the northern part of the east limb, Shubany anticline (Zeynalov et al., 2017)

Results of the XRD measurements of sandstone samples from the Balakhany suite show that they have abrupt changes in volumes of minerals in the whole mineralogical composition (Fig.6). Based on this measurement calcite cement precipitation makes up 10-18% of rocks in the SE limb while in the NE limb of the Subany anticline, it makes up 40-45%, comprising almost half of the rock composition. Feldspar and clay minerals are of low percentages, and, hence, calcite is the dominant cementing material in observed sandstones.

A higher concentration of deformation bands was observed in the northern part of the eastern limb of the Shubany anticline, where calcite precipitation occurred. Calcite cement-rich sandstones undergo strong diagenesis and are abundant in deformation bands commonly displaying a clustered pattern (Fig.7).

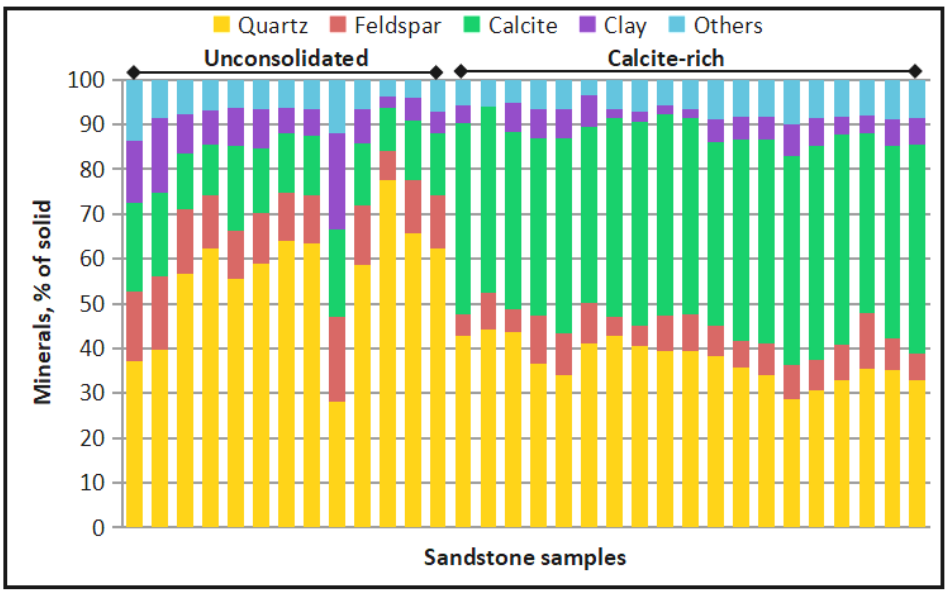


Fig. 6. Bar chart displaying fractions of per mineral species from sandstone plugs on the Balakhany VIII and Balakhany VI sandstones based on XRD measurements

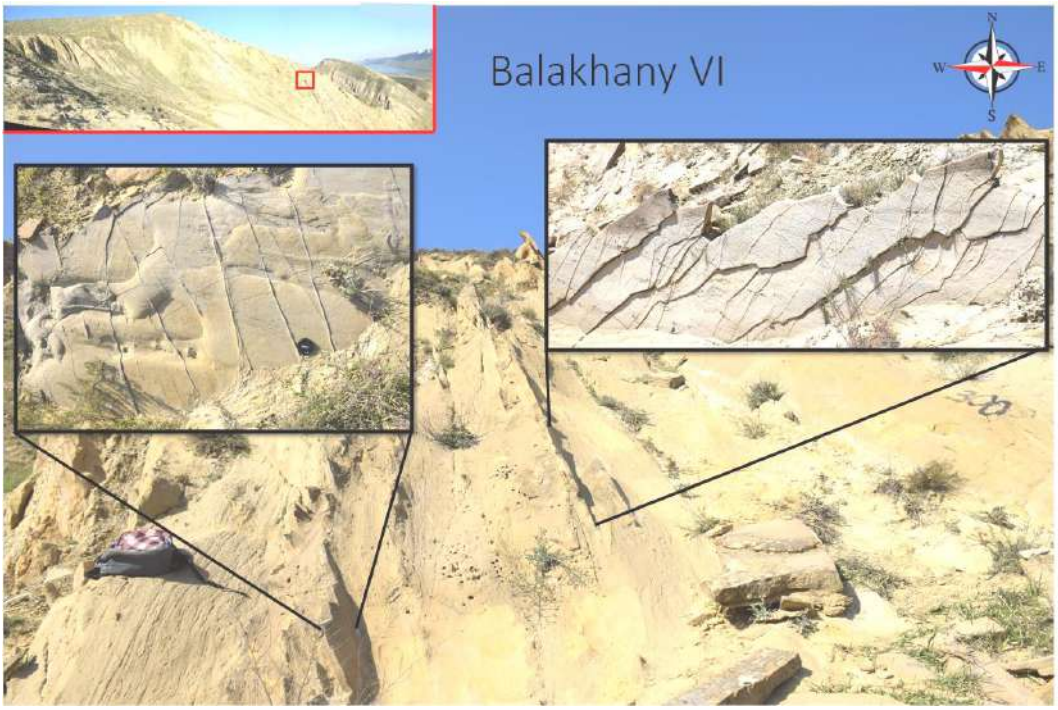
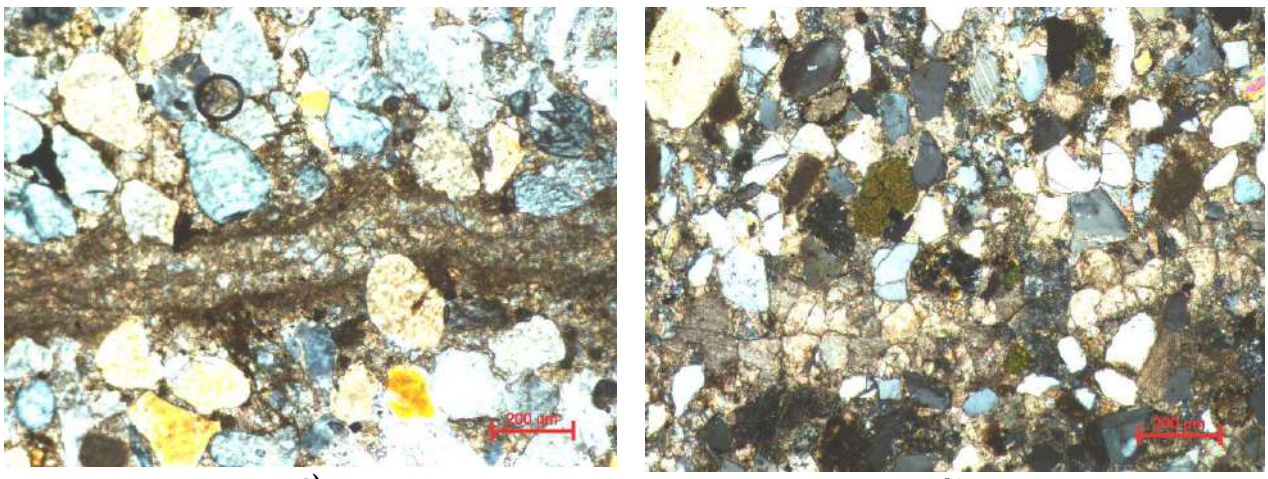


Fig. 7. Calcite-rich sandstone layers of the Balakhany VI complicated by deformation bands in the NE limb of the Shubany anticline (Zeynalov et al., 2017)

Thin sections allowed checking grain arrangements in rock bodies filled with calcite cement (Fig.8). The photomicrographs of the thin sections display a high degree of compaction and cementation in both examples of calcite-rich sandstones. Grain morphology varies from subangular to subrounded, and grain size is medium to fine with uniform distribution. These samples display the dissolution of grains generated by deterioration with grain size reduction (Fig. 8a) and calcite cement concretions deteriorated within the deformation band, meaning calcite precipitated prior to formation of deformation band (Fig. 8b).

The SEM images allowed visualization of pore space filling by calcite cement. Quartz grains were outlined based on the distribution of Si elements inside the sample (Fig. 9c). Si can be a constituent of several minerals other than quartz, such as feldspars and clays. Therefore, to separate quartz (SiO_2) those grains with only Si responses were selected. Any other element responds, such as K, Na, Ca, and Al along with Si are indicators of feldspar/clay minerals. Calcite cement was outlined in the same way based on the distribution of Ca inside of the sample (Fig.9d). As seen in Fig. 9c and Fig. 9d, calcite cement fills up much of the pore space. Figure 9b shows a quartz grain coated by calcite crystals. Based on XRD measurements, calcite comprises 45% of this sandstone sample.



a) **b)**

Fig. 8. Photomicrographs of calcite-rich sandstone samples: (a) a mixture of quartz, feldspar, and calcite-cement with deformation band (Balakhany VI sample); (b) Calcite cement-rich, minor feldspar with deformation band (Balakhany VIII sample)

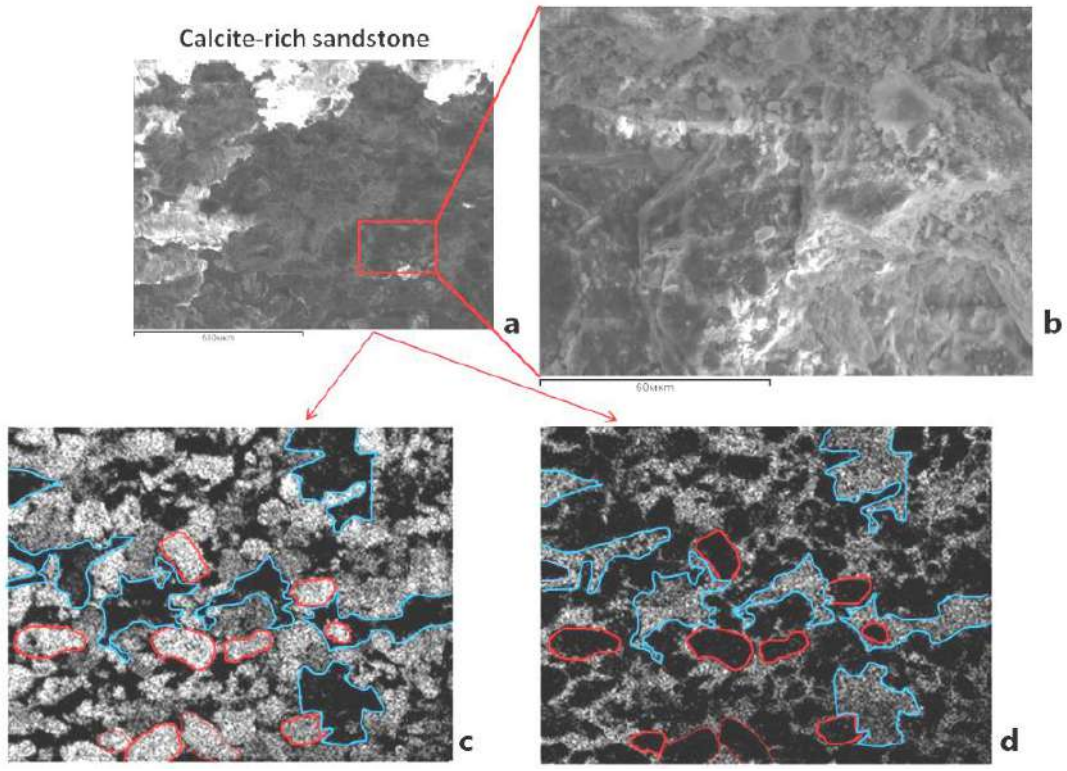


Fig. 9. SEM images visualizations of pore space filled by calcite cement in the Bal VIII horizon sandstone: (a) stacked SEM image of a calcite-rich sample; (b) zoomed in section of A, displaying coating of a quartz grain by calcite cement; (c) distribution of Si, and (d) distribution of Ca inside of the sample. Example quartz grains and calcite cement are outlined in red and blue, respectively

Since a lot of the pore space is occupied, calcite cementation significantly reduces porosity and, hence, the permeability of the rocks. It is observed in comparison of the petrophysical properties of calcite-rich and unconsolidated sandstones (Fig.10).

There is a sharp decrease in porosity and permeability as calcite cement volume increases in the Balakhany VIII horizon sandstones, which negatively impacts to reservoir quality in the northern part of the east limb of the anticline.

A comparison of porosity with the amount of calcite fraction in its mineral composition is also considered. Here, an increase of 40-45% in the amount of calcite fraction increased the consolidation of the rock, which caused a significant decrease in porosity (Fig. 11a). The same pattern is observed in comparison with the permeability. The amount of calcite fraction in the rock is more than 40% increasing its consolidation degree, so the permeability is significantly reduced (Fig. 11a).

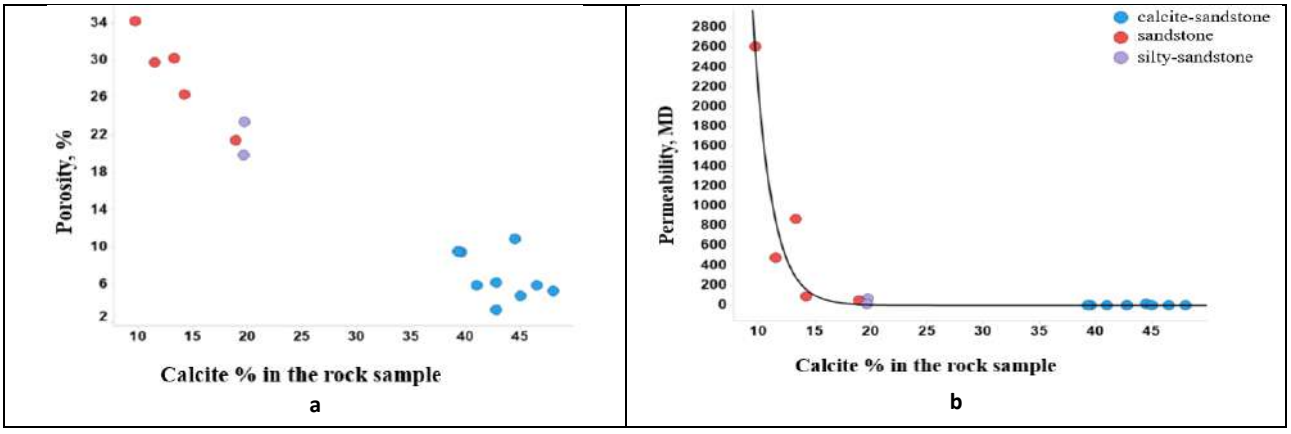


Fig. 10. (a) Porosity vs calcite fraction plots for rock sample; (b) Permeability vs calcite fraction plots for rock sample

The amounts of total clay and calcite cement content and their effect on the porosity of sandstone rock samples from the Balakhany VIII and Balakhany VI horizons were also studied. Results of the laboratory measurement show that the porosity is 20-30% when the content of both total clay and calcite in rock samples is no more than 10-15 %. Conversely, when the clay content exceeded 20%, the porosity dropped below 20%, especially with lower volumes of calcite cement (10-12 %) (Fig.11c).

If we make the same comparison of the permeability properties of the rock, a similar case can be observed here. Thus, when the amount of both total clay and calcite in the rock sample varies between 10-12%, it can be observed that the permeability value is more than 1000 mD, and if the percentage of total clay is more than 20% and the amount of calcite is low, the permeability decreases significantly to less than 20 mD (Fig.11d).

Discussion of results

The presence of calcite cement concretions in the pore space of sandstone rocks increased consolidation reducing the porosity and permeability of reservoirs for fluid flow in the Balakhany suite, primarily in the Balakhany VIII and Balakhany VI horizons in the north-eastern limb of the Shubany. These are potentially good analogues of the ACG reservoirs in the South Caspian Basin and the Lesser Harami, Greater Harami, and Pirsagat fields in the Kur Basin. Most of the sandstone reservoirs in these areas are related to the upper part of the Productive Series. Based on well data, high-volume calcite cement is distributed irregularly in these sandstones.

The highest calcite cement fraction significantly reduced effective porosity in the lower permeable facies. The increasing calcite cement fraction is caused by increasing concretion size. Analysis of these features reveals that concretions make flow paths more tortuous and retard flow in the coarser facies near the top of the sandstone. The fastest path through the sandstone is in the lightly cemented, high net-to-gross center of the sandstone body. The upward-increasing cement fraction is caused by upward-increasing concretion size.

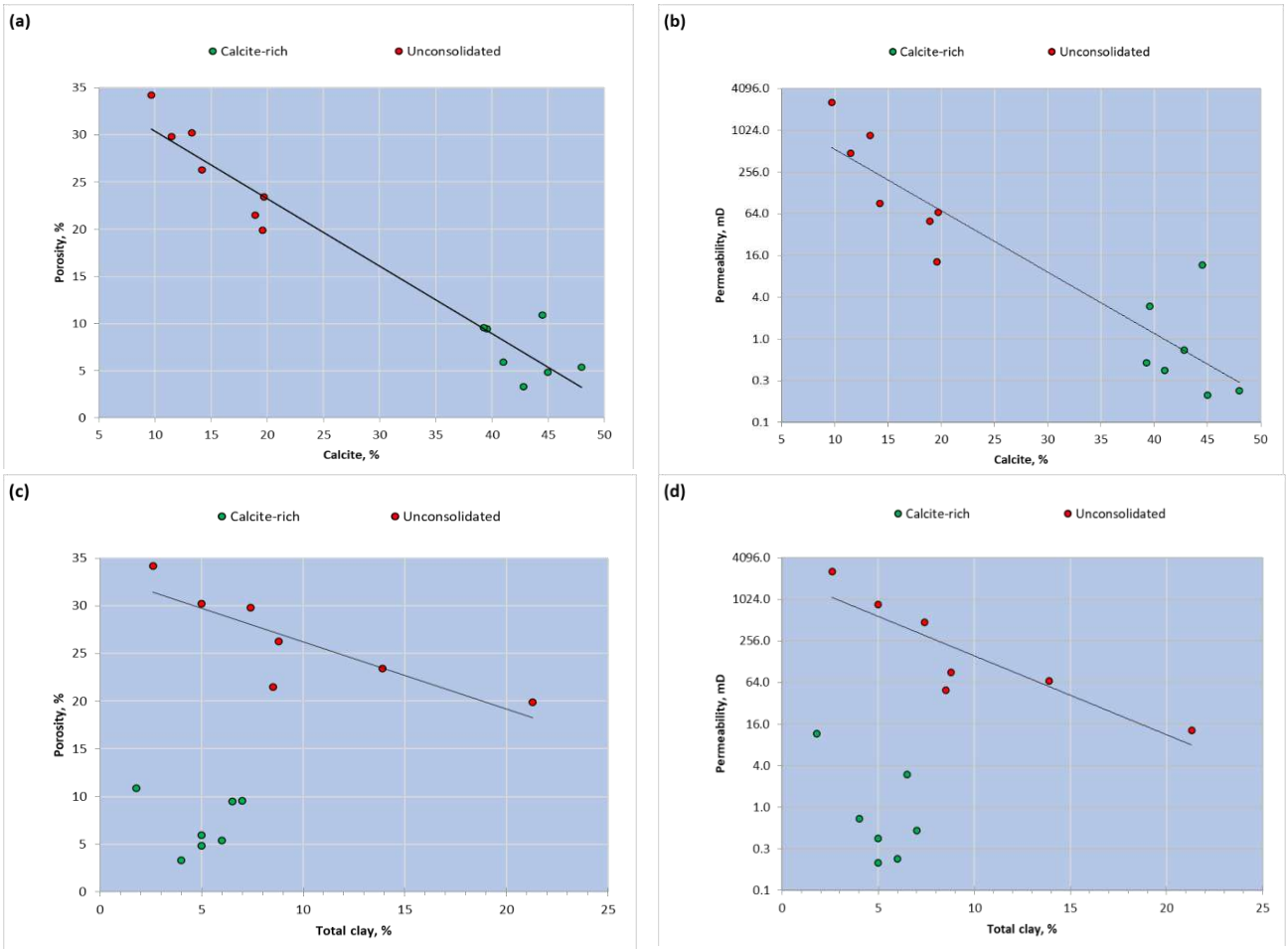


Fig. 11. (a) – Porosity vs calcite cement volume for rock sample; (b) – Permeability vs calcite cement volume plots for rock sample; (c) – Porosity vs total clay volume for rock sample; (b) – Permeability vs total clay volume for rock sample of the Balakhany VIII and Balakhany VI horizons

The Balakhany suite sandstone facies of the Productive series were formed during the period of increased fluvial-deltaic discharge and sediment supply, while mudstone-prone settings. Fresh groundwater is considered the primary source for the precipitation of calcite cement concretions in this suite. Climatic changes, fluctuations of the Caspian Lake, and groundwater flow direction influenced on the formation of calcite concretions in fluvial channel sandstones in the NE limb of the Shubany anticline.

Understanding the depositional environment of calcite cement precipitation observed in the sandstones of the Balakhany suite in Shubany field of the South Caspian Basin is crucial in evaluating the quality of the analogue's reservoirs in the Kur Basin. The varying volume of calcite cement in sandstones can significantly affect the petrophysical properties of reservoirs, making its study essential.

Conclusions

The sandstones of the Balakhany VI and Balakhany VIII horizons in the South Caspian Basin, and their analogues in the Kur Basin, were formed due to a high amount of sediment input and fluvial-deltaic discharge deposits. Fresh groundwater is considered the primary source for the precipitation of calcite cement concretions in these horizons.

The calcite cement concretions observed in the sandstones of the Balakhany VI and Balakhany VIII horizons can be used to indicate the presence of groundwater calcrete. These concretions formed during both humid and arid climatic periods and are linked to the high-frequency base-level fluctuations of Caspian Lake, which are caused by the oscillation of the water table and groundwater flow direction influenced on the formation of calcite concretions in braided fluvial channel sandstones.

A large amount of calcite cement precipitation (more than 30%) in the sandstones of the Balakhany VIII and Balakhany VI horizons has reduced the porosity and permeability, while a small amount of these cements (less than 15%) played a significant role in increasing quality of reservoirs in the South Caspian Basin.

Irregular distribution of calcite cement concretions is strong evidence of their fluvial-deltaic depositional environments which is revealed by labyrinth type of architecture of calcite cement rich sandstones of the Balakhany VIII and Balakhany VI horizons in the Shubany field of the South Caspian Basin. These results can be applied to the nearby Kur Basin to evaluate the properties of similar reservoirs. These results can be applied to the nearby Kur Basin to evaluate the properties of similar reservoirs.

Acknowledgments

The author expresses his gratitude to the co-authors of previously published joint papers on the considered problem.

REFERENCES

Abdullayev NR, Weber J, van Baak GC et al (2018) Detrital zircon and apatite constraints on depositional ages, sedimentation rates and provenance: Pliocene Productive Series South Caspian, Basin, Azerbaijan. Basin Res 30(5):835–862. https://doi.org/10.1111/bre.12283

Aliev AK (1960) Geology and hydrocarbons of the Kura-Araks Region. Azerneftneshr, Baku, p 361 (in Russian)

Aliyeva EGM (2005) Reservoirs of the lower Pliocene productive series at the western flank of the south Caspian basin. Lithology and Mineral Resources 40(3):267–278

Alizadeh AA, Ahmedov HA, Ahmedov AM et al (1966) Geology of oil and gas fields in Azerbaijan. Nedra, Moscow, p 392 (in Russian)

Alizadeh AA, Guliev IS, Mamedov PZ (2018) Productive strata of Azerbaijan. vol 2, Nedra, Moscow, p 236 (in Russian)

Alizadeh AA, Guliyev IS, Kadirov FA, Eppelbaum LV (2016) Geosciences in Azerbaijan. Geology, vol 1, Springer. Heidelberg, New York, p 239

Alkhasli S, Zeynalov G, Shahtakhtinskiy A (2022) Quantifying occurrence of deformation bands in sandstone as a function of structural and petrophysical factors and their impact on reservoir quality: an example from outcrop analog of Productive Series (Pliocene), South Caspian Basin. Journal of Petrol Explor Prod Technol 12:1977–1995. https://doi.org/10.1007/s13202-021-01448-z

Allen MB, Vincent SJ, Alsop GI, Ismail-zadeh AJ, Flecker R (2003) Late Cenozoic deformation in the South Caspian region: effects of a rigid basement block within a collision zone. Tectonophysics 366(3–4):223–239. https://doi.org/:10.1016/S0040-1951(03)00098-2

Allen MB, Jones S, Ismail-Zadeh A et al (2002) Onset of subduction as the cause of rapid Pliocene–Quaternary subsidence in the South Caspian Basin. Geology 30(9):775–778

Artyushkov EV (2007) Formation of the superdeep South Caspian basin: subsidence driven by phase change in continental crust. Russian Geology and Geophysics 48(12):1002–1014

Bjørkum PA, Walderhaug O (1990) Lateral extent of calcite cemented zones in shallow marine sandstones. In: Buller AT, Berg E, Hjelmeland O (eds) North Sea oil and gas reservoirs–II. Graham and Trotman, London, pp 331–336

Boles JR, Ramseyer K (2002) Diagenetic carbonate in Miocene sandstone reservoir, San Joaquin Basin, California. Am Assoc Pet Geol Bull 71(12):1475–1487

Brunet MF, Korotaev MV Ershov AV, Nikishin AM (2003) The South Caspian basin: a review of its evolution from subsidence modeling. In: Brunet M-F, Cloetingh S (eds) Integrated Peri-Tethyan Basins Studies (Peri-Tethys Programme). Sedimentary Geology 156(4):119–148

Crossey LJ, Loucks R, Totten MW (1996) Siliciclastic diagenesis and fluid flow: concepts and applications. SEPM Special Publication 55, p 222

Delu Xie, Suping Yao, Jian Cao, Wenxuan Hu, Yang Qin (2020) Origin of calcite cements and their impact on reservoir heterogeneity in the Triassic Yanchang Formation, Ordos Basin, China: A combined petrological and geochemical study. Marine and Petroleum Geology 117(104376). https://doi.org/10.1016/j.marpetgeo.2020.104376

Devlin WJ, Cogswell JM, Gaskins GM et al (1999) South Caspian Basin: Young, Cool, and Full of Promise. GSA TODAY A Publication of the Geological Society of America 9(7):1–2

Dutton SP (2008) Calcite cement in Permian deep-water sandstones Delaware Basin, west Texas: origin, distribution, and effect on reservoir properties. Am Assoc Pet Geol Bull 92(6):765–787

Dutton SP, White CD, Willis BJ, Novakovic J (2002) Calcite cement distribution and its effect on fluid flow in a deltaic sandstone, Frontier Formation, Wyoming. AAPG Bulletin 86(12):2007–2021

Dutton SP, Willis BJ, White CD, Bhattacharya JP (2000) Outcrop characterization of reservoir quality and interwell-scale cement distribution in a tide-influenced delta, Frontier Formation, Wyoming, USA. Clay Minerals 35(1): 95–105. https://doi.org/: 10.1180/000985500546756

Forte A, Cowgill E, Bernardin et al (2012) Late Cenozoic deformation of the Kur fold-thrust belt, southern Greater Caucasus. Geological Society of America Bulletin 122(3):465–486

Gamkrelidze I (1986) Geodynamic evolution of the Caucasus and adjacent areas in Alpine time. Tectonophysics 127(3-4):261–277. https://doi.org/10.1016/0040-1951(86)90064-8

Golonka J (2004) Plate tectonic evolution of the southern margin of Eurasia in Mesozoic and Cenozoic. Tectonophysics 381(1):233–273

Gorin VA (1939) Productive Series of Absheron Peninsula. AzGonti, Baku, p 12–19 (in Russian)

Granath JW, Baganz OW (1996) A review of Neogene subsidence mechanisms for the South Caspian basin. In: 3rd Annual meeting and fieldtrip of IGCP project N 369 ‘‘Comparative evolution of Peri-Tethyan rift basins’’, Centennial Celebration of EGSMA, 19 – 24 November, Cairo, Egypt, pp 24–25

Green T, Abdullayev N, Hossack J, Riley G, Roberts AM (2009) Sedimentation and subsidence in the South Caspian Basin, Azerbaijan. In: Brunet M-F, Wilmsen M, Granath JW (eds.) South Caspian to Central Iran Basins. Geological Society of London, Special Publication, London, vol 312, pp 241–260

Guliyev IS, Mamedov PZ, Feyzullayev AA et al (2003) Hydrocarbon systems of the South Caspian Basin, Nafta-press, Baku, p 205

Hinds D, Simmons MD, Allen MB, Aliyeva E (2007) Architecture variability in the Pereriva and Balakhany suites of the Neogene productive series, Azerbaijan: implications for reservoir quality. In: Yilmaz PO, Isaksen GH (eds) Oil and Gas of the Greater Caspian Area, AAPG Studies in Geology, Tulsa, vol 55, pp 87–107. https://dx.doi.org/10.1306/1205841St553010

Hinds DJ, Aliyeva E, Allen MB, Davies CE et al (2004) Sedimentation in a discharge dominated fluvial-lacustrine system: the Neogene Productive Series of the South Caspian Basin, Azerbaijan. Mar Pet Geol 21(5):613–638. https://doi.org/10.1016/ j.marpetgeo.2004.01.009

Jackson J, Priestley K, Allen M, Berberian M (2002) Active tectonics of the south Caspian basin. Geophysics Journal International 148(2):214–245. https://doi.org/10.1046/j.1365-246X.2002.01588.x

Javanshir RJ, Riley GW, Duppenbecker SJ, Abdullayev NR (2015) Validation of lateral fluid flow in an overpressured sand-shale sequence during development of Azeri-Chirag-Gunashli oil field and SD gas field: South Caspian Basin, Azerbaijan. Mar Pet Geol 59:593-610.

Jones RW, Simmons MD (1996) A review of the stratigraphy of Eastern Paratethys (Oligocene-Holocene). Bulletin of the National History Museum, London 52(1):25–49

Kadirov FA (2004) Gravity model of lithosphere in the Caucasus-Caspian Region. In: South Caspian Basin: Geology, geophysics, oil and gas content, Nafta Press. Baku, Azerbaijan, p 333

Kadirov FA, Safarov RT (2014) Current crustal deformation within the Azerbaijan territory. Seismoprognosis observations in the territory of Azerbaijan 11(1):34–37

Kantorowicz JD, Bryant ID, Dawans JM (1987) Controls on the permeability and distribution of carbonate cements in Jurassic sandstones: Bridport Sands, southern England, and Viking Group, Troll field, Norway. In: Marshall JD (ed) Diagenesis of sedimentary sequences, Oxford, Blackwell, p 103–118

Khain VE, Shardanov AN (1952) Geological history and structure of the Kura basin. Baku, Azerbaijan Academy of Sciences Publ, p 348

Klein JS, Mozley P, Campbell A, Cole R (1999) Spatial distribution of carbon and oxygen isotopes in laterally extensive carbonate-cemented layers: implications for mode of growth and subsurface identification. J Sedim Res 69:184–191

McBride EF, Milliken KL, Cavazza W et al (1995) Heterogeneous distribution of calcite cement at the outcrop scale in Tertiary sandstones, northern Apennines, Italy. AAPG Bulletin 79(7): 1044–1063

Milliken KL, McBride EF, Cavazza W et al (1998) Geochemical history of calcite precipitation in Tertiary sandstones, northern Apennines, Italy. In: Morad S (ed) Carbonate cementation in sandstones: International Association of Sedimentologists, Special Publication 26:213–239

Morad S (1998) Carbonate cementation in sandstones: distribution patterns and geochemical evolution. In: Morad S (ed) Carbonate cementation in sandstones: International Association of Sedimentologists, Special Publication 26:1–26

Morton A, Allen M, Simmons M et al (2003) Provenance patterns in a neotectonic basin: Pliocene and Quaternary sediment supply to the South Caspian. Basin Research 15(3):321–337

Mozley PS, Davis JM (1996) Relationship between oriented calcite concretions and permeability correlation structure in an alluvial aquifer, Sierra Ladrones Formation, New Mexico. J Sed Res 66:11–16

Nemcok M, Feyzullayev AA, Kadirov FA et al (2011) Neotectonics of the Caucasus and Kura Valley, Azerbaijan. Global Engineers and Technologists Review 1:1–14

Ortoleva PJ (ed) (1994) Basin compartments and seals. AAPG Memoir 61, p 477

Reynolds AD, Simmons MD, Bowman MBJ et al (1998) Implications of outcrop geology for reservoirs in the Neogene productive series: Apsheron Peninsula, Azerbaijan. AAPG Bulletin 82(1):25–49

Saigal GC, Bjørlykke K (1987) Carbonate cements in clastic reservoir rocks from offshore Norway – relationships between isotopic composition, textural development and burial depth. In: Marshall JD (ed) Diagenesis of sedimentary sequences, Oxford, Blackwell, Geological Society, Special Publication 36:313–324

Sullivan KB, McBride EF (1991) Diagenesis of sandstones at shale contacts and diagenetic heterogeneity, Frio Formation. AAPG Bulletin 75(1):121–138

Taylor KG, Gawthorpe RL, Curtis CD, et al (2000) Carbonate cementation within a sequence stratigraphic framework: the Upper Cretaceous sandstones of Book Cliffs, Utah–Colorado. Journal of Sedimentary Research 70:360–372

Uskin NI (1916) Stratigraphy and tectonics of the Productive Series of the Balakhany-Sabunchi-Ramany oil-producing region. Baku, p 80 (in Russian)

Walderhaug O, Bjørkum PA (1998) Calcite growth in shallow marine sandstones: growth mechanisms and geometry. In: Morad S (ed) Carbonate cementation in sandstones: International Association of Sedimentologists, Special Publication 26:179–192

Walderhaug O, Bjørkum PA, Nordgard-Bolas HM (1989) Correlation of calcite-cemented layers in shallow-marine sandstones of the Fensfjord Formation in the Brage field. In Collinson JD (ed) Correlation in hydrocarbon exploration, Graham and Trotman, London, p 367–375

Worden RH, Matray JM (1998) Carbonate cement in the Triassic Chaunoy Formation of the Paris basin: distribution and effect on flow properties. In: Morad S (ed) Carbonate cementation in sandstones, International Association of Sedimentologists, Special Publication 26:163–177

Zeynalov G**,** Alkhasli S, Shahtakhtinskiy A (2017) Outcrop analogue study of deformation bands and their impact on rock properties of the Productive Series in South Caspian Basin. OnePetro, Society of Petroleum Engineers, p 20. https://doi.org/10.2118/189018-MS

Zeynalov G, Alkhasli Sh (2018) Structural deformation and its impact to sandstone reservoirs in Eastern Azerbaijan. The 80th EAGE Conference & Exhibition,11-14 June 2018, Copenhagen, Denmark, EarthDoc, Vol 2018, p 1–5. https://doi.org/10.3997/2214-4609.201801590

Zeynalov GA (2024) Calcite diagenesis impact on sandstone reservoirs of the Productive Series in South Caspian and Kura Basins, 85th EAGE Annual Conference & Exhibition, Jun 2024, Oslo, Norway, EarthDoc, Volume 2024, p 1–5. https://doi.org/10.3997/2214-4609.202410156

Zeynalov GA (2022) Environmental facies analysis of the Productive Series in the Kura Basin, Azerbaijan. 83rd Annual EAGE Conference Proceedings, Exhibition, Spain, Madrid, Jun 2022, EarthDoc, Volume 2022, p 1–5. https://doi.org/10.3997/2214-4609.202210479

Zonenshain LP, Le Pichon X (1986) Deep basins of the Black Sea and Caspian Sea as remnants of Mesozoic back-arc basins. Tectonophysics 123:2181–211

РАСПРЕДЕЛЕНИЕ КАЛЬЦИТОВЫХ ЦЕМЕНТОВ И ИХ ВЛИЯНИЕ НА РЕЗЕРВУАРЫ В ПРОДУКТИВНОЙ ТОЛЩЕ ЮЖНО-КАСПИЙСКОГО И КУРИНСКОГО БАССЕЙНОВ

Зейналов Г.А.
Бакинская Высшая Нефтяная Школа, Азербайджан
Баку, Сабаильский район, Новая Сальянская трасса, 3 км, 25

Резюме. Качество коллекторов продуктивной толщи нижнего плиоцена в бассейнах Южного Каспия и Куры напрямую контролируется кальцитовой цементацией и уплотнением, связанными с седиментационными условиями. Изучение взаимодействия этих процессов в коллекторах даёт возможность проанализировать закономерности диагенеза в флювиально-дельтовых песчаниках, особенно с учётом малоизученного влияния карбонатной цементации в флювиально-дельтовых фациях. Выпадение кальцитового цемента при уплотнении осадочных пород существенно влияет на проницаемость песчаных коллекторов и фильтрацию флюидов при добыче нефти и газа. С этой точки зрения изучены особенности распределения конкреций кальцитового цемента в песчаниках верхней продуктивной толщи Южно-Каспийского и Куринского бассейнов и их влияние на пористость, проницаемость и фильтрацию флюидов. Распределение кальцитовых конкреций было картировано в выходах песчаников верхней части продуктивной толщи Ясамальской (Шубанинской) антиклинали на западном фланге Южно-Каспийской впадины. Крупные пластинчатые кальцитовые конкреции в этих флювиально-дельтовых песчаниках, как правило, следуют наклону слоистости в сторону бассейна. По данным рентгеновской дифракции (XRD) и сканирующей электронной микроскопии (SEM) высокое содержание кальцитовых цементных конкреций, присутствующих в песчаниках верхней части продуктивной толщи (балаханский VIII и балаханский VI горизонты) Ясамальской (Шубанинской) антиклинали, значительно снижает пористость и проницаемость для потока флюида. Понимание условий осадконакопления кальцитовой цементации, наблюдаемых в песчаниках продуктивной толщи на западном борту Южно-Каспийского бассейна, имеет важное значение для оценки качества аналоговых коллекторов в песчаниках соседнего Куринского бассейна. Наличие большого объёма кальцитового цемента существенно влияет на петрофизические свойства коллекторов, что обуславливает важность изучения их происхождения.

Ключевые слова*: кальцитовый цемент, Южно-Каспийский бассейн, Куринский бассейн, диагенез, поток жидкости, продуктивная толща*

CƏNUBİ XƏZƏR VƏ KÜR HÖVZƏLƏRİNDƏ MƏHSULDAR QAT ÇÖKÜNTÜLƏRİNDƏ KALSİT SEMENTLƏRİNİN PAYLANMASI VƏ ONLARIN KOLLEKTOR SÜXURLARINA TƏSİRİ

Zeynalov Q.Ə.
Bakı Ali Neft Məktəbi, Azərbaycan
Bakı, Səbail rayonu, Yeni Salyan şossesi 3-cü km, 25

Xülasə. Cənubi Xəzər və Kür hövzələrində Alt Pliosenin Məhsuldar qat çöküntülərinin kollektor süxurlarının keyfiyyəti çöküntü toplanma şəraiti ilə əlaqədar olaraq, birbaşa kalsit sementləşməsinin və sıxlaşmasının xarakterindən asılıdır. Çay-delta qumdaşı kollektorlarında bu proseslərin qarşılıqlı öyrənilməsi həmin qumdaşıların diagenetik xüsusiyyətlərini, xüsusən də çay-delta fasiyasında zəif öyrənilmiş karbonat sementləşməsinin təsirini təhlil etməyə imkan verir. Çökmə süxurların sıxlaşması zamanı kalsit sementin-

in çökməsi neft və qazın hasilatı dövründə qumlu kollektorların keçiriciliyinə və mayelərin süzülməsinə əhəmiyyətli dərəcədə təsir göstərir. Bu nöqteyi nəzərdən Cənubi Xəzər və Kür hövzələrində Məhsuldar qatın üst hissəsinin qumdaşılarında kalsit sement konkresiyalarının paylanmasının xüsusiyyətləri və onların məsaməliyə, keçiriciliyə və mayelərin süzülməsinə təsiri öyrənilmişdir. Cənubi Xəzər hövzəsinin qərb kənarında Yasamal (Şubanı) antiklinalında Məhsuldar qatın üst hissəsinin qumdaşı süxurlarının yerüstü çıxıntılarında kalsit konkresiyalarının paylanması xəritəyə alınmışdır. Bu çay-delta qumdaşılarında qat-qat kalsit konkresiyaları adətən hövzəyə doğru laylanma yamacı istiqamətində yayılmışlar. Rentgen Difraksiyası (XRD) və Skan Edən Elektron Mikroskop (SEM) məlumatlarına əsasən, Yasamal (Şubanı) antilkinalında Məhsuldar qatın üst hissəsinin (Balaxanı VIII və Balaxanı VI horizontlarında) qumdaşılarının tərkibində mövcud olan yüksək miqdarda kalsit sement konkresiyaları məsaməliyi və maye axını keçiriçiliyini əhəmiyyətli dərəcədə azaldır. Cənubi Xəzər hövzəsinin qərb kənarında Məhsuldar qatın qumdaşılarında müşahidə olunan kalsit sementininin çökmə şəraitinin başa düşülməsi qonşu Kür hövzəsindəki qumdaşı kollektorlarının keyfiyyətinin qiymətləndirilməsi üçün çox vacibdir. Qeyd edilən qumdaşıların tərkibində böyük həcmdə kalsit sementinin mövcud olması onların kollektorlarının petrofizik xüsusiyyətlərinə əhəmiyyətli dərəcədə təsir göstərir və bu da onun mənşəyinin öyrənilməsinin vacibliyini şərtləndirir.

Açar sözlər: *kalsit sementi, Cənubi Xəzər hövzəsi, Kür hövzəsi, diagenez, maye axını, Məhsuldar qat*

ANAS Transactions Earth Sciences 2 / 2025

http://www.journalesgia.com

POSSIBILITIES FOR DETECTING RESERVOIR WETTABILITY AND BITUMINISATION BASED ON INTEGRATED PETROPHYSICAL CORE AND WELL-LOGGING DATA

Galkin S.V.[1], Kolychev I.J.[2], Savitsky Y.V.[3*], Shumilov A.V[4], Gurbanov V.Sh.[5,6], Abbasova G.G.[7]

[1-4]Perm National Research Polytechnic University, Russia
[5]Ministry of Science and Education of the Republic of Azerbaijan, Institute of Oil and Gas, Azerbaijan
9, Baku, F.Amirov str., Baku, AZ1000
[6]Baku State University, Azerbaijan
33 Acad. Zahid Khalilov str., Baku, AZ1148
[7]Azerbaijan State Oil and Industry University, Azerbaijan
20, Azadlig ave., Baku, AZ1010
Corresponding author: yansavitsky@yandex.ru

Keywords: *hydrophobisation, wettability, bituminisation, porosity, electrical resistivity of rocks, X-ray core tomography, laterolog, microlaterolog*

Summary. For some complex Visean oil-saturated intervals of the fields of the Perm Krai, a high electrical resistance has been established. This can be explained by the hydrophobicity and bitumen content of the reservoirs. The assessment of these parameters was carried out analysing a petrophysical and geophysical data for a number of large oilfields. X-ray tomography was used to assess the wettability of the core samples, which was compared with lateral log data. Comparison of core X-ray tomography results with electrical logging data shows that at resistivity over 200 ohm·m the rocks are hydrophobic, and at a resistivity over 600 ohm·m they practically do not take water. The bituminisation of the reservoirs was analysed from the core material, taking into account the porosity according to the nuclear logging data, as well as the electrical resistivity from the lateral and micro-lateral logs. We demonstrate that log porosity and resistivity data can be used in developing algorithms, in building wettability and bituminisation maps of the main fields. These maps can be further utilized in building 3D reservoir models and in optimization of the secondary recovery operations in the field. The analysis of all the data suggests that open porosity is the key parameter controlling bituminisation. According to the obtained results, algorithms have been developed to predict the formation bituminisation using a set of logging methods. The results of the developed method were applied in digital geological and technological modelling of deposits with different types of wettability and bitumen content.

© 2025 Earth Science Division, Azerbaijan National Academy of Sciences. All rights reserved.

1. Introduction

Pore characteristics are fundamental to understanding the subsurface heterogeneity and constituent fluid flow in reservoir rocks (Johnson et al., 2006).

The north of the Perm region in Russia is a promising area for oil production development, where several new oil fields have recently been discovered. In this area, recoverable reserves of a single field often exceed 40 million barrels of oil. Most of the production facilities are characterized by a low degree of reserves recovery. High economic prospects of this region are also associated with low oil viscosity (1-3 mPa • s) and relatively high reservoir permeability (100 • 10-3 μm^2). The Visean complex is one of the largest in terms of oil reserves and it is represented by fine-grained and medium-fine-grained sandstones with porosity of 8-20%.

High porosity intervals are typically light grey sandstones, while low porosity intervals can be bituminous and dark in colour. For a significant number of oil-saturated intervals, a high electrical resistivity of rocks of more than 200 Ohm·m, and in some cases more than 1000 Ohm·m, has been established. According to theoretical concepts, abnormal-

ly high resistivity can be explained by rocks hydrophobicity. This topic was covered in reports Salah Al-Ofi et al. (2017 and 2018), as well as in paper (D'jakonova et al., 2021).

Data of reservoirs wettability is extremely important for efficient planning of oil production and especially for water flooding. The possibility of using wettability change as the main recovery mechanism in the process of enhanced oil recovery has only become an important topic in the research region in recent years. This is despite the fact that it was first recognized in 1959 by Wagner, Leach and tested in the field in 1962 (Wagner and Leach, 1959; Leach and Wagner, 1962).

Efimov et al. (2016) show that problems with reservoir injection optimization in the Visean objects of Perm region are often related to the rocks of increased resistivity. In case of low porosity reservoirs, the increased resistivity is typically associated with their bituminous content (Mukhametshin and Galeev, 2014), which reduces well productivity.

2. Materials and methods

The tomographic method has been applied to 47 core samples, 30 mm in size from the Perm region. All core samples were preliminarily extracted, open porosity (ϕ), irreducible water saturation (Swi), specific electrical resistivity of water-saturated sample (Rws) and the sample with residual water (Rrw) were determined. Open porosity was determined by the liquid saturation and hydrostatic weighing method; irreducible water saturation was determined by the capillarimetric method with air displacement pressure of up to 0.3 MPa through semipermeable membranes with a breakthrough pressure of 1.5 MPa. Oil-saturated core samples are characterised by a wide range of reservoir properties: ϕ of 10.1-22.3% (16.2% on average), Swi of 3.3-24.2% (9.0% on average).

The experimental tomograms of the cores in their dry state and saturated with sodium iodide aqueous solution with NaI concentration of 300 g/l were acquired. Saturation was achieved by gradually filling an evacuated sample chamber with preliminary evacuated NaI solution. This step was followed keeping the samples in the solution. White colour on the tomograms corresponds to calcification sites characterised by relatively high density; their configuration can be used to compare the tomograms of dry and saturated samples.

Tomography of dry and saturated samples was performed using the same parameters of the position and rotation of the stage, as well as the distance to the X-ray gun and the detector. The shooting parameters were as follows: voltage of 155-175 kV, current of 60-80 μA, copper filter was 0.5 mm thick. After 3D reconstruction of the tomography results, the sample volumetric models were compared. For comparison, both reconstructions were reduced to the same brightness according to the histogram; the upper and lower 2.5 mm ends of each sample were avoided to eliminate artifacts arising during X-ray shooting (Gurbanov et al., 2019).

For the pore volume calculation, image binarisation was carried out with the purpose to discriminate the pore space. Subsequently, the cutoff corresponding to the "rock-air" interface was drawn on the histogram to highlight the pore volume. Tomographic porosity of dry and saturated samples was calculated as the ratio of the pore volume to the entire sample volume. The use of the NaI additive to the aqueous solution does not change its filtration characteristics. The density of the solution with NaI differs sharply from the density of the void space in the dry state. Thus, the sample wettability can be assessed comparing the dry and NaI solution-saturated tomograms. The dry pores on the tomograms are displayed as black, while the saturated ones will change colour to light grey. This makes it possible to determine the fraction of the pore volume saturated with fluid (Berg et al., 2014). The coefficient of impregnation CI was calculated as the ratio of the difference in the pore volume between the dry (V1) and the saturated sample (V2) to the pore volume in the dry sample (V1):

$$CI = \frac{V_1 - V_2}{V_1} * 100\%. \quad (1)$$

The impregnation coefficient is used as an indicator of the reservoir wettability. We have established a conditional division into three classes. Notably, at CI values over 90% the sample was classified as hydrophilic, at 90-50% – as having signs of hydrophobicity, at 50-10% – as mainly hydrophobic, and, finally, if the impregnation was below 10% – as hydrophobic.

Pore-type reservoirs are distinguished by complex interpretation of gamma-ray, neutron-neutron, sonic, and caliper logs. The formation saturation is determined from electrical resistivity using induction (IK), laterolog (BK), and microlaterolog (MBK).

To create an algorithm for forecasting bituminisation, data from 376 wells with lateral logging data, 155 wells with micro-lateral logging data, and 27 wells with coring were analyzed. In addition to BK and MBK data, all intervals of the well section are characterized by the values of porosity and residual water saturation according to logging interpretation data, as well as in the case of sampling with a core description, indicating the presence of bituminisation. All wells belong to the fields of the Solikamsk depression (Gurbanov, Narimanov, 2019).

The water saturation is most reliably evaluated in the far field by the laterolog, including formation resistivity greater than 100 ohm·m. Due to the usage of

the shielding electrodes, the drilling fluid effect is minimised and the vertical resolution can be as low as 50 cm (20 inches), allowing thin bed evaluation. The most reliable formation resistivity from BK (RBK) is obtained in wells filled with water-based mud having resistivity of 0.03-3 ohm·m and for the intervals with bed thickness greater than 0.8 m (30 inches).

A subset of 47 core samples was analysed to compare wettability from X-ray tomography with the laboratory measurements of resistivity. The resistivity of the core samples was measured using the two-electrode method at a frequency of 1000 Hz with complete (100%) and residual saturation of cylindrical samples with formation water marked by the X-ray contrast agent (Gurbanov et al., 2021).

Oil-saturated intervals of several fields are classified according to the signs of wettability changes (hydrophobisation) and bituminisation. The data on the results of the predictive assessment are entered into 3D digital geological models. The models were built for two fields of the Solikamsk depression – Unvinskoye and Sukharevskoye. As a result, the fraction of hydrophobised and bituminised sections in the overall oil-saturated thickness was calculated for the entire territory.

3. Results

3.1. Hydrophobisation evaluation from core X-ray tomography

Previous studies have applied a variety of conventional techniques to porous media to qualitatively and quantitatively characterise the pore size of complex geological materials. Centrifugation, isometric drying, Amott and adsorption methods are most frequently used for assessing wettability on cores (Dixit et al., 2000). Comparison of wettability determination by different methods shows different results (Gurbatova et al., 2016), due to indirect characterisation. According to these authors, the X-ray core tomography method is the most informative for wettability. Using this direct imaging method, studies have examined pore systems and the surrounding matrix visually (Bultreys et al., 2016; Milliken, Curtis, 2016).

This method allows visualizing the rock pore space including the assessment of the degree of aqueous solution penetration into the core samples (Efimov et al., 2015).

Examples of tomograms of sandstones with different types of wettability are shown in Fig. 1. The NaI solution fills almost the entire pore space of the hydrophilic sample, changing the general background colour of the rock skeleton to light grey (Fig. 1a). For the saturated sample with CI in the 50-90% range, we observe that some of the larger pores are displayed in black in the central part of the tomogram, i.e. those pores were not accessed by the NaI solution (Fig. 1b). The proportion of such pores increases for the samples with strong signs of hydrophobicity at CI of 10-50% (Fig. 1c). For hydrophobic sandstones the images of the dry and saturated pores volumes in the central part of the tomograms are practically the same, which indicates absence of NaI impregnation (Fig. 1d).

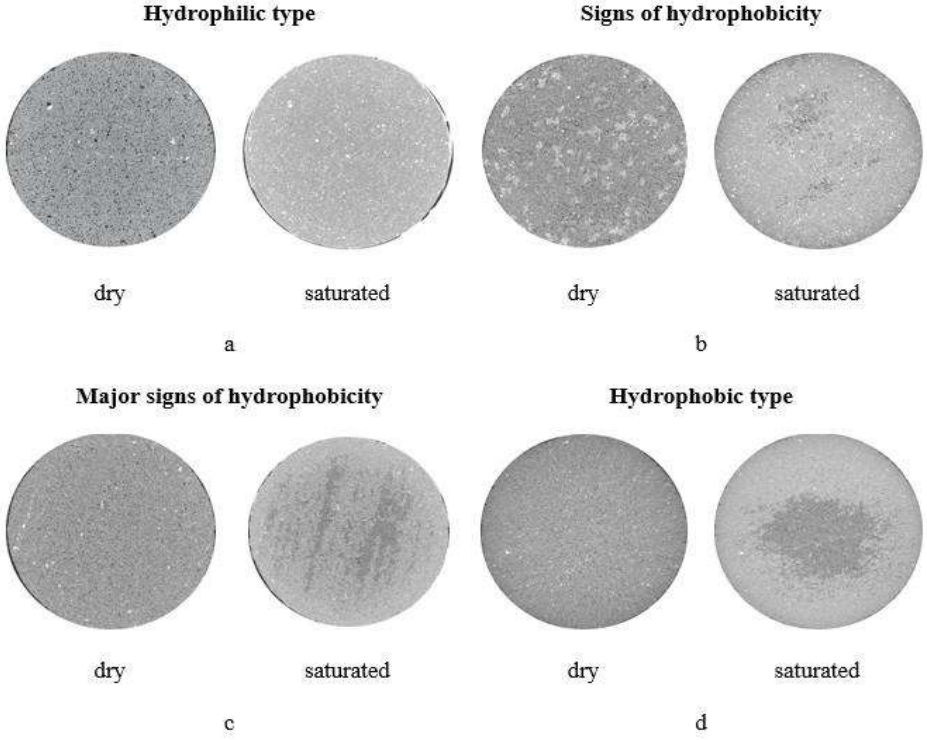


Fig. 1. X-ray tomograms of dry and NaI solution-impregnated sandstone cores with different wettability

Fig. 2a and 2b are log plots of the Visean interval from two wells in the Unvinskoye Field.

Increased values of resistivity from microlaterolog (R_{MBK}) are interpreted as intervals of bituminisation, represented in cores as dark-coloured (almost black) sandstones with reduced open porosity. These intervals are characterised by low value of GR log and are often included in recoverable oil reserves, although their real share in oil production is minimal.

Comparison of core X-ray tomography results with electrical logging data shows that the rocks are hydrophobic at resistivity over 200 ohm·m, and they practically do not take water at a resistivity over 600 ohm·m. At the same time "black sandstones" were encountered in less than 20% of the Perm region wells, that is why this problem has not been studied in detail so far. Fig. 2 shows the wells that penetrated dark grey to black bitumen-filled sandstones sampled by core.

In well A (Fig. 2a), the formations Bb1 and Bb2 are characterized by relatively low resistivity R_{BK} due to their hydrophilic nature. The only exception is the lowest interval with a thickness of 1 m (2048 m depth), for which resistivity exceeds 200 ohm·m in both BK and MBK. Thus, drilling mud does not enter this hydrophobic interval, and it can be interpreted as bituminous. Wettability assessment results from electrical logging is fully consistent with the core data analysis, including X-ray tomography. Except of the lowest interval with dark grey bituminised core, the rest are light grey sandstones of different grains. The Bb3 and Bb4 formations are interpreted as bitumen-saturated according to logs, as they have increased BK and MBK values. Moreover, the resistivity exceeds 1400 ohm·m for the Bb3 formation. Cores obtained from both formations are bituminised, and the entire Bb3 formation is represented by the classic “black sandstone” and Bb4 formation – by dark grey sandstone.

In well B (Fig.2b), the Bb2 formation reservoirs (2043 m depth) are characterised by relatively low BK and MBK readings and light grey core without signs of bituminisation. These intervals can be identified by the hydrophilic type of the oil-saturated sandstone. The upper part of the Bb3 formation (2049 m depth) is also made up of light core for which resistivity R_{BK} exceeds 200 ohm·m and R_{MBK} is greater than 100 ohm·m. Decreased MBK values show that drilling mud has entered the hydrophobic reservoir reducing the resistivity in the bottomhole zone. The bottoms of the Bb3 (2051 m depth) and the Bb4 formations are represented by dark bituminised core. These intervals have BK and MBK readings over 200 ohm·m. High MBK values in this case show that drilling fluid has not filtrated into the formation due to its bituminisation. Therefore, three possible cases of reservoirs with different wettability can be distinguished: (1) hydrophilic with reduced BK and MBK readings, (2) hydrophobic oil-saturated with high BK and low MBK readings, and (3) bituminous with high BK and MBK readings.

As a result of core analysis, it was found that all samples saturated with formation water have resistivity within the range of 0.6 to 4 ohm·m. The ratio of the studied samples to the permeable part of the section confirms the low values of the water-saturated samples. The low resistivity values in the water-saturated samples confirms their affinity to the permeable reservoir sections. The samples with residual water saturation show a dramatic core resistivity increase to 24 -1200 ohm·m.

Comparison of the core resistivity values with log resistivity shows positive correlation, as sandstone hydrophobisation universally reduces their conductivity. It should be noted that core preparation for laboratory experiments (extraction, heating etc.) affects resistivity measured, whereas shoulder effects, vertical resolution, and washouts can impact log resistivity data. Further complication results from the sample size discrepancies: inches in core samples versus meters in logs (Kerimov et al., 2020).

Interval resistivity from logs shows that in several cases abnormally high values were observed, in 53% of the cases they were exceeding 200 ohm·m and in 13% of the cases the reading were above 600 ohm·m. Core samples wettability results (CI) are compared with interval laterolog resistivity in Table 1.

For the intervals with R_{BK}< 30 ohm·m all X-ray tomography-studied core samples were assessed as hydrophilic (CI > 0.90). Cores with R_{BK} of up to 120 ohm·m were classified as mainly hydrophilic. At resistivity readings of 200-600 ohm·m most samples show some signs of hydrophobic behaviour with 0.5-0.9 CI range, whereas higher log resistivity mostly corresponds to samples with CI < 0.5, i.e., showing significant signs of hydrophobisity. Finally, two out of three samples with CI < 0.1 (hydrophobic) come from intervals with log resistivity above 1000 ohm·m.

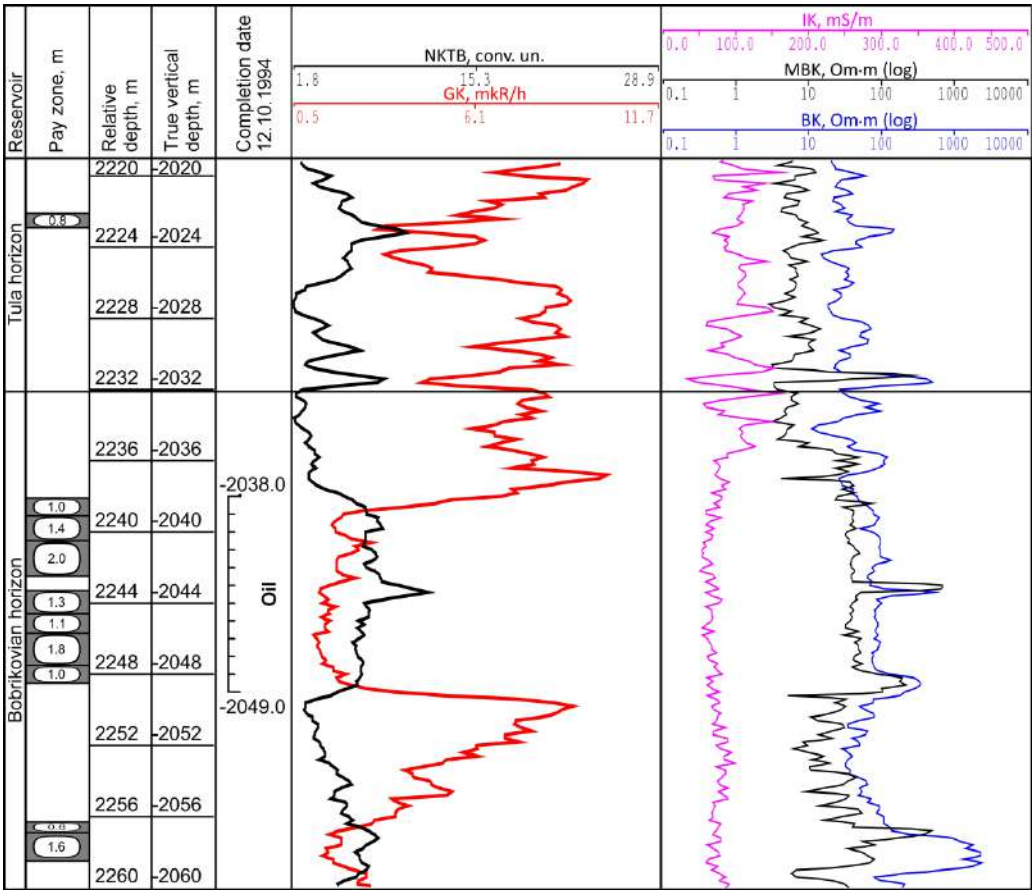
Therefore, the following criteria for the wettability classification of the oil-saturated Visean reservoirs can be formulated:

– in the intervals with R_{BK} below 120 ohm·m, the reservoirs are hydrophilic;

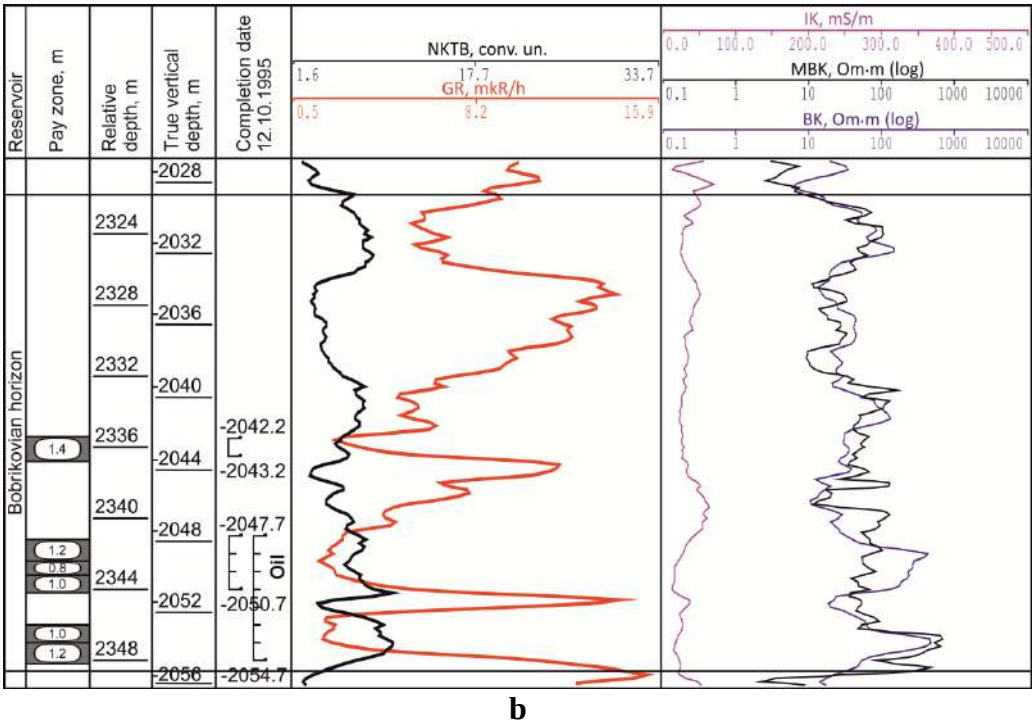
– in the R_{BK} range from 120-200 ohm·m, the wettability assessment is unclear;

– starting from R_{BK} over 200 ohm·m, reservoirs hydrophobisation processes start to manifest, rendering mostly hydrophobic reservoirs;

– at R_{BK} over 600 ohm·m, the reservoirs are totally hydrophobic.



a



b

Fig. 2. Log displays of two wells (a) and (b) from the Unvinskoye Field. Horizontal scales: NKTB – dual spacing thermal decay-time logging, conventional unit; GK – gamma-ray logging, μR/hour; IK – induction well logging, mS/m; BK – laterolog, Om·m; MBK – microlaterolog, Om·m

Table 1

Core wettability evaluation from X-ray tomography compared with corresponding interval resistivity from laterolog (BK). Number of cores in each category is shown.

Electrical resistivity from BK (R_{BK}) ohm·m	Impregnation coefficient (CI), unit fraction			
	<0,10	0,10-0,50	0,50-0,90	>0,90
<30	0	0	0	4
30-80	0	0	3	7
80-120	0	1	0	4
120-200	0	0	2	1
200-300	1	1	2	1
300-400	0	1	5	1
400-600	0	1	4	2
600-1000	0	1	1	0
>1000	2	0	2	0
Total	***3***	***5***	***19***	***20***

3.2. Reservoirs bituminisation evaluation from petrophysical core and electrical logs

Table 2 shows data on core bituminisation occurrence as compared to core open porosity (ϕ). All five samples with ϕ <12% show bituminisation, whereas all 22 samples with ϕ > 16% show none. Within 12-16% porosity range, bituminisation probability gradually decreases.

Table 2

Bitumen occurrence in core data set of 47 samples versus core porosity

Core porosity	Without bitumen	With bitumen	Total	Percentage of samples whith bitumen
below 12%	0	5	5	100
12% to 14%	3	6	9	66.6
14% to 16%	8	3	11	37,5
16% to 18%	4	0	4	0
18% to 20%	9	0	9	0
over 20%	9	0	9	0
Total	***33***	***14***	***47***	***29.8***

Petrophysical indicators of sandstone bituminisation obtained on core can only be useful if they can be also applied in log interpretation. To determine the error in wireline log-based open porosity (ϕwl) and irreducible water saturation (Swiwl) we used our core data and compared with the corresponding log interval averages. A combination of GR and Neutron logs was used to quantify ϕwl. The ϕwl = f (ϕc) dependence can be described by the positive linear function. In general, the correlation between them is positive, albeit not strong (r = 0.55). Nonetheless, it does show that log data on ϕwl can be feasible in reservoir bituminisation delineation. On the contrary, the comparison of residual water saturation in core (Swic) and log data (Swiwl) shows no correlation between them (r = 0.14). Therefore, the Swiwl indicator is excluded from further analysis.

Analysis of 68 oil-saturated sandstone intervals shows bituminisation in 21% of cases (14 out of 68). The complex log interpretation was available for almost the entire data set with a few exceptions for microlaterolog (MBK). Based on the joint analysis of core and wireline log-based petrophysical we established that bituminous content is practically excluded at a porosity ϕwl>16% (30 out of 31 intervals). Reservoirs bituminisation is most probable at ϕwl<12% (3 out of 4 intervals). In the ϕwl range from 12-16% reservoir bituminisation probability naturally decreases (Table 3).

Table 3

Bitumen occurrence in cores as compared to log porosity

Log porosity	Without bitumen	With bitumen	Total	Percentage of samples with bitumen
below 12%	1	3	4	75.0
12% to 14%	4	6	10	60.0
14% to 16%	19	4	23	17.3
16% to 18%	11	1	12	8.3
18% to 20%	12	0	12	0
over 20%	7	0	7	0
Total	***54***	***14***	***68***	***20.6***

Reservoirs bituminisation is not typical for hydrophilic reservoirs with R_{BK} below 60 ohm·m (13 out of 14 intervals) (Table 4).

Table 4

Bitumen occurrence in core and corresponding BK resistivity values

BK log ranges	Without bitumen	With bitumen	Total	Percentage of samples whith bitumen
below 60 ohm·m	13	1	14	7.1
60—120 ohm·m	13	3	16	18.7
120—200 ohm·m	6	4	10	40.0
200—600 ohm·m	15	5	20	25.0
over 600 ohm·m	5	1	6	16.7
Total	***52***	***14***	***66***	***21.2***

Analysis of the data presented in Table 5 suggests that low MBK values are characteristic of good mud filtrate penetration into the formation, which is a consequence of no reservoir bituminisation (at MBK < 10 ohm·m 18 out of 18 core show none). As

the MBK values grow, bituminisation probability gradually increases, and at MBK > 200 ohm·m bituminised core was found in 3 of 3 cases.

Table 5

Bitumen occurrence in core and corresponding MBK resistivity values

MBK log ranges	Without bitumen	With bitumen	Total	Percentage of samples whith bitumen
below10 ohm·m	18	0	18	0
10–30 ohm·m	13	3	16	18.7
30–100 ohm·m	6	3	9	33.3
100–200 ohm·m	2	3	5	40.0
Over 200 ohm·m	0	3	3	100
Total	***39***	***12***	***51***	***23.5***

The analysis of all the data suggests that open porosity is the key parameter controlling bituminisation. In absence of interval porosity data the bituminisation forecast may be unreliable. With consideration of the results obtained algorithms have been developed for reservoir bituminisation forecasting using a complex of radioactive and electrical logging methods. The bituminous content forecast algorithm of the intervals with oil-saturated reservoirs can be formulated as follows:

– $\phi wl < 12\%$ – pervasive bituminisation, $\phi wl \geq 16\%$ – no bituminisation,

– $R_{BK} < 60$ ohm·m – no bituminisation,

– $R_{MBK} < 15$ ohm·m – no bituminisation, $R_{MBK} \geq 200$ ohm·m – pervasive bituminisation,

– when $R_{BK} \geq 60$ ohm·m, $15 \leq R_{MBK} < 200$ ohm·m, and at ϕwl =12-14%, the intervals are assessed as bituminous, but for ϕwl = 14-16%, it is concluded that there is no bituminisation.

The forecast error when using this classification in field studies with the complete log data set is estimated as 4% (2 out of 50 intervals analysed). The error slightly increases when no MBK data is available (7 out of 65 intervals). In the absence of resistivity logs, the forecast error increases to 15% (7 out of 65 intervals). This clearly indicates that the most reliable prediction of reservoir bituminisation can be achieved when full set of wireline data is available.

3.3. Lateral distribution of wettability and bituminisation of oil-saturated sandstone reservoirs

Based on the formulated criteria and the results of 3D modelling, the calculation of hydrophobised and bituminised sections for the entire study area was carried out. Figs 3 and 4 show maps of the reservoir hydrophobisation and bituminisation built for two oil fields. Complete absence of hydrophobisation (bituminisation) in the maps is depicted with light grey colour, whereas dark color corresponds to the maximum hydrophobisation (bituminisation).

The Unvinskoye Field section is mainly characterized by high resistivity, allowing pervasive hydrophobisation being predicted (Fig. 3a). However, the western and central parts of the field are mainly characterised by high porosity reservoir sandstones, so that the bituminisation is limited. Intense bituminisation is forecasted in the eastern flank of the field (Fig. 3b), where reservoirs with low porosity are localized. Core data from the Unvinskoye Field confirm that oil-saturated reservoir bituminisation is typical for it. In 9 cases out of 18 analysed intervals bitumen was found in the core (Gurbanov et al., 2022).

The wettability zonation in the Sukharevskoye Field section shows the hydrophobised reservoir areas localize in the crestal part of the structure, whereas the hydrophilic section is predicted in the northern part of the structure (Fig. 4a).

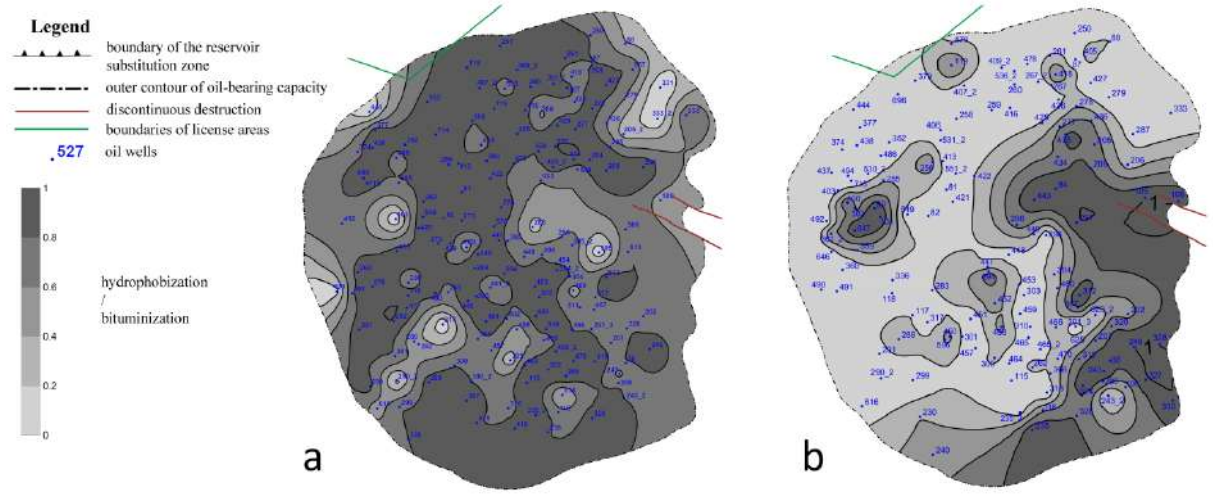


Fig. 3. Reservoir hydrophobisation (a) and bituminisation (b) maps of the Bb Formation, Unvinskoye Field

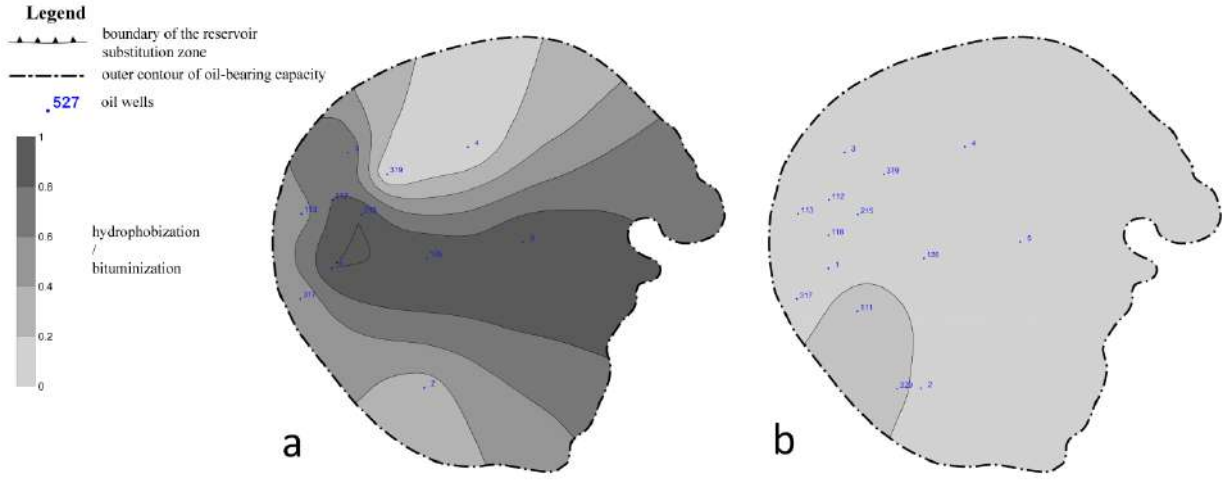


Fig. 4. Reservoir hydrophobisation (a) and bituminisation (b) maps of the Bb Formation, Sukharevskoye Field

Nonetheless, the bituminisation prediction of the crestal zone is unlikely, as it is characterised by high reservoir porosity. Core data from the Sukharevskoye Field reveal no bituminisation, as any signs of bituminisation were detected in any of the 28 sampled intervals.

4. Discussion

The results of identifying zones of hydrophobic and bituminous reservoirs can be used when planning measures to increase oil production. Under such conditions, the implementation of standard water flooding of reservoirs may be ineffective due to hydrophobisation of the rocks. According to the experience, proppant hydraulic fracturing can be proposed for the study area in areas of highly porous reservoirs with high potential production rates (Votinov et al., 2018; Zhang et al., 2019; Galkin et al., 2022)., Hydraulic fracturing can be economically ineffective for bituminous rocks, due to high costs; in such conditions, radial drilling technology can be recommended (Kochnev et al., 2018; Reinsch et al., 2018; Galkin et al., 2019).

Abnormally high resistivity of oil-saturated reservoirs of the Perm region is considered to be related to their wettability alteration (hydrophobisation) and bituminisation. To predict these processes, both core and log data must be jointly analysed. High porosity measured in cores and log data interpretation is indicative of hydrophilic sandstone reservoir, whereas low porosity and relatively high resistivity are the most reliable indicators of wettability changes resulting in bituminisation. We demonstrate that log porosity and resistivity data can be successfully used in developing algorithms, when applied to field data, can be instrumental in building wettability and bituminisation maps of the main fields. These maps can be further utilized in building 3D reservoir models and in optimization of the secondary recovery operations in the field.

5. Conclusions

As a result of the studies, it was found that according to the data of combining the methods of lateral and microlateral electric logging, the areas of development of bituminisation and hydrophobisation of reservoirs can be identified. The operation of injection wells in such areas is often characterised by reduced injectivity, which makes standard flooding ineffective. One of the ways to optimise injection is to create relatively long highly conductive channels that allow increasing the degree of reservoir sweep by the displacement process, which can be solved by using radial drilling technology. Under the conditions of development of hydrophobic sandstones, the alkaline flooding technology can also be considered promising, which can lead to an increase in oil mobility due to the removal of rock of poorly soluble substances. Thus, for reservoir hydrophobisation development zones established according to the developed method, a number of promising reservoir stimulation technologies can be recommended.

Funding: The research was funded by the Ministry of Science and Higher Education of the Russian Federation (Project No. FSNM-2023-0005).

Acknowledgments: The tomography of core samples was carried out on a unique scientific installation "Complex for studying the structure of the reservoir space of rocks" of the collective use centre "Centre for the reservoir properties of rocks" of the Perm National Research Polytechnic University.

Conflicts of Interest: The authors declare no conflict of interest. The funders had no role in the design of the study; in the collection, analyses, or interpretation of data; in the writing of the manuscript, or in the decision to publish the results.

REFERENCES

Berg S, Armstrong R, Ott H, Georgiadis A et al (2014) Multiphase flow in porous rock imaged under dynamic flow conditions with fast X-ray computed microtomography. Petrophysics 55(4):304–312

Bultreys T, Boone MA, Boone MN et al (2016) Fast laboratory-based micro-computed tomography for pore-scale research: Illustrative experiments and perspectives on the future. Advances in water resources 95:341–351

Dixit AB, Buckley JS, McDougall SR et al (2000) Empirical measures of wettability in porous media and the relationship between them derived from pore-scale modelling. Transp Porous Media 40(1):27–54

D'jakonova TF, Bata LK, Gurbatova IP (2021) The electrical resistivity of rocks according to logging is an independent diagnostic indicator for the identification of non-hydrophilic reservoirs in a productive formation, Karotazhnik 3(309):66–75 (in Russian)

Efimov AA, Galkin SV, Savitckii IaV, Galkin VI (2015) Estimation of heterogeneity of oil and gas field carbonate reservoirs by means of computer simulation of core X-ray tomography data. Ecology, Environment and Conservation 21(Nov):79–85

Efimov AA, Savitskii IaV, Galkin SV et al (2016) Study of wettability of reservoirs of oil fields by the method of X-ray tomography cores. Neftegaz GNKAR 4(4):55–63. https:// doi.org/10.5510/OGP20160400298

Galkin SV, Savitskiy YV, Osovetsky BM et al (2022) Detailed study of hydraulic fracturing of kashiro-verey rocks by electron microscopy. ANAS Transactions, Earth Sciences 1:17–27

Galkin SV., Kochnev AA., Zotikov VI (2019) Estimate of radial drilling technology efficiency for the bashkir operational oilfields objects of Perm Krai. Journal of Mining Institute 238:410–414. https:// doi.org/: 10.31897/PMI.2019.4.410 (in Russian)

Gurbanov VSh, Hasanov AB, Abbasova GG (2019) The stochastic character of distribution of granulometric content and fractality of porous structure in oil reservoirs. ANAS Transactions, Earth Sciences 2:54–60

Gurbanov VSh, Galkin SV, Narimanov NR et al (2021) Petrophysical characteristics of the Meso-Cenozoic deposits of the South-Eastern subsidence of the Greater Caucasus in connection with their oil and gas potential. SOCAR Proceedings 3:9–21. https://doi.org/10.5510/OGP20210300524

Gurbanov VSh, Hasanov AB, Abbasova GG (2022) Breakthrough technologies in solving problems of geological exploration for oil and gas. SOCAR Proceedings 1:84–89 (in Russian)

Gurbanov VSh, Narimanov NR (2019) Forecast of oil and gas potential of the basement of the South Caspian megadepression. Proceedings of the International Scientific and Practical Conference, Kazan, 1-2 September, p 37-39 (in Russian)

Gurbanov VSh, Sultanov LA, Babaev MS, Mustaev RN (2020) Geological structure and results of petrophysical studies of the deposits of the Pliocene strata of the Baku Archipelago. Mining Journal, Moscow 8(2277):51–55 (in Russian)

Gurbatova IP, Melekhin SV, Chizhov DB, Fairuzova IuV (2016) Features of study complex carbonate reservoir rocks`wetting using laboratory methods. Bulletin of PNRPU, Geology, Oil and Gas Engineering and Mining 15(20):240–245. https://doi.org/10.15593/2224-9923/2016.20.4 (in Russian)

Hasanov AB, Gurbanov VSh, Abbasova GG (2022) Variations in reservoir properties of productive horizons of offshore fields in Azerbaijan. Russia Mining Journal, Moscow, 12:10–15 (in Russian)

Johnson DL, Koplik J, Dashen R (2006) Theory of dynamic permeability and tortuosity in fluid-saturated porous media. Journal of Fluid Mechanics 176(1):379–402

Kerimov VYu, Gasanov AB, Gurbanov VSh, Abbasova GG (2020) Petrophysical characteristic of deep oil and gas reservoirs in inland and offshore fields in Azerbaijan. Eurasian Mining 1:3–8

Kochnev AA, Zotikov VI, Galkin SV (2018) Analysis of the influence of geological technological parameters on the effectiveness of radial drilling technology on the example of operational objects in Perm region. Bulletin of the Tomsk Polytechnic University, Geo Assets Engineering 329(12):20–29 (in Russian)

Leach RO, Wagner OR, Wood HW, Harpke CF (1962) A laboratory and field study of wettability adjustment in water flooding. J Petrol Technol 14(2):206–212. https://doi.org/10.2118/119-PA

Milliken KL, Curtis ME (2016) Imaging pores in sedimentary rocks: Foundation of porosity prediction. Marine and Petroleum Geology 73(C):590–608

Mukhametshin RZ, Galeev AA (2014) Diagnostics of ancient oil-water contacts by instrumental methods. Oil industry 10:28–33 (in Russian)

Reinsch T, Paap B, Hahn S et al (2018) Insights into the radial water jet drilling technology – Application in a quarry. Journal of Rock Mechanics and Geotechnical Engineering 10(2):236–248

Rozhkova YuA, Gurbanov VS, Efendiyev GM, Galkin SV (2022) Assessment of applicability of preformed particle gels for Perm region oil fields. IOP Conference Series: Earth and Environmental Science 1021(1):012073. https:// doi.org/10.1088/1755-1315/1021/1/012073

Salah Al-Ofi et al (2017) Influence of rock wettability alteration on dielectric dispersion data. Paper presented at the SPE Kingdom of Saudi Arabia Annual Technical Symposium and Exhibition, Dammam, Saudi Arabia, April 2017. Paper Number SPE-188028-MS. https://doi.org/10.2118/188028-MS

Salah Al-Ofi et al (2018) Technical Presentation: Correlating Dielectric Dispersion Data and Wettability Index of Carbonate Rock, SPE Kingdom of Saudi Arabia Annual Technical Symposium and Exhibition, Dammam, Saudi Arabia, April 23-26, Paper Number SPE-192224-MS. https://doi.org/10.2118/192224-MS

Votinov AS, Drozdov SA, Malysheva VL, Mordvinov VA (2018) Recovery and increase of the productivity of wells of Kashirskiy and Podolskiy reservoirs of the certain Perm region oil field. Perm Journal of Petroleum and Mining Engineering 18(2):140–148. https://doi.org/10.15593/2224-9923/2018.4.4

Wagner OR, Leach RO (1959) Improving oil displacement efficiency by wettability adjustment. Trans AIME 216(01):65–72. https://doi.org/10.2118/1101-G

Zhang G, Zhang Y, Xu A, Li Y (2019) Microflow effects on the hydraulic aperture of single rough fractures. Advances in GeoEnergy Research 3(1):104–114. https://doi.org/10.26804/ager.2019.01.09

ВОЗМОЖНОСТИ ОБНАРУЖЕНИЯ СМАЧИВАЕМОСТИ И БИТУМИЗАЦИИ КОЛЛЕКТОРОВ ПО КОМПЛЕКСНЫМ ПЕТРОФИЗИЧЕСКИМ ДАННЫМ КЕРНА/КАРОТАЖА

Галкин С.В.[1], Колычев И.Ю.[2], Савицкий Ю.В.[3*], Шумилов А.В.[4], Гурбанов В.Ш.[5,6], Г.Г. Аббасова[7]
[1-4]Пермский национальный исследовательский политехнический университет, Россия
614990, Пермь, Комсомольский просп., 29
[5]Министерство науки и образования Республики Азербайджан, Институт нефти и газа, Азербайджан
AZ1000, Баку, ул. Ф. Амирова, 9
[6]Бакинский государственный университет, Азербайджан
AZ1148, Баку, ул. акад. Захида Халилова, 33
[7]Азербайджанский государственный университет нефти и промышленности, Азербайджан
AZ1010, Баку, просп. Азадлыг, 20
**Автор, отвечающий за переписку: yansavitsky@yandex.ru*

Резюме. Для некоторых нефтенасыщенных интервалов визейских отложений Пермского края по каротажу установлено аномально высокое электрическое сопротивление, что можно объяснить гидрофобизацией и битумизацией коллекторов. Оценка данных параметров проведена путем сопоставления петрофизических и геофизических исследований по ряду эксплуатационных объектов. Для оценки смачиваемости применена рентгеновская томография керна, результаты которой сравнивались с данными бокового электрического каротажа. Сравнение результатов рентгеновской томографии керна с данными электрического каротажа показывает, что при удельном сопротивлении более 200 Ом·м породы являются гидрофобными, а при значениях более 600 Ом·м практически не впитывают воду. Битумизация коллекторов оценивалась по данным исследований керна, что сопоставлялось с результатами определения пористости по гамма-каротажу, а также с удельным электрическим сопротивлением по боковому и микробоковому каротажу. Мы демонстрируем, что данные о пористости и удельном сопротивлении могут быть использованы при разработке алгоритмов, построении карт смачиваемости и битумизации основных месторождений. Эти карты могут быть далее использованы при построении трехмерных моделей пластов и оптимизации операций вторичного извлечения на месторождении. Анализ всех данных показывает, что открытая пористость является ключевым параметром, контролирующим битумизацию. С учетом проведенного анализа разработаны алгоритмы прогнозирования битумизации коллекторов на основе комплекса геофизических исследований скважин. Результаты разработанного метода применены при цифровом геолого-технологическом моделировании нефтяных месторождений с различными типами смачиваемости и битумизации. Также результаты выявления зон гидрофобных и битуминозных коллекторов могут быть использованы при планировании мероприятий по повышению нефтеотдачи.

Ключевые слова: *гидрофобизация, смачиваемость, битумизация, пористость, удельное электрическое сопротивление горных пород, рентгеновская томография керна, боковой электрический каротаж, микробоковой каротаж*

KERN/KAROTAJIN KOMPLEKS PETROFİZİKİ MƏLUMATLARINA GÖRƏ KOLLEKTORLARIN BİTUMLAŞMASININ VƏ İSLANMASININ MÜƏYYƏN EDİLMƏSİ İMKANLARI

Qalkin S.V.[1], Kolychev I.Y.[2], Savitsky Y.V.[3*], Şumilov A.V.[4], Qurbanov V.Ş.[5,6], Abbasova Q.Q.[7]
[1-4]Perm Milli Tədqiqat Politexnik Universiteti, Rusiya
614990, Perm, Komsomolski prosp., 29
[5]Azərbaycan Respublikasının Elm və Təhsil Nazirliyi, Neft və Qaz İnstitutu, Azərbaycan
AZ1000, Bakı, F.Əmirov küç., 9
[6]Bakı Dövlət Universiteti, Azərbaycan
AZ1148, Bakı, akad. Zahid Xəlilov küç., 33
[7]Azərbaycan Dövlət Neft və Sənaye Universiteti, Azərbaycan
AZ1010, Bakı, Azadlıq prosp., 20
**Yazışmalara məsul:yansavitsky@yandex.ru*

Xülasə. Quyuların karotaj məlumatlarından istifadə etməklə Perm diyarının Visean yataqlarının bəzi neftlə doymuş intervallarında anomal yüksək elektrik müqaviməti aşkar edilmişdir. Bu, anbarların hidrofobizasiyası və bitumlaşması ilə izah edilə bilər. Bu parametrlər bir sıra hasilat hədəfləri üçün petrofiziki və geofiziki tədqiqatların müqayisəsi yolu ilə qiymətləndirilmişdir. Nəmlənmə qabiliyyətini qiymətləndirmək üçün əsas rentgen tomoqrafiyası istifadə edildi, nəticələri yanal elektrik qeydləri ilə müqayisə edildi. Əsas rentgen tomoqrafiyasının nəticələrinin elektrik qeydiyyatı məlumatları ilə müqayisəsi göstərir ki, müqaviməti 200 Ohm·m-dən çox olan süxurlar hidrofobikdir, 600 Ohm·m-dən çox olduqda isə onlar demək olar ki, heç bir su qəbul etmirlər. Rezervuarın bitumlaşdırılması əsas məlumatlardan istifadə edilməklə qiymətləndirilmişdir, bu məlumatlar qamma şüaları ilə qeydiyyatdan istifadə etməklə məsaməliliyin təyini ilə, eləcə də yanal və mikroquyuların girişindən istifadə etməklə müəyyən edilmiş elektrik müqaviməti ilə müqayisə edilmişdir. Biz nümayiş etdiririk ki, məsaməlilik və müqavimət məlumatlarından əsas sahələr üçün alqoritmlər hazırlamaq və nəmlənmə qabiliyyəti və bitum xəritələrini qurmaq üçün istifadə etmək olar. Bu xəritələr daha sonra 3D rezervuar modellərinin qurulması və yataqda ikinci bərpa əməliyyatlarının optimallaşdırılması üçün istifadə oluna bilər. Bütün məlumatların təhlili göstərir ki, açıq məsaməlilik bitum əmələ gəlməsinə nəzarət edən əsas parametrdir. Bu təhlil əsasında quyuların karotaj məlumatlarının hərtərəfli toplusu əsasında lay bitumunun əmələ gəlməsinin proqnozlaşdırılması üçün alqoritmlər hazırlanmışdır. İşlənib hazırlanmış metodun nəticələri müxtəlif nəmlilik və bitum əmələgəlmə növlərinə malik neft yataqlarının rəqəmsal geoloji və texnoloji modelləşdirilməsinə tətbiq edilmişdir. Bundan əlavə, hidrofobik və bitumlu lay zonalarının müəyyən edilməsi gücləndirilmiş neftçıxarma tədbirlərinin planlaşdırılmasında istifadə edilə bilər.

Açar sözlər: *hidrofobizasiya, nəmlənmə qabiliyyəti, bitumlaşma, məsaməlilik, süxurların elektrik müqaviməti, rentgen nüvəli tomoqrafiya, Lateroloq, mikrolateroloq*

ANAS Transactions Earth Sciences 2 / 2025

http://www.journalesgia.com

REDUCTION OF THE FRACTIONAL DIFFERENTIAL MODEL OF FLAT-RADIAL FLUID FLOW IN A FRACTAL MEDIUM TO A SECOND-KIND FREDHOLM EQUATION

Aliyev N.A.[1], Rasulov M.A.[2*], Jalalov G.I.[2], Sinsoysal B.[3], Xanbabayeva M.H.[2]

[1]Baku State University, Faculty of Applied Mathematics and Cybernetics, Azerbaijan
23, acad. Zahid Khalilov str., Baku AZ1148
[2]Ministry of Science and Education of the Republic of Azerbaijan,
Institute of Oil and Gas, Azerbaijan,
9, Fikret Amirov str., Baku, AZ1000
[3]Istanbul Beykent University, Faculty of Engineering and Architecture,
Department of Computer Engineering, Turkey
34396, Sariyer, Istanbul
**Corresponding author: mresulov@gmail.com*

Keywords: *mass transfer in fractal media, non-stationary diffusion equation in the plane-radial region, the Laplace transform, a Volterra integral equation of the second kind with a regular kernel, the method of successive substitution*

Summary. Over the last decade, interest in the theory of mass transfer in fractal media stems from geophysical and experimental data demonstrating the non-linearity of porous media, including their block structure and fractal properties. In such media, the filtration process, even for homogeneous mixtures, is modelled by non-integer-order differential equations, complicating theoretical research. In this paper, a solution is constructed for the fractional-order non-stationary diffusion equation describing the plane-radial motion of single-phase fluids in fractal porous media. To solve the reduced spectral problem for the derivative of the Laplace transform function, a Volterra integral equation of the second kind with a regular kernel is derived. For this integral equation, a resolvent in the form of a rapidly converging series is obtained by successive substitution. A necessary condition for the convergence of the series is found, and an analytical expression for the derivative of the Laplace transform of the desired pressure function is obtained. By integrating the resulting analytical expression for the Laplace transform with respect to the spatial variable, an integral representation is found. Finally, by applying the inverse Laplace transform, an expression for the dynamic distribution of the desired pressure function is obtained. The resulting expression, firstly, allows one to study the problem of unsteady fluid flow in a radial medium of fractal nature, and secondly, also answers the question of the existence and uniqueness of the problem under consideration. Using numerical integration methods, one can calculate the values of the pressure function at any point r and any time t, with an error estimate. Furthermore, the obtained results allow one to evaluate the solution found using approximate methods.

© 2025 Earth Science Division, Azerbaijan National Academy of Sciences. All rights reserved.

Introduction

In many fields of science and technology, the application of the theory of fractals, which describes the laws of irregular heterogeneous environments new research directions have begun to intensively develop. Many scientific sources in the literature are devoted to the statistical classification of porous media with fractal character. In this classification, either the pore space, or the rock (collector), or the surface of the pore system, or the volume of the liquid filling the porous medium can be considered fractal (Afonin, Sukhinov, 2009; Barabanov, 2016; Belevtsev, Lukashchuk, 2020; Gazizov, Lukashchuk, 2017; Nigmatullin, 1986), laboratory experiments show that the sand-clay medium has a fractal nature and the fractal dimension can vary from 2.6 to 2.8.

The equations involved in this process are described by means of a fractional form ordinary or partial differential equation or a system of equations. In addition to being an unusual differential equation, fractional differential equations reveal an unexpected simplicity in revealing the essence of many natural phenomena – complex systems found in

modern physics, mechanics, biology, chemistry, engineering, etc.

Fractional differential equations are not only a unique type of differential equation, but they also exhibit a surprising simplicity in capturing the essence of many natural phenomena including intricate systems found in contemporary physics, mechanics, biology, chemistry, engineering, and other fields. In this regard, fractional derivative and differential calculus has recently become a rapidly developing field of mathematical analysis.

R.R.Nigmatullin showed that the diffusion process in media with a "Koch tree" type fractal structure is described by a generalised

$$\frac{\partial^{\alpha} c_1(x,t)}{\partial t^{\alpha}} = D_1 \frac{\partial^2 c_1(x,t)}{\partial x^2}$$

equation of motion in special derivatives, and this model can serve as a model of a porous medium in which the diffusion process occurs. Here, D_1 is a positive constant characterising the flow and the medium. From this model, a fractional derivative relaxation equation related to the fractal dimension of the medium can also be obtained (Afonin, Sukhinov, 2009; Mirzadzhanzade et.al., 2004).

As it is known in the literature, this aspect, whose geometric structure retains its basic properties while considering at different length scales, i.e., it has the property of self-similarity, has found application in the geosciences including the solution of oilfield development problems, and development work continues. The application of models expressed by fractional order equations allows the development of general methods modeling flow processes in porous media with complex inhomogeneous permeability and facilitates the consideration of the influence of physical processes occurring in these media.

The filtration process in fractured media usually occurs under anomalous kinetic conditions, i.e. it does not obey normal Gaussian statistics. The presence of cracks in a porous medium creates a nonlocal effect due to spatial variation. Sometimes cracks are formed as a result of explosions in the beds and cause severe inhomogeneities (Mirzadzhanzade et.al., 2004).

In the case of fractal-like fractures around the well, fluid filtration can be accomplished not by classical Darcy's law but by means of a modified, i.e. fractional order derivative.

In the case of radial flow, the modified Darcy's law is expressed by

$$w = -\frac{k_{\nu}}{\mu} D^{\nu}_{r_w+} p(r,t),\ \nu \in (0,1), \qquad (1)$$

(Barabanov, 2016; Gazizov, Lukashchuk, 2017). Here w is the filtration velocity, p is the pressure, k_{ν} is the fractional analog of permeability, μ is the viscosity of the fluid, r is the distance from the center of the well, t is the time variable and

$$D^{\nu}_{r_w+} p(r,t) = \frac{1}{\Gamma(1-\nu)} \frac{d}{dr} \int_{r_w}^{r} \frac{p(\rho,t)d\rho}{(r-\rho)^{\nu}},$$

(Kilbas et al., 2006; Oldham, Spanier, 1974; Podlubny, 1999; Samko et al., 1993).

If we substitute expression (1) into the classical

$$\frac{\partial(\phi\rho)}{\partial t} + \text{div}\,(\rho w) = q,$$

continuity equation, we get

$$\frac{\partial p(r,t)}{\partial t} = a_{\nu} \frac{1}{r} \frac{\partial}{\partial r} \left[r\, D^{\nu}_{r_w+} p(r,t) \right] + q,$$
$$0 < r_w < r < r_c,\ t > 0. \qquad (2)$$

Here, r_w and r_c are constants that describe the contour of the well and the bed in the reservoir, respectively. $a_{\nu} = \frac{k_{\nu}}{\mu\, \phi c_f}$ is a positive constant coefficient, ϕ is the porosity, q is the source function, and $\rho = \rho(p)$ is the classical equation of state. Previously, let us first consider the case where k_{ν}, μ and ϕ are constant.

Now, let's investigate the solution of equation (2) under the following conditions

$$p(r,0) = p_0(r), \qquad (3)$$

$$p(r_w,t) = p_w(t),\ p(r_c,t) = p_c(t), \qquad (4)$$

where, $p_0(r)$, $p_w(t)$ and $p_c(t)$ are known continuous functions. Equation (2) was studied in (Aliyev et al., 2023) in the case of rectilinear fluid flow in a porous medium with fractal nature and when the pressure function p does not depend on t (Suleymanov et al., 2005).

Converting the differential problem into the integral equation

It can be expressed equation (2) as

$$D_t p(r,t) = \frac{a_{\nu}}{r} \left(rD\, D^{\nu}_{r_w+} p(r,t) + D^{\nu}_{r_w+} p(r,t) \right) + q,$$
$$t \in (0,\infty), r \in (r_w, r_c) \qquad (5)$$

using the notation $D. = \frac{\partial .}{\partial r}$. Applying the Laplace transform

$$\tilde{p}(r,\lambda)=\int_0^{\infty} e^{-\lambda t}p(r,t)dt$$

to both sides of equation (5), we get

$$D_{r_{w+}}^{1+\nu}\tilde{p}(r,\lambda)+\frac{1}{r}D_{r_{w+}}^{\nu}\tilde{p}(r,\lambda)-\frac{\lambda}{a_\nu}\tilde{p}(r,\lambda)=-F(r,\lambda), \quad (6)$$

where

$$F(r,\lambda)=\frac{p_0(r)+\tilde{q}(r,\lambda)}{a_\nu},$$
$$D_{r_{w+}}^{\nu}\tilde{p}(r,\lambda)=\frac{1}{\Gamma(1-\nu)}\frac{d}{dr}\int_{r_w}^{r}\frac{\tilde{p}(\rho,\lambda)d\rho}{(r-\rho)^{\nu}}. \quad (7)$$

If we apply operator

$$I_{r_{w+}}^{\nu}(\cdot)=\frac{1}{\Gamma(\nu)}\int_{r_w}^{r}\frac{(\cdot)}{(r-\rho)^{1-\nu}}d\rho \quad (8)$$

to both sides of equation (6), we obtain

$$D_{r_{w+}}^{1}\tilde{p}(r,\lambda)+I_{r_{w+}}^{\nu}\left(\frac{1}{r}D_{r_{w+}}^{\nu}\tilde{p}(r,\lambda)\right)-$$
$$-\frac{\lambda}{a_\nu}I_{r_{w+}}^{\nu}\left(\tilde{p}(r,\lambda)\right)+C_1\frac{r^{\nu-1}}{(\nu-1)!}=$$
$$=-I_{r_{w+}}^{\nu}\left(F(r,\lambda)\right)+D_{r_{w+}}^{1}\widetilde{p'}(r,\lambda)\big|_{r=r_w}. \quad (9)$$

Using the relation

$$\int_{r_w}^{r}\frac{(r-\rho)^{-\nu}}{(-\nu)!}\tilde{p}(\rho,\lambda)d\rho=\tilde{p}(r_w,\lambda)\frac{(r-r_w)^{1-\nu}}{(1-\nu)!}+$$
$$+\int_{r_w}^{r}\frac{(r-\rho)^{1-\nu}}{(1-\nu)!}\widetilde{p'}(\rho,\lambda)d\rho,$$

we can express (7) as

$$D_{r_{w+}}^{\nu}\tilde{p}(r,\lambda)=\tilde{p}(r_w,\lambda)\frac{(r-r_w)^{-\nu}}{(-\nu)!}+$$
$$+\int_{r_w}^{r}\frac{(r-\rho)^{-\nu}}{(-\nu)!}\widetilde{p'}(\rho,\lambda)d\rho.$$

In this instance, (9) takes on the following form

$$D_{r_{w+}}^{1}\tilde{p}(r,\lambda)+I_{r_{w+}}^{\nu}\left(\frac{1}{r}\int_{r_w}^{r}\frac{(r-\rho)^{-\nu}}{(-\nu)!}\widetilde{p'}(\rho,\lambda)d\rho\right)-$$
$$-\frac{\lambda}{a_\nu}I_{r_{w+}}^{\nu}\left(\tilde{p}(r,\lambda)\right)=-C_1\frac{r^{\nu-1}}{(\nu-1)!}-$$
$$-I_{r_{w+}}^{\nu}\left(\frac{1}{r}\tilde{p}(r_w,\lambda)\frac{(r-r_w)^{-\nu}}{(-\nu)!}\right)-$$
$$-I_{r_{w+}}^{\nu}\left(F(r,\lambda)\right)+D_{r_{w+}}^{1}\widetilde{p'}(r,\lambda)\big|_{r=r_w}. \quad (10)$$

Let's consider the

$$J_1=I_{r_{w+}}^{\nu}\left(\frac{1}{r}\int_{r_w}^{r}\frac{(r-\rho)^{-\nu}}{(-\nu)!}\widetilde{p'}(\rho,\lambda)d\rho\right),$$
$$J_2=\frac{\lambda}{a_\nu}I_{r_{w+}}^{\nu}\left(\tilde{p}(r,\lambda)\right)$$

expressions included in the equation (10). According to the definition of the integral, we can write J_1 as

$$J_1=I_{r_{w+}}^{\nu}\left(\frac{1}{r}\int_{r_w}^{r}\frac{(r-\rho)^{-\nu}}{(-\nu)!}\widetilde{p'}(\rho,\lambda)d\rho\right)=$$
$$=\int_{r_w}^{r}\frac{(r-\eta)^{\nu-1}}{(\nu-1)!}d\eta\frac{1}{\eta}\int_{r_w}^{\eta}\frac{(\eta-\rho)^{-\nu}}{(-\nu)!}\widetilde{p'}(\rho,\lambda)d\rho=$$
$$=\int_{r_w}^{r}\widetilde{p'}(\rho,\lambda)d\rho\int_{\rho}^{r}\frac{1}{\eta}\frac{(r-\eta)^{\nu-1}}{(\nu-1)!}\frac{(\eta-\rho)^{-\nu}}{(-\nu)!}d\eta. \quad (11)$$

Using the equation

$$\tilde{p}(\rho,\lambda)=\int_{r_w}^{\rho}\widetilde{p'}(\eta,\lambda)d\eta+\tilde{p}(r_w,\lambda),$$

for J_2 we have

$$J_2=\frac{\lambda}{a_\nu}\int_{r_w}^{r}\frac{(r-\rho)^{\nu-1}}{(\nu-1)!}d\rho\left[\int_{r_w}^{\rho}\widetilde{p'}(\eta,\lambda)d\eta+\tilde{p}(r_w,\lambda)\right]=$$
$$=\frac{\lambda}{a_\nu}\int_{r_w}^{r}\frac{(r-\rho)^{\nu-1}}{(\nu-1)!}d\rho\int_{r_w}^{\rho}\widetilde{p'}(\eta,\lambda)d\eta+$$
$$+\frac{\lambda}{a_\nu}\int_{r_w}^{r}\frac{(r-\rho)^{\nu-1}}{(\nu-1)!}\tilde{p}(r_w,\lambda)d\rho=$$
$$=\frac{\lambda}{a_\nu}\int_{r_w}^{r}\widetilde{p'}(\eta,\lambda)d\eta\int_{\eta}^{r}\frac{(r-\rho)^{\nu-1}}{(\nu-1)!}d\rho+J_3, \quad (12)$$

where

$$J_3=\frac{\lambda}{a_\nu}\int_{r_w}^{r}\frac{(r-\rho)^{\nu-1}}{(\nu-1)!}\tilde{p}(r_w,\lambda)d\rho.$$

Substituting (11) and (12) into (10) yields

$$D^1_{r_w+}\tilde{p}(r,\lambda)+\int_{r_w}^{r}\widetilde{p'}(\rho,\lambda)d\rho\left[\int_{\rho}^{r}\frac{1}{\eta}\frac{(r-\eta)^{\nu-1}}{(\nu-1)!}\frac{(\eta-\rho)^{-\nu}}{(-\nu)!}d\eta-\frac{\lambda}{a_\nu}\int_{\rho}^{r}\frac{(r-\eta)^{\nu-1}}{(\nu-1)!}d\eta\right]=$$

$$=-C_1\frac{r^{\nu-1}}{(\nu-1)!}+\frac{\lambda}{a_\nu}\int_{r_w}^{r}\frac{(r-\rho)^{\nu-1}}{(\nu-1)!}\tilde{p}(r_w,\lambda)d\rho-I^{\nu}_{r_w+}\left(\frac{1}{r}\tilde{p}(r_w,\lambda)\frac{(r-r_w)^{-\nu}}{(-\nu)!}\right)-$$

$$-I^{\nu}_{r_w+}\big(F(r,\lambda)\big)+D^1_{r_w+}\widetilde{p'}(r,\lambda)\big|_{r=r_w}. \tag{13}$$

Some integrals in the last equation can be calculated as follows:

$$\int_{\rho}^{r}\frac{(r-\eta)^{\nu-1}}{(\nu-1)!}d\eta=-\frac{1}{(\nu-1)!}\int_{\rho}^{r}(r-\eta)^{\nu-1}\,d(r-\eta)=\frac{(r-\rho)^{\nu}}{\nu!},$$

$$\frac{\lambda}{a_\nu}\int_{r_w}^{r}\frac{(r-\eta)^{\nu-1}}{(\nu-1)!}\tilde{p}(r_w,\lambda)\,d\eta=\frac{\lambda}{a_\nu}\tilde{p}(r_w,\lambda)\frac{(r-r_w)^{\nu}}{\nu!},$$

$$J_4=I^{\nu}_{r_w+}\left(\frac{1}{r}\tilde{p}(r_w,\lambda)\frac{(r-r_w)^{-\nu}}{(-\nu)!}\right)=\int_{r_w}^{r}\frac{(r-\eta)^{\nu-1}}{(\nu-1)!}\frac{1}{\eta}\tilde{p}(r_w,\lambda)\frac{(\eta-r_w)^{-\nu}}{(-\nu)!}d\eta=$$

$$=\tilde{p}(r_w,\lambda)\int_{r_w}^{r}\frac{(r-\eta)^{\nu-1}}{(\nu-1)!}\frac{1}{\eta}\frac{(\eta-r_w)^{-\nu}}{(-\nu)!}d\eta.$$

In this case, equation (13) can be expressed as

$$D^1_{r_w+}\tilde{p}(r,\lambda)+\int_{r_w}^{r}\widetilde{p'}(\rho,\lambda)d\rho\left[\int_{\rho}^{r}\frac{1}{\eta}\frac{(r-\eta)^{\nu-1}}{(\nu-1)!}\frac{(\eta-\rho)^{-\nu}}{(-\nu)!}d\eta-\frac{\lambda}{a_\nu}\frac{(r-\rho)^{\nu}}{\nu!}\right]=$$

$$=-C_1\frac{r^{\nu-1}}{(\nu-1)!}+\frac{\lambda}{a_\nu}\tilde{p}(r_w,\lambda)\frac{(r-r_w)^{\nu}}{\nu!}-\tilde{p}(r_w,\lambda)\int_{r_w}^{r}\frac{(r-\eta)^{\nu-1}}{(\nu-1)!}\frac{1}{\eta}\frac{(\eta-r_w)^{-\nu}}{(-\nu)!}d\eta-$$

$$-I^{\nu}_{r_w+}\big(F(r,\lambda)\big)+D^1_{r_w+}\widetilde{p'}(r,\lambda)\big|_{r=r_w}. \tag{14}$$

Finally, denoted by

$$K(r,\rho,\lambda)=\int_{\rho}^{r}\frac{1}{\eta}\frac{(r-\eta)^{\nu-1}}{(\nu-1)!}\frac{(\eta-\rho)^{-\nu}}{(-\nu)!}d\eta-\frac{\lambda}{a_\nu}\frac{(r-\rho)^{\nu}}{\nu!}, \tag{15}$$

$$\Phi(r,\lambda)=-C_1\frac{r^{\nu-1}}{(\nu-1)!}+\Phi_1(r,\lambda), \tag{16}$$

$$\Phi_1(r,\lambda)=\frac{\lambda}{a_\nu}\tilde{p}(r_w,\lambda)\frac{(r-r_w)^{\nu}}{\nu!}-\tilde{p}(r_w,\lambda)\int_{r_w}^{r}\frac{(r-\eta)^{\nu-1}}{(\nu-1)!}\frac{1}{\eta}\frac{(\eta-r_w)^{-\nu}}{(-\nu)!}d\eta-$$

$$-I^{\nu}_{r_w+}\big(F(r,\lambda)\big)+D^1_{r_w+}\widetilde{p'}(r,\lambda)\big|_{r=r_w},$$

for $\widetilde{p'}(r,\lambda)$ we obtain the following Volterra type-II integral equation

$$\widetilde{p'}(r,\lambda)+\int_{r_w}^{r}K(r,\rho,\lambda)\widetilde{p'}(\rho,\lambda)d\rho=\Phi(r,\lambda). \tag{17}$$

As can be seen from (15) and (16), for $\rho\le r$, the functions $K(r,\rho,\lambda)$ and $\Phi(r,\lambda)$ are continuous functions with respect to the variable r.

Applying the method of successive substitution to the (17) Volterra integral equation, we find that

$$\tilde{p}'(\rho,\lambda)=\Phi(\rho,\lambda)-\int_{r_w}^{\rho}K_1(\rho,\theta,\lambda)\tilde{p}'(\theta,\lambda)d\theta. \tag{18}$$

Here, $K_1(r,\rho,\lambda)=K(r,\rho,\lambda)$. Considering (18),

$$\tilde{p}'(r,\lambda)=\Phi(r,\lambda)-\int_{r_w}^{r}K_1(r,\rho,\lambda)\tilde{p}'(\rho,\lambda)d\rho=$$

$$=\Phi(r,\lambda)-\int_{r_w}^{r}K_1(r,\rho,\lambda)\left[\Phi(\rho,\lambda)-\int_{r_w}^{\rho}K_1(\rho,\theta,\lambda)\tilde{p}'(\theta,\lambda)d\theta\right]d\rho=$$

$$=\Phi(r,\lambda)-\int_{r_w}^{r}K_1(r,\rho,\lambda)\Phi(\rho,\lambda)\,d\rho+\int_{r_w}^{r}K_1(r,\rho,\lambda)d\rho\int_{r_w}^{\rho}K_1(\rho,\theta,\lambda)\tilde{p}'(\theta,\lambda)d\theta.$$

Changing the order of integration in the last expression, we get

$$\tilde{p}'(r,\lambda)=\Phi(r,\lambda)-\int_{r_w}^{r}K_1(r,\rho,\lambda)\Phi(\rho,\lambda)\,d\rho\ +\int_{r_w}^{r}K_2(r,\rho,\lambda)\tilde{p}'(\rho,\lambda)d\rho, \tag{18$_1$}$$

where

$$K_2(r,\theta,\lambda)=\int_{\rho}^{r}K_1(r,\rho,\lambda)K_1(\rho,\theta,\lambda)d\rho. \tag{19$_1$}$$

By repeating this process n times, we have

$$\tilde{p}'(r,\lambda)=\Phi(r,\lambda)-\int_{r_w}^{r}K_1(r,\rho,\lambda)\Phi(\rho,\lambda)d\rho+\int_{r_w}^{r}K_2(r,\rho,\lambda)\Phi(\rho,\lambda)d\rho-$$
$$-\int_{r_w}^{r}K_3(r,\rho,\lambda)\Phi(\rho,\lambda)d\rho+\cdots+(-1)^n\int_{r_w}^{r}K_{n-1}(r,\rho,\lambda)\Phi(\rho,\lambda)d\rho+$$
$$+\int_{r_w}^{r}K_n(r,\rho,\lambda)\tilde{p}'(\rho,\lambda)d\rho. \tag{18$_n$}$$

Here,

$$K_n(r,\rho,\lambda)=\int_{\rho}^{r}K_1(r,\theta,\lambda)K_{n-1}(\rho,\theta,\lambda)d\theta. \tag{19$_n$}$$

We can write equation (18$_n$) as

$$\tilde{p}'(r,\lambda) = \Phi(r,\lambda) + \sum_{m=1}^{n-1}(-1)^m \int_{r_w}^{r} K_m(r,\rho,\lambda)\,\Phi(\rho,\lambda)d\rho + \int_{r_w}^{r} K_n(r,\rho,\lambda)\tilde{p}'(\rho,\lambda)d\rho =$$

$$= \Phi(r,\lambda) + \int_{r_w}^{r}\left[\sum_{m=1}^{n}(-1)^m\,K_m(r,\rho,\lambda)\right]\Phi(\rho,\lambda)d\rho + \int_{r_w}^{r} K_n(r,\rho,\lambda)\tilde{p}'(\rho,\lambda)d\rho\,. \qquad (20)$$

Taking into account the summation $\sum_{m=1}^{n}(-1)^m\,K_m(r,\rho,\lambda)$, the solution of the integral equation (18) is

$$\tilde{p}'(r,\lambda) = \lim_{n\to\infty}\left\{\Phi(r,\lambda) + \int_{r_w}^{r}\left[\sum_{m=1}^{n}(-1)^m\,K_m(r,\rho,\lambda)\right]\Phi(\rho,\lambda)d\rho\right\} +$$

$$+ \int_{r_w}^{r} K_n(r,\rho,\lambda)\tilde{p}'(\rho,\lambda)d\rho,$$

$$\tilde{p}'(r,\lambda) = \Phi(r,\lambda) + \int_{r_w}^{r} R(r,\rho,\lambda)\,\Phi(\rho,\lambda)d\rho\,. \qquad (21)$$

Here, the expression

$$R(r,\rho,\lambda) = \sum_{m=1}^{\infty}(-1)^m\,K_m(r,\rho,\lambda) \qquad (22)$$

is called resolvent.

Let us now examine whether the series (22) converges. $K(r,\rho,\lambda)$ is a continuous and bounded function, i.e., for $\rho < r$ the following evaluations are valid

$$|K_1(r,\rho,\lambda)| \le M,$$

$$|K_2(r,\theta,\lambda)| = \left|\int_{\theta}^{r} K_1(r,\rho,\lambda)K_1(\rho,\theta,\lambda)d\rho\right| \le M^2(r-\theta),$$

$$|K_3(r,\theta,\lambda)| = \left|\int_{\theta}^{r} K_1(r,\theta,\lambda)K_2(\rho,\theta,\lambda)d\rho\right| \le M^3\int_{\rho}^{r}(\rho-\theta)d\rho = M^3\frac{(r-\theta)^2}{2!},$$

.....

$$|K_n(r,\theta,\lambda)| = \left|\int_{\theta}^{r} K_1(r,\rho,\lambda)K_{n-1}(\rho,\theta,\lambda)d\rho\right| \le M^n\int_{\rho}^{r}\frac{(\rho-\theta)^{n-2}}{(n-2)!}d\rho = M^n\frac{(r-\theta)^{n-1}}{(n-1)!}.$$

For the upper bound of the resolvent (22) we obtain the following estimate

$$\frac{M}{(n-1)!}[M(r-\theta)]^{n-1} \le \frac{M}{(n-1)!}q^{n-1},$$

where

$$q = M(r_c - r_w).$$

Thus, the series

$$M + Mq + M\frac{q^2}{2} + \cdots + M\frac{q^{n-1}}{(n-1)!} + \cdots$$

is absolutely and regularly convergent in the triangle domain ($r_w \le r \le r_c$, $r_w \le \rho \le r$), for arbitrary q.

Now, to find the function $\tilde{p}(r,\lambda)$, let us integrate equation (21) with respect to r from r_w to r_c

$$\tilde{p}(r,\lambda)=\int_{r_w}^{r}\Phi(\rho,\lambda)d\rho+\int_{r_w}^{r}\left[\int_{r_w}^{\rho}R(\rho,\eta,\lambda)\,\Phi(\eta,\lambda)d\eta\right]dr+C_2.$$

Considering (17), the last equation can be written as follows:

$$\tilde{p}(r,\lambda)=-C_1\left\{\int_{r_w}^{r}\frac{\rho^{\nu-1}}{(\nu-1)!}d\rho+\int_{r_w}^{r}\left[\int_{r_w}^{\rho}R(\rho,\eta,\lambda)\frac{\eta^{\nu-1}}{(\nu-1)!}d\eta\right]d\rho\right\}+C_2+$$

$$+\left\{\int_{r_w}^{r}\Phi_1(\rho,\lambda)d\rho+\int_{r_w}^{r}\left[\int_{r_w}^{\rho}R(\rho,\eta,\lambda)\Phi_1(\eta,\lambda)\,d\eta\right]d\rho\right\}. \tag{23}$$

Using the following expressions

$$A(r)=\int_{r_w}^{r}\frac{\rho^{\nu-1}}{(\nu-1)!}d\rho+\int_{r_w}^{r}\left[\int_{r_w}^{\rho}R(\rho,\eta,\lambda)\frac{\eta^{\nu-1}}{(\nu-1)!}d\eta\right]d\rho,$$

and

$$B(r)=\int_{r_w}^{r}\Phi_1(\rho,\lambda)d\rho+\int_{r_w}^{r}\left[\int_{r_w}^{\rho}R(\rho,\eta,\lambda)\Phi_1(\eta,\lambda)\,d\eta\right]d\rho$$

the equation (23) can be rewritten as follows

$$C_1A(r)-C_2=\tilde{p}'(r,\lambda)-B(r). \tag{24}$$

Using the following conditions

$$\tilde{p}(r_w,\lambda)=\tilde{p}_w(\lambda),\ \ \tilde{p}(r_c,\lambda)=\tilde{p}_c(\lambda)$$

to find the unknown constants, we get

$$\begin{cases}C_1A(r_w)-C_2=\tilde{p}_w(\lambda)-B(r_w),\\ C_1A(r_c)-C_2=\tilde{p}_c(\lambda)-B(r_c).\end{cases}$$

The solution of the obtained system of algebraic equations by using Cramer's method is

$$C_1=\frac{\tilde{p}_c(\lambda)-\tilde{p}_w(\lambda)-\big(B(r_c)-B(r_w)\big)}{A(r_c)},$$
$$C_2=\frac{-A(r_c)\big(\tilde{p}_w(\lambda)-B(r_w)\big)}{A(r_c)}=-\big(\tilde{p}_w(\lambda)-B(r_w)\big).$$

Substituting these expressions into (24), for $\tilde{p}(r,\lambda)$ we obtain the following expression

$$\tilde{p}(r,\lambda)=-\frac{\tilde{p}_c(\lambda)-\tilde{p}_w(\lambda)-\big(B(r_c)-B(r_w)\big)}{A(r_c)}\left\{\int_{r_w}^{r}\frac{\rho^{\nu-1}}{(\nu-1)!}d\rho+\int_{r_w}^{r}\left[\int_{r_w}^{\rho}R(\rho,\eta,\lambda)\frac{\eta^{\nu-1}}{(\nu-1)!}d\eta\right]d\rho\right\}-$$

$$-\big(\tilde{p}_w(\lambda)-B(r_w)\big)+\left\{\int_{r_w}^{r}\Phi_1(\rho,\lambda)d\rho+\int_{r_w}^{r}\left[\int_{r_w}^{\rho}R(\rho,\eta,\lambda)\Phi_1(\eta,\lambda)\,d\eta\right]d\rho\right\}. \tag{25}$$

Using the obtained Laplace transform $\tilde{p}(r,\lambda)$ with the help of the inverse transform

$$p(r,t) = \frac{1}{2\pi i}\int_{\gamma-i\infty}^{\gamma+i\infty} e^{\lambda t}\tilde{p}(r,\lambda)d\lambda, \gamma = $$

$$= Re\lambda > \lambda_0, i = \sqrt{-1}$$

we can find the values of the original pressure function at arbitrary points r and t.

Conclusion

The fractional with $1+\alpha$ ($0<\alpha<1$) order diffusion equation modelling of the flat-radial flow of one-phase liquids in porous media with fractal structure is transformed into the spectral boundary value problem for derivatives with respect to the Laplace transformation.

The solution of the spectral problem reduces to the second type Volterra integral equation.

In order to find the solution of the integral equation, the method of successive substitution is used to construct a resolvent for the solution and the solution is obtained as a convergent series.

The obtained representation allows for the proof of the existence of a solution of the considered problem and discovery of its approximate solution provided that the error is evaluated.

REFERENCES

Aliyev NA, Rasulov MA, Jalalov GI, Huseynova FM (2023) Study of the problem of straight-line flow of homogeneous fluids in fractal environments. In: Materials of the Republican scientific conference "Problems and prospects of oil and gas fields exploration", Baku, 5-6 December 2023, p 72–77 (in Azerbaijani)

Afonin AA, Sukhinov AI (2009) Mathematical models of geofiltration and geomigration in porous media with a fractal structure. Izvestiya SFedU, Technical sciences 97(8):62–70 (in Russian)

Barabanov VL (2016) Fractal model of the initial stage of capillary impregnation of rock. Georesources, Geoenergy, Geopolitics 1(13):1–15. https://doi.org/10.29222/ipng.2078-5712.2016-13.art5 (in Russian)

Belevtsov NS, Lukashchuk SYu (2020) Study of fractional-differential model of single-phase filtration with Riesz potential. Multiphase systems 1–2:14. https://doi.org/10.21662/mfs2020.1 (in Russian)

Gazizov RK, Lukashchuk SYu (2017) Fractional-differential approach to modelling filtration in complex inhomogeneous porous media. Bulletin of UTAMU 21(4):104–112 (in Russian)

Kilbas AA, Srivastava HM, Trujillo JJ (2006) Theory and applications of fractional differential equations. Elsevier, North-Holland

Miller KS, Ross B (1993) An introduction to the fractional calculus and fractional differential equations. John Wiley and Sons, New York, p 366

Mirzadzhanzade AKh, Khasanov MM, Bakhtizin RN (2002) Modeling of oil and gas production processes. Nonlinearity, nonequilibrium, uncertainty. Institute of Computer Research, Moscow–Izhevsk, p 368 (in Russian)

Nigmatullin RR (1986) The realization of the generalized transfer equation in a medium with fractal geometry. Phys. Stat. SolCfcD 133:425–430

Oldham KB, Spanier J (1974) The fractional calculus. Academic Press, New York, p 234

Podlubny I (1999) Fractional differential equations. Academic Press, San Diego

Samko SG, Kilbas AA, Marichev OI (1993) Fractional integrals and derivatives: Theory and applications. Gordon and Breach Science Publishers, Switzerland, p 976

Suleimanov BA, Abbasov EM, Efendieva AO (2005) Stationary filtration in a fractally inhomogeneous porous medium. Engineering Physics Journal 78(4):194–196 (in Russian)

СВЕДЕНИЕ ЗАДАЧИ ДРОБНОГО ДИФФЕРЕНЦИАЛЬНОГО УРАВНЕНИЯ, ОПИСЫВАЮЩЕГО ПРОЦЕСС ПЛОСКО-РАДИАЛЬНОГО ДВИЖЕНИЯ ЖИДКОСТИ ВО ФРАКТАЛЬНОЙ СРЕДЕ, К ИНТЕГРАЛЬНОМУ УРАВНЕНИЮ ФРЕДГОЛЬМА ВТОРОГО РОДА

Алиев Н.А.[1], Расулов М.А.[2*], Джалалов Г.И.[2], Синсойсал Б.[3], Ханбабаева М.Х.[2]

[1]Бакинский Государственный Университет, Факультет прикладной математики и кибернетики, Азербайджан AZ1148, Баку, ул. акад. Захида Халилова, 23

[2]Министерство науки и образования Азербайджанской Республики, Институт нефти и газа, Азербайджан AZ1000, Баку, ул. Фикрета Амирова, 9

[3]Стамбульский Университет Бейкент, Факультет Инженерии и Архитектуры, Кафедра Компьютерной Инженерии, Турция 34396, Сарыер, Стамбул

**Автор, отвечающий за переписку: mresulov@gmail.com*

Резюме. В последнее десятилетие теория массопереноса во фрактальных средах привлекает как практический, так и теоретический интерес. Этот интерес обусловлен геофизическими и экспериментальными данными, демонстрирующими нелинейность пористых сред, включая их блочную структуру и фрактальные свойства. В таких средах процесс фильтрации даже для однородных смесей моделируется дифференциальными уравнениями нецелого порядка, что затрудняет теоретические исследования. В данной работе построено решение нестационарного уравнения диффузии дробного порядка, описывающего плоскорадиальное движение однофазных жидкостей во фрактальных пористых средах. Для решения редуцированной спектральной задачи для производной функции преобразования Лапласа выведено интегральное уравнение Вольтерры второго рода с регулярным ядром. Для этого интегрального уравнения методом последовательной подстановки получена

резольвента в виде быстро сходящегося ряда. Найдено необходимое условие сходимости ряда и получено аналитическое выражение для производной функции преобразования Лапласа искомой функции давления. Интегрируя полученное аналитическое выражение для преобразования Лапласа по пространственной переменной, находим интегральное представление. Наконец, применяя обратное преобразование Лапласа, получаем выражение для динамического распределения искомой функции давления. Полученное выражение, во-первых, позволяет исследовать задачу нестационарного течения жидкости в радиальной среде фрактальной природы, а во-вторых, также отвечает на вопрос о существовании и единственности рассматриваемой задачи. Используя методы численного интегрирования, можно вычислить значения функции давления в любой точке r и в любой момент времени t с оценкой погрешности. Кроме того, полученные результаты позволяют оценить найденное решение приближенными методами.

***Ключевые слова**: массоперенос во фрактальных средах, нестационарное уравнение диффузии в плоскорадиальной области, преобразование Лапласа, интегральное уравнение Вольтерра второго рода с регулярным ядром, метод последовательной подстановки*

FRAKTAL MÜHITDƏ MAYENİN MÜSTƏVİ-RADİAL HƏRƏKƏT PROSESİNİ TƏSVİR EDƏN KƏSR TƏRTİBLİ DİFFERENSİAL MƏSƏLƏNİN İKİNCİ NÖV FREDHOLM İNTEQRAL TƏNLİYİNƏ GƏTİRİLMƏSİ

Əliyev N.A.[1], Rəsulov M.A.[2*], Cəlalov G.İ.[2], Sinsoisal B.[3], Xanbabayeva M.X.[2]
[1]Bakı Dövlət Universiteti, Tətbiqi Riyaziyyat və Kibernetika Fakültəsi, Azərbaycan
AZ1148, Bakı, akad. Zahid Xəlilov küç., 23
[2]Azərbaycan Respublikasının Elm və Təhsil Nazirliyi, Neft və Qaz İnstitutu, Azərbaycan
AZ1000, Bakı, Fikrət Əmirov küç., 9
[3]İstanbul Beykent Universiteti, Mühəndislik və Memarlıq Fakültəsi, Kompüter Mühəndisliyi Bölümü, Türkiyə
34396, Sarıyer, İstanbul
**Yazışmalara məsul:mresulov@gmail.com*

Xülasə. Son onillikdə fraktal materiallarda kütlə köçürmə nəzəriyyəsi həm praktiki, həm də nəzəri cəhətdən diqqətləri cəlb etmişdir. Bu maraq məsaməli mühitin qeyri-xəttiliyini, o cümlədən onların blok strukturu və fraktal xassələrini nümayiş etdirən geofiziki və eksperimental məlumatlara əsaslanır. Belə mühitlərdə süzülmə prosesi, hətta bircins qarışıqlar üçün də, kəsr tərtibli differensial tənliklərlə modelləşdirilir ki, bu da nəzəri tədqiqatları çətinləşdirir. Bu işdə fraktal məsaməli mühitlərdə birfazalı mayelərin müstəvi-radial hərəkətini təsvir edən qeyri-stasionar kəsr tərtibli filtrasiya tənliyinin analitik həlli qurulmuşdur. Təzyiq funksiyasının Laplas çevirməsinin törəməsi üçün gətirilmiş spektral məsələni həll etmək üçün müntəzəm nüvəli ikinci növ Volterra inteqral tənliyi alınmışdır. Bu inteqral tənlik üçün ardıcıl əvəzetmə metodundan istifadə etməklə sürətlə yığılan sıra şəklində rezolventa tapılmışdır. Sıranın yığılması üçün zəruri şərt tapılır və naməlum təzyiq funksiyasının Laplas çevirməsinin törəməsi üçün analitik ifadə alınır. Laplas çevrilməsi üçün tapılmış analitik ifadəni fəza dəyişəninə görə inteqrallamaqla orijinal funksiyanın Laplas cevirməsi üçün inteqral təsviri tapılır. Nəhayət, tərs Laplas çevrilməsini tətbiq edərək, biz axtarılan orijinal təzyiq funksiyasının dinamik paylanması üçün ifadə alırıq. Alınan ifadə, birincisi, fraktal təbiətli radial mühitdə qeyri-sabit maye axını problemini öyrənməyə imkan verir, ikincisi, baxılan problemin mövcudluğu və yeganəlyi suallarına da cavab verir. Ədədi inteqrallama üsullarından istifadə edərək, yatağın hər hansı bir r nöqtəsində və istənilən t anında təzyiq funksiyasının qiymətlərini xətanın qiymətləndirməsi ilə hesablaya bilərik. Bundan əlavə, əldə edilən nəticələr təqribi üsullardan istifadə edilərək alınan həlləri də qiymətləndirməyə imkan verir.

***Açar sözlər:** fraktal mühitdə kütlə ötürülməsi, müstəvi-radial bölgədə qeyri-stasionar diffuziya tənliyi, Laplas çevrilməsi, requlyar nüvəli ikinci növ Volterra inteqral tənliyi, ardıcıl əvəzetmə üsulu*

ANAS Transactions Earth Sciences 2 / 2025

http://www.journalesgia.com

MECHANICAL PROPERTIES OF OIL-BEARING ROCKS AND STABILITY OF THE BOTTOM HOLE ZONE

Hasanov A.B.[1,2*], Ramazanova N.A.[2], Bayramov K.T.[1]

[1]Azerbaijan State Oil and Industry University, Azerbaijan
20, Azadlig ave., Baku, AZ1010
[2]Ministry of Science and Education of the Republic of Azerbaijan,
Oil and Gas Institute, Azerbaijan
9, F.Amirov str., Baku, AZ1000
**Corresponding author: adalathasanov@yahoo.com*

Keywords: *bottom hole zone, terrigenous reservoirs, mechanical properties, confining pressure*

Summary. The paper discusses the relationship between the mechanical properties of oil-saturated reservoirs and stability of the near-wellbore zone during the long-term exploitation of an oil field. The relevance of this task is associated with on one hand the choice of the most rational wellbore design, and on the other – the necessity to consider the mechanisms of rock pressure manifestation, reservoir destruction during fluid movement, etc. These interconnected factors are typically assessed through studies of dynamic petrophysics in the field of oil and gas reservoir development. During the operation of producing wells, a significant decrease is observed in reservoir pressure as a result of the formation of a depression cone in the near-wellbore zone. The most optimal approach is to analyse changes in reservoir pressure over time. The paper provides an example of tracer studies of the averaged filtration parameters of reservoir rocks in the interval between injection and production wells. The paper describes cases of modelling in-reservoir fluid dynamics, where the injection well is located on the flank of the structure, and the production well is at its crest, and vice versa. The paper also presents assessments of mechanical properties (hardness, yield strength, etc.) of core samples at various levels of confining pressure. Terrigenous and volcano-clastic-sedimentary reservoirs with a specific cavernous pore structure were used for testing. The results of these studies allowed the classification of the tested samples according to the criteria of Deere and Miller, as well as the establishment of correlation relationships between individual physiccal and mechanical properties.

© 2025 Earth Science Division, Azerbaijan National Academy of Sciences. All rights reserved.

Introduction

As is known, in terms of efficiency, the well bottom and adjacent bottom hole part of the productive interval, are fundamentally important during the entire period of active exploitation of deposits (Mirzajanzadeh, Ametov, 1983). Ensuring the required reliability of this part of the well is associated with the necessity to maintain the mechanical stability of the bottom hole zone to damage under the conditions of changing field development. In the practice of oil and gas production, various bottom hole designs were used, however the most rational bottom hole design should consider the mechanisms of rock pressure, reservoir fracture during fluid movement, etc. These interrelated indicators usually evaluated by dynamic petrophysics studies in the area of oil and gas field development (Khristianovich et al., 1957; Baklashov, 2005; Mori, Furmentro, 1994). Thus, in particular, academician S.A.Kristianovich proposed an idea of the geo-discharge method (Khristianovich et al., 1957). Later, specialists and scientists from the Institute of Problems of Mechanics of the Russian Academy of Sciences proposed a method of the directed discharge (drainage) of a reservoir (hydraulic fracturing method - HFM) based on increasing the permeability of the bottom hole zone of the reservoir by creating artificial stresses within the reservoir (Baklashov, 2005; Mori, Furmentro, 1994). The idea of the directional drainage method (DDM) consists of an idea that it is not necessary to restore the permeability of natural filtration channels blocked during drilling and operation of wells, but much better to additionally create a new system of cracks in the rock – filtration channels. At the same time, the permeability of these channels can exceed the natural permeability by tens or even hundreds of times. During hydraulic fractur-

ing method (HFM), high-pressure liquid injected into the existing cracks porous, causing high stresses within these cracks and ensured their further growth (Baklashov, 2005; Mori, Furmentro, 1994). As a result, the rock unevenly released from compressive stresses in different directions occurring tangential stresses, and at a certain value of these stresses, the rock begins to crack (Gasanov et al., 2016). However, unlike rocks tectonic fracturing, which often produces one or more extended cracks, hydraulic fracturing produces multiple cracks within the single formation volume. In the whole, cracking and loosening of the rock carried out due to the release of elastic compression energy accumulated in it by rock pressure.

Theory

In the practice of development oil and gas fields, the methodology to justify the choice of the design of the bottom holes of oil producing wells is well known (RD 39-2-771-82, Krasnodar, VNIIKRNEFT), according to which the stability of rocks in the bottom hole zone of wells is determined on the following cases:

1. Liquid or gas extracted from the reservoir;
2. The liquid injected into the reservoir;
3. There is no any fluid movement.

At the same time, a significant decrease in reservoir pressure is observed during the operation of producing wells as a result of the formation of a depression funnel in the bottom hole zone of the formation (Gladkov, Gladkova, 2008). As a result, the formation, especially in the bottom hole zone, begins to growth additional vertical load leading to deformation of the pore space. In this case, both elastic and plastic, decreases in the capacitance and filtration properties of rocks occur. The extending of such bottom hole deformations can be detected only based on special, rather laborious monitoring, or by theoretical methods to predict the stability of reservoir properties of real sediments at great depths (Gladkov, Gladkova, 2011; Gladkov, 2011). However, the analysis of reservoir pressure changes in area and depth of oil deposits over time could consider being the most optimal (Trofimov et al., 2007). Based on these data, the nature of the variation of reservoir properties in each producing and injection well of the field is estimated, and isobar maps are constructed. Such isobar maps used to calculate the area- and volume-weighted average reservoir pressures within the outer oil-bearing contours or within the testing zone. In addition to isobar maps, maps of the difference in reservoir pressure in the same well are composed of the current date and previous measurement date. Based on the totality of maps compiled, the effectiveness of water injection into the reservoir assessed, as well as the presence of falls, zones of replacement of the porous reservoir with dense impermeable rocks, etc. was revealed.

As an example, tracer studies of the average values of reservoir filtration parameters in the interval between injection and production wells were cited. The mutual arrangement of injection and production wells within the geological structure and the direction of the intra-reservoir fluid flow were commonly modelled. In particular, the results of the study of formation of fluid dynamics were described (Trofimov et al., 2007; Zhang, Rykus, 2015).

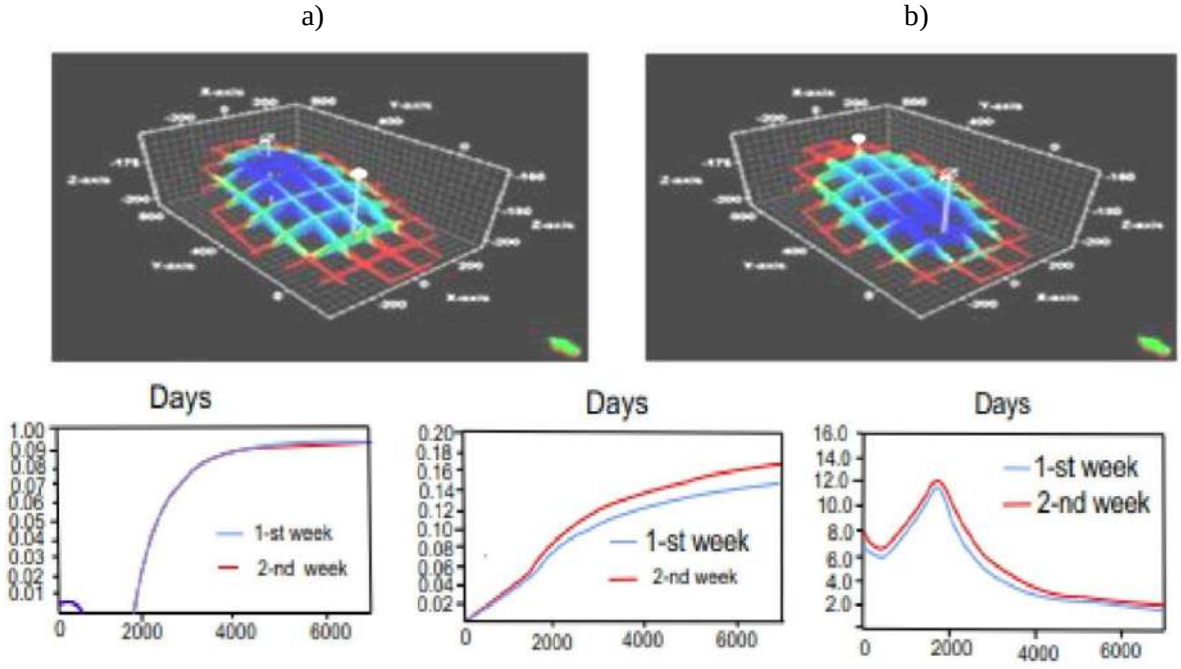


Fig. 1. The results of modelling of the watering, production and flow rates at different positions of injection and production wells (Trofimov et al., 2007)

In this research, two principal locations of the injection and production wells were considered relatively to the overall structure of the field:

1) the injection well is located on the wing of the structure, and the production well is on its roof (Fig. 1a);
2) the injection well is located on the roof of the structure, and the production well is located on its wing (Fig. 1b).

According to the modelling results, it turned out that the location of the injection and production wells relative to the elements of the field structure does not significantly affect the watering availability of wells (Trofimov et al., 2007). In both cases, the first and second, the beginning of reservoir flooding and its steady growth over a long time occurred after 1800 days. Simultaneously, oil production rate under the second model turned out to be slightly higher than under the first one.

Discussions of results

Tracer methods similar as the described above are applicable in any flooding system and any degree of watering of production wells. These methods have found wide application in many oil-producing companies in the study of oil reservoirs, and the resistance of productive reservoirs to secondary deformations that occur during development studied sufficiently in (Imanov, 2001, 2012). These studies provide estimates of the hardness and yield strength of core samples at various values of all-round pressure (Fig. 2). In particular, it is noted that siltstones at pressures up to and including 25 MPa collapsed elastically. In this case, the hardness and yield strength of siltstones under atmospheric conditions are 58.8 and $42.7 \cdot 10^7$ N/m^2, respectively (Hasanov et al., 2022).

Unlike terrigenous reservoirs, volcanogenic-sedimentary reservoirs with a specific cavernous pore structure also differ in the nature of deformation under the influence of an external compressive load. Thus, Table 1 shows the results of a series of tests on the deformation of the pore structure and permeability under uniaxial pressure (Heap et al., 2022, 2024).

A review of the data in Table 1 shows (Teymen, 2018) that the density of dry U_w rocks varies from 1.34 to 2.02 g/sm^3, open porosity P_a – 14.2-37.5%, water saturation W — 7.0 – 27.9%, velocity of propagation of longitudinal waves V_p – 1.25-2.85 km/s, index point load I_s – 1.30-4.69 MPa, compressive strength U_{cs} – 6.6-69.2 MPa. According to the classification of Deere and Miller (Deere, Miller, 1966), among the data given in Table 1, 5 samples belong to moderately strong $U_{cs}\geq$ (110-55MPa), 9 to weakly strong $U_{cs}\geq$ (55.0-27.5 MPa) and 13 to very weakly strong $U_{cs}\geq$ (27.5MPa). The bending strength of the studied samples (F_{ts}) varies from 1.23 to 6.35 MPa, kick strength (D_n) — 2-17 MPa, resistance to abrasive wear (B_{sa}) – 28.3-139.1 sm^3 / 50 sm^2, and hardness (HB) – 1.9-49.2 kg/mm^2.

Their compressive strength, bending strength, kick strength and resistance to abrasive wear were tested to identify correlations between the physical parameters of some samples and their mechanical properties (Table 2) (Heap et al., 2024).

However, it should be noted that the hardness of rocks does not increase indefinitely due to increase of hydrostatic pressure. Thus, the curves of the dependence of hardness on hydrostatic pressure at 200 MPa begin to flatten out (especially noticeable on the curves of sandstone hardness). The observed process illustrates the structural resistance to deformation characteristics of most solids including rocks.

In addition to the above-mentioned geomechanical properties, the stability of the bottom-hole zone of wells is closely related to the initial stress state and structural features of the mountain range as a whole (Gasanov, 2021; Alimzhanov, 1999; Zaalishvili et al., 2023).

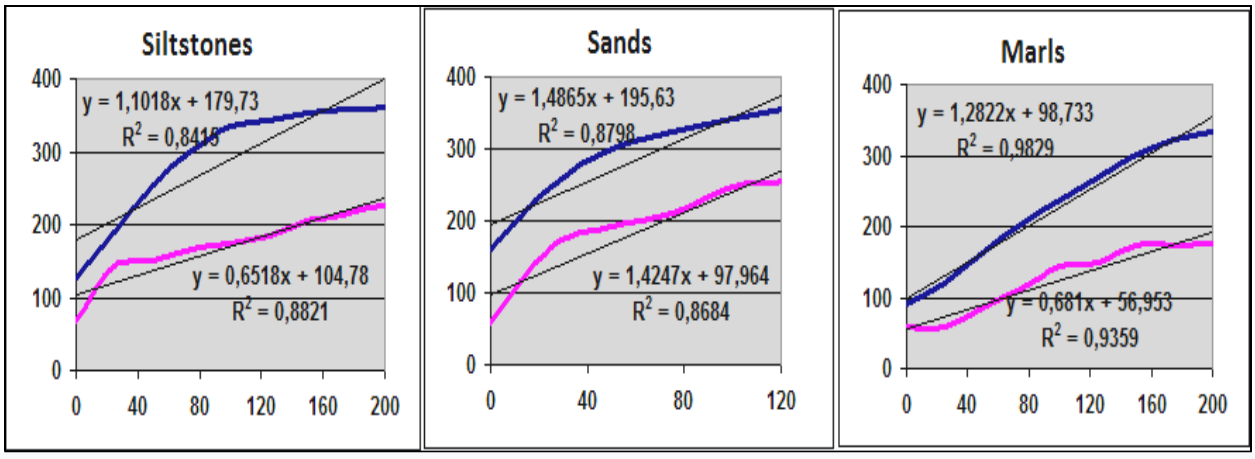


Fig. 2. Different values of confining pressure

Table 1

The test results of tuff samples (average values and standard deviation)

Code Sample	U_{cs}	F_{ts}	D_n	B_{sa}	HB	I_s	V_p	U_w	P_a	W
	MPa			sm³/50sm²	κg/mm²	MPa	κm/s	g/sm³	%	
T-1	69.2±3.9	6.24±0.7	17.0±1.5	27.2±1.6	49.2±3.4	4.69±0.4	2.94±0.1	1.97±0.0	14.5±0.2	7.4±0.0
T-2	59.9±1.2	5.50±0.2	11.8±1.3	28.3±1.1	32.1±1.6	3.60±0.2	2.75±0.2	2.02±0.0	13.9±0.5	6.9±0.2
T-3	54.7±3.0	5.37±0.6	12.0±1.7	34.5±3.1	39.2±3.5	2.97±0.3	2.55±0.1	1.96±0.0	16.7±0.4	8.5±0.3
T-4	61.5±7.4	6.35±0.4	14.4±1.3	29.8±2.4	30.7±1.8	3.74±0.5	2.71±0.0	1.89±0.1	18.7±0.6	9.9±0.2
T-5	55.9±4.9	5.16±0.7	11.8±1.4	30.4±1.5	42.1±4.6	3.34±0.4	2.84±0.4	1.91±0.0	17.9±0.2	9.4±0.1
T-6	43.9±1.2	5.00±0.3	10.3±0.8	41.2±3.7	27.8±2.8	2.86±0.5	2.71±0.3	1.89±0.1	19.8±1.2	10.5±1.0
T-7	40.4±3.8	4.12±0.4	10.6±0.8	43.9±4.4	25.4±2.0	3.02±0.3	2.81±0.1	1.87±0.0	18.7±1.0	10.4±0.6
T-8	39.8±2.8	5.41±0.6	10.3±0.9	52.9±3.8	23.8±1.2	3.25±0.2	2.84±0.3	1.93±0.0	18.5±0.4	9.6±0.1
T-9	32.8±0.5	3.88±0.3	8.2±0.8	58.5±3.5	10.9±0.4	1.90±0.1	1.92±0.0	1.74±0.0	20.7±2.3	11.9±1.6
T-10	31.9±2.6	4.58±0.3	8.9±0.6	54.1±4.3	19.6±1.8	2.29±0.2	2.23±0.0	1.77±0.0	22.4±1.4	12.7±0.8
T-11	26.4±4.8	4.32±0.4	9.4±2.1	41.1±3.7	17.9±2.0	2.45±0.4	2.04±0.2	1.87±0.0	23.5±0.9	12.9±0.4
T-12	26.9±1.0	4.20±0.3	6.6±1.7	52.3±5.2	7.5±0.6	1.97±0.5	2.03±0.0	1.55±0.0	29.5±0.6	18.8±0.3
T-13	26.1±0.7	4.82±0.2	5.9±1.1	57.3±2.9	12.1±0.7	2.55±0.4	2.21±0.2	1.58±0.0	25.8±1.5	16.3±1.1
T-14	20.9±1.1	3.29±0.3	7.4±1.2	56.7±6.2	8.1±1.0	2.11±0.4	2.32±0.1	1.60±0.0	29.2±0.1	18.2±0.1
T-15	16.8±1.1	3.62±0.4	5.9±0.5	86.4±5.2	11.5±0.6	2.17±0.3	2.22±0.3	1.47±0.0	33.2±0.2	23.0±0.5
T-16	7.8±0.5	1.23±0.2	2.0±0.2	122.2±8.6	3.7±0.1	1.32±0.2	1.30±0.2	1.36±0.1	34.4±0.4	25.4±0.4
T-17	15.1±1.0	3.32±0.5	5.9±0.9	94.2±4.7	12.6±1.0	2.14±0.4	2.15±0.2	1.44±0.0	33.4±0.9	24.7±0.7
T-18	25.5±1.7	4.56±0.4	8.8±0.8	56.0±5.0	15.8±1.1	2.42±0.5	2.29±0.2	1.88±0.0	26.7±0.3	12.8±0.1
T-19	6.6±0.9	1.37±0.1	2.0±0.3	139.1±14	1.9±0.2	1.51±0.3	1.36±0.3	1.34±0.0	37.5±0.2	27.9±0.7
T-20	25.1±2.0	4.12±0.3	5.9±0.6	67.0±5.4	7.5±0.4	2.29±0.1	2.53±0.4	1.70±0.1	21.5±0.4	12.6±0.5
T-21	35.7±2.5	4.72±0.4	8.9±1.1	68.3±2.7	16.7±1.0	2.86±0.3	2.85±0.3	1.77±0.0	18.2±0.0	10.3±0.3
T-22	6.7±0.8	1.55±0.2	2.0±0.1	130.0±7.8	2.2±0.2	1.65±0.4	1.25±0.3	1.52±0.1	31.6±0.5	20.8±0.2
T-23	14.6±1.4	2.22±0.1	2.7±0.2	113.1±6.8	2.7±0.2	1.86±0.3	1.85±0.2	1.50±0.0	30.3±0.8	19.5±0.4
T-24	30.3±2.8	3.87±0.2	8.2±0.7	58.6±4.1	22.1±2.2	1.76±0.1	2.28±0.1	1.83±0.0	25.8±0.4	14.2±0.5
T-25	19.4±2.4	3.15±0.1	3.5±0.4	70.2±6.3	6.4±0.6	1.43±0.1	1.55±0.1	1.57±0.0	28.1±0.7	18.0±1.2
T-26	28.8±3.8	4.45±0.4	7.8±0.7	63.7±3.8	15.6±0.6	1.90±0.2	2.78±0.1	1.61±0.0	26.9±1.3	16.6±1.6
T-27	34.2±2.3	4.55±0.3	8.2±0.8	65.6±4.6	12.0±0.8	2.29±0.1	2.23±0.2	1.89±0.0	18.2±0.6	9.7±0.8

Table 2

Correlations between physical properties of the tested samples

No	Interdependent parameters	The optimal regression equation	The correlation coefficient
1	Compressive strength (MPa) and point load index (MPa)	Y = 19.5 (X) - 16.2	R = 0.82
2	Compressive strength (MPa) and open porosity (%)	Y = -56.48 Ln (X) + 209.84	R = 0.84
3	Compressive strength (MPa) and hardness (kg/mm^2)	Y = 1.2581 X + 9.6626	R = 0.87
4	Compressive strength (MPa) and longitudinal wave velocity (km /s)	Y = 4.5314 X $^{2.2296}$	R = 0.68
5	Bending strength (MPa) and point load index (MPa)	Y = 3.7946 Ln (X) + 0.877	R = 0.77
6	Bending strength (MPa) and water saturation in weight proportion (g/cm^3)	Y = -0.1948 X + 6.9885	R = 0.73
7	Bending strength (MPa) and hardness (kg/mm^2)	Y = 1.3792 Ln (X) + 0.5732	R = 0.82
8	Bending strength (MPa) and longitudinal wave velocity (km/s)	Y = 1.1068 X $^{1.555}$	R = 0.80
9	Impact resistance (MPa) and point load index (MPa)	Y = 10.965 Ln (X) -1.3277	R = 0.82
10	Impact strength (MPa) and dry rock density (g/cm^3)	Y = 16.117 X -19.7	R = 0.76
11	Impact resistance (MPa) and hardness (kg/mm^2)	Y = 1.1068 X $^{0.6394}$	R = 0.90
12	Impact strength (MPa) and longitudinal wave velocity (km/s)	Y = 1.2375 X $^{2.1686}$	R = 0.81

Possible deformations and subsidence of the Earth's surface during the development of oil and gas deposits are commonly found in the following cases (Alimzhanov, 1999):

– the presence of abnormally high reservoir pressures (AHRP) by the development of productive facilities without maintaining reservoir pressure;
– low strength and deformation characteristics of the reservoir;
– the presence of high porosity of reservoir rocks (up to 30-40%);
– relatively small depth of the developed deposits (up to 2000 m);
– significant total capacity of productive deposits.

Conclusions

A summary of the results of the study of the physical and mechanical properties of a number of terrigenous and sedimentary-volcanogenic rocks showed the presence of a significant relationship between the values of porosity, density and deformation-strength properties. In particular, it was found that the compressive strength U_{cs}, bending F_{ts} and impact toughness D_n decrease logarithmically with increasing open porosity P_a, while abrasive wear resistance B_{sa} nonlinearly increases with increasing open porosity Pa for sedimentary-volcanogenic rocks. Density U_w and water saturation Ware linearly interrelated with the mechanical properties of the rock; compressive strength U_{cs}, bending F_{ts} and impact toughness D_n increase with increasing density U_w. The speed of sound is an important indicator for predicting the mechanical properties of rocks; U_{cs}, F_{ts} and D_n are linearly related to the speed of sound, but the relationship between B_{sa} and V_p is represented by an inverse logarithmic function with a low correlation coefficient R = 0.66. The velocities of longitudinal waves V_p in rocks are determined by lower values of standard deviation than the velocities in porous media. Since the tested samples were highly porous, the correlation coefficients obtained on the longitudinal wave velocity V_p are somewhat lower than on other parameters. The point load index I_s is a very significant parameter in predicting the main mechanical properties of geological media, since the calculation of U_{cs}, F_{ts}, B_{sa} and D_n values is impossible without this characteristic. The higher the point load index, the greater the values of U_{cs}, F_{ts} and D_n. In addition, there is a close correlation between s - cs and I - U, with a correlation coefficient R> 0.80. However, a weak inverse correlation with R = 0.69 was found between B_{sa} and I_s.

REFERENCES

Alimzhanov AM (1999) Non-axisymmetric elastic-plastic state around the wellbore under the softening effect of drilling mud. Paper presented at Proc. intern. conf. "Geodynamics and stress state of the Earth's interior". Akademgorodok, Novosibirsk, 4-7 October 1999, p 184–189 (in Russian).

Baklashov IV (2005) Geomechanics. Volume I. Fundamentals of geomechanics, Publishing House of Moscow State Mining University, Moscow, p 280 (in Russian).

Deere DU and Miller RP (1966) Engineering classification and index properties for intact rock, Illinois Univ. at Urbana Dept. of Civil Engineering, Tec. Rep. No. AFWL-TR-65-116, p 327

Gasanov AB (2021) Geological and geophysical knowledge and productivity issues of the sedimentary complex of the South Caspian Basin. Leman, Baku, p 240 (in Russian)

Gasanov AB, Kyazimov RR, Mamedova DN, Mutallimova OM (2016) Variations in reservoir pressure and filtration-capacity properties of reservoirs of deep-seated fields in the South Caspian Sea. Presented in the collection of materials from the scientific practical conference 'Geology, Geodynamics and Geoecology of the Caucasus: Past, Present and Future' Makhachkala, p 242–247 (in Russian)

Gladkov EA (2011) Polygenic formation of hydrocarbons in fractured-cavernous carbonate reservoirs. Geology, geophysics and development of oil and gas fields 11:23–27 (in Russian)

Gladkov EA, Gladkova EE (2008) Ambiguity of geological and technological information in the process of adaptation of the hydrodynamic model. Drilling and Oil 10:40–41 (in Russian)

Gladkov EA, Gladkova EE (2011) Changes in the filtration-capacitive properties of deposits during their development. Oil and Gas Journal, Russia 9:75–79 (in Russian)

Hasanov AB, Isfandiyarov OA, Mehraliyeva NH, Abbasov TS (2022) Stability conditions of oil-saturated reservoirs porosity with deep overlaying. ANAS Transactions, Earth Sciences 2:46–53. https://doi.org/10.33677/ggianas20220200081

Heap MJ et al. (2024) Compaction and permeability evolution of tuffs from Krafla volcano (Iceland). Journal of Geophysical Research: Solid Earth 129(8), e2024JB029067. https://doi.org/10.1029/2024JB029067

Heap MJ, Meyer GG, Noel C et al., (2022) The permeability of porous volcanic rock through the brittle-ductile transition. Journal of Geophysical Research: Solid Earth 127(6), e2022JB024600. https://doi.org/10.1029/2022jb024600

Imanov AA (2001) Comprehensive assessment of the properties of sedimentary rocks and oil and gas potential of the South Caspian Basin at great depths. Elm, Baku, p 256 (in Russian)

Imanov AA (2012) Physic mechanical properties of sedimentary rocks of the South Caspian Basin in deep conditions: hydrocarbon resources of great depths. Baku, p 203 (in Russian).

Khristianovich SA, Zheltov YuP, Barenblatt GI (1957) On the mechanism of hydraulic fracturing of the reservoir. Oil industry 5:44–53 (in Russian)

Mirzajanzadeh AKh, Ametov IM (1983) Forecasting the field efficiency of thermal stimulation methods on oil reservoirs. Nedra, Moscow, p 205 (in Russian)

Mori V, Furmentro D (ed) (1994) Rock mechanics as applied to problems of oil exploration and production: collection of articles. Mir, Elf Akiten, Moscow, p 416 (in Russian)

Teymen A (2018) Prediction of the main mechanical parameters of tuffs based on test results. Physical and technical problems of mineral development 5:18–32 (in Russian)

Trofimov AS, Krivova NR, Ponyaev SV, Galliev FF (2007) Tracer studies of the formations of the "Yu" group of the Kottyn area. Bulletin of the subsoil user 18:44–46 (in Russian)

Zaalishvili VB, Hasanov AB, Abbasov EY, Mammadova DN (2023) Detailing the pore structure of productive intervals of oil wells using the Colour 3D Imaging. Energies 16(1):217. https://doi.org/10.3390/en16010217

Zhang C, Rykus MV, (2015). On the influence of geological heterogeneity of the mouth bar on the hydrodynamics of the Red Forest reservoir (China). Electronic scientific journal Oil and Gas Engineering 1:33–46 (in Russian)

МЕХАНИЧЕСКИЕ СВОЙСТВА НЕФТЕНОСНЫХ ПОРОД И УСТОЙЧИВОСТЬ ПРИЗАБОЙНОЙ ЗОНЫ СКВАЖИН

Гасанов А.Б.[1,2*], Рамазанова Н.А.[2], Байрамов К.Т.[1]
[1]Азербайджанский Государственный университет нефти и промышленности, Азербайджан
AZ1010, Баку, просп. Азадлыг, 20
[2]Министерство науки и образования Азербайджана, Институт нефти и газа, Азербайджан
AZ10009, Баку, ул. Ф. Амирова, 9
**Автор, отвечающий за переписку: adalathasanov@yahoo.com*

Резюме. В статье рассматриваются данные зависимости механических свойств нефтенасыщенных коллекторов и устойчивости призабойной зоны скважин в процессе разработки месторождения. Актуальность данной задачи связана, с одной стороны, с выбором наиболее рациональной конструкции забоя скважины, а с другой – с необходимостью учета механизмов изменения горного давления, разрушения пласта-коллектора при движении флюида и т.п. Эти взаимосвязанные показатели обычно оцениваются методами динамической петрофизики, согласно которым в процессе эксплуатации добывающих скважин в призабойной зоне пласта формируется воронка депрессии и наблюдается значительное снижение пластового давления. При этом наиболее оптимальным считается анализ изменений пластовых давлений нефтяных залежей во времени. Для иллюстрации этого в работе приведены трассерные исследования осредненных значений фильтрационных параметров пластов в интервале между нагнетательной и добывающей скважинами. Описаны случаи моделирования внутрипластовой флюидодинамики, когда нагнетательная скважина находится на крыле структуры, а добывающая скважина – на ее вершине и наоборот. В работе также приведены оценки механических свойств (твердости, предела текучести и т.п.) для проб кернов при различных значениях всестороннего давления. Причем к испытаниям привлекались как терригенные, так и вулканогенно-осадочные коллекторы со специфической – кавернозно-поровой структурой. В частности, установлено, что прочность на сжатие Ucs, изгиб Fts и ударная вязкость Dn логарифмически уменьшаются с ростом открытой пористости Pa, в то время как абразивная износостойкость Bsa нелинейно увеличивается с ростом открытой пористости Pa для осадочно-вулканогенных пород. Плотность Uw и водонасыщенность W линейно взаимосвязаны с механическими свойствами породы; прочность на сжатие Ucs, изгиб Fts и ударная вязкость Dn увеличиваются с ростом плотности Uw. Результаты позволили классифицировать испытанные пробы соответственно критериям Дира и Миллера, а также установить корреляционные связи между отдельными физико-механическими свойствами.

Ключевые слова: *призабойная зона, терригенные коллекторы, механические свойства, всестороннее давление*

NEFTLİ SÜXURLARIN MEXANİKİ XÜSUSİYYƏTLƏRİ VƏ QUYUDİBİ ZONASININ DAYANIQLIĞI

Həsənov Ə.B.[1,2], Ramazanova N.A.[2], Bayramov K.T.[1]
[1]Azərbaycan Dövlət Neft və Sənaye Universiteti, Azərbaycan
AZ1010, Bakı, Azadlıq prosp., 20
[2]Azərbaycan Respublikası Elm və Təhsil Nazirliyi, Neft və Qaz İnstitutu, Azərbaycan
AZ1009, Bakı, F.Əmirov küç., 9
**Yazışmalara məsul:adalathasanov@yahoo.com*

Xülasə. Məqalədə yatağın işlənməsi zamanı neftlə doymuş süxurların mexaniki xassələrinin və quyu dibi zonasının dayanıqlığının şəraiti haqqında məlumatlar araşdırılır. Bu mövzunun aktuallığı bir tərəfdən quyu dibinin ən səmərəli dizaynının seçilməsi, digər tərəfdən isə lay təzyiqinin dəyişmə mexanizmlərinin, mayenin hərəkəti zamanı kollektorluq xüsusiyyətlərinin dəyişilməsi və s. amillərin nəzərə alınması zərurəti ilə bağlıdır. Bu, bir-biri ilə əlaqəli göstəricilər adətən dinamik petrofizika metodlarından istifadə etməklə qiymətləndirilir. Nəticə etibari ilə, quyu dibinin neft hasilatı zamanı təzyiq depressiyasının formalaşması, eləcə də lay və lay təzyiqinin əhəmiyyətli dərəcədə azalması müşahidə edilməsi mümkün olur. Bu araşdırmalarda ən optimal təhlil neft yataqlarının lay təzyiqinin zamanla dəyişməsi hesab olunur. Məsələnin həlli məqsədilə məqalədə basqı və hasilat quyuları arasındakı intervalda layların filtrasiya parametrlərinin orta qiymətlərini izləyən tədqiqatlar metodu təqdim olunur. Laydaxili maye dinamikasının modelləşdirilməsi halları, basqı quyusunun yataq strukturu qanadında, hasilat quyusu isə onun tağ hissəsində və əksinə olduqda təsvir edilir. Həmçinin, məqalədə məhdudlaşdırıcı təzyiqin müxtəlif dəyərlərində bəzi süxur nümunələri üçün mexaniki xassələrin (sərtlik, məhsuldarlıq və s.) təxminləri təqdim olunur. Bundan başqa, tədqiqatlara spesifik kavernoz-məsaməli struktura malik həm terrigen, həm də vulkanogen-çökmə kollektorlar nümunələri cəlb edilmişdir. Nəticələr sınaqdan keçirilmiş nümunələri Deere və Miller meyarlarına uyğun təsnif etməyə, həmçinin fərdi fiziki və mexaniki xassələr arasında korrelyasiya asılıqlarını təyin etməyə imkan vermişdir.

Açar sözlər*: quyudibi zona, terrigen süxurlar, mexaniki xassələr, qapalı təzyiq*

ANAS Transactions Earth Sciences 2 / 2025

http://www.journalesgia.com

RESEARCH ON THE EFFECTIVENESS OF THE COMBINED METHOD OF POLYMER AND WATER-GAS IMPACT ON OIL RESERVOIRS

Hadiyeva A.S.[1*], Bissembayeva K.T.[1], Mamalov E.N.[2], Sabyrbayeva G.S.[1]

[1] *Caspian University of Technology and Engineering named after Sh.Yessenova, Kazakhstan*
Building 1, Microdistrict 32, Aktau, Mangistau region, 130003

[2] *Ministry of Science and Education Republic of Azerbaijan, Oil and Gas Institute, Azerbaijan*
9, F.Amirova str., Baku, AZ1000

**Corresponding author: hadieva_albina@mail.ru*

Keywords: *polymer, concentration, solution, water-gas mixture, oil recovery factor*

Summary. This paper focuses on the issue of effective technology for extracting high-viscosity oil from heterogeneous reservoirs. The study examines methods for enhancing oil recovery from depleted fields containing high-viscosity oil. Three different reservoir impact methods are analysed in this research. Two of these methods are well known in oil production practice: polymer flooding and oil displacement using a water-gas mixture. The results obtained from these experiments are compared with the outcomes of the proposed combined impact method. The experiments utilized oil with a viscosity of 205 mPa·s at 20°C. In all conducted experiments, the first stage involved oil displacement using distilled water. In the first scenario, after the initial stage, a slug of polymer solution was injected and subsequently pushed forward by distilled water. In the second scenario, a slug of polymer solution was injected and then displaced using a water-gas mixture. In the third scenario, after the initial stage, oil displacement continued by injecting a water-gas mixture into the porous medium. A comparative analysis of the conducted experiments showed that the worst result was obtained when only the polymer solution slug was used. The effectiveness of the combined impact technology based on a polymer solution slug with a 0.25% concentration and a water-gas mixture was found to be approximately equal to that of using only a water-gas mixture with a high water-gas ratio.

© 2025 Earth Science Division, Azerbaijan National Academy of Sciences. All rights reserved.

Introduction. Currently, the development of oil fields with complex geological structures and the physical-chemical properties of fluids saturated in productive reservoirs are carried out using active recovery methods.

The early detection of complications that arise under diverse geological and operational conditions in high-viscosity oil fields is a critical challenge. This is because each oil reservoir depending on the field differs significantly in terms of structural volume changes and technological parameters.

The widespread application of advanced oil recovery technologies aimed at effectively reducing residual oil saturation through the displacement of oil with viscous compositions will allow for the long-term maintenance of stable production levels in most fields with complex geological structures that are in the final stages of development. It has been proven that the viscosity of liquids can be controlled using various types of polymers. These substances are capable of altering the rheological properties of aqueous solutions and forming gel structures with varying densities (Kukin, Solyakov,1982; Polymers for Oil Production, accessed 2025; Shevtsov et al., 2001). A detailed analysis of studies has shown that polymer compositions have been used both to enhance oil recovery due to their flow-diverting properties and as water-isolating components in production wells (Babaev et al., 2016; Fyodorova et al., 2012; Manzhay et al., 2017; Thomas et al., 2017; Veliyev, 2020). The use of polymer solutions enables the implementation of various methods to reduce permeability or block the water-saturated porous structure. The reduction of water inflow into oil wells is due to the ability of polyacrylamide (PAA) to adsorb onto pore surfaces or form cross-linked polymer networks that hinder fluid filtration. It has been found that as the polymer concentration increases, the mobility of the solution decreases (Sparlin, 1976; Smith, 1970). Among the numerous studies confirming the effectiveness of polymer flooding, some indicate its low efficiency in the final stages of field development (Aleazar-Vara et al., 2016).

Many researchers have dedicated their work to the use of water-gas mixtures to increase oil production from fields developed in the later stages (Drozdov et al., 2007; Mullaev et al., 2016).

A detailed study of polymer and water-gas injection technologies (Mamalov et al., 2022) suggests their combined application.

The combination of polymer and water-gas injection allows the following results:

- Increased reservoir coverage due to better penetration of the polymer solution and foam into low-permeability zones;
- Enhanced oil displacement from the reservoir by reducing interfacial tension between oil and water, as well as forming more stable emulsions;
- Reduction of residual oil in the reservoir due to the formation of more stable emulsions and oil displacement by foam;
- Lower risk of fracture formation in the reservoir through more uniform pressure distribution;
- Improved waterflood efficiency by increasing the viscosity of the polymer solution.

Methods and Materials of the Study

To evaluate the effectiveness of the combined polymer and water-gas injection method, a series of experiments were conducted in this study. These experiments, which varied in terms of displacement agents, were performed using a reservoir model setup, as shown in Figure 1. The reservoir model length is 0.84 m, with a diameter of 0.025 m. The experiments used oil with a viscosity of 205 mPa·s at 20°C.



Fig. 1. Reservoir Model Setup

Quartz sand with a particle size of less than 0.2 mm was used as the porous medium. Polyacrylamide (PAA) was used as the polymer. The initial experimental data are presented in Table 1.

In experiments No.1 and No.2, oil displacement was carried out using only a PAA solution slug with different concentrations. In experiments No.3, No.4, and No.5, oil displacement was performed using PAA solutions of varying concentrations combined with a water-gas mixture. In experiments No.6 and No.7, after depletion mode, oil displacement was conducted solely with a water-gas mixture. The polymer slug volume was nearly identical in all experiments.

These studies were necessary to conduct a comparative analysis of the combined reservoir stimulation method.

Results and Discussion

Based on this analysis, the effectiveness of different stimulation methods for an oil reservoir developed after depletion was determined. Initially, two experiments were conducted to displace oil from a depleted reservoir using a polyacrylamide (PAA) slug.

The experiments were carried out in the following sequence: first, a depleted reservoir was formed (Stage I). It is important to note that in all experiments the initial oil displacement was performed using distilled water, thereby simulating the depletion phase of the reservoir.

To eliminate the influence of salts contained in natural waters, oil displacement from the reservoir model was carried out using distilled water.

The extraction process was halted after injecting 3-4 pore volumes of water or upon detecting signs of oil in the outgoing flow. At this stage, a significant amount of oil remained in the reservoir.

The results of the conducted experiments are presented in Table 2.

This Table presents the values of the oil recovery factor and residual oil saturation in all seven experiments after Stage I. The variation in the oil recovery factor and residual oil saturation across the experiments is influenced by the initial oil saturation of the porous medium. At the same time, a high water saturation of the porous medium is observed.

The results obtained after Stage I indicate the need for further development of the depleted reservoir, where significant oil reserves remain. To address this and potentially reduce the amount of water in the produced fluid from the reservoir model, it was decided to apply secondary recovery methods.

In our case, three reservoir stimulation options were considered. The first option involves oil displacement using a slug of PAA solution, which is mobilized by injecting distilled water. The second option examines a combined method, where a slug of PAA solution is injected into the reservoir and then displaced using a water-gas mixture. The third option considers oil displacement using only a water-gas mixture. A comparative analysis of these options will help determine the most effective approach.

Table 1

Initial Experimental Data

EXPERIMENT № / PARAMETERS	1	2	3	4	5	6	7
Water Permeability, μm²	1.8	1.88	1.79	1.82	1.39	1.23	1.39
Oil Saturation, %	86.3	81.8	81.5	81.8	79.9	85.9	81.8
Water Saturation, %	13.7	18.2	18.5	18.2	20.1	14.1	18.2
PAA Solution Concentration, %	0.5	0.25	0.5	0.1	0.25	-	-
PAA Slug Volume, pore volumes	43.8	42.4	41.2	42.4	41.4	-	-

Table 2

Experimental results

EXPERIMENT № / PARAMETERS	1	2	3	4	5	6	7
Oil recovery factor for stage I (without polymer injection), %	51.5	42	41.6	43.0	42	42	49.0
Final oil recovery factor, %	65.9	54.5	74.5	60.7	67	58.5	81.5
Additional oil recovery factor, %	14.4	12.5	32.9	17.7	25	16.5	32.5
Residual oil saturation after Stage I, %	41.7	50.1	47.6	44.8	40	48.1	40
Volume of produced water after Stage I, pore volumes	4	3.1	4	3.6	2.5	1.35	2.5
Volume of produced water after Stage II, pore volumes	2	2.4	1.6	3.4	5.6	1.36	5.6
Reduction in Water Cut, times	2	1.3	2.5	1.05	1.93	-	-
Residual Resistance Factor (average), R	2.6	1.3	6.7	2.4	3.8	-	-
Residual Oil Saturation after Stage II, %	29.4	37.0	20.8	32.1	26.0	35.9	15.2
Water-Gas Mixture, m³/nm³	-	-	0.008	0.013	0.009	0.0015	0.105
Viscosity of PAA Solution, mPa·s	188	38	188	12	38	-	-

Let's consider the first option. In this case, a slug of PAA solution with a concentration of 0.5% (experiment No. 1) and 0.25% (experiment No. 2) is injected into the reservoir. The PAA solution slug moves through the reservoir under the influence of distilled water. The viscosity of the PAA solution slugs depending on the concentration is significantly higher than that of water (Table 2). This leads to a reduction in the mobility of the injected water and partial adsorption of the polymer on the surface of quartz sand grains. As a result, the residual resistance factor increases, and the water production at the outlet of the reservoir model decreases. All of the above is well confirmed by Figure 2. Figure 2 shows the water production dynamics from the end of the depletion phase to the beginning of PAA solution slug injection.

As seen in Fig. 2, from the beginning of the injection of the PAA solution slug ($\tau = 3.5$) until its completion ($\tau = 0.6$), there is a sharp decrease in the amount of water in the produced fluid from the reservoir model. After the complete injection of the slug, a gradual increase in the produced water is observed. From the moment the PAA slug is injected into the reservoir, an increase in the amount of produced oil is observed in both cases.

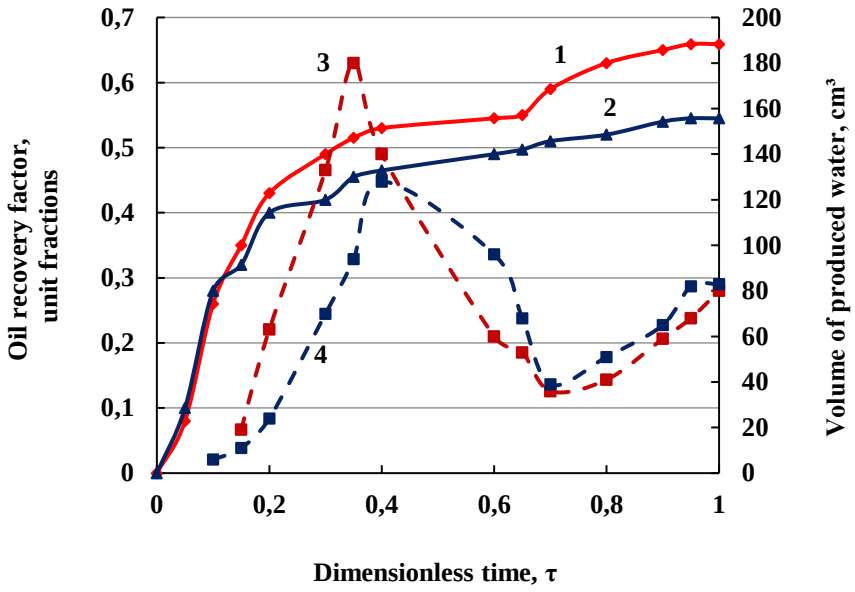


Fig. 2. Dynamics of the oil recovery factor (ORF) and water withdrawal from the reservoir model
1 and 3 – ORF and water withdrawal, respectively, in experiment No. 1,
2 and 4 – ORF and water withdrawal, respectively, in experiment No. 2,
$\tau = t_i / \sum t_i$, where t_i is the current time, h; $\sum t_i$ is the total process time, h

Injection of the PAA slug into the porous medium increases the residual resistance factor (R), which prevents water breakthrough at the outlet of the reservoir model, thereby reducing the water content in the produced oil. In Experiment No.1, the residual resistance factor (R) reached 2.6, while in Experiment No.2, it was 1.3. According to Table 2, the volume of water exiting the reservoir model decreased by a factor of 1.89 in Experiment No 1 and 1.29 in Experiment No.2.

As the PAA slug moves through the porous medium, polymer absorption and dilution occur leading to a decrease in solution viscosity. This results in partial water breakthrough increasing the volume of produced water and reducing oil recovery. The final oil recovery factor in Experiment No.1 was 65.9%, while in Experiment No.2, it was 54%. Higher PAA concentration improves process efficiency, as a more viscous PAA solution enhances water thickening and flow control. This confirms that increasing PAA concentration enhances the efficiency of the polymer flooding process, leading to better oil displacement and reduced water production.

The results of these experiments indicate the need to implement a new technology for more efficient oil recovery from the reservoir. Based on this, a combined technology was tested, which involves injecting a slug of PAA solution along with a water-gas mixture (in this case, air was used as the gas).

After completing oil displacement under depletion mode, the combined technology was introduced. In the second stage, during Experiments No.3, No.4, and No.5, a slug of PAA solution with concentrations of 0.5%, 0.1%, and 0.25% was injected into the reservoir. The slug volume ranged from 41.2% to 43.8% of the pore space (as shown in Table 2).

The polymer displacement through the reservoir was carried out using a water-air mixture. This mixture was chosen as the displacing agent due to its ability to form an emulsion within the reservoir.

The viscosity of the resulting emulsion differs from that of the injected water and, in particular, from that of air. Viscosity under reservoir conditions is a crucial parameter that influences the efficiency of polymer flooding. The higher the viscosity of the mixture, the better it displaces oil from the reservoir. However, if the viscosity is too high, it can cause difficulties in injecting the mixture into the reservoir.

Using the viscosity formula for the mixture provided in reference (Mamalov et al., 2022), we calculate the change in mixture viscosity depending on the water-gas ratio.

The following assumptions are made:

$$V_{g.r} = V_{g,\,n.c.}/P_r \; ; \; B = \sum V_{water} / \sum V_{g,\,n.c.} \; ,$$

where $V_{g,\,n.c}$ – is the gas volume under normal conditions, P_r – is the reservoir pressure, B – is the water-gas ratio, $\sum V_{water}$ – is the cumulative injected water volume, $\sum V_{g,\,n.c}$ – is the cumulative injected gas volume under normal conditions. The calculation results are presented in Table 3.

Increasing the viscosity of the water-gas mixture can indeed contribute to more effective propagation of the polyacrylamide (PAA) solution slug.

As the volume of injected water decreases, the volumetric fraction of gas in the gas mixture increases. This leads to an increase in the viscosity coefficient of the mixture. A higher viscosity mixture can improve its ability to move efficiently through a porous medium, such as the PAA solution slug. Increased viscosity of the mixture can help achieve better control and uniform distribution of the PAA solution in the pores and fractures of rock formations, which in turn can enhance the efficiency of the treatment process or other operations.

At the same time, the volume of extracted water decreases. Figure 3 presents the dynamics of viscosity changes in the water-gas mixture depending on the water-gas ratio for the three conducted experiments. It can be noted that up to a certain limit of the water-gas ratio, the viscosity of the mixture increases, after which it reaches a stable state. The point at which stable viscosity values are established is determined by the content of the PAA solution.

Table 3

Results of calculations

Dimensionless time	$V_{g,\ n.c.}$ cm^3	$\sum V_{g,\ n.c}$ cm^3	V_{water} cm^3	$V_{g,r}$ cm^3	$(V_{g,r}+V_{water})$ cm^3	R_c	μ_{cm} mPa·s	$\sum V_{water}$ cm^3	B x10^{-3} m^3/nm^3
0.4	-	-	-	-	-	-			
0.6	-	-	-	-	-	0	0,7679	0	0
0.65	6000	6000	13	1875	1838	0.99	2.6	13	2.0
0.7	4000	10000	32	667	699	0.98	2.57	45	4.5
0.75	3000	13000	52	366	418	0.97	2.56	97	7.5
0.8	4000	17000	72	487	559	0.95	2.52	169	9.9
0.85	4000	21000	78	487	565	0.94	2.50	247	11.8
0.9	6000	27000	76	732	808	0.93	2.48	323	12.0
0.95	7000	34000	79	854	933	0.93	2.48	402	11.8
1.0	3000	37000	98	366	464	0.92	2.46	500	13.5

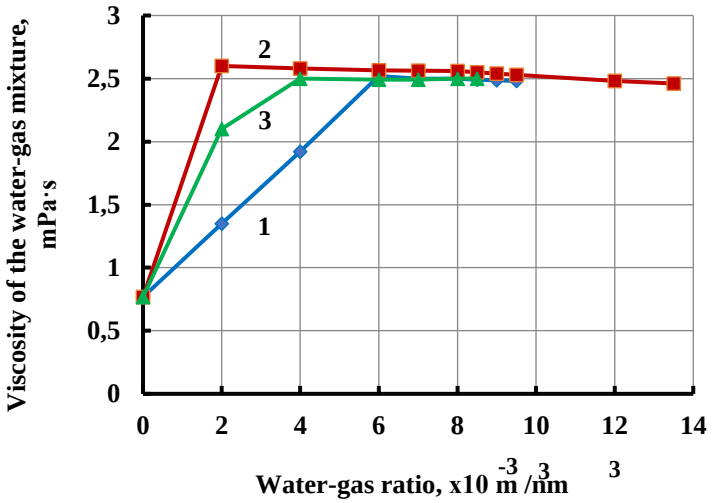


Fig. 3. Dependence of mixture viscosity on the water-gas ratio
1 – Experiment No.3 (C = 0.5%), 2 – Experiment No.5 (C = 0.25%),
3 – Experiment No.4 (C = 0.1%)

With a decrease in the solution concentration, its viscosity reaches the maximum value more quickly and then remains practically unchanged, even with a further increase in the water-gas ratio. This is likely due to differences in the residual resistance factor values observed in the experiments (Table 2). At a lower concentration, and consequently a lower residual resistance factor, a high-viscosity emulsion forms more quickly in the reservoir. Such an emulsion is less susceptible to thinning of the polymer slug retains its characteristics for a longer period, and thus contributes to more effective oil displacement even with low water injection rates. The viscosity of the mixture (usually with added polymers) can vary depending on the water-gas ratio. The water-gas ratio determines the proportion of gas to water in the mixture. As the water-gas ratio increases, the viscosity of the mixture typically decreases. This occurs due to the reduction in interactions between polymer molecules (or other additives) in the mixture, as water is diluted by gas. Increasing the water-gas ratio can enhance the process efficiency for several reasons:

A decrease in mixture viscosity is usually associated with an increase in rock permeability. This can facilitate better penetration of the mixture (containing polymers and other additives) into the rock, ultimately enhancing the efficiency of the oil extraction process.

At lower viscosity, the mixture can be more evenly distributed within the reservoir, promoting more uniform and efficient oil recovery.

Lower viscosity also requires less energy for movement through the reservoir, allowing the mixture to penetrate the rock more easily, which can increase the oil production rate.

Reducing mixture viscosity by increasing the water-gas ratio can enhance the efficiency of the oil recovery process. However, other factors such as reservoir structure, polymer type, well operation parameters, and specific conditions must also be considered to optimize the process and achieve the best results.

Injection of a polymer solution and a water-gas mixture helps create resistance to fluid filtration in the porous medium. Based on the obtained results, the dynamics of the residual resistance factor were determined for each experiment. Figure 4 presents the dynamics of the residual resistance factor for the three considered experiments (No. 3, 4, 5).

At the beginning of the filtration process, the resistance factor is high because the fluid penetrates the porous medium and fills the pores. Then, the resistance factor decreases as the fluid begins to displace gas or oil from the porous medium. Eventually, the resistance factor increases again as the porous medium becomes saturated with fluid, making further fluid movement more difficult. The graph of the resistance factor versus dimensionless time is used to evaluate the efficiency of the filtration process in the porous medium. It is also applied to predict the pressure required to maintain a specific fluid flow rate in the porous medium.

In Fig. 5, the dynamics of the oil recovery factor and the water-gas ratio are presented. As seen in the figure, with the initiation of water-gas mixture injection into the porous medium, a sharp increase in the amount of displaced oil is observed. The combined effect of the PAA solution mechanism and the water-gas mixture enhances the filtration capacity of the injected fluids.

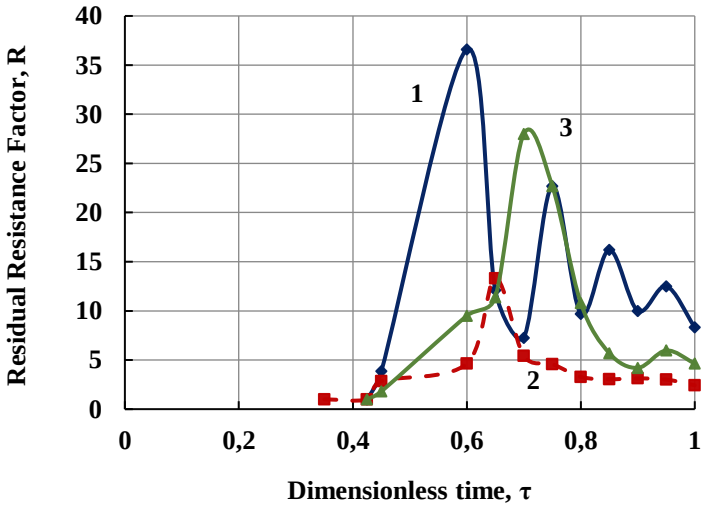


Fig. 4. Dependence of the resistance factor on dimensionless time
1 – Experiment No.3 (C=0.5%), 2 – Experiment No.4 (C=0.1%),
3 – Experiment No.5 (C=0.25%)

It is important to note the well-known fact that an increase in the polymer concentration in the slug leads to a corresponding increase in the oil recovery factor. In Experiment No.4, with a polymer concentration of C=0.1%, the oil recovery factor (ORF) reached 60.7% (with an additional oil production of 17.7%); in Experiment No.5, with C=0.25%, the ORF was 67% (25% additional recovery); and in Experiment No.3, with C=0.5%, ORF – 74.5% (32.9%).

Thus, it is clearly evident that the combined application of the polymer solution slug and the water-gas mixture is more effective than using only the polymer solution. In the third series of experiments, oil displacement after the depletion phase was studied using a water-gas mixture. The residual oil saturation after Stage I was:

Experiment No.6 – 48.1%

Experiment No.7 – 40%

To obtain additional oil recovery, a water-gas mixture was injected into the reservoir. The viscosity of this mixture differs significantly from that of water, which enhances oil displacement. According to the formula provided in reference (Mamalov et al., 2022), the viscosity of the water-gas mixture depends on the volumetric fraction of air (gas) in the water-gas mixture (R). Figure 6 presents this dependency for all experiments. The figure demonstrates a linear relationship. Under combined treatment conditions, the viscosity curve as a function of the gas fraction is positioned higher than the viscosity obtained from oil displacement using only the water-gas mixture. The presence of a high-viscosity polymer solution in the reservoir likely contributes to a partial increase in the viscosity of the water-gas mixture. The dependency of viscosity on the volumetric gas fraction (R) during combined treatment falls within a narrow range of variation.

At a certain water-gas ratio, the viscosity of the mixture reaches stabilisation. The average stabilised viscosity of the water-gas mixture in the experiments was 2.5 mPa·s. Moreover, when the water-gas ratio exceeds 0.006 m^3/nm^3, the viscosity remains stable for all concentrations (Fig. 3).

Additionally, some portion of the gas (air) in the mixture may break through into the oil zone dissolving in it and reducing its viscosity. This process enhances the efficiency of oil displacement from the porous medium. The final oil recovery factor was 58.5% in Experiment No.6 and 81.5% in Experiment No.7. The additional oil recovery amounted to 16.5% in Experiment No.6 and 32.5% in Experiment No.7.

The research results indicate that the higher the viscosity of the mixture (i.e., the higher the water-gas ratio), the more effective the process.

Further the comparative analysis will be provided. Figure 7 presents the dynamics of oil recovery and water-gas mixture displacement of three experiments (Nos.1, 3, and 7), taken as examples from each variation. The starting point for comparison is the moment when oil displacement is ceased by distilled water (Stage I, i.e., depletion drive).

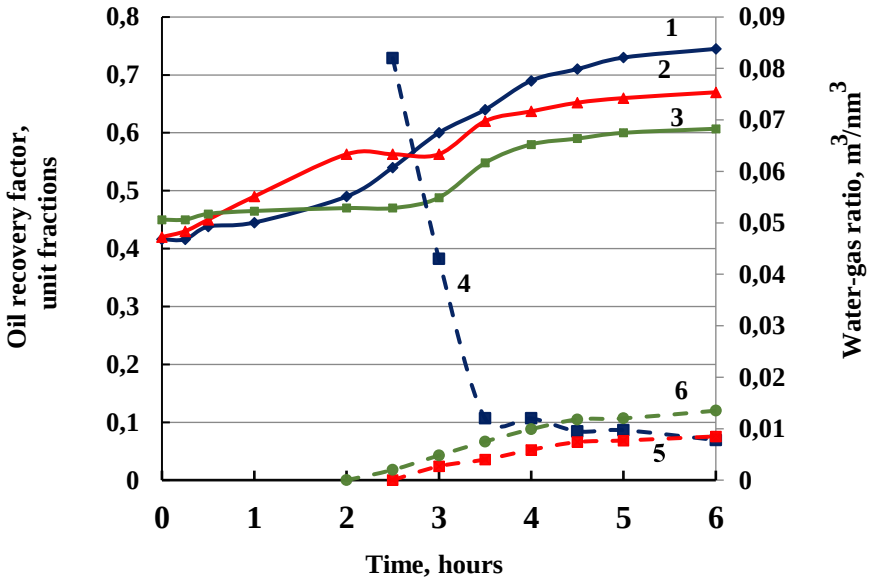


Fig. 5. Dynamics of changes in the oil recovery factor (ORF) and the water-gas ratio
1 and 4 – ORF and water-gas ratio for Experiment No.3, respectively;
2 and 5 – ORF and water-gas ratio for Experiment No.5, respectively;
3 and 6 – ORF and water-gas ratio for Experiment No.4, respectively.

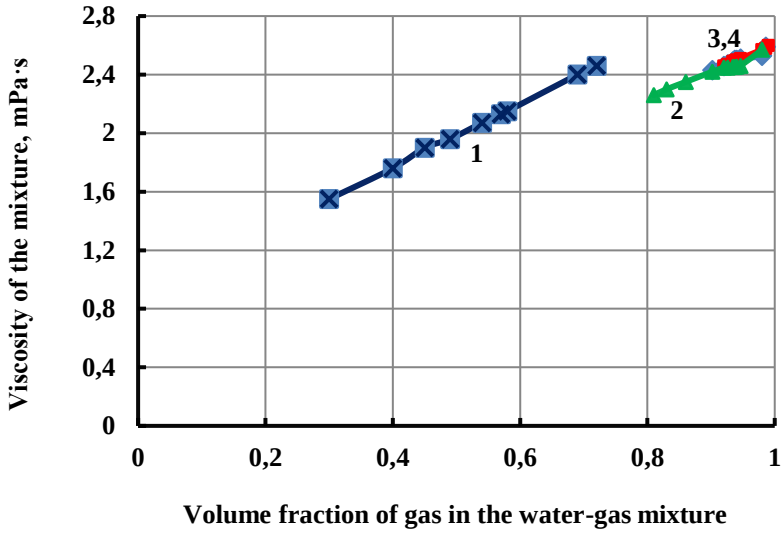


Fig. 6. Dependence of mixture viscosity on the gas volume fraction in the water-gas mixture under reservoir conditions
1 – Experiment No.7; 2 – Experiment No.3; 3 – Experiment No.5; 4 – Experiment No.4

The figure shows that during oil displacement with a polymer solution slug (curve 1) oil recovery increases gradually. However, in experiments No.3 and No.7, once the water-gas mixture is injected, the rate of oil production accelerates significantly. Consequently, the oil recovery factor increases. The highest final oil recovery factor is observed when only the water-gas mixture is injected, while the lowest is observed during displacement using only the polymer solution slug.

At first glance, oil displacement by the water-gas mixture appears to be the most efficient method. However, when comparing the actual increase in recovered oil, the water-gas method (32.9%) and the combined method using a 0.5% polymer solution slug followed by a water-gas mixture (32.5%) show nearly identical effectiveness. This is likely due to variations in the initial residual oil saturation at the beginning of the process.

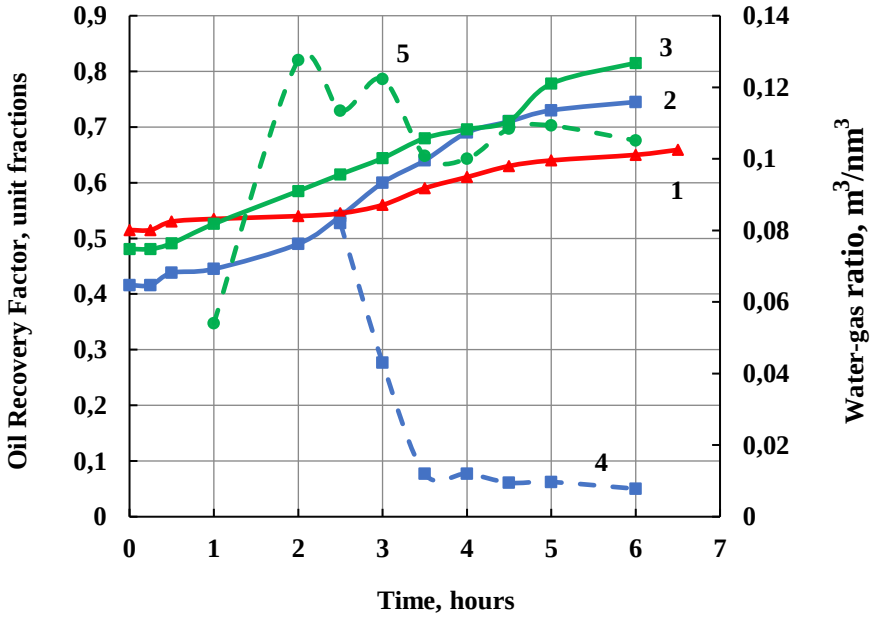


Fig. 7. Dynamics of Oil Recovery Factor (ORF) and Water-Gas Ratio (WGR)
1 – ORF of experiment No.1 (oil displacement by a polymer solution slug with C=0.5%);
2 – ORF of experiment No.3 (oil displacement by a polymer solution slug with C=0.5% and WGR);
3 – ORF of experiment No.7 (oil displacement by a water-gas mixture);
4 – WGR of experiment No.3;
5 – WGR of experiment No.7.

Conclusions

A comparative analysis of the conducted studies showed that the process of combined oil displacement (polymer + water-gas mixture) and oil displacement using a water-gas mixture are the most promising methods. By adjusting the polymer solution concentration and the water-gas ratio, the best results can be achieved. The experiments confirm the potential to improve the oil recovery factor in high-viscosity oil fields using the proposed methods.

Funding. This research was funded by the Science Committee of the Ministry of Education and Science of the Republic of Kazakhstan (grant AR22685524).

REFERENCES

Aleazar-Vara LA, Zamudio-Rivera LS, Buenrostro-Gonzalez E (2016) Application of multifunctional agents during enhanced oil recovery. In: Dr. Laura Romero-Zeron (ed) Chemical enhanced oil recovery (cEOR) – A Practical overview. https://doi.org/0.5772/64792

Babaev ER, Mamedova PSh, Soltanova ZG (2016) Compositions based on water-soluble polymers for use in oil displacement. Oil and Gas Chemistry (NefteGazoHimiya) 3:17–19 (in Russian)

Drozdov AN, Egorov YuA, Telkov VP (2007) Water-gas injection: investigation of oil displacement processes for various viscosity oils in the Shumovskoye field. Oil And Gas Territory (Territoriya Neftegas) 4:56–61 (in Russian)

Fyodorova AF, Portnyagin AS, Shits EYu (2012) Oil-displacing properties of polymer solutions under formation conditions at South-West Yakutia oilfields. Electronic scientific journal Oil and Gas Business (Neftegazovoe delo), Moscow 2:189–193 (in Russian)

Kukin VV, Solyakov YuV (1982) Application of water-soluble polymers for enhancing oil recovery from reservoirs. VNIIOENG, Moscow p 44 (in Russian)

Mamalov EN, Djalalov GI, Gorshkova EV et al (2022) Intensification of oil production using water-air mixture. SOCAR Proceedings, Baku 2:78–83 (in Russian)

Manzhay VN, Polikarpov AV, Rozhdestvensky EA (2017) Application of insoluble polymers for enhancing oil recovery from reservoirs. Bulletin of Tomsk Polytechnic University, Engineering of Georesources 328(12):29–35 (in Russian)

Mullaev BT, Abitova AZh, Saenko OB (2016) Uzen field: Problems and Solutions. vol 2, LitRes, Almaty, p 513 (in Russian)

Polymers for Oil Production. https://www.ecohim.spb.ru/neftedobycha/reagenty-dobychi-nefti. Accessed 17 Sep 2025

Shevtsov IA, Kabo VYa, Rumyantseva EL et al (2001) New technologies for the application of polymer reagents in oil production. Oil Industry 7:28–30 (in Russian)

Smith FW (1970) Behavior of partially hydrolyzed polyacrylamide solutions in porous media. J Pet Technol 22(2):148-156

Sparlin DD (1976) An evaluation of polyacrylamides for reducing water production. J Pet Technol 28(08):906–914

Thomas A, Sahuk B, Abirov Zh et al (2017) Polymer flooding to increase oil recovery at light and heavy oil. Oil and Gas Territory (Territoriya Neftegas), Kazakhstan, 7-8:58–67 (in Russian)

Veliyev EF (2020) Review of modern methods for enhancing oil recovery using flow-blocking technologies. SOCAR Proceedings (Scientific Papers of NIPI NEFTEGAS) 2:50–66 (in Russian)

ИССЛЕДОВАНИЕ ЭФФЕКТИВНОСТИ КОМПЛЕКСНОГО МЕТОДА ПОЛИМЕРНОГО И ВОДОГАЗОВОГО ВОЗДЕЙСТВИЯ НА НЕФТЯНЫЕ ПЛАСТЫ

Хадиева А.С.[1*], Бисембаева К.Т.[1], Мамалов Е.Н.[2], Сабырбаева Г.С.[1]

[1]Каспийский университет технологий и инжиниринга им.Ш.Есенова, Актау, Казахстан
130003, Мангистауская область, г. Актау, Микрорайон 32, дом 1
[2]Министерство науки и образования Республики Азербайджан, Институт нефти и газа, Азербайджан
AZ1000, Баку, ул.Ф.Амирова, 9
**Автор, отвечающий за переписку: hadieva_albina@mail.ru*

Резюме. Данная статья посвящена эффективной технологии добычи высоковязской нефти в неоднородных пластах. В работе рассматриваются вопросы увеличения нефтеотдачи с истощенных месторождений, содержащих высоковязкую нефть. В работе изучаются три варианта метода воздействия на нефтяной пласт. Два метода хорошо известны в нефтяной практике. Это полимерное заводнение и вытеснение нефти водогазовой смесью. Результаты, полученные в этих экспериментах, сравниваются с результатами предлагаемого комбинированного метода воздействия. Суть комбинированного метода в следующем. В пористую среду нагнетается оторочка раствора полиакриламида разной концентрации. Перемещение оторочки осуществляется нагнетанием водогазовой смеси (в наших исследованиях в качестве газа использовался воздух). Экспериментальные исследования производились на однородной модели пласта длиной 0,84 м и диаметром 0,025 м. В качестве пористой среды брался кварцевый песок с фракцией ≤0,20 мм. В экспериментах использовалась нефть вязкостью 205мПа*с при 20ºС. Во всех проведенных экспериментах на первом этапе осуществлялось вытеснение нефти дистиллированной водой. В первом варианте после первого этапа произвели закачку оторочки раствора полимера с последующим проталкиванием ее дистиллированной водой, во втором варианте – закачку оторочки раствора полимера с последующим проталкиванием ее водогазовой смесью. В третьем варианте дальнейшее вытеснение нефти после окончания первого этапа продолжили нагнетанием в пористую среду водогазовой смеси. Сравнительный анализ проведенных исследований показал, что худший результат получен при использовании только оторочки раствора полимера. Эффективность применения комбинированной технологии воздействия на основе оторочки раствора полимера с концентрацией 0,25% и водогазовой смесью и применение только водогазовой смеси с высоким водогазовым отношением примерно одинаковы.

Ключевые слова: *полимер, концентрация, раствор, водогазовая смесь, коэффициент извлечения нефти*

NEFT LAYLARINA POLİMER VƏ SU-QAZ TƏSİRİNİN KOMPLEKS ÜSULUNUN EFFEKTİVLİYİNİN TƏDQİQİ

Hadıyeva A.S.[1]*, Bisembayeva K.T.[1], Mamalov Y.N.[2], Sabirbayeva G.S.[1]
[1]Ş.Yesenov adına Kaspi Texnologiya və Mühəndislik Universiteti, Aktau, Qazaxıstan
130003, Mangistau vilayəti, Aktau, Mikrorayon 32, Bina 1
[2]Azərbaycan Respublikasının Elm və Təhsil Nazirliyinin Neft və Qaz İnstitutu, Azərbaycan
AZ1000, Bakı, F.Əmirov küçəsi, 9
**Yazışmalara məsul:hadieva_albina@mail.ru*

Xülasə. Bu məqalə qeyri-bircins laylarda yüksək özlülüklü neftin çıxarılmasının effektiv texnologiyasına həsr olunmuşdur. İşdə yüksək özlülüklü tükənmiş yataqlardan neftvermə əmsalının artırılması məsələlərinə baxılır. İşdə neft layına təsir üsulunun üç variantına baxılmışdır. Bunlardan iki üsul neft praktikasında yaxşı tanınır. O üsullardan biri neftin laydan polimerlə, digəri isə neftin su-qaz qarışığı ilə sıxışdırılması üsuludur. Bu üsullarla təcrübələr aparılmış və alınan nəticələr laya kombinə edilmiş təsir üsulu ilə alınmış nəticələrlə müqayisə edilmişdir. Kombinə edilmiş üsulun mahiyyəti aşağıdakılardan ibarətdir. Müxtəlif konsentrasiyalı poliakrilamid məhlulu məsaməli mühitə vurularaq val yaradılır və onun yerdəyişməsi su-qaz qarışığının vurulması ilə həyata keçirilir (tədqiqatlarda qaz əvəzinə havadan istifadə edilmişdir). Eksperimental tədqiqatlar 0,84 m uzunluğunda və 0,025 m diametrində homogen təbəqə modelində aparılmışdır və ≤ 0,20 mm fraksiyalı kvars qum məsaməli mühit kimi götürülmüşdür. Təcrübələrdə 20^{o} C-də 205mPa*s özlülüklü neftdən istifadə edilmişdir. Aparılan bütün təcrübələrdə birinci mərhələdə neftin distilə edilmiş su ilə sıxışdırılması həyata keçirilmişdir. Birinci mərhələdən sonra, polimer məhlulu uyğun olaraq distilə edilmiş su və su-qaz qarışığı ilə sıxışdırılmışdır. Üçüncü variantda birinci mərhələ başa çatdıqdan sonra neftin sıxışdırılması su-qaz qarışığının məsaməli mühitə vurulması ilə davam etdirilmişdir. Aparılan tədqiqatların müqayisəli təhlili göstərdi ki, ən pis nəticə yalnız polimer məhlulunun valından istifadə edildikdə əldə edilir. 0,25% konsentrasiyalı polimer məhlulu və su-qaz qarışığı əsasında kombinəli təsir texnologiyasının tətbiqinin effektivliyi və yüksək su-qaz nisbəti ilə yalnız su-qaz qarışığının tətbiqi təxminən eynidir.

Açar sözlər: *polimer, konsentrasiya, məhlul, su-qaz qarışığı, neftvermə əmsalı*

ANAS Transactions Earth Sciences 2 / 2025

http://www.journalesgia.com

CHARACTERIZATION OF UNDERGROUND RIVER PASSAGES CONTROLLED BY ALLOGENIC RECHARGE: INSIGHTS FROM AN ARTIFICIAL TRACER TEST IN THE GUNUNGSEWU KARST AREA, INDONESIA

Cahyadi A.[1*], Adji T.N.[1], Haryono E.[2], Widyastuti M.[1], Agniy R.F.[3], Naufal M.[2], Setiawan N.[2], Fathoni H.[2], Pratama A.D.[2], Riyanto I.A.[4], Fatchurohman H.[5]

[1]Department of Environmental Geography, Faculty of Geography, Universitas Gadjah Mada, Indonesia
Yogyakarta, 55281
[2]Karst Research Group, Faculty of Geography, Universitas Gadjah Mada, Indonesia
Yogyakarta, 55281
[3]Department of Geography Information Science, Faculty of Science, Technology, Engineering and Mathematics, Universitas Maha Karya Asia, Indonesia
Yogyakarta, 55282
[4]Doctoral Program on Geography, Faculty of Geography, Universitas Gadjah Mada, Indonesia
Yogyakarta, 55281
[5]Department of Earth Technology, Vocational College, Universitas Gadjah Mada, Indonesia
Yogyakarta, 55281
**Corresponding author: ahmad.cahyadi@ugm.ac.id*

Keywords: *allogenic river, artificial tracer test, dissolution passage, fluorescent dyes*

Summary. The Ponjong Hydrogeological Subsystem is a part of the Gunungsewu Karst Area on Java Island, Indonesia, and is uniquely influenced by allogenic recharge. This allogenic river system exists because the karst in this subsystem develops over a Tertiary volcanic formation. The contact between the Wonosari Formation limestone and the volcanic rocks, primarily composed of explosive volcanic materials from the Semillir Formation, allows this system forming. In this area, allogenic river catchments are dominated by relatively impermeable volcanic rocks and steep gradients, which often lead to flash floods. This study aimed to determine the characteristics of the cave and conduit networks within the underground river system influenced by allogenic recharge. An artificial tracer test using fluorescent dyes with breakthrough curves recorded by a fluorometer was conducted. Data analysis revealed that large, single conduits predominantly shape the cave networks in the study area. Due to the large discharge and steep gradient of the underground river system, a single conduit is formed instead of a maze-like cave system. The identification of connectivity between the allogenic rivers and the Gremeng Resurgence highlights that the karst drainage basin of the Gremeng Resurgence is not part of the Beton Karst Drainage Basin, as previously suggested by researchers who used methods other than artificial tracer tests. The development of large underground river systems indicates a high vulnerability to groundwater pollution and the ability to release groundwater reserves quickly. This poses a challenge for future environmental management, particularly in relation to water quality and water resource quantity management.

© 2025 Earth Science Division, Azerbaijan National Academy of Sciences. All rights reserved.

Introduction

The Gunungsewu karst area is located in the south-central part of the island of Java, Indonesia. This karst area is one of the most extensive karst areas in Indonesia with enormous water resource potential. Several underground rivers and springs have been utilized to meet the water needs of the communities in the karst area and also the surrounding areas.

The Gunungsewu Karst Area has six hydrogeological subsystems (Fig. 1) (Haryono et al., 2017). One of which is Ponjong Subsystem (Cahyadi et al., 2018a; Riyanto et al., 2018). This subsystem consists of springs and resurgence with large discharges

and a well-developed underground river system (Haryono, 2011).

Ponjong differs from the other subsystems in Gunungsewu in the presence of allogenic recharge (Cahyadi et al., 2018b). Allogenic is a type of water recharge that supplies an underground river or groundwater in karst areas and originate in non-karst areas (Ford & Williams, 2007; Gilli, 2015). In Ponjong Subsystem, the allogenic recharge flows from the north, which is a hilly area with tertiary volcanic rocks (Adji, 2011; 2012). Some experts refer to the catchment area of this subsystem as Panggung Massive (van Bemmelen, 1949).

The allogenic river emerging in Ponjong Subsystem is attributable to the contact between tertiary volcanic rocks and the underlying limestone that forms Gunungsewu Karst Area. These volcanic rocks are part of the four ancient volcanoes, namely Panggung, Manyaran Wonodadi, and Wuryantoro ancient volcano (Fig. 2) (Akmaluddin et al., 2005; Surono, 2008; Bronto et al., 2009). On the 1:100,000 Geologic Map of Surakarta published by the Geological Agency, these volcanic materials are constituents of the Semilir Formation (Tms) and Wonosari Formation (Tmwl) (Surono et al., 1992).

Allogenic recharge in underground rivers/groundwater systems in karst areas is thought to have a considerable influence on the development of cave networks (Palmer, 2007; 2001). Open systems in allogenic rivers allow the entry of water with high concentrations of carbon dioxide into the karst groundwater system, and the dissolution process is thereby more intensive than in areas controlled by autogenic recharge (closed system) (Auler, 2013). Moreover, large amounts of water likely cause highly intensive erosion on the walls of caves and underground rivers, although not throughout the year (White, 1988; Palmer, 2007).

Characterizing dissolution passages and flow connectivity is the first part of defining karst drainage basins. Defining the karst drainage basin (KDB) or catchment area is very important in environmental management (Abdulrazzaq et al., 2022, Imrani et al., 2023). Karst areas with highly developed dissolution passages have very different characteristics from undeveloped karst areas. In addition to the vulnerability to pollution, these conditions are also related to the storage and release properties of karst aquifers, thus determining the condition of water resources in a region.

This study aimed to determine the characteristics of the cave passages and their connectivity within the Ponjong Hydrogeological Subsystem. Understanding the effects of allogenic recharge on the network shape is crucial for managing karst areas in general (Eppelbaum et al., 2014), and particularly those regions affected by allogenic recharge in the future. This paper presents a case study of the Kalimati Sinking Stream - Gremeng Resurgence system, an underground river system at the research site.

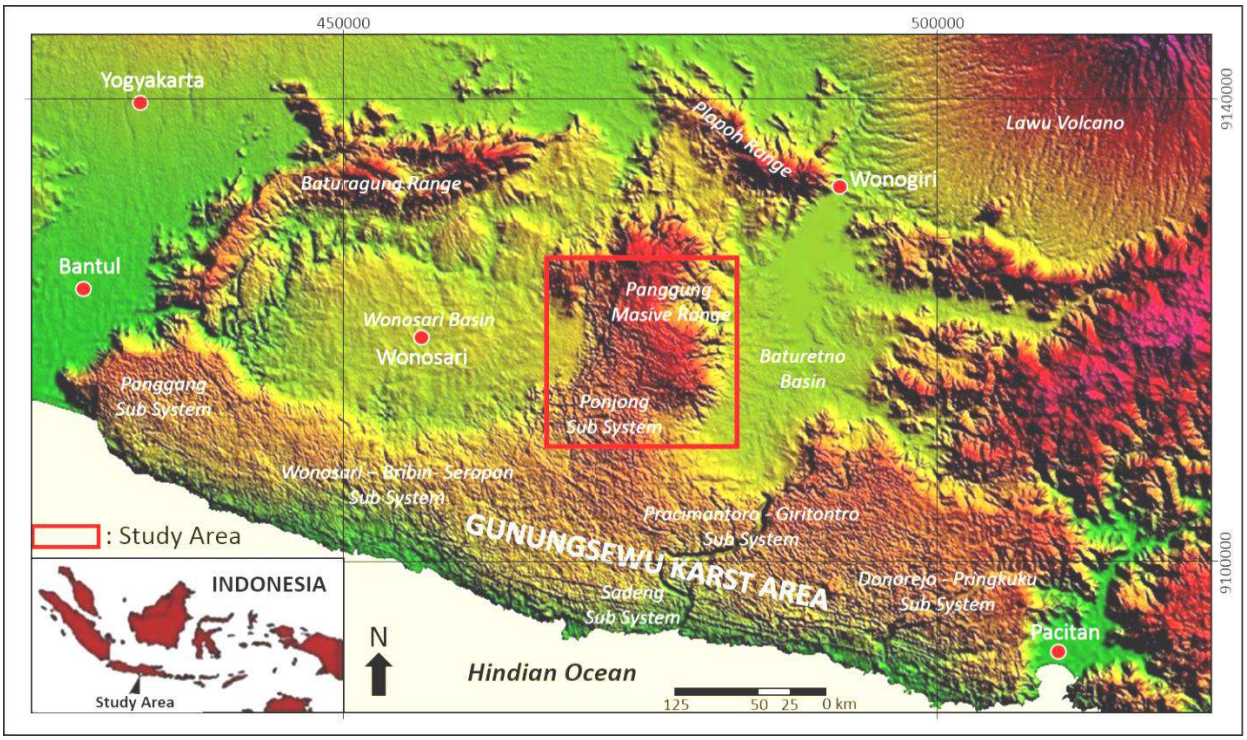


Fig. 1. The Hydrogeological System of Gunungsewu Karst Area
(Sources: Shuttle Radar Topography Mission United States Geological Survey)

Methods

The artificial tracer test resulted in breakthrough curve from which the characteristics of the karst cave networks were identified. Breakthrough curve recording was done with 2 fluorometers placed in Gremeng and Beton Resurgence. Tracer test is a method of tracking or tracing subsurface channels using water tracing agents (Stanley et al., 1980; Käss, 1998; Field, 2003; Field, 2005; Worthington, 2011). This research used two tracing agents or fluorescent dyes, namely uranine and tinopal. Both substances were selected because they are safe to use and easily detected even in minute concentrations (Hess and White, 1989; Behrens et al., 2001; Benischke et al., 2007).

The quantities of dye tracer used in this study are based on the equation proposed by Benischke et al. (2007), as shown in Equation 1. This equation was chosen because it generally does not overestimate the amount of dye tracer needed and does not result in a flat curve in the breakthrough curve (BTC) recording, as it does not exceed the maximum concentration that the fluorometer can detect. M represents the quantity of dye tracer required, in kilograms (kg). L is the distance from the injection point to the observation point, where the fluorometer is installed, measured in kilometres (km). Q is the discharge during artificial tracer tests conducted at the study site, in litres per second (L/s). C is the target peak concentration to be obtained, measured in micrograms per litre (µg/L). The peak concentration refers to the maximum concentration recorded by the fluorometer.

$$M = 1{,}9.10^{-5}(LQC)^{0{,}95} \qquad 1)$$

The fluorescent dye was injected into Kalimati Sinking Stream (Fig. 3), and its appearance was observed at Beton and Gremeng Resurgences. This procedure was carried out because underground rivers controlled by allogenic recharge can form maze caves, which are underground passageways with many branches (Palmer, 2007). The observation results were recorded in a fluorometer and analysed based on the shape of the resultant breakthrough curve. Some conduits that are identifiable by the breakthrough curve analysis are shown in Fig. 4.

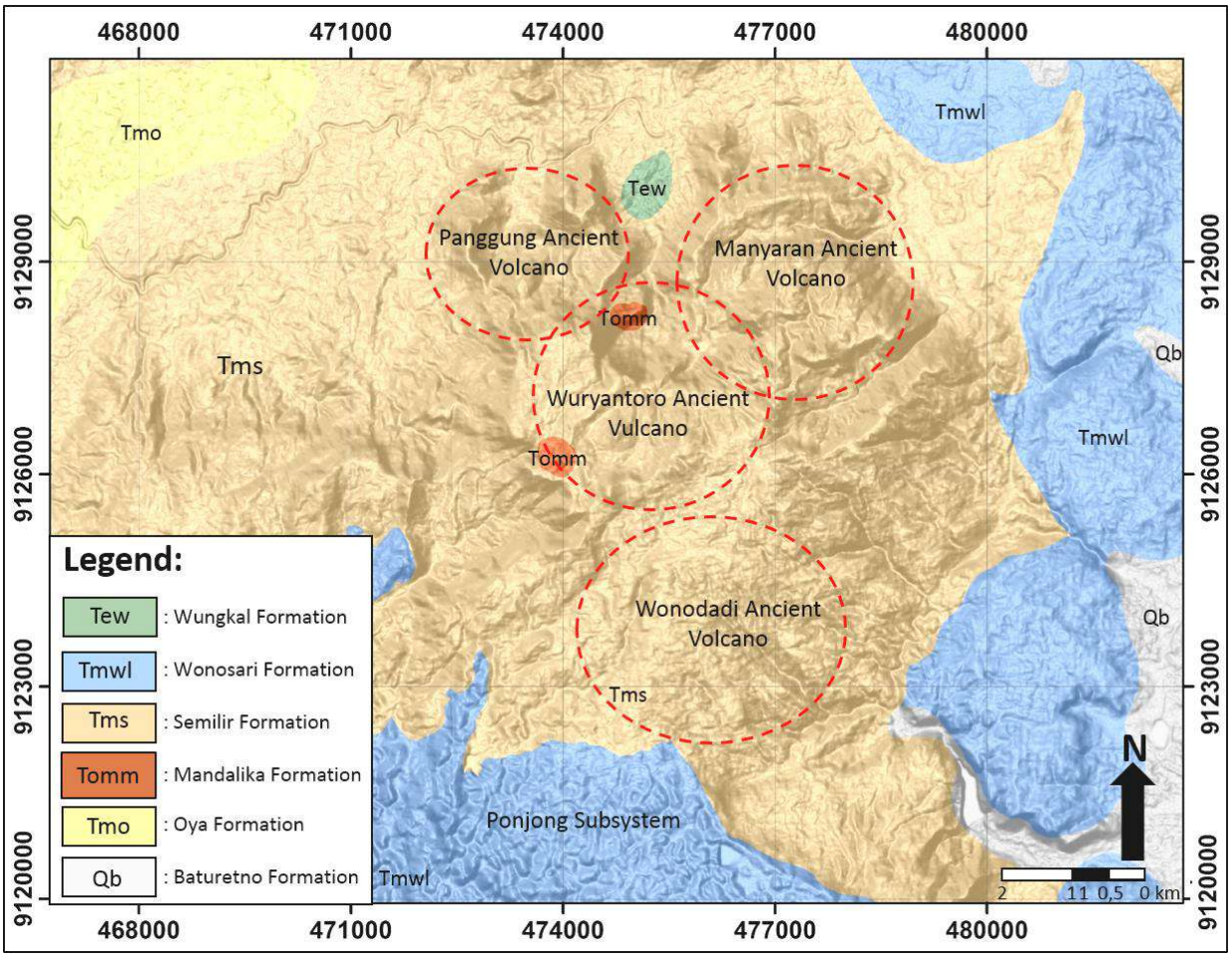


Fig. 2. The Ancient Volcanoes around the Ponjong Hydrogeological Subsystem
(Sources: Geological Map from Geological Agency of Indonesia and DEMNAS from Geospatial Information Agency of Indonesia)

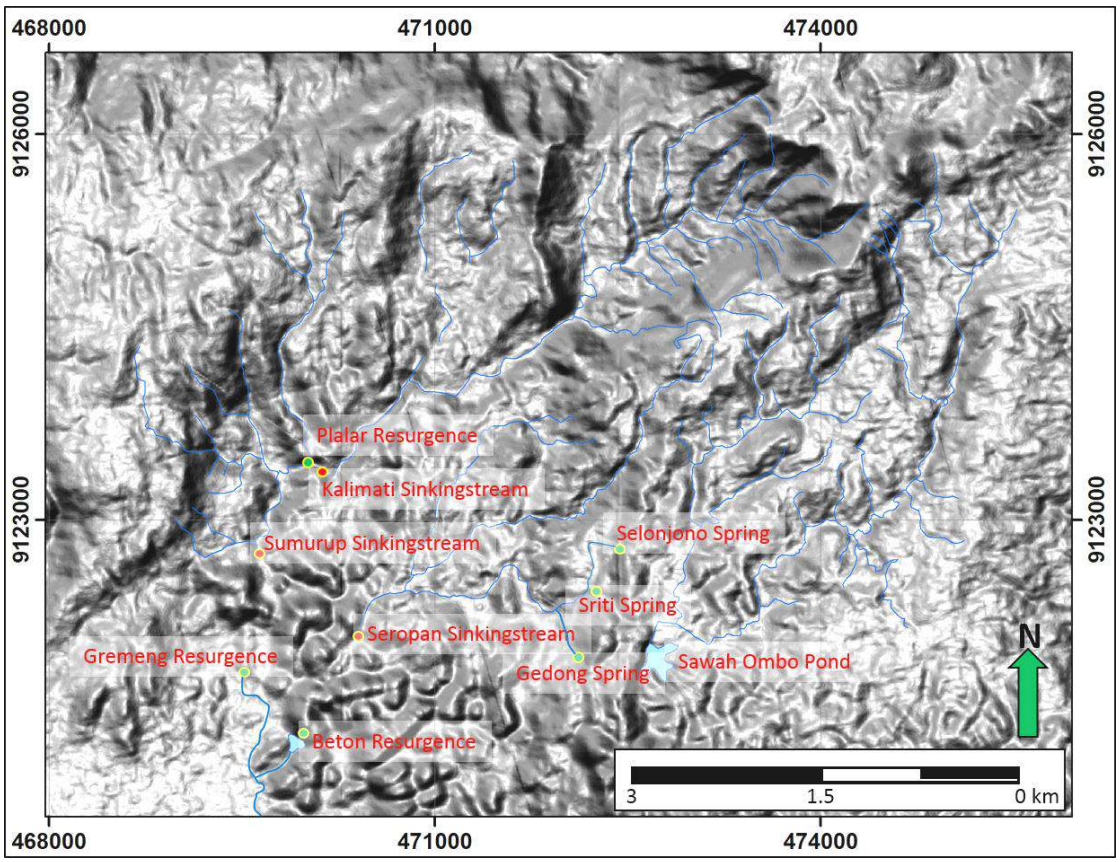


Fig. 3. The Hydrological Conditions of the Karst Area with Ponjong Hydrogeological Subsystem (Sources: Shuttle Radar Topography Mission United States Geological Survey and Field Survey)

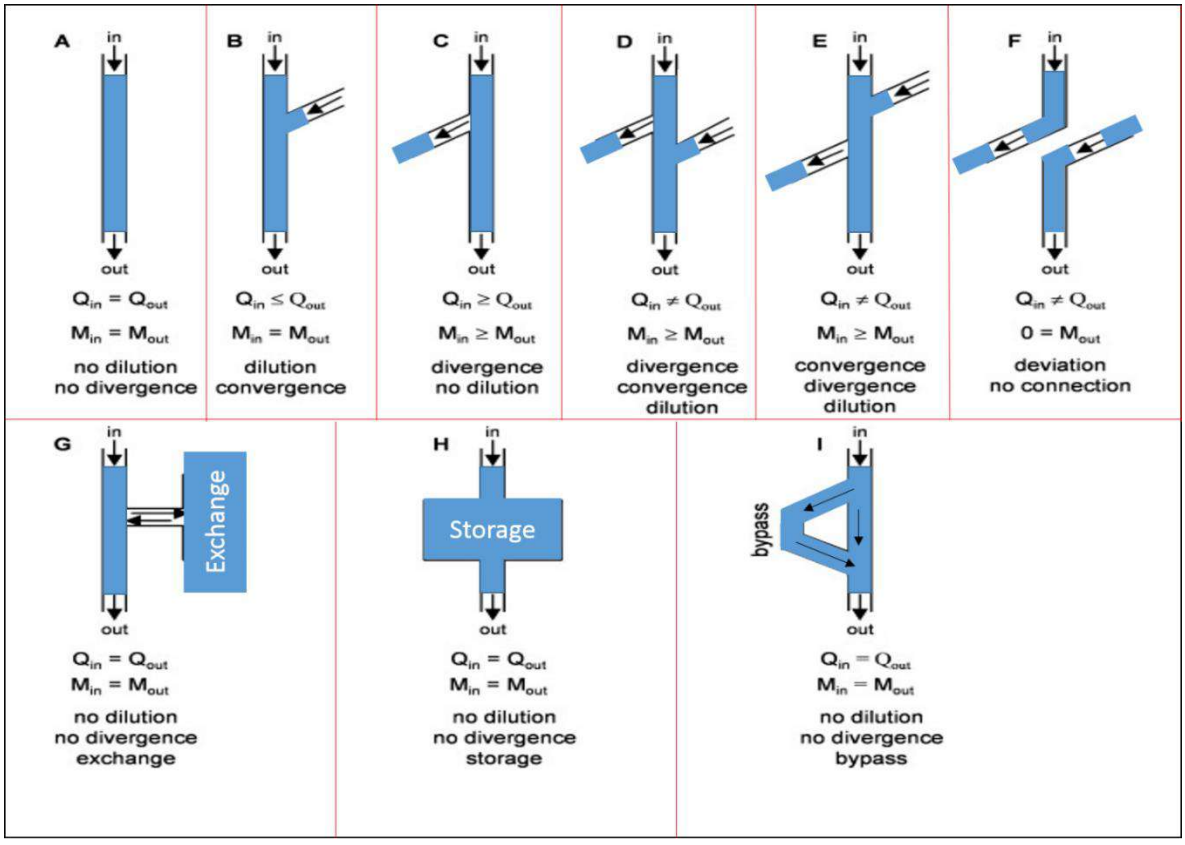


Fig. 4. Several Types of Cave Networks in Karst Underground River (Modification from Goldscheider et al., 2008)

Results and Discussion

The analysis results showed that the fluorescent dye (uranine) injected into Kalimati Sinking Stream appeared in Plalar Resurgence. From this resurgence site, the monitoring detected that the karst water flew through a surface river toward Sumurup Sinking Stream before re-emerging in Gremeng Resurgence. Since the fluorometer at Beton Resurgence did not read the presence of uranine, it implies that the allogenic system of Kalimati is not part of the networks that shape Beton Resurgence. This finding is different from previous studies in the same location because they employed different methods, namely topographic considerations (Budiyanto, Lestari, 2019), topography, cave distribution, and sinking stream (Pratiwi, 2013), and water balance (Lestari et al., 2014). Fig. 5 illustrates the complete connectivity between the sinking streams and resurgences at the research site.

In addition to Kalimati, the tracer dye was injected into Seropan Sinking Stream. Although this dye did not appear at Gremeng Resurgence, it was detected in Beton Resurgence. It indicates that Seropan Sinking Stream and Gremeng Resurgence are from two separate systems. These results are in line with Pratiwi (2013) and Lestari et al. (2014) but contrary to Budiyanto, Lestari (2019) that include Seropan Sinking Stream into the Gremeng Resurgence system.

Recording by fluorometer at Gremeng Resurgence produced a breakthrough curve, as presented in Fig. 6. The breakthrough curve was in a single form, representing a single conduit (Goldscheider et al., 2008; Leibundgut et al., 2009; Gilli, 2015). The steep curve with a short transit time shows that the cave network is well-developed and somewhat large. A single conduit is the characteristic of caves affected by allogenic recharge in addition to maze cave.

The BTC of artificial tracer test results at Kalimati Sinking Stream – Gremeng Resurgence showed that the dye tracer was first detected after 82 minutes. This indicates the rapid flow of water in the underground river, the highly developed dissolution tunnels, and the very high susceptibility to contamination. The dye tracer concentration peaked approximately 22 minutes after injection and was last detected after 223 minutes.

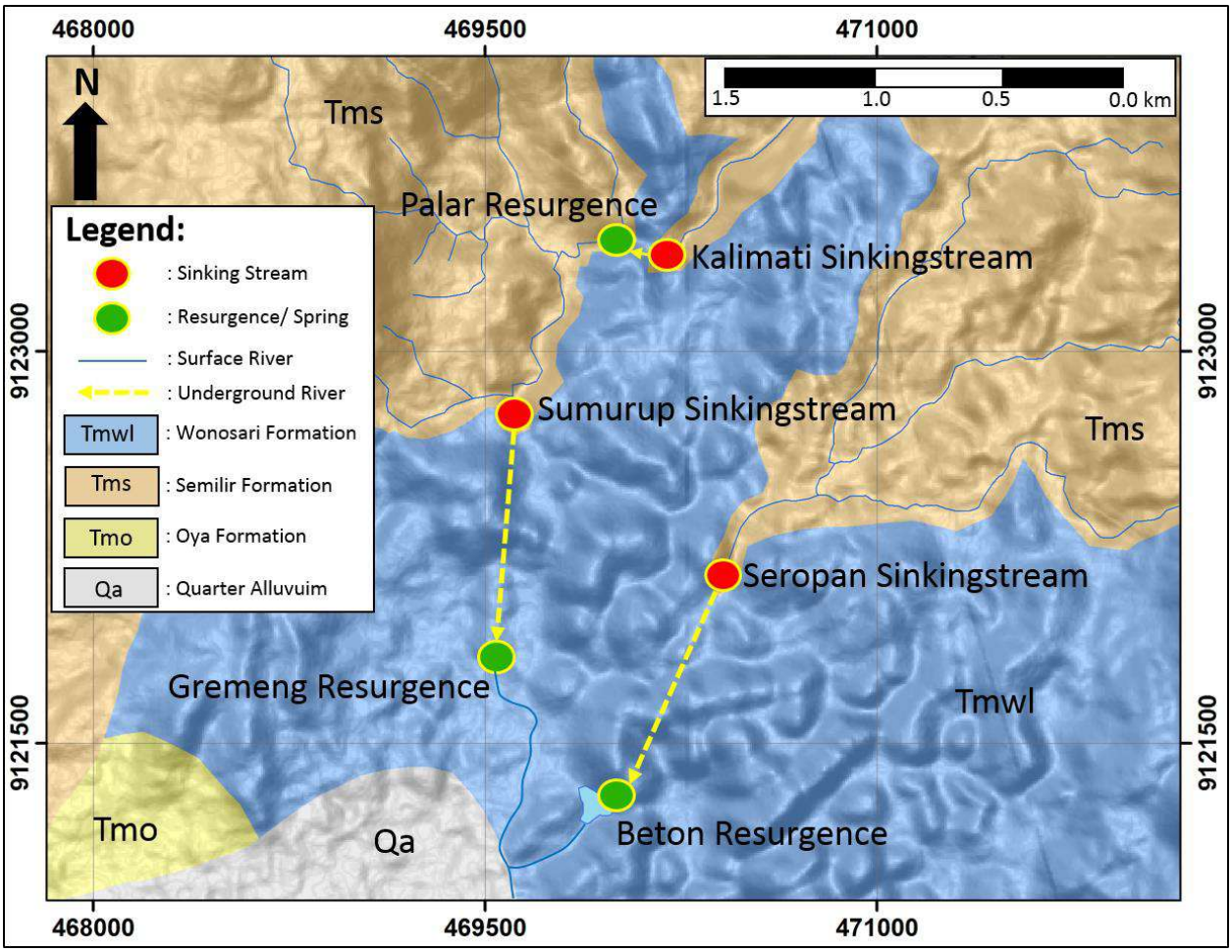


Fig. 5. The Connectivity Between the Sinking Streams and Resurgences in Ponjong Hydrogeological System Based on Tracer Test (Sources: Shuttle Radar Topography Mission United States Geological Survey and Field Survey)

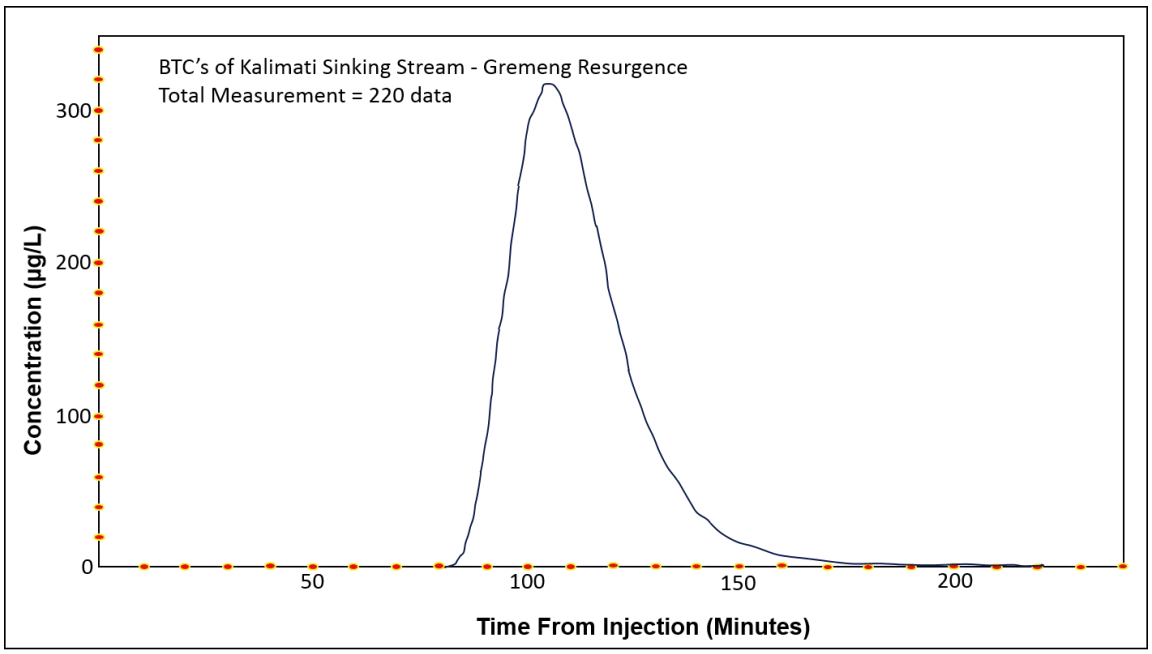


Fig. 6. The Breakthrough Curve at Gremeng Resurgence

Single conduits develop in karst areas controlled by allogenic recharge because the water intermittently flows in a large quantity (for example, flash floods) and at a fast rate as a consequence of underground river flow with high gradient. The high gradient is caused by the vast difference in elevation of sinking stream and resurgence over a short horizontal distance. Cahyadi et al. (2022) mentioned that underground river passages formed in Beton Karst Drainage Basin / KDB (located east of Gremeng KDB) also have single conduit characteristics for all dissolution passages formed (Fig. 7). The BTC recorded at Beton Resurgence shows a shorter time span between the first and last detections compared to the BTC at Gremeng Resurgence. With relatively similar spacing, this suggests a more developed dissolution tunnel in the Beton KDB.

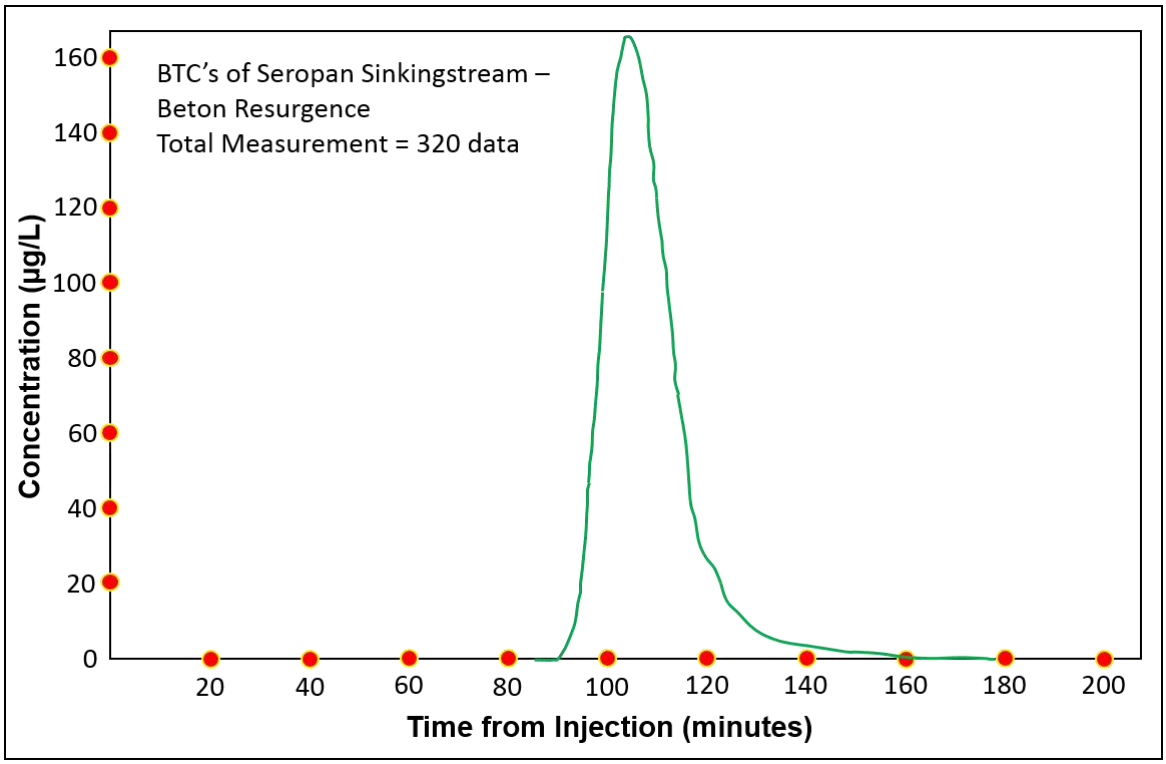


Fig. 7. The Breakthrough Curve at Beton Resurgence

The catchment area of the allogenic river system that enters Gremeng Resurgence is 13.25 km^2 (Cahyadi et al., 2018b). It is mostly composed of volcanic rocks like basaltic-andesitic lava, tuff, volcanic breccia, and agglomerates. Because these rocks poorly absorb water, the rain falling on them transform to high amounts of runoff. Also, the elevations of Sumurup Sinking Stream and Gremeng Resurgence differ by 60 m with a horizontal distance of 800 m, creating a high gradient. Area of watershed of allogenic river, the geological character of the catchment, and high gradient are the factors that form a single conduit system. Unlike this network system, Pindul – an underground river system in Wonosari Basin – has multiple conduit networks and a slightly sloping breakthrough curve (Cahyadi, Agniy, 2016). Despite its broader catchment area, Pindul has a low gradient that allows the development of these networks.

The development of advanced dissolution tunnels with large single conduits allows for rapid flow of underground rivers. This will certainly lead to rapid release of water from the aquifer. This causes the water that enters the underground river to be discharged quickly. On the other hand, the connectivity of the Gremeng Resurgence with the allogenic rivers at the ground surface causes the vulnerability to pollution from the Gremeng Resurgence to be very high. Protection of the karst drainage basin in Gremeng Resurgence requires management of the area outside the karst area which is an allogenic watershed. It is an integral part of the karst area that feeds the Gremeng Resurgence through autogenic recharge.

Conclusions

The breakthrough curve represents the development of an extensive, single conduit cave network in the Ponjong Hydrogeological Subsystem. Also, the absence of fluorescent dye emerging at springs or other resurgences indicates that maze cave does not form in the study area. Single conduits are the result of intermittent allogenic recharge with a substantial quantity. Kalimati Sinking Stream is located at a significantly different elevation than Gremeng Resurgence, results in high gradient and rapid flow of water in the underground river system. Consequently, instead of a maze cave, a single conduit dominates this system.

Acknowledgement

This research is part of the first author's dissertation and is funded by the 2019 Research Grant for Young Lecturers of Universitas Gadjah Mada. Authors would like to thank all parties who have assisted in this research.

REFERENCES

Abdulrazzaq ZT, Ahmed MM, Salih SA, Asfahani J (2022) Hydro-geophysical parameters estimation of porous aquifer using geoelectrical technique – case study from Baiji-Tikrit Sub-Basin, Iraq. ANAS Transactions Earth Sciences 1:3–16. https://doi.org/10.33677/ggianas20220100068

Adji TN (2011) Baseflow separation of the Bribin River Upstream in Gilap Cave Flowage, Sewu Mountain Karst, Gunung Kidul, Yogyakarta. Jurnal Geologi Indonesia 6(3):165–175. https://doi.org/10.17014/ijog.6.3.165-175 (in Indonesian)

Adji TN (2012) Wet season hydrochemistry of Bribin Cave in Gunung Sewu Karst, Indonesia. Environmental Earth Sciences 67(6):1563–1572. http://dx.doi.org/10.1007/s12665-012-1599-x

Akmaluddin, Setijadji DL, Watanabe K, Itaya T (2005) New interpretation on magmatic belts evolution during the Neogene-Quaternary periods as revealed from newly collected K-Ar ages from Central-East Java, Indonesia. Proceedings Joint Convention Surabaya 2005 – HAGI-IAGI-PERHAPI. The 30th HAGI, The 34th IAGI, and The 14th PERHAPI Annual Conference and Exhibition. http://repository.ugm.ac.id/digitasi/download.php?file=3261

Auler AS (2013) Sources of water aggressiveness – the driving forces of karstification. In: Treatise on Geomorphology, vol. 6. Elsevier Inc., London p 23–28, https://doi.org/10.1016/B978-0-12-374739-6.00099-3

Behrens H, Beims U, Dieter H et al. (2001) Toxicological and ecotoxicological assessment of water tracer. Hydrogeology Journal 9: 321–325. https://doi.org/10.1007/s100400100126

Benischke R, Goldscheider N, Smart C (2007) Tracer techniques. In: Methods in karst hydrogeology. Taylor and Francis Group, London, p 147–170

Bronto S, Mulyaningsih S, Hartono G, Astuti B (2009) Waduk Parangjoho and Songputri Reservoirs: alternative eruption sources of Semilir Formation in Eromoko Area, Wonogiri Regency, Central Java. Jurnal Geologi Indonesia 4(2):79–92. http://dx.doi.org/10.17014/ijog.4.2.77–92 (in Indonesian)

Budiyanto E, Lestari EP (2019) Sensitivity of Gremeng Karst Spring to rainfall in its catchment area. Jurnal Geografi: Geografi dan Pengajarannya 17(1):63–70 (in Indonesian)

Cahyadi A, Agniy RF (2016) Breakthrough curve analysis for passage characterization in Pindul underground river system. https://osf.io/preprints/inarxiv/3bs2v/ (in Indonesian)

Cahyadi A, Riyanto IA, Adji TN et al (2018a) Hydrostratigraphy and its impact on the emergence of springs in the Panggang Sub-System, Gunungsewu Karst Region, Gunungkidul Regency. Proceedings of Seminar Nasional Geografi II organized by Himpunan Mahasiswa Pascasarjana Geografi (HMPG) UGM. https://doi.org/osf.io/preprints/inarxiv/pc9fv/ (in Indonesian)

Cahyadi A, Riyanto I, Irshabdillah MR et al (2018b) Inventory and characterization of allogenic river flow system in Karst Gunungsewu Area of Gunungkidul Regency. Research Report (Faculty of Geography, Universitas Gadjah Mada), Yogyakarta, Indonesia, 92 p. https://acadstaff.ugm.ac.id/karya_files/inventarisasi-dan-karakterisasi-sistem-aliran-sungai-alogenik-di-kawasan-karst-gunungsewu-kabupaten-gunungkidul-0eab08e1810838be9e4be72cdfe44ac7 (in Indonesian)

Cahyadi A, Adji TN, Haryono E, Widyastuti M, Agniy RF (2022) Tracing flow directions of the Pentung Allogenic River in Gunungsewu Karst Area, Gunungkidul, using artificial tracer test. IOP Conference Series: Earth and Environmental Science, vol. 1098 (1). https://iopscience.iop.org/article/10.1088/1755-1315/1098/1/012048

Davis SN, Thompson GM, Bentley HW, Stiles G (1980) Ground-water tracers – a short review. Groundwater Journal 18(1):14–21. https://doi.org/10.1111/j.1745-6584.1980.tb03366.x

Eppelbaum L, Zheludev V, Averbuch A (2014) Diffusion maps as a powerful tool for integrated geophysical analysis to detecting hidden karst terranes. ANAS Transactions Earth Sciences 1-2:36–46

Field MS (2003) A review of some tracer-test design equations for tracer-mass estimation and sample-collection frequency. Environmental Geology 43:867–881. https://doi.org/10.1007/s00254-002-0708-7

Field MS (2005) Tracer-Test design for losing stream-aquifer systems. International Journal of Speleology 35(1):25–36. http://dx.doi.org/10.5038/1827-806X.35.1.4

Ford D, Williams P (2007) Karst hydrology and geomorphology. John Wiley and Sons Ltd., Chichester, West Sussex, United State of America, p 576. https://doi.org/10.1002/9781118684986

Gilli E (2015) Karstology – karst, caves and springs: elements of fundamental and applied karstology. CRC Press, Boca Raton, Florida, United State of America, p 256. http://dx.doi.org/10.1201/b18380.

Goldscheider N, Meiman J, Pronk M, Smart C (2008) Tracer tests in karst hydrogeology and speleology. International Journal of Speleology 37(1):27–40. http://dx.doi.org/10.5038/1827-806X.37.1.3

Haryono E (2011) Introduction to Gunungsewu karst. Field Guide. Asian Trans-Disciplinary Karst Conference. https://osf.io/preprints/inarxiv/7w2sh_v1

Haryono E, Barianto DH, Cahyadi A (2017) Hydrogeology of Gunungsewu Karst Area: field guide for the 2nd annual scientific week of the association of Indonesian groundwater experts. https://osf.io/preprints/inarxiv/t5dgp/ (in Indonesian)

Hess JW, White WB (1989) Chemical hydrology. In: Karst hydrology: concepts from the Mammoth Cave Area. Springer, New York, United State of America, p 145–174

Imrani ZT, Zeynalova KZ, Hidayati GA (2023) A study of caves and their speleotourism potential in Azerbaijan. ANAS Transactions Earth Sciences 1:100–110. http://doi.org/10.33677/ggianas20230100097

Käss W (1998) Tracing technique in geohydrology. Balkema, Rotterdam, Netherland, 602 p

Leibundgut C, Maloszewski P, Külls C (2009) Tracers in hydrology. Wiley Blackwell, New York, USA, 432 p

Lestari Y, Haryono E, Fatchurohman H (2014) Identification of catchment area criticality level to determine management direction: case study of Beton Spring Catchment, Ponjong, Gunungkidul. In: Environmental ecology of Indonesian Karst Areas: maintaining the preservation of Indonesia's Karst Areas, Second Edition. Deepublish, Yogyakarta, Indonesia, p 52–65 (in Indonesian)

Palmer AN (2001) Dynamics of cave development by allogenic water. Acta Carsologica 30(2):13–32

Palmer AN (2007) Cave geology. Caves Books, Dayton, Ohio, United State of America, p.454

Pratiwi ES (2013) Weaknesses and constraints of the application of the EPIK method in determining intrinsic groundwater vulnerability zoning in the Gunungsewu Karst Area, Indonesia. In: Environmental ecology of Indonesian Karst Areas: maintaining the preservation of Indonesia's Karst Areas, First Edition, Deepublish, Yogyakarta, Indonesia, p 53–63. https://books.google.co.id/books/about/Ekologi_lingkungan_Kawasan_Karst_Indones.html?id=i05iEQAAQBAJ&redir_esc=y (in Indonesian)

Riyanto IA, Cahyadi A, Adji TN, Haryono E et al (2018) Connectivity analysis and characterization of passage using tracer test in epikarst spring of Panggang Sub system, Gunungsewu Karst Area. Proceeding of Indonesian Hydrogeologist Expert Community Annual meeting (in Indonesian)

Surono BT, Sudarno I, Wiryosujono S (1992) Geology of the Surakarta-Giritontro Quadrangles, Java: Bandung, geological research and development center, Indonesia, scale 1:100,000

Surono S (2008) Sedimentation of the Semilir formation in Sendang Village, Wuryantoro, Wonogiri, Central Java. Jurnal Sumber Daya Geologi 28(1):29–41 (in Indonesian)

van Bemmelen RW (1949) The geology of Indonesia. Vol. IA, General geology. Martinus Nijhoff, The Hague, Netherland

White WB (1988) Geomorphology and hydrology of karst terrains. Oxford University, New York, p 480

Worthington SRH (2011) Management of carbonate aquifers. In: Karst management. Springer, Dordrecht, Netherland, p 241–263

ОСОБЕННОСТИ ПОДЗЕМНОГО СТОКА РЕК С АЛЛОГЕННЫМИ ВОДАМИ, ВЫЯВЛЕННЫЕ МЕТОДОМ ИСКУССТВЕННОГО ТРАССИРОВАНИЯ В КАРСТОВОМ РЕГИОНЕ ГУНУНГСЕВУ (ИНДОНЕЗИЯ)

Кахиади А.[1*], Аджи Т.Н.[1], Харьоно Э.[2], Видьястути М.[1], Агний Р.Ф.[3], Науфал М.[2], Сетиаван Н.[2], Фатони Г.[2], Пратама А.Д.[2], Рийанто И.А.[4], Фатчурохман Г.[5]

[1]Кафедра экологической географии, географический факультет, Университет Гаджах Мада, Индонезия Джокьякарта, 55281

[2]Группа по исследованию карста, географический факультет, Университет Гаджах Мада, Индонезия Джокьякарта, 55281

[3]Кафедра геоинформатики, факультет науки, технологии, инженерии и математики, Университет Маха Карья Азия, Индонезия Джокьякарта 55282

[4]Докторская программа по географии, географический факультет, Университет Гаджах Мада, Индонезия Джокьякарта, 55281

[5]Отделение технологии Земли, Профессиональный колледж, Университет Гаджах Мада, Индонезия Джокьякарта, 55281

**Автор, отвечающий за переписку: ahmad.cahyadi@ugm.ac.id*

Резюме. Гидрогеологическая подсистема Понджонг является частью карстовой области Гунунгсеву на острове Ява, Индонезия и находится под уникальным влиянием аллогенного питания. Эта аллогенная речная система существует потому, что карст в этой подсистеме развивается над третичной вулканической формацией. Контакт между известняками фор-

мации Воносари и вулканическими породами, состоящими в основном из эксплозивных вулканических материалов формации Семиллир, позволяет сформироваться этой системе. Было установлено, что в этом районе в водосборах аллогенных рек преобладают относительно непроницаемые вулканические породы и крутые уклоны, что часто приводит к неожиданным паводкам. Целью данного исследования было определить характеристики карстовой системы подземных каналов под влиянием аллогенного питания. Был проведен искусственный индикаторный тест с использованием флуоресцентных красителей, кривые прорыва регистрировались флуориметром. Погружающийся ручей Калимати расположен на существенно отличающейся высоте, нежели Гременгский источник, что приводит к высокому уклону и быстрому течению воды в подземной речной системе. Анализ данных показал, что пещерные сети в районе исследования формируются преимущественно крупными одиночными каналами. Из-за большого расхода и крутого уклона подземной речной системы вместо лабиринтообразной пещерной системы образуется одиночный канал. Выявление связи между аллогенными реками и Гременгским источником подчеркивает, что карстовый водосборный бассейн Гременгского источника не является частью Бетонского карстового водосборного бассейна, как предполагали ранее исследователи, использовавшие при исследовании иные, кроме искусственных индикаторных тестов, методы.

Ключевые слова: *аллогенная река, искусственный индикаторный тест, размывание пещерного прохода, флуоресцентные индикаторы*

QUNUNQSEVU KARST REGİONUNDA (İNDONEZİYA) SÜNİ İZLƏMƏ ÜSULU İLƏ TƏDQİQ EDİLMİŞ ALLOGEN SULARLA QİDALANAN ÇAYLARIN YERALTI AXIN XÜSUSİYYƏTLƏRİ

Cahyadi A.[1]*, Aji T.N.[1], Haryono E.[2], Widiyastuti M.[1], Agniy R.F.[3], Naufal M.[2], Setiawan N.[2], Fatoni G.[2], Pratama A.D.[2], Riyanto I.A., Fatchurohman H.[5]

[1]Ətraf Mühit Coğrafiyası Kafedrası, Coğrafiya Fakültəsi, Gadjah Mada Universiteti, Cokyakarta, 55281, İndoneziya

[2]Karst Tədqiqat Qrupu, Coğrafiya Fakültəsi, Gadjah Mada Universiteti, Cokyakarta, 55281, İndoneziya

[3]Coğrafi İnformasiya Texnologiyaları Kafedrası, Elm, Texnologiya, Mühəndislik və Riyaziyyat Fakültəsi, Maha Karya Asiya Universiteti, Cokyakarta, 55282, İndoneziya

[4]Coğrafiya üzrə Doktorantura Proqramı, Coğrafiya Fakültəsi, Gadjah Mada Universiteti, Cokyakarta, 55281, İndoneziya

[5]Yer Elmləri Texnologiyası Bölməsi, Peşəkar Kollec, Gadjah Mada Universiteti, Cokyakarta, 55281, İndoneziya

**Yazışmalara məsul: ahmad.cahyadi@ugm.ac.id*

Xülasə. Ponjong hidrogeoloji alt sistemi İndoneziyanın Yava adasında yerləşən Qununqsevu karst bölgəsinin bir hissəsidir və allogen qidalanmanın özünəməxsus (unikal) təsiri altındadır. Bu allogenik çay sistemi, karstın üçüncü dövr vulkanik süxurları üzərində inkişaf etməsi nəticəsində mövcuddur. Bu bölgədə Vonosari formasiyasına aid əhəngdaşı süxurları ilə əsasən Semilir formasıyasına mənsub, partlayış mənşəli vulkanik süxurlardan ibarət piroklastik qatlar arasında müşahidə olunan litoloji kontakt bu sistemin formalaşmasına şərait yaradır. Aparılmış tədqiqatlar nəticəsində müəyyən edilmişdir ki, bu regionda allogen çay hövzələrində nisbətən zəif sukeçirən vulkanik süxurların və kəskin yamacların üstünlük təşkil etməsi qəfil sel hadisələrinin baş vermə ehtimalını artırır. Bu işin məqsədi allogen qidalanma şəraitində fəaliyyət göstərən yeraltı karst kanalları sisteminin hidrogeoloji xüsusiyyətlərini və axın dinamikasını öyrənməkdir. Bunun üçün flüoresan indikatorlardan istifadə edilərək süni trasser təcrübəsi aparılmış, əldə edilən nəticələr flüorimetr vasitəsilə qeydə alınmışdır. Kalimati udulan axarı, Gremenq bulağına nisbətən əhəmiyyətli dərəcədə fərqli hipsometrik səviyyədə yerləşir ki, bu da yeraltı çay sistemində yüksək hidrogeoloji qradiyent və sürətli axın rejiminin formalaşmasına səbəb olur. Aparılmış məlumat təhlili göstərmişdir ki, tədqiqat sahəsindəki karst boşluqları və mağara şəbəkələri əsasən iri ölçülü, tək axınlı kanallardan ibarətdir. Yeraltı çay sistemində böyük su sərfi və kəskin meyillik nəticəsində labirintvari mağara sistemi formalaşmır, əksinə, nisbətən stabil hidrodinamik rejimə malik tək (monokanal) tipli karst kanalı inkişaf edir. Allogen çaylarla Gremenq bulağı arasında əlaqənin müəyyənləşdirilməsi göstərir ki, Gremenq bulağının karst mənşəli su toplanma hövzəsi, əvvəlki tədqiqatçılar tərəfindən irəli sürüldüyü kimi, Beton karst hövzəsinin bir hissəsi deyil. Bu nəticə, süni indikator sınaqları istisna olmaqla, müxtəlif tədqiqat üsullarından istifadə etmiş əvvəlki tədqiqatların fərqli nəticələrini təkzib edir və bulağın müstəqil hidrogeoloji sistemə mənsub olduğunu vurğulayır.

Açar sözlər: *allogen çay, süni trasser sınağı, mağara keçidinin yuyulması, flüoresan indikatorlar*

ANAS Transactions **Earth Sciences** **2 / 2025**

http://www.journalesgia.com

IMPACT ASSESSMENT OF CASPIAN SEA LEVEL VARIATIONS ON GROUNDWATER IN THE ABSHERON COASTAL ZONE AND ASSOCIATED ECOLOGICAL PROBLEMS

Sultanov B.N.[1*], Gadirly F.R.[2], Hajiyeva G.N.[3]

[1]Ministry of Science and Education of the Republic of Azerbaijan,
Institute of Geology and Geophysics, Azerbaijan
119, H. Javid Ave., Baku, AZ1073
[2]Ministry of Science and Education of the Republic of Azerbaijan,
Institute of Geography named after acad. H.A.Aliyev, Azerbaijan
117, H. Javid Ave., Baku, AZ1073
[3]Baku State University, Azerbaijan
33, acad. Zahid Khalilov str., Baku, AZ 1148
**Corresponding author: bsaultanov@mail.ru*

Keywords: *groundwater, climate action, sea level, Boussinesq equation, Caspian sea, Absheron peninsula*

Summary. The presented paper is devoted to the current problem of assessing the dynamics of changes in the groundwater level on the coast of the Absheron peninsula in the context of the anticipated decline in the level of the Caspian Sea over the upcoming years. This decrease directly affects the hydrological regime of coastal aquifers, which can entail a number of serious geo-ecological consequences, including changes in the groundwater level, activation of saltwater intrusion, changes in the bearing properties of soils, degradation of vegetation cover, and the emergence of potential risks for existing coastal infrastructure and ecosystems. In this paper, an approach based on the use of analytical and semi-analytical methods is chosen, which represents an effective compromise for obtaining a rapid and physically sound assessment of hydrodynamic processes in porous soil materials. The aim of this work is to study the change in groundwater levels in order to control the aridification of the coastal zone of the Caspian Sea. The object of the study is the coastal zone of the Absheron peninsula, and the upper horizons of the Pliocene deposits are considered as a model geological section. A mathematical model based on the Boussinesq equation is used to predict the dynamics of groundwater level decline. The study focuses on the groundwater response to a fairly sharp drop in the Caspian Sea level, using data on the Palchig Pilpilasi (mud volcano) deposits to the east of Chilov island. This problem simulates a fairly sharp drop in sea level by or about 1 meter over 10 years (3650 days).

© 2025 Earth Science Division, Azerbaijan National Academy of Sciences. All rights reserved.

1. Introduction

The Absheron peninsula is the most important industrial and densely populated centre of Azerbaijan on the shores of the Caspian Sea. One of the key factors influencing the geoecological situation of the coastal zone is the long-term and ongoing decline in the level of the Caspian Sea. This process directly affects the hydraulic regime of coastal aquifers, leading to a change in the level of groundwater, activation of saltwater intrusion processes, changes in the bearing properties of soils and potential risks to coastal infrastructure and ecosystems.

Salt water makes up 97.5% of the Earth's water resources. Fresh water reserves are small, and almost 70% of them are actively melting Arctic and Antarctic glaciers (Shishelova, Tolstoy, 2016). One of the most important reserves of fresh water suitable for use is groundwater. In many regions, especially those with a shortage of surface water, groundwater is the main source of satisfying both drinking and agricultural and industrial needs, and people use these resources very actively.

Currently, humanity extracts 3.5 times more water than is formed underground. At the same time, in most regions of the Earth, dependence on groundwater continues to grow. For example, in the same India, pumping groundwater accounts for up to 85% of all freshwater consumption, while in Europe this figure

is 75% (Rahul et al., 2021). The use of groundwater in Azerbaijan accounts for approximately 20% of the total freshwater demand (Mammadov, 2002). In recent years, climate change, anthropogenic impact, as well as such factors as the lowering of the Caspian Sea level have had a negative impact on the level of groundwater in the Absheron Peninsula. Continuation of this process from year to year increases the risk in terms of environmental sustainability, since groundwater plays an important role in providing water to the population living on the peninsula.

The geological and geomorphological structure of the Absheron Peninsula has affected the formation of groundwater in this area. Since the ancient clay rocks exposed in the northwestern and western parts of the peninsula, following in the eastern direction, became deeper and deeper, covered with Quaternary sediments, which created favourable conditions for the accumulation of groundwater. Climatic factors also play a special role in the formation of groundwater, as well as in the formation of their quantitative and qualitative characteristics, for example, studies show that over the period 1991–2017, there was an increase in the amount of precipitation on the Absheron Peninsula, and the most significant increase in precipitation was recorded in Baku meanwhile a decrease in the amount of precipitation was observed on the sea surface, which can lead to a further decrease against the background of increased evaporation in the level of the Caspian Sea (Safarov et al. 2020). Every year, 184.8 kg/ha of salts, of which 12.9% is NaCl, come to the Earth's surface with precipitation, which affects the chemical composition of groundwater (Shishelova, Tolstoy, 2016). Water vapour condensation also plays an important role in the formation of groundwater.

General patterns of the location and chemical composition of groundwater on the peninsula indicate that these waters are widespread only in the northern coastal strip, the Baku Basin and the eastern part of the Absheron Peninsula, and are distributed to a much lesser extent in other areas (Javadzade, 2014). The depth of groundwater varies up to a depth of 50-60 meters starting from the surface.

In the villages of Jorat, Fatmayi and Pirshaghi, the flow of these waters is directed to the north, while in the Baku basin and in the eastern part of Absheron, it is directed to the northeastern and southern coastline (Aliyev, 2000). In the western part of the peninsula, groundwater occurs at a depth of 0.5 m to 18 m, in the eastern part – from 2 m to 29 m. In the western section, groundwater is chloride-sulphate and chloride-sodium in chemical composition, with a total mineralization of 6.4-88.6 g/l, and in some cases less than 0.8 g/l (Aliyev, 2000).

In the East, these indicators vary from 0.3 to 11.7 g/l, respectively, and in chemical composition they are hydrocarbonate-chloride, sulphate-chloride, chloride-calcium-sodium-magnesium, sodium and sodium-magnesium. The total mineralization of waters increases from north to south with a depth of 0.6 g/l to 16 g/l and more. The chemical composition of the water is mainly hydrocarbonate-chloride, sulfate-hydrocarbonate-chloride, sulfate-chloride and chloride-sulfate sodium-calcium (Mammadov, 2002).

The chemical composition of pressure waters, the total mineralization of which increases with depth and fluctuates mainly from 0.4 to 5.7, rarely up to 97.7 g/l, varies from hydrocarbonate-sulfate, calcium-magnesium-sodium to sulfate-chloride and chloride-sulfate-sodium, sodium-magnesium. In some cases, the water contains hydrogen sulfide (Surakhany settlement, Bakhcha natural zone), the content of H_2S fluctuates from 112 to 229 mg/l (Surakhany settlement) (Mammadov, 2002).

According to the results of the calculations, 33 million m^3 of water is extracted on the peninsula annually (Aliyev, 2000). An analytical analysis of the entire complex of hydrogeological conditions, as well as an approximate calculation of the possibilities for increasing groundwater production made it possible to identify zones of rock aquifers and total mineralisation of groundwater within each hydrogeological region. The most promising area in terms of groundwater reserves is the northern coast of the Absheron Peninsula – the Baku and Gyuzdek troughs, where the villages of Bilgah, Nardaran, Buzovna, Shuvalan are located, as well as the villages of Bina, Zira, Turkan and the settlement of Yeni Gala, as well as the territory to the northwest of the Garadagh stone quarry (Mammadov, 2002).

In recent years, the groundwater level in the area of our research has begun to decrease. The depletion of aquifers as a result of active exploitation has a negative impact on both the environment and the local population using groundwater. If the problem becomes widespread, it can lead to serious economic, humanitarian and environmental problems. A decrease in the water level will lead to the drying up of rivers and lakes, which will also have a negative impact on animals and plants. The ecological state of the territory is determined mainly by the level of groundwater and its mineralisation.

The most well-known classification is according to which an environmental disaster occurs when the decrease of groundwater level exceeds 50% of the critical value for soils and agricultural landscapes, and when it exceeds 25-50%, the condition is assessed as an environmental emergency (Shcheglov, Semionova, 2011). As it is known, a decrease in the water level leads to an increase in the concentration

of ions and soil salinisation. For instance, Na^+ and HCO_3^- ions can bind into soda $NaHCO_3$ and cause soil alkalinization (Shcheglov, Semionova, 2011). In addition to the chemically toxic effect on plants, soils with a noticeable soda content are characterised by poor water-physical and physical-mechanical properties. In addition, they are characterised by low water permeability and a sharp decrease in the amount of moisture available to plants (Shcheglov, Semionova, 2011). It is believed that when groundwater occurs at a depth of more than 3-4 m, the water flow regime becomes neutral and does not affect the development of plants. When groundwater occurs closer than 0.5-1.0 m from the surface, its regime is considered critical. When the groundwater level is from 0.5 (1.0) m to 3.0 (4.0) m, its regime can be considered optimal (neutral) if it is fresh or slightly mineralised (Aliyev, 2000). However, if the mineralisation increases, this will have a negative impact on plants even at these deep depths (Shestakov, 1979).

However, the process of lowering the groundwater level in the studied territory develops at an active pace. The decrease in the water level has led to a decrease in agricultural productivity, a reduction in the diversity of flora and fauna, a decrease in soil fertility and an acceleration of the desertification process (Hajiyeva, Ibrahimova, 2024).

The presented article is devoted to a topical issue. The article studies the impact of the decrease in the level of the Caspian Sea on groundwater using modern methods and analyses the prediction of the ecological disaster that may occur in the future.

The level of the Caspian Sea has been subject to rise and fall at various times. The highest sea level was recorded in 1995. Later, it began to fall again, and by the year 2000 it had declined for 35 cm. Since 2001, the level rose by 30 cm in the next five years. Currently, a further decline in sea level has been observed since 2005 (Mammadov, 2015; Safarov et al., 2024).The decrease in the level has led to the globalization of a number of socio-economic including environmental problems. Thus, the decrease in the water level and changes in the climate have led to the loss of soil fertility, the deterioration of vegetation cover, in short, the activation of the desertification process. This event has also brought to the fore problems such as salinization and increase in the depth of groundwater. Therefore, it is very important to study the impact of the Caspian Sea level on groundwater (Mammadov, 2007).

The geological structure of the peninsula is characterized by exceptional complexity. The basis of the section is made up of thick, up to 3 km and in places more, strata of Pliocene deposits represented by alternation and mixing of sandstones, argillites and clays formed under dynamic conditions of geological activity in the past of the Caspian basin. These deposits, known as the Productive Stratum, have historically been the object of oil and gas production and have complex filtration and capacity properties (Buryakovsky et al., 2001). The presence of volcanic rocks and mud volcanic inclusions brought to the surface further complicates the geological model.

In these conditions, quantitative assessment of the nature of changes in the groundwater system to changes in the Caspian Sea level becomes an important task (Aliyev, 2024). The use of analytical and semi-analytical methods based on the fundamental laws of liquid filtration through porous soil material is an effective compromise that allows for a quick and physically substantiated assessment of hydrodynamic processes. The object of the study is the coastal zone of the Absheron Peninsula. The upper horizons of the Pliocene deposits are considered as a model geological section.

The aim of this work is to study the change in groundwater levels in order to control the aridification of the coastal zone of the Caspian Sea.

2. Methodology of the research

In this paper, a mathematical model based on the Boussinesq equation (Turcotte, Schubert, 1985) is applied to predict the dynamics of groundwater level decrease in the coastal areas of the Absheron Peninsula in response to a sharp or gradual decrease in the Caspian Sea level using data from Pliocene deposits. This equation, being a classical model of filtration effectively describes non-stationary hydrodynamic processes in unconfined aquifers, where the cross-sectional area of the flow varies proportionally to its pressure. This represents an effective compromise for obtaining a fast and physically correct estimate. To obtain an analytical solution, the nonlinear Boussinesq equation was linearised by replacing the variable flow power. This linearisation allows the original equation to be transformed into a parabolic equation, mathematically identical to the diffusion equation, which makes it convenient for the analytical solution and description of the process of attenuation and propagation of hydraulic disturbance in a porous medium.

The present study proposes a physically and mathematically sound approach to assess the consequences of the Caspian Sea level decline for coastal groundwater of the Absheron Peninsula. The key elements of the model are the consideration of real petrophysical data of the Pliocene deposits characterised by low permeability together with the universal hydrogeological laws of liquid filtration through porous soil materials. The constructed model, although somewhat generalised, reflects real physical processes and can allow obtaining a quite realistic

forecast of the rather slow nature of the reaction of the hydrogeological system of groundwater in response to a rapid change in the Caspian Sea level.

3. Results and discussions

3.1. Statement of the problem and physical characteristics of the soil material

The rock of the coastal line is allowed consisting mainly of sandstone as well as with inclusions in the form of siltstone, clay and various volcanic rocks. To build the model, laboratory data from samples collected in the Palchig Pilpilasi area had been used (Buryakovsky et al., 2001). These data can be considered representative for the averaged assessment of the characteristics of the filtration-capacity properties of the soil material of the coastal line of the Absheron Peninsula. In its structure, such material contains particle sizes of granules in the following range (Buryakovsky et al., 2001):

More than 0.25 mm (medium and coarse sand): 2.7%

From 0.25 to 0.1 mm (fine sand): 13.8%

0.01 mm (dusty sand, silt): 53.5%

Less than 0.01 mm (pelite fraction, clay): 30.0%

Analysis of the granulometric composition fully confirms the low permeability values. The dominant fraction (53.5%) is represented by fine-grained rocks (silty sand and silt), and a significant content (30%) of the (clay) fraction acts as a cementing and binding material sharply reducing the effective diameter of the filtration channels. Thus, despite the high overall porosity, the effective permeability of the system is limited precisely by the predominance of fine particles. The porosity of this material is 22.3% (Buryakovsky et al., 2001). This value is quite high and indicates a significant volume of void space capable of containing fluids. Permeability of the material is k_{perm}= 54 mD (Buryakovsky et al., 2001). This value indicates low or moderately low permeability of rocks. To convert it to a filtration coefficient used in hydrogeology, the formula (1) can be used:

$$K = \frac{k_{perm} \cdot \rho \cdot g}{\mu} \quad (1)$$

Here $\rho -$ water density within 1020 kg/m³, $g -$ acceleration due to gravity equals on average 9.81 m/s², $\mu -$ the dynamic viscosity of water at 20 degrees Celsius is taken to be equal to $1.003 \cdot 10^{-3}$ Pa · s. Thus, the filtration coefficient is K = 5.316×10^{-7} m/s ≈ 0.046 m/day. Such a low value is a key factor determining the inertia and slow nature of hydrodynamic processes.

To describe the non-stationary process of lowering the groundwater level in an unconfined formation, the classical Boussinesq equation (2) is used (Shestakov, 1979; Turcotte & Schubert, 1985). For the one-dimensional case (when water moves only in one direction, perpendicular to the shore), it has the form (Shestakov, 1979):

$$\mu \frac{\partial h}{\partial t} = \frac{\partial}{\partial x}\left(kh \frac{\partial h}{\partial x}\right), \quad (2)$$

where $h(x,t)$ – is the height of groundwater above the aquiclude at point *x* and at time *t*. This is the desired groundwater level.

x – is a distance from the shore of a reservoir.

t – is time since the water level in the reservoir dropped.

μ – is a coefficient of soil water yield (a dimensionless value showing what volume of water the soil can give up when the sea level drops). For sands μ is usually 0.1-0.3. For soils with high clay fraction content μ is significantly less than the total porosity and can be estimated in the range of 0.05-0.1. Thus, the coefficient μ can be taken as an average of 0.1 (Maksimov, 1979).

k – is soil filtration coefficient (m/day) characterizing its permeability.

This equation is nonlinear due to the term $h\frac{\partial h}{\partial x}$, which complicates its solution. To obtain an analytical solution, the Boussinesq equation is linearised. This is done by replacing the variable flow power h with some constant averaged power h_{avar}. Although it was derived for relatively simple conditions, its linearised form is a parabolic-type equation, mathematically identical to the diffusion equation, and perfectly describes the process of attenuation and propagation of a hydraulic disturbance in a porous medium.

The linearized one-dimensional Boussinesq equation has the following form:

$$\frac{\partial h}{\partial t} = a \frac{\partial^2 h}{\partial x^2} \quad (3)$$

Here the coefficient *a* is calculated using the formula:

$$a = \frac{K \cdot h_{avar}}{\mu}, \quad (4)$$

where *K* – is a filtration coefficient (adopted as 0.046 m/day);

h_{avar} – is average aquifer thickness (estimated parameter);

μ – is water loss coefficient.

To solve this problem, the following initial and boundary conditions are established:

1. Initial condition ($t = 0$): The groundwater level throughout the area is equal to the initial sea level H_0. $h(x,0) = H_0$. We take the initial level to be 10 meters near the seashore.

2. Boundary condition on the coast ($x = 0$): The groundwater level is equal to the new, lowered sea level H_k. $h(0,t) = H_k$. We take the lowered sea level to be equal to 8 meters.

3. Boundary condition at a distance ($x \to \infty$): The groundwater level remains unaffected $h(\infty,t) = H_0$.

The solution to this problem allows obtaining the distribution of the groundwater level $h(x,t)$ for any time and at any distance from the shore. We take the distance inland from the shore to be 1 km.

The solution to the linearised Boussinesq equation (3) for such conditions describes what the groundwater level *h* will look like at any point *x* and at any time *t*. The solution is often expressed through the decrease in level $S(x,t) = H_0 - h(x,t)$. In turn, the total decrease in level at the boundary with the reservoir will be $S_0 = H_0 - H_k$. The analy-tical solution for the decrease in level has the following form of solution through an additional error function (Turcotte, Schubert, 1985):

$$S(x,t) = S_0 \cdot erfc\left(\frac{x}{2\sqrt{at}}\right) \quad (5)$$

Here $S(x,t)$ – is a decrease in the groundwater level at a distance *x* from the shore at time t, $erfc -$ is an error function, S_0 – is a sharp decrease in the level in the reservoir.

The change in the Caspian Sea level, in ge-neral, over previous geological periods of time shows an oscillatory and uncertain nature due to the huge variety of factors affecting it, including the anthropogenic factor, which has begun to exert an active influence in recent centuries (Kenzhegaliev et al., 2021; Naderi Beni et al., 2013). Due to the fact that the Caspian Sea is the largest closed water body, its level is sensitive to global and regional climate changes (Lahijani et al., 2023; Safarov et al., 2024).

At the moment, it can be said that over the past decades, the level of the Caspian Sea has tended to decrease by about 1 meter (Lahijani et al., 2023; Naderi Beni et al., 2013). According to the latest scientific data (Court et al., 2025; Samant et al., 2023), a decline of approximately 1.4 m over 16 years (2006–2021) was considered and it is predicted that the Caspian Sea level may fall by an average of approximately ~9 cm/year. Let us assume in our problem a fairly sharp drop in sea level by 1 meter and construct a model that approximately characterizes the change in the level of coastal groundwater over a period of 3650 days, approximately equal to ≈ 10 years.

3.2. Graphical representation of the modelled dynamics of groundwater level changes and discussion of the numerical results

The modelling was performed using "Python" code and the "Matplotlib", "Numpy" and "Scipy" additional library packages.

Thus, taking into account all of the above mentioned, the following graphs of changes in groundwater levels near the shore of the Caspian Sea can be presented in Figure below.

According to the obtained data of the constructed model, it is expected that in the first year the decrease in the groundwater level will start to appear at a distance of approximately 200 meters from the seashore and would be only slightly reduced (to about 999.96 cm) and at a distance of 500 meters with groundwater level of approximately 999.49 cm in 10 years. The results obtained are shown in discrete tabular form in Table below.

4. Conclusion

The model shows that the process of lowering the groundwater level will be extremely slow and inertial. A significant lowering will be observed only in a narrow coastal strip, while at a distance of se-veral kilometres from the coast the effect will appear only after many decades. However, the slow but constant decrease in the level of the Caspian Sea will certainly affect the level of coastal groundwater, and at the same time change the geoecological situation of the region.

As a result of the conducted studies, it was determined that the decrease in the level of the Caspian Sea will lead to the globalisation of environmental problems such as the drying up of groundwater in the future. This, in turn, will lead to the destruction of the vegetation cover currently existing here, the complete loss of mineral substances present in the soil cover, the destruction of agriculture and, most importantly, the emergence of the problem of drought. Therefore, it is necessary to quickly eliminate the factors that cause the decrease in the level of the Caspian Sea.

Financing of the work

The research was carried out at the expense of budgetary financing of the Institute of Geology and Geophysics of the Ministry of Science and Education of the Republic of Azerbaijan.

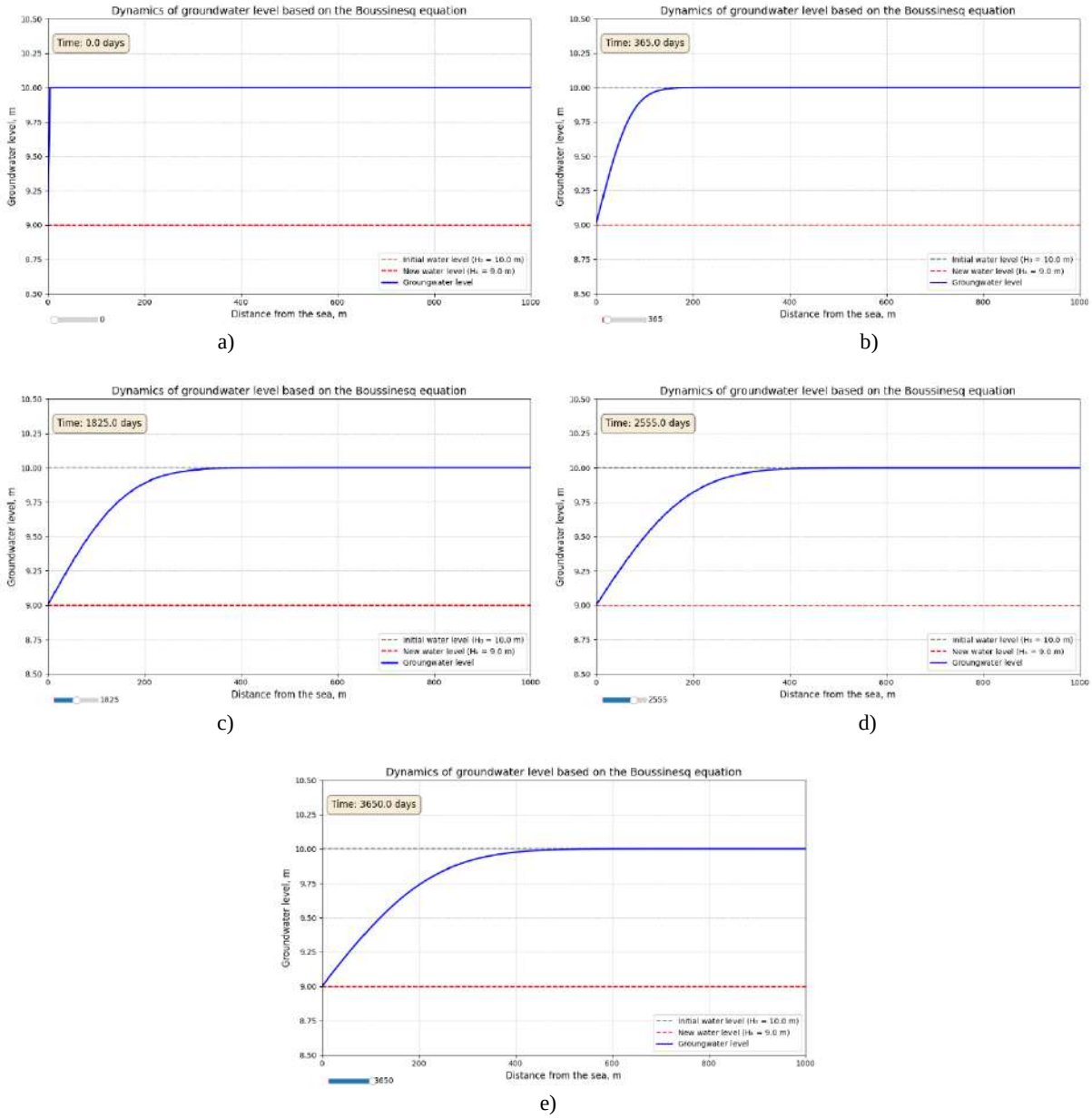


Fig. Dynamics of changes in groundwater levels based on the solution of the Boussinesq equation: a) at initial moment in time (exactly 0 days); b) approximately over a year (exactly 365 days); c) after about 5 years (exactly 1825 days); d) after about 7 years (exactly 2555 days); e) after about 10 years (exactly 3650 days)

Table

The groundwater level at a given distance from the shore at a given point in time

Distance from the shore in meters	Groundwater level on day 0 of measurements (in centimetres)	Groundwater level after 1 year (in centimetres)	Groundwater level after 5 years (in centimetres)	Groundwater level after 7 years (in centimetres)	Groundwater level after 10 years (in centimetres)
0	900.00	900.00	900.00	900.00	900.00
100	1000.00	992.36	957.18	949.69	942.47
200	1000.00	999.96	988.70	981.95	973.75
300	1000.00	1000.00	998.25	995.55	990.72
400	1000.00	1000.00	999.85	999.26	997.50
500	1000.00	1000.00	999.99	999.92	999.49

REFERENCES

Aliyev AS (2024) Changes in the level of the Caspian Sea in the modern period: causes and results. The Reports of National Academy of Sciences of Azerbaijan, LXXX(1-2):15–19. https://doi.org/10.59423/gnr.2024.83.40.012

Aliyev FSh (2000) Groundwater of the Republic of Azerbaijan, use of resources and geoecological problems. Baku, p 323 (in Azerbaijani)

Buryakovsky LA, Chilingar GV, Aminzadeh F (2001) Petroleum Geology of the South Caspian Basin. Gulf Professional Publishing (an imprint of Butterworth–Heinemann), p. 442

Court R, Lattuada M., Shumeyko N et al (2025) Rapid decline of Caspian Sea level threatens ecosystem integrity, biodiversity protection, and human infrastructure. Communications Earth & Environment 6(1)261

Hajiyeva GN, Ibrahimova LP (2024) Ecological problems of technogenically disturbed lands on the Absheron Peninsula. Journal Geology, Geogeography and Geoecology 33(1):70–76. https://doi.org/10.15421/112408

Javadzade EB (2014) Groundwater resources and their use in Azerbaijan. Proceedings of the 2nd Caspian International Conference "Water Technologies", Baku, Azerbaijan, p 99–101 (in Azerbaijani)

Kenzhegaliev A, Kanbetov A. et al (2021) Fluctuation in the level of the Caspian Sea and its consequences. International Symposium Sustainable Energy and Power Engineering 2021 (SUSE-2021). E3S Web of Conferences, vol 288, 01064, Kazan, Russia, 18–20 February 2021

Lahijani H, Leroy S, Arpe K, Crétaux JF (2023) Caspian Sea level changes during instrumental period, its impact and forecast: A review. Elsevier, Earth-Science Reviews 241(44):104428. https://doi.org/10.1016/j.earscirev.2023.104428

Maksimov VM (1979) Reference manual of hydrogeologist. Nedra, Leningrad, vol 1, p 512 (in Russian)

Mammadov RM (2007) Hydrometeorology variability and ecogeographical problems of the Caspian Sea. Issue 1.Elm, Baku, p 474

Mammadov RM (2015) Impact of climate changes on the Caspian Sea Level. J of Resources and Ecology 6(2):87–92. https://doi.org/10.5814/j.issn.1674-764x.2015.02.004

Mammadov MA (2002) Hydrography of Azerbaijan. Nafta-Press, Baku, 266 p (in Azerbaijani)

Naderi Beni A, Lahijani H et al (2013) Caspian sea-level changes during the last millennium: historical and geological evidence from the south Caspian Sea. Journal of European Geosciences Union 9(4):1645–1665. https://doi.org/10.5194/cp-9-1645-2013

Rahul Sh, Ravi K, Pinki A, Ittishree B et al (2021) Groundwater extractions and climate change. In: Water Conservation in the Era of Global Climate Change, p 23–45. https://doi.org/10.1016/B978-0-12-820200-5.00016-6

Safarov ES, Safarov SH, Bayramov EA (2024) Changes in the hydrological regime of the Volga River and their influence on Caspian Sea level fluctuations. Water, 16(12):1–19. https://doi.org/10.3390/w16121744

Safarov SH, Safarov ES, Huseynov JS, Ismayilova NN (2020) Modern changes in precipitation on the Caspian coast of Azerbaijan. Journal of Oceanological Research 48(1):27–44. https://doi.org/10.29006/1564-2291.JOR-2020.48(1).2

Samant R, Prange M et al (2023) Climate-driven 21st century Caspian Sea level decline estimated from CMIP6 projections. Commun Earth Environ 4(1)357:1–12. https://doi.org/10.1038/s43247-023-01017-8

Shcheglov DI, Semionova LA (2011) Influence of groundwater level on properties and fertility of soil. Science Prospects 5(20):18–20 (in Russian)

Shestakov VM (1979) Dynamics of groundwater. Moscow University Publishing House, Moscow, p 368 (in Russian)

Shishelova TI, Tolstoy MYu (2016) Current state of water science. Problems and prospects. Scientific Review Abstract Journal 4:61–80 (in Russian)

Turcotte D, Schubert J (1985) Geodynamics, vol 2, Mir, Moscow, p 376 (in Russian)

ОЦЕНКА ВОЗДЕЙСТВИЯ КОЛЕБАНИЙ УРОВНЯ КАСПИЙСКОГО МОРЯ НА ПОДЗЕМНЫЕ ВОДЫ ПРИБРЕЖНОЙ ЗОНЫ АБШЕРОНСКОГО ПОЛУОСТРОВА И ЭКОЛОГИЧЕСКИЕ ПРОБЛЕМЫ

Султанов Б.Н.[1*], Кадирли Ф.Р.[2], Гаджиева Г.Н.[3]

[1]Министерство науки и образования Азербайджанской Республики,
Институт геологии и геофизики, Азербайджан
AZ1073, Баку, просп. Г.Джавида, 119
[2]Министерство науки и образования Азербайджанской Республики,
Институт географии имени академика Г.А.Алиева, Азербайджан
AZ1073, Баку, просп. Г.Джавида, 117
[3]Бакинский Государственный Университет, Азербайджан
AZ1148, Баку, ул. акад. Захида Халилова, 33
**Автор, отвечающий за переписку:bsaultanov@mail.ru*

Резюме. Представленная статья посвящена актуальной проблеме оценки динамики изменения уровня подземных грунтовых вод на побережье Абшеронского полуострова в контексте ожидаемого снижения уровня Каспийского моря на протяжении ближайших лет. Это снижение напрямую влияет на гидрологический режим прибрежных водоносных горизонтов, что может повлечь за собой ряд серьезных геоэкологических последствий, включая изменение уровня подземных грунтовых вод, активизацию интрузии соленых морских вод, изменение несущих свойств грунтов, деградацию растительного покрова и возникновение потенциальных рисков для существующей прибрежной инфраструктуры и экосистем. В этой статье выбран подход, основанный на применении аналитических и полуаналитических методов, что представляет собой эффективный компромисс для получения быстрой и физически обоснованной оценки гидродинамических процессов в пористых материалах грунта. Объектом исследования является прибрежная зона Абшеронского полуострова, а в качестве модельного геологического разреза рассмотрены верхние горизонты плиоценовых отложений. Для прогнозирования динамики понижения уровня грунтовых вод используется математическая модель, основанная на уравнении Буссинеска. Исследование фокусируется на реакции грунтовых вод на достаточно резкое снижение уровня Каспийского моря, используя при этом данные по отложениям

Палчыг Пилпилясы (Грязевая Сопка) к востоку от острова Чилов. Актуальность работы также подкрепляется общими тенденциями снижения уровня Каспийского моря в последние десятилетия и прогнозами дальнейшего падения на 10-20 метров в течение ближайших 100 лет. В рамках данной задачи моделируется достаточно резкое падение уровня моря на 1 метр в течение 10 лет (3650 дней).

Ключевые слова: *грунтовые воды, борьба с изменением климата, уровень моря, уравнение Буссинеска, Каспийское море, Абшеронский полуостров*

XƏZƏR DƏNİZİNİN SƏVİYYƏ TƏRƏDDÜDÜNÜN ABŞERON YARIMADASININ SAHİL ZONASINDAKI YERALTI SULARA TƏSİRİNİN QİYMƏTLƏNDİRİLMƏSİ VƏ EKOLOJI PROBLEMLƏR

Sultanov B.N.[1*], Qədirli F.R.[2], Hacıyeva G.N.[3]
[1] Azərbaycan Respublikasının Elm və Təhsil Nazirliyi,
Geologiya və Geofizika İnstitutu, Azərbaycan
AZ1073, Bakı, H.Cavid prosp., 119
[2] Azərbaycan Respublikasının Elm və Təhsil Nazirliyi,
akad. H.Əliyev adına Coğrafiya İnstitutu, Azərbaycan
AZ1073, Bakı, H.Cavid prosp., 117
[3] Bakı Dövlət Universiteti, Azərbaycan
AZ1148, Bakı, akad. Zahid Xəlilov küç., 33
**Yazışmalara məsul:bsaultanov@mail.ru*

Xülasə. Təqdim olunan məqalə, gələcək illərdə Xəzər dənizinin səviyyəsinin aşağı düşməsi fonunda Abşeron yarımadası sahillərində yerləşən yeraltı suların səviyyəsinin dinamikasını qiymətləndirilməsi kimi aktual bir mövzuya həsr olunmuşdur. Bu enmə sahilyanı yeraltı su daşıyan təbəqələrin hidroloji rejiminə birbaşa təsir edir ki, bu da bir sıra ciddi geoekoloji problemlərə gətirib çıxara bilər. Bura yeraltı suların səviyyəsinin dəyişməsi, duzlu dəniz sularının intruziyasının (daxil olmasının) aktivləşməsi, torpaqların süxur qatlarının mexaniki daşıyıcılıq xüsusiyyətlərinin dəyişməsi, torpaqların münbitliyinin itirlməsi, bitki örtüyünün kasadlaşması, mövcud sahil infrastrukturu və ekosistemləri üçün potensial risklərin yaranması daxildir. Bu məqalədə məsaməli torpaq materiallarında hidrodinamik proseslərin sürətli və fiziki cəhətdən əsaslandırılmış qiymətləndirilməsi üçün effektiv bir kompromis təqdim edən analitik və yarı-analitik metodların tətbiqinə əsaslanan bir yanaşma seçilmişdir. Tədqiqatın obyekti Abşeron yarımadasının sahil zonası, model kimi isə Pliosen çöküntülərinin yuxarı təbəqələrinin geoloji kəsiyi seçilmişdir. Yeraltı suların səviyyəsinin enməsinin dinamikasını proqnozlaşdırmaq üçün Bussinesk (Boussınesq) tənliyinə əsaslanan riyazi modeldən istifadə olunur. Tədqiqatda, Xəzər dənizinin səviyyəsinin kifayət qədər kəskin enməsinə yeraltı suların əks reaksiyası öyrənilir. Tədqiqat modelini qurmaq məqsədilə, Çilov adasından şərqdə yerləşən "Palçıq pilpiləsi" çöküntülərindən əldə edilən geofiziki məlumatlardan istifadə olunub. Yeni tədqiqatların məlumatları əsasına, son onilliklərdə Xəzər dənizinin səviyyəsinin ümumi enmə tendensiyaları və gələcək 100 il ərzində 10-20 metr daha da enməsi proqnozları əsasında işin aktuallığı təmin olunur. Bu məsələnin çərçivəsində, dəniz səviyyəsinin 10 il ərzində (3650 gün) 1 metr kəskin enməsi modelləşdirilir.

Açar sözlər*: yeraltı sular, iqlim dəyişikliyi ilə mübarizə, dəniz səviyyəsi, Bussinesk tənliyi, Xəzər dənizi, Abşeron yarımadası*

ANAS Transactions Earth Sciences 2 / 2025

http://www.journalesgia.com

ASSESSMENT OF EXOGENIC GEOLOGICAL PROCESS DYNAMICS IN THE YANARDAG AREA OF ABSHERON PENINSULA (AZERBAIJAN) BASED ON VERTICAL ELECTRICAL SOUNDING DATA

Salamov A.M.[1], Safarov R.T.[1*], Zamanova A.H.[1], Ahmadova E.V.[2], Gahramanov M.R.[1]

[1]Ministry of Science and Education of the Republic of Azerbaijan,
Institute of Geology and Geophysics, Azerbaijan
119, H.Javid ave., Baku, AZ1073
[2]Faculty of Geology, Baku State University, Azerbaijan
33, acad. Z.Khalilov str., Baku, AZ1148
**Corresponding author: rafiqsafarov@gmail.com*

Keywords: *geophysics, mud volcano, electrical prospecting, resistivity, rock, density, faults*

Summary. This paper examines the investigation of exogenic geological processes in the Yanardagh area located in the northern part of the Absheron peninsula at a distance of 27 km from Baku. The peninsula is orographically the southeastern continuation of the Greater Caucasus and occupies an area of approximately 2,000 sq. km. This area was formed as a result of volcanic-tectonic processes and the ignition of natural gas flows that emerged to the surface through cracks. Field geophysical measurements using Vertical Electrical Sounding method were carried out along nine profiles using a symmetrical four-electrode AMNB installation. As a result of the conducted geophysical studies, the following tasks: detailed subdivision of the geological section to a depth of 30 m; identification and tracking of probable faults; determination of some probable physical parameters of the rocks forming the geological section were solved. Three main layers composed of clays with different thickness and electrical resistivity were identified. Based on the plotted maps of the averaged values of the expected physical parameters, it was established that the western part of the area is most susceptible to the impact of exogenic geological processes. Presumably, the main cause of the exogenic geological processes development is an aqueous solution flowing from the mud volcano manifestation located in the southwestern part of the study area. It is proposed the necessity to eliminate the ingress of water flowing from the mud volcano into the geological environment in order to reduce the rate of the exogenic geological processes development in the study area.

© 2025 Earth Science Division, Azerbaijan National Academy of Sciences. All rights reserved.

Introduction

The Yanardagh geophysical research area, which is one of the rare natural phenomena and also attracts tourists, is located in the northern part of the Absheron Peninsula at a distance of 27 km from Baku. These rare natural phenomena are treated and protected with special care all over the world. Therefore, the study of such phenomena is mandatory and relevant.

The peninsula is orographically the southeastern continuation of the Greater Caucasus, occupies an area of approximately 2,000 square kilometres, and its eastern part extends deep into the Caspian Sea.

According to orographic features, the peninsula is divided into four main parts: northwestern and southwestern – low mountainous, northern (or central) – hilly-ridged plain, and eastern – flat. The study area is located in the north-western part of the peninsula (Fig.1).

The development of exogenic geological processes (EGP) occurs everywhere, both on plains along the banks of rivers, lakes, water reservoirs and seas, and in mountainous areas. Developing in areas of intensive economic exploration, EGPs pose a threat to all open engineering structures without exception (Aliyev, 2002).

Reasonable assessment of the EGPs hazard requires the solution of a number of specific issues related to the structure of the slope, its lithological composition, condition, properties, bedding and thickness of individual rock strata, their water abundance and groundwater regime (Ogilvi, 1990).

Among EGPs, landslides are one of the most widespread and hazardous. Landslides cause significantly greater total damage than volcanic eruptions, floods, hurricanes, and even earthquakes (Goryainov et al., 1987).

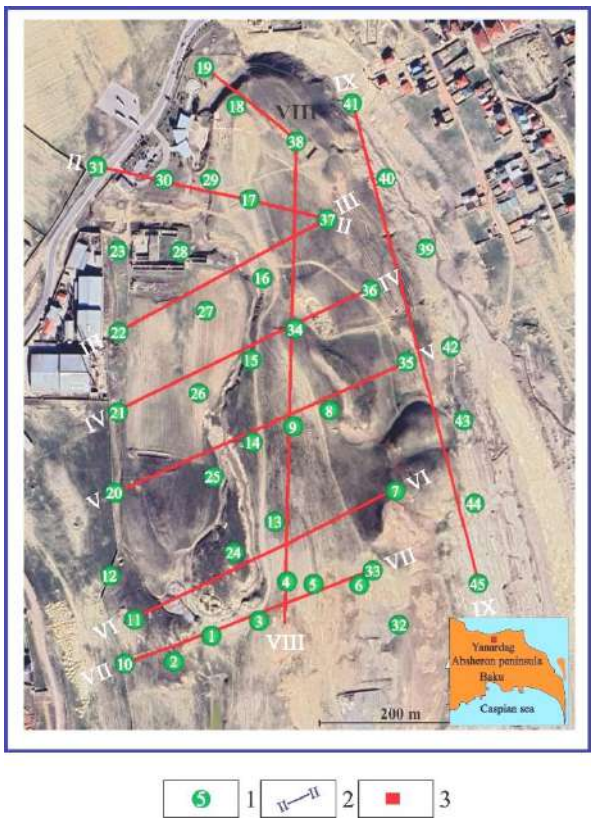


Fig. 1. Location of geophysical profiles in the study area
1 – VES points and their sequence numbers; 2 – geophysical profiles; 3 – location of the geophysical research area – Yanardagh site

This is due to the high prevalence of landslide processes and the fact that the mentioned natural disasters often turn out to be the cause of landslides that are more destructive than they themselves, which cause the death of huge numbers of people.

The most spectacular of the known landslide disasters was the 2.2 km^3 landslide that formed in the Pamirs and created Lake Sarez in 1911.

According to R.Shuster, the amount of direct and indirect losses associated with landslides reaches 1 billion dollars per year in the USA (Goryainov et al., 1987). In Japan, this number is much higher. Therefore, study of EGPs, including landslides, is always an actual issue in the world and in Azerbaijan.

Since 1929, the study of landslides in Azerbaijan, including the Absheron Peninsula has been the subject of numerous works by researchers Alizade et al. (1990), Kashkai (1952), Azizbekov (1961), Popov et al. (1990), Shirinov (1965, 1993), Budagov (1982), etc. Various EGPs, including landslides of the Absheron Peninsula were studied by I.A.Israfilbekov, V.A.Listengarten, A.D.Shakhsuvarov (1983), Gul (2003), Konovalov, Gul (1956), Aliyev (2002), Salamov (2015, 2020).

The purpose of the research was to study the geophysical-engineering conditions of the Yanardagh site. In order to achieve this goal, the following tasks were set on geophysical work studies:

- detailed subdivision of the geological section to a depth of 30 m;
- identification and tracing of suspected faults;
- determination of some probable physical parameters of rocks forming the geological section.

To solve the task, the electrical prospecting method – Vertical Electrical Sounding was used.

As it is known, the intensity of EGPs development and landslides depends on numerous geological, natural factors and anthropogenic activities.

Method

Field geophysical measurements were carried out along nine profiles using a symmetrical four-electrode AMNB installation.

As it is known, the modern theory of VES is based on the Schlumberger mathematical model, which allows calculating the specific apparent electrical resistivity ρ_a of a multilayer medium with horizontal interfaces. This method relies on specific electrical resistivity, thickness of individual layers, as well as the dimensions of the VES survey setup (Salamov et al., 2017; Salamov et al., 2023).

The distance between the profiles and between the VES observation points was selected depending on the terrain ruggedness and passability. The survey setup is oriented along the profiles. In order to achieve the detailed subdivision of the geological section and more accurate estimation of sliding plane depth based on the experimental studies results, an additional network with denser AB/2 spacing interval was used: the step was 1 m up to 10 m, then it was 2 m up to 30 m.

Taking into account the above mentioned aim of the detailed subdivision of the geological section and more precise depth determination of the individual lithological varieties, the sizes of the transmitter line AB/2 (AB/2 =1; 2; 3; 4; 5; 6; 7; 8; 9; 10,10; 12,12; 14; 16; 18; 20; 22; 24,24; 26,26; 28; 30) and the receiving line MN/2 (MN/2=0,3; 0,3; 0,3; 0,3; 0,3; 0,3; 0,3; 0,3; 0,3; 0,3;1; 0,3;1; 1; 1; 1; 1; 1; 1;2; 1;2; 2; 2) were adopted based on the results of conducted VES experiments (Salamov et al., 2017).

Following formula was used to calculate the apparent electrical resistivity ρ_a, (Yakubovski, Renard, 1991)

$$\rho_{ai} = K_{VES}\frac{\Delta U_{mV}}{I_{mA}} \quad (1)$$

To determine the specific electrical resistivity of individual layers, formula (2) is used, when $\rho_i > \rho_{i-1}$, (Galin, 1989; Popov et al., 1990)

$$\rho_i = [\rho_{ai} \times (AB/2)_i - \rho_{ai-1} \times (AB/2)_{i-1}]/ \\ /[(AB/2)_i - (AB/2)_{i-1}] \quad (2)$$

When $\rho_{i-1} > \rho_i$, formula (3) was used (Salamov et al., 2015)

$$\rho_i = \left\{\left[\left(\frac{AB}{2}\right)_i - \left(\frac{AB}{2}\right)_{i-1}\right] \times \rho_{ai-1} \times \rho_{ai}\right\}/ \\ / [\rho_{ai-1} \times (AB/2)_i - \rho_{ai} \times (AB/2)_{i-1}] \quad (3)$$

Expressions (1), (2) and (3) are the main calculation formulas in the proposed method to determine the parameters of a geoelectric section based on VES data for installations where, MN<<AB.

Surfer 25, CorelDRAWX6 and ZOND2 software were used to process and illustrate the field geophysical materials.

ERA-MAX electrical prospecting equipment with an operating frequency of 4.88 Hz was used on field measurements.

The Yanardagh volcano research area belongs to the Caspian seismically active zone, and elevations vary within the range from 80.0 m to 30.0 m.

The VES surveys were conducted along nine (I…IX) profiles with a total length of 3174 running meters. The directions of profiles I-I…VII-VII are northeast-southwest, and of profiles VIII-VIII and IX-IX are north-south.

As a result of the conducted researches on apparent electrical resistivity ($\rho_{a.e.r.}$), vertical sections of apparent electrical resistivity were constructed. Then, based on specific electrical resistivity ($\rho_{s.e.r.}$), geoelectric sections were constructed and then transformed into lithological-geophysical sections. The maps characterising some average physical properties of rocks forming the geological section of the study area were also created.

Geological structure of the study area

The study area is approximately 25 hectares. This area surrounds the Northern local zone of the Gyrmaki mud volcano. In the general background, due to the development of mud volcano structure, a wide and deep gorge (valley) of Gyrmaki is formed (Alizadeh et al., 2016).

In the area of the Gyrmaki mud volcano location, generally, predominant deposits are from the Pliocene. The maximum thickness of such deposits, which have an oval distribution, is 30 m. They are known as grey and brownish-grey sticky clays in the Absheron peninsula. Carbonate-sand deposits are recorded in the eastern foothill zones and on the slopes of both the southern and northern ridges in the direction of the Gyrmaki valley.

Hydrogeology

In the study area, groundwater basins are present in closed synclines and moldstypical for this territory, which explains the sporadic distribution of groundwater. In the molds, groundwater confined to all stratigraphic levels forms a single radial flow directed from the sides of the mold towards the Caspian Sea (Alizadeh et al., 2016).

Discussion

It should be noted that analogical geophysical studies were not carried out in this area before.

As a result of the conducted field geophysical studies, the apparent electrical resistivity of rocks was calculated. These data were subjected to interpretation, and the specific electrical resistivity of rocks was determined.

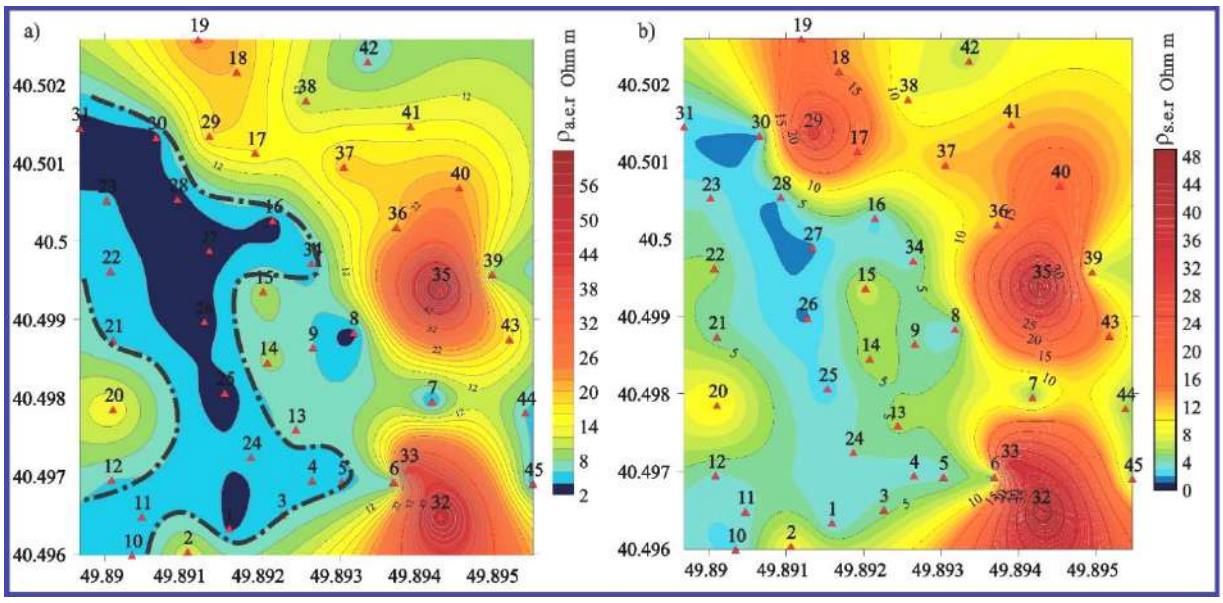


Fig. 2. Maps of the averaged electrical parameters of rocks (a- $\rho_{a.e.r.}$ and b – $\rho_{s.e.r.}$) in the geological section of the Yanardagh study area

As it can be seen from the constructed maps based on the averaged values (particularly – $\rho_{a.e.r.}$, Fig.2a) on rocks in the geological section, the study area conditionally can be divided into two parts. According to the constructed maps, from west to east, an increase in the averaged values of $\rho_{a.e.r.}$, and $\rho_{s.e.r.}$ in rocks in the geological section is observed (Fig. 2 a, b). This indicator may be associated with both the lithological composition of rocks and a decrease in their moisture (water) content.

In the eastern part of the study area, where the averaged values ($\rho_{a.e.r.}$) varies approximately in the range of 12-38 Ohm-m, and in the western part, this indicator is 2-8 Ohm-m.

A similar picture is observed on the map compiled with the averaged values of the specific electrical resistivity ($\rho_{s.e.r.}$) of rocks that make up the geological section of the study area under water (here, rocks are considered to be under the influence of water). In the western part of the area, rock $\rho_{s.e.r.}$ values decrease and vary in the range of 2-5 Ohm-m. This indicator of rocks varies in the range of 10-16 Ohm-m in the eastern and northern parts.

In the western part of the study area, a strip of very low $\rho_{a.e.r.}$values in northwest-southeast direction was identified, which is of certain geological interest.

In the southwestern (VES No. 10, 11, 12) part of the study area there is a manifestation of the mud volcano apophysis and an outlet of an aqueous solution from it, which flows to the north and some part of the water disappears in the geological environment around VES No. 30, 31, 23, 28, 27, 25, 26, and the rest flows to the east. Part of the water, which flows in the north direction penetrates the geological environment and moistens it to the middle of the area approximately. Therefore, in the eastern part of the area, there is a decrease in all, except for natural humidity, the probable physical parameters of rocks forming the geological section.

In order to get the detailed subdivision of the geological section, field measurements were carried out using the VES method and vertical sections of the apparent electrical resistivity of rocks and probable lithological and geophysical sections were constructed (Fig. 3).

As can be seen from the constructed sections of profiles VI-VI and VIII-VIII, three rock layers of different thickness were identified. The top of the first layer was identified at a depth of approximately 7-8 m and the lithology is presumably composed of clays with a thickness of 12-14 m and with $\rho_{s.e.r.}$ of 2-4 Ohm-m. This layer is traced in the VES No.11-13 of profile VI-VI and VES No.3-16 of profile VIII-VIII.

On the top of this layer, a layer with a thickness of 3-7 m and $\rho_{s.e.r.}$ of 0.5-1 Ohm-m is traced. It is assumed that this layer is the sliding plane of a potential landslide and the main factor of EGPs development. In our opinion, this is true for the eastern part of the study area, since the dip of relief increases towards the east.

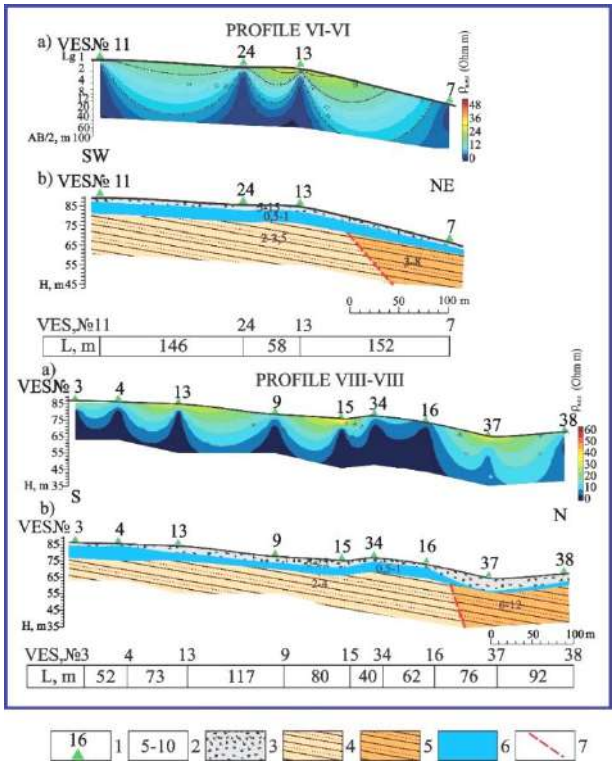


Fig. 3. Vertical sections of apparent electrical resistivity of rocks (a) and probable lithological-geophysical sections (b) along profiles VI-VI, VIII-VIII in Yanardagh area
1 – VES survey points and their sequence numbers; 2 – specific electrical resistivity of rocks forming the geological section; 3 – deposits composed of different rock fragments; 4 – clayey rocks; 5 – clays with alternating thin layers of sand; 6 – heavily watered layer; 7 – probable fault

The uppermost layer with a thickness of 3-7 m and $\rho_{s.e.r.}$ of 5-30 Ohm-m can be traced along the entire extent of the profiles. This layer is composed of different rock fragments and it is possible that these deposits are a potential landslide mass.

Profile VI-VI in the interval of VES No. 13-17 and profile VIII-VIII of VES No. 16-37 revealed probable faults in the north-south direction with a dip towards south-east (Fig. 3.).

To the northeast of the identified fault line, an increase in the $\rho_{s.e.r.}$ values of the rocks can be traced and presumably composed of clays with thin layers of sand.

In our opinion, the identified fault and the second layer of the section, which has very low electrical resistivity will provoke the movement of the landslide mass to the east.

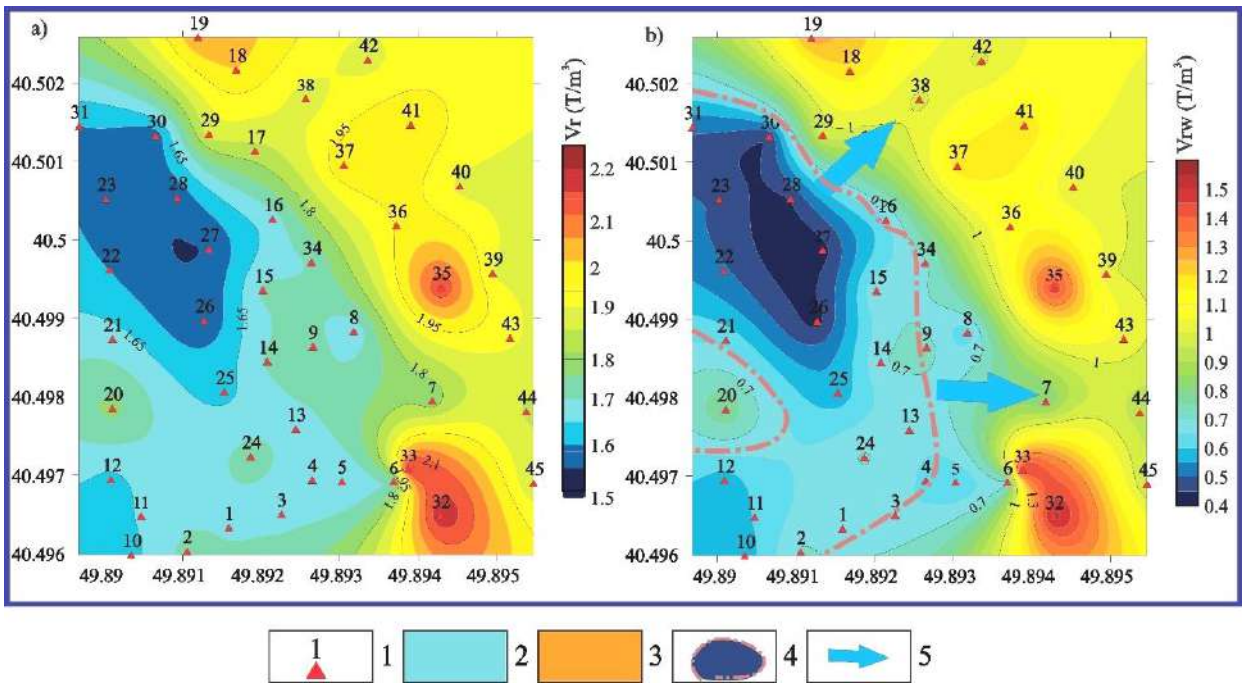


Fig. 4. Maps of expected averaged density values on rocks in the geological section (a) and rocks of the geological section under influence of water (b)
1 – VES points and their sequence numbers; 2 – area with an estimated density of 0.5-1.7 t/m^3; 3 – area with an estimated density of 1.7-2.1 t/m^3; 4 – area with an abnormally lower estimated density of 0.4-0.6 t/m^3; 5 – estimated direction of landslide mass movement

In order to more accurately identify the area most susceptible to the influence of EGP, maps of the probable average density of rocks forming the geological section (a) and the density of rocks under water (Fig. 4, b) were constructed.

According to the constructed maps, the probable density of rocks varies in the range of 1.5-2.1 t/m^3 (a) in the study area and in the range of 0.5-1.4 t/m^3 (b) under water respectively.

As can be seen from the maps compiled using the averaged values of rock densities (a) and (b), the study area is divided into two parts – the western part with low rock densities and the eastern part with relatively high rock densities.

On the map of the average rock density of under water, an area with density of 0.4-1.0 t/m^3 is distinguished, which is presumably an area subject to the intensive influence of EGPs. This area coincides with disappearance of part of the aqueous solution that flows out from the mud volcano mentioned above.

According to the map of the probable under water rock density, the allocated anomalous area seems to tend to connect with the apophysis of the mud volcano, which is located at the southwestern end of the study area.

As a result of acquired data analysis, it can be assumed with some confidence that in the event of activation of geodynamic and EGPs, the potential landslide mass will move to the south and south-east directions, approximately, towards VES No. 38-42, and 7-44 (Fig. 4, b).

As a result of the field data interpretation, maps of the potential landslide mass thickness (Fig.5a) and thickness of the probable sliding plane (Fig.5b) were constructed.

The potential landslide mass thickness (a) varies in the range of 1.5-8.5 m, and increases to the east. The thickness of the supposed sliding plane varies in the range of 1.5-6.5 m.

The map shows a pattern in which the probable sliding plane thickness decreases relatively from the west to east.

In order to obtain additional data on the rock water content degree, a map of the probable natural water content of the study area was constructed.

According to the probable natural water content distribution, the study area is approximately divided into two parts, i.e. the west is over-moistened and the east is relatively less moistened (Fig.6a).

It is confirmed that the water solution from the mud volcano manifestation penetrates into the geological environment and moistens it. It can be said that the main reason for the EGPs development is the soil subsidence formation, as well as the potential landslide massif formation in the study area is the water solution that flows from the mud volcano manifestation.

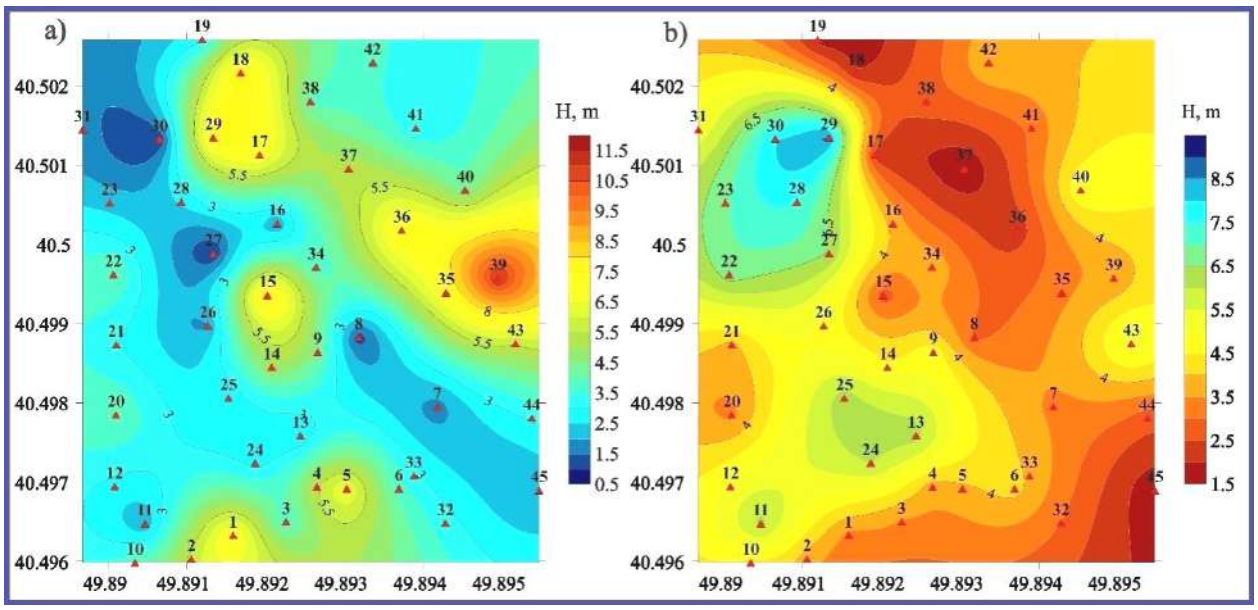


Fig. 5. Maps of the potential landslide mass thickness (a) and the probable sliding plane of the landslide (b) of the Yanardagh study area

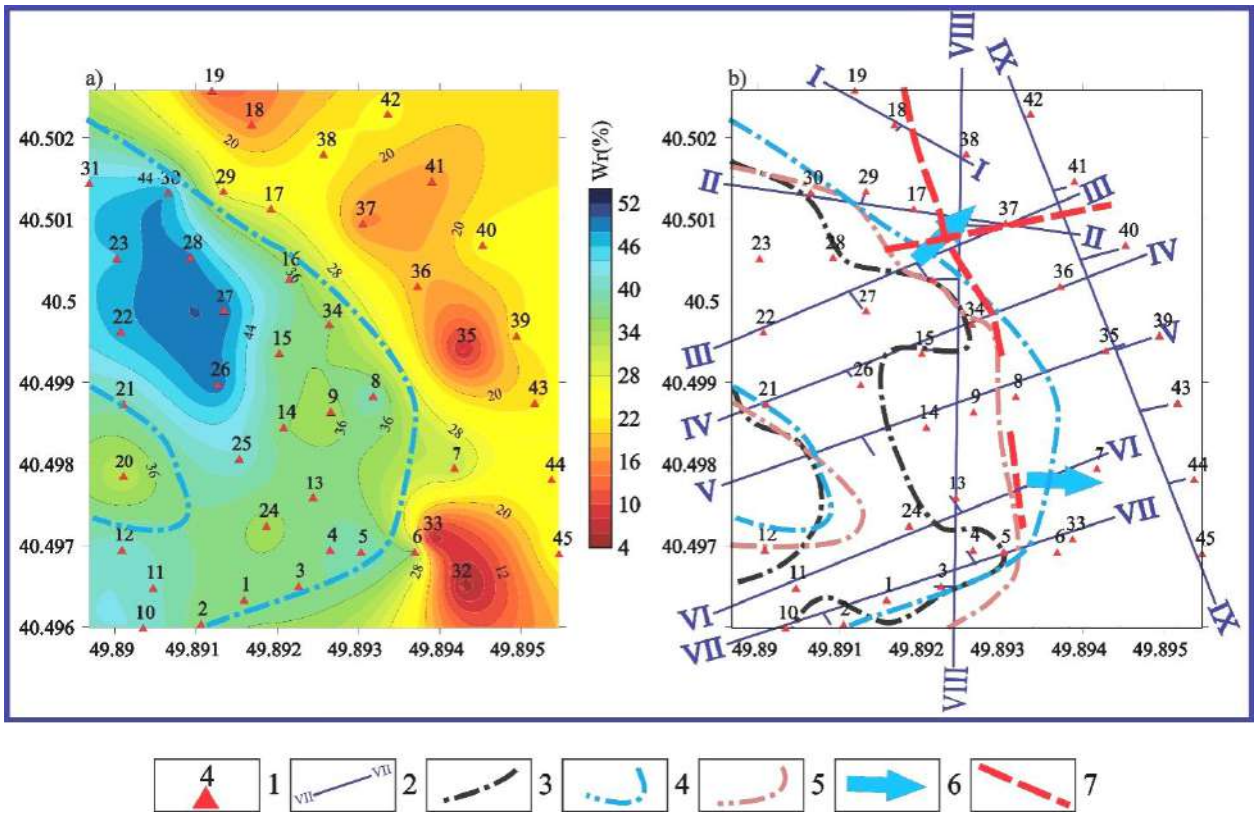


Fig. 6. Maps of natural rock moisture in the geological section (a) and the results of the Yanardagh geophysical research (b) area
1 – VES points and their sequence numbers; 2 – geophysical profiles; 3 – contour of low apparent electrical resistivity; 4 – contour of the abnormally moistened sediments; 5 – contour of the abnormal under water rock density; 6 – probable movement direction of potential landslide mass; 7 – probable fault identified based on VES data

Conclusion

As a result of the interpretation, we obtained:

– Three main layers were identified and subdivided to a depth of 30 m in the geological section of the study area;

– Three layers mainly composed of clays with different thickness and electrical resistivity were identified;

– Faults in the north-south and west-east directions were identified (Fig.6b);

– It was presumably established that in the western part of the study area the rock apparent and specific resistivity and their probable density decreases relative to the eastern part, and the rock natural water content increases;

– Water solution from the mud volcano manifestation flows to the north and along its way is absorbed to the east moistening the eastern part of the study area;

– As a result of moistening the eastern part, a potential landslide area is formed;

– The main reasons of EGPs development are flowing water solution (atmospheric precipitation) and revealed faults.

REFERENCES

Aliyev FSh (2002) Egzogenic geological processes in Azerbaijan Republic, their investigation methods and prognosis principles. Chashioglu, Baku, p 208 (in Azerbaijani)

Alizade AS, Aliyev FSh, Krasilshikov LA et al (1990) Geology and hydrogeology of foothill plains. Nedra, Moscow, p 284 (in Russian)

Alizadeh AA, Guliyev IS, Kadirov FA et al (2016) Geosciences in Azerbaijan. Vol I, Geology, Springer, Heidelberg, NY, p 239

Azizbekov ShA (1961) Geology of Nakhichevan ASSR. Nedra, Moscow, p 503 (in Russian)

Budagov BA (1982) Zoning of the territory of the Azerbaijan SSR by the intensity of landslide manifestation. Proceedings of the Academy of Sciences of the Azerbaijan SSR. The Sciences of Earth 6:63–71 (in Russian)

Galin DL (1989) Interpretation of engineering geophysics data. Nedra, Moscow, p 114 (in Russian)

Goryainov NN, Bogolyubov AN, Varlamov NM et al (1987) Landslide investigation using geophysical methods. Nedra, Moscow, p 157 (in Russian)

Gul AK (2003) Problems of landslides in Baku. Proceedings of Azerbaijan National Academy of Sciences. The Sciences of Earth, Baku 2:73–77 (in Russian)

Israfilbekov IA, Listengarten VA, Shahsuvarov AS (1983) Album of hydrogeological and engineering-geological maps of the Apsheron Peninsula at a scale of 1:50000. Main Directorate of Geodesy and Cartography of USSR, Moscow (in Russian)

Kashkai MA (1952) Mineral springs of Azerbaijan. Publishing House of Azerb.SSR, Baku, p 503 (in Russian)

Konovalov IM, Gul AK (1956) Water content of landslide slopes. Reports of the Academy of Sciences of the Azerbaijan SSR 12(9) (in Russian)

Ogilvi AA (1990) Principles of engineering geophysics. Nedra, Moscow, p 501 (in Russian)

Popov EA, Ten KM, Funtikov GN et al (1990) Guidelines for the use of VES for the detailed dissection of the section in solving geological and engineering-geological problems. Rotaprint, Moscow, p 52 (in Russian)

Salamov AM, Kadirov AG, Salamov FA, Pashayev TR (2015) Investigation of the landslide in the Khizi region of Azerbaijan by the method of Vertical Electrical Sounding. Inzhenerniye izyskaniya (engineering survey) 5-6:50–56 (in Russian)

Salamov AM, Kadirov AH, Mukhtarov ASh, Zamanova AH, Gasimov EE (2020) Development of the landslide processes on the eastern wing of the Bibiheybat brachyanticline using the electrical survey. ANAS Transactions, Earth Sciences 1:19–27. https://doi.org/10.33677/ggianas20200100039 (in Russian)

Salamov AM, Mammadov SG, Gadirov AH, Safarov RT (2017) High-resolution vertical electrical sounding survey: investigation of subsurface structures at Dashgil´s mud volcano, Azerbaijan. International Journal of Development Research 7(1):16688–16692

Salamov AM, Mammadov VA, Rashidov TM, Zamanova AG, Gasimov EE (2023) Electrical resistivity tomography of Lokbatan mud volcano: inner structure and formation mechanism. ANAS Transactions, Earth Sciences 1:49-59. https://doi.org/10.33677/ggianas20230100093

Shirinov NSh (1993) Absheron Peninsula. In the collection: Relief of Azerbaijan. Elm, Baku, p 164–167 (in Russian)

Shirinov NSh (1965) Geomorphology of the Absheron oil-bearing region. Publishing House of the Academy of Sciences of the Azerb. SSR, Baku, p 188 (in Russian)

Yakubovski YuV, Renard IV (1991) Electrical prospecting. Nedra, Moscow, p 347 (in Russian)

ИССЛЕДОВАНИЕ РАЗВИТИЯ ЭКЗОГЕННЫХ ГЕОЛОГИЧЕСКИХ ПРОЦЕССОВ ВЕРТИКАЛЬНЫМ ЭЛЕКТРИЧЕСКИМ ЗОНДИРОВАНИЕМ НА ПЛОЩАДИ ЯНАРДАГ АБШЕРОНСКОГО ПОЛУОСТРОВА (АЗЕРБАЙДЖАН)

Саламов А.М.[1], Сафаров Р.Т.[1], Заманова А.Г.[1], Ахмедова Э.В.[2], Кахраманов М.Р.[1]

[1]Министерство науки и образования Азербайджанской Республики, Институт геологии и геофизики, Азербайджан AZ1073, Баку, просп. Г.Джавида, 119

[2]Геологический факультет, Бакинский государственный университет, Азербайджан AZ1148, Баку, ул. акад. З. Халилова, 33

**Автор, отвечающий за переписку: rafiqsafarov@gmail.com*

Резюме. В данной работе приводятся результаты изучения экзогенных геологических процессов на площади Янардаг, расположенной в северной части Абшеронского полуострова на расстоянии 27 км от Баку. В орографическом отношении полуостров является юго-восточным продолжением Большого Кавказа и занимает площадь около 2000 кв. км. Район геофизических исследований относится к числу редких памятников природы и образовался в результате вулкано-тектонических процессов и возгорания природных газовых потоков, вышедших на поверхность по трещинам. Эта территория окружает северную локальную зону грязевого вулкана Гырмаки. Полевые геофизические измерения методом вертикального электрического зондирования проводились по девяти профилям с использованием симметричной четырехэлектродной установки AMNB. В результате проведенных геофизических исследований были решены следующие задачи: детальное расчленение геологического разреза до глубины 30 м; выявление и трассирование вероятных разломов; определение некоторых вероятных физических параметров пород, слагающих геологический разрез. Были выделены три основных сложенных глинами

слоя, имеющих различную толщину и электрическое сопротивление. На основе построенных карт усредненных значений предполагаемых физических параметров установлено, что западная часть площади наиболее подвержена воздействию экзогенных геологических процессов. Предположительно, основной причиной развития экзогенных геологических процессов является водный раствор, вытекающий из грязевулканического проявления, расположенного в юго-западной части исследуемой территории. В целях снижения скорости развития экзогенных геологических процессов, на исследуемой территории предлагается исключить попадание в геологическую среду вод, стекающих с грязевого вулкана.

Ключевые слова: *геофизика, грязевой вулкан, электроразведка, сопротивления, порода, плотность, разрывные нарушения*

ABŞERON YARIMADASININ YANARDAĞ SAHƏSİNDƏ EKZOGEN GEOLOJİ PROSESLƏRİN İNKİŞAFININ ŞAQULİ ELEKTRİK ZONDLAMA ÜSULU İLƏ TƏDQİQİ (AZƏRBAYCAN)

Salamov Ə.M.[1], Səfərov R.T.[1], Zamanova A.H.[1], Əhmədova E.V.[2], Qəhrəmanov M.R.[1]
[1]*Azərbaycan Respublikasının Elm və Təhsil Nazirliyi, Geologiya və Geofizika Institutu, Azərbaycan*
AZ1073, Bakı, H.Cavid prosp., 119
[2]*Geologiya fakültəsi, Bakı Dövlət Universiteti, Azərbaycan*
AZ1148, Bakı, akad. Z.Xəlilov küç., 33
**Yazışmalara məsul: rafiqsafarov@gmail.com*

Xülasə. Bu tədqiqat işində Abşeron yarımadasının şimal hissəsində, Bakıdan 27 km məsafədə yerləşən Yanardağ ərazisində ekzogen geoloji proseslər araşdırılır. Oroqrafik cəhətdən yarımada Böyük Qafqazın cənub-şərq davamıdır və təxminən 2000 km^2 ərazini əhatə edir. Geofiziki tədqiqat sahəsi nadir təbii abidələrdən biridir və vulkanik-tektonik proseslər və çatlardan səthə çıxan təbii qaz axınlarının alovlanması nəticəsində əmələ gəlmişdir. Bu ərazi Qırməki palçıq vulkanının şimal hissəsini əhatə edir. Şaquli Elektrik Zondlama metodundan istifadə edərək çöl geofiziki ölçmələri simmetrik dörd elektrodlu AMNB qurğusundan istifadə edərək doqquz profil boyunca aparılmışdır. Yerinə yetirilmiş geofiziki tədqiqatlar nəticəsində aşağıdakı məsələlər həll edilmişdir: geoloji kəsilişin 30 m dərinliyə qədər müfəssəl bölünməsi; ehtimal olunan qırılmaların müəyyən edilməsi və izlənilməsi; geoloji kəsilişi təşkil edən süxurların bəzi ehtimal olunan fiziki parametrlərinin müəyyən edilməsi. Müxtəlif qalınlığa və elektrik müqavimətinə malik gillərdən ibarət üç əsas lay müəyyən edilmişdir. Ehtimal olunan fiziki parametrlərin tərtib edilmiş orta qiymətlərinin paylanma xəritələri əsasında müəyyən edilmişdir ki, ərazinin qərb hissəsi ekzogen geoloji proseslərin təsirinə daha çox həssasdır. Güman edilir ki, ekzogen geoloji proseslərin inkişafının əsas səbəbi tədqiqat sahəsinin cənub-qərb hissəsində yerləşən palçıq vulkanı təzahüründən axan sulu məhluldur. Təklif olunur ki, tədqiq olunan ərazidə ekzogen geoloji proseslərin inkişaf sürətini azaltmaq üçün palçıq vulkanından axan suyun geoloji mühitə daxil olmasını aradan qaldırmaq lazımdır.

Açar sözlər: *geofizika, palçıq vulkanı, elektrik kəşfiyyatı, müqavimət, süxur, sıxlıq, qırılmalar*

ANAS Transactions Earth Sciences 2 / 2025

http://www.journalesgia.com

МОДЕЛИРОВАНИЕ РАБОТЫ ПОРОДОРАЗРУШАЮЩЕГО ИНСТРУМЕНТА ДЛЯ БУРЕНИЯ СКВАЖИН

Ибрагимов Р.С.*, Бахшалиева Ш.О.

Азербайджанский Государственный Университет Нефти и Промышленности, Азербайджан

AZ1101, Баку, просп. Азадлыг, 34

**Автор, отвечающий за переписку*: *rafiq.ibrahimov@yahoo.com*

MODELING THE OPERATION OF A ROCK-DESTRUCTING TOOL FOR WELL DRILLING

Ibrahimov R.S.*, Bakshaliyeva Sh.O.

Azerbaijan State Oil and Industrial University, Azerbaijan

AZ1101, Baku, Azadlig ave.,34

**Corresponding author*: *rafiq.ibrahimov@yahoo.com*

Keywords: *sinking, well, jet bits, rocks, rock pressure, fluid density, flushing liquid*

Summary. The paper discusses the results of a study of blast hole drilling. The occurrence of pressure in the hole under the influence of a high pressure jet flowing from the nozzles of a jet cone bit is pulsating in nature. In the rock, where rock pressure acts, stress occurs, resulting in rock fatigue. Experiments have shown that the relaxation period, when the liquid retains the properties of a solid body, is measured in millionths of a second, while the spreading period lasts hundreds of times longer. Moreover, the relaxation period is very difficult to detect in experiments. With constant axial load and rotation speed, the mechanical rate of penetration increases with increasing fluid flow. The paper indicates that due to a sharp change in pressure in the pores of the rocks, the liquid enclosed in them is compressed, a hydraulic shock occurs, as a result of which the walls of the pores, expanding, are brittle destroyed. This process occurs when the critical value of the tensile stress is reached. In calculations, hydromechanical destruction of the bottom occurs. In general, the analysis of accumulated experience in modeling the processes of interaction of a rock-destroying tool with a rock has shown the insufficiency of the study of the mechanism of the tool's impact on the rock. The paper shows the need to take into account the elastic characteristics of rocks when calculating the speed of the jet during hydromechanical destruction.

© 2025 Earth Science Division, Azerbaijan National Academy of Sciences. All rights reserved.

Введение

Горные породы являются телами неоднородными как по составу, так и по строению. В связи с этим у пород по сравнению с минералами имеется большое количество дефектов и главным образом по границам зерен. Поэтому силы взаимодействия по границам зерен за редким исключением (у сливных пород) всегда меньше, чем внутри зерен (минералов), слагающих ту или иную породу.

Наличие большого количества дефектов и неоднородность горных пород приводят к тому, что их механические свойства резко отличаются от свойств минералов даже в том случае, если порода является мономинеральной (Spivak, Popov,1986).

При процессе бурения породоразрушающими долотами на скважинах в результате гидромеханического взаимодействия струи жидкости с горной породой в условиях забоя скважины из-за удара струи происходит дополнительное гидромеханическое разрушение породы. Как известно, физиком Д.Максвеллом было указано, что при определенных условиях жидкость обладает вязко-упругим характером (Maxwell, 2012; Milne-Thomson, 1964). В момент удара жидкость в струе вначале сжимается и только затем начи-нает растекаться. Опыты показали, что релаксационный период, когда жидкость сохраняет свойства твердого тела, измеряется миллионными долями секунды, а период растекания длится в сотни раз дольше.

Причем период релаксации весьма трудно обнаружить в опытах (Loitsyansky, 2003; Efendiyev et al., 2017). При неизменных осевой нагрузке и скорости вращения механическая скорость проходки во взрывных скважинах с увеличением расхода жидкости возрастает. Существенно улучшить очистку забоя от выбуренных частиц и повысить механическую скорость проходки можно (Stepanova,1983; Sadovenko, Inkin, 2015), если гидравлическую мощность потока промывочной жидкости реализовать в насадках гидромониторного шарошечного долота.

Цель работы

Целью данной работы являлось исследование процесса бурения, при котором возникает давление в скважине под воздействием напора струи промывочного раствора.

Материалы и методы

Известно, что в горном деле происходит возникновение гидромеханического давления под воздействием высокого напора струи. Промывочный раствор, вытекающий из насадок долота, по своей природе является пульсирующим во время процесса бурения скважины. Следовательно, в породе, где действует горное давление, возникает знакопеременное напряжение, в результате чего происходит усталость породы (Ibrahimov et al., 2022; Efendiyev et al., 2021). Величина небольшого увеличения давления в поровом пространстве за счет распространения упругих продольных волн может быть определена по формуле Н.Е.Жуковского (Rabotnov, 1979):

$$P = \rho_{ж}\, v c \qquad (1)$$

где, $\rho_{ж}$ – плотность жидкости;
v – скорость струи, потерянная при встрече с поверхностью забоя скважины;
c – скорость распространения упругих волн расширения, определяемая по формуле (Kozyrev, Shalnev, 1970):

$$c = \sqrt{\frac{1}{\rho_{п}}\left[\frac{\bar{E}(1-\mu)}{(1+\mu)(1-2\mu)} + (am+b)(1-\mu)\right]} \qquad (2)$$

где $\rho_{п}$ – плотность породы; $\bar{E}$ – модуль объемной упругости пористой среды; μ – коэффициент Пуассона породы; m – коэффициент объемной пористости среды; a и b – экспериментальные коэффициенты.

Результаты и Обсуждения

Экспериментально (Fedorenko, 2008; Sadovenko, 1991) было установлено, что модуль упругости для хрупких тел при динамической нагрузке больше, чем при статической.

Так как коэффициент Пуассона при сжатии больше, чем при расширении, следовательно, с ростом глубины скважины его значение должно возрастать. По данным американских и отечественных исследователей (Gavrilenko, Ermakova, 2004; Efendiyev et al., 2024) для песчаника с коэффициентом пористости $m = 0.30$ коэффициент Пуассона равен μ=0.25, а модуль упругости колеблется в пределах $E=2.87\cdot10^{8}\div1.05\cdot10^{9}$ Н/м^2.

Экспериментальные коэффициенты, входящие в формулу (2), вычислены для пористого песчаника с коэффициентом пористости $m = 0.25 - 0.30$, плотностью $\rho_{п} = 2.598 \cdot 10^3$ Н/м^3 и модулем упругости E_n=4.79· 10^{10} Н/м^2 и составляют: $a = 2.87 \cdot 10^9 - 1.92 \cdot 10^{10}$ Н/м^2; $b = 2.39 \cdot 10^8 - 9.58 \cdot 10^8$ Н/м^2. Величина коэффициента деформации скелета порового пространства определяется по формуле (Sudakov, 2020; Brown et al., 2000):

$$\varepsilon = \frac{P \cdot d_n}{4\delta_0 E_n}(2-\mu) \qquad (3)$$

где $d_{п}$ – диаметр пор; δ_0 – толщина перегородок порового пространства.

Эффективный напор для разрушения угла составляет: $h_{эф} = (30-50)f$,где f – коэффициент крепости по Л.А.Шрейнеру, К.В.Руппенейту и др. При напоре струи 3-5 MPa разрушаются породы крепостью f≤1.

Плотность однородного изотропного пористого песчаника определяется по формуле:

$$\rho = (1-m)\rho_n + m\rho_{ж}. \qquad (4)$$

С ростом глубины скважины плотность пористой породы изменяется под влиянием давления и температуры.

Было установлено, что при условиях t >130^{0}C плотность промывочной жидкости с ростом давления возрастает по линейному закону (Stepanova, 1983; Sadovenko,1991; Simonov, Vyskrebtsov, 1990).

$$\Delta\rho_p = 4\cdot10^{-10} P(I), \qquad (5)$$

а с ростом температуры – по квадратичному закону:

$$\Delta\rho_t = 4\cdot10^{-5}\rho_0 t + 3\cdot10^{-6}t^2 - 0,4\rho_0\left(\frac{t-130}{t}\right)^2 . \quad (6)$$

Таким образом, плотность песчаника, насыщенного жидкостью, возрастает с ростом давления и уменьшается с ростом температуры, т.е.

$$\rho_{б.р.} = \rho_0 + \Delta\rho_p - \Delta\rho_t . \quad (7)$$

Принимая эффективную пористость породы за абсолютную, для среднего значения объемной упругости можно написать:

$$\bar{E} = \frac{E_{ж}\cdot E_n}{E_{ж}(1-m)+mE_n} . \quad (8)$$

Фактически модуль упругости породы также является функцией давления и температуры.

Скорость распространения звука в жидкости является линейной функцией температуры. Для воды эта зависимость описывается формулой:

$$c_t = 1390 + 3,3t$$

Скорость распространения звука в промывочном растворе в зависимости от давления аппроксимируется согласно линейному закону:

$$c_p = 1512 + 0,275P . \quad (9)$$

При возникновении гидромеханического давления в поровом пространстве в результате взаимодействия высоконапорной струи промывочной жидкости с поверхностью забоя скважины, относительное изменение объема промывочной жидкости в порах породы равно:

$$\frac{\Delta V}{V} = \frac{3(1-2\mu)}{\bar{E}}P , \quad (10)$$

где, P – давление жидкости, действующее в поровом пространстве породы.

Т.к. плотность промывочной жидкости является функцией давления и температуры, то относительное изменение объема промывочного раствора в поровом пространстве может быть записано в виде (Stepanova, 1983; Kyazimov, Islamov, 2023):

$$\frac{\Delta V}{V} = \frac{\rho_{б.р.} - \rho_0}{\rho_{б.р.}} . \quad (11)$$

Приравнивая (10) и (11), получим:

$$P = \frac{(\rho_{б.р.} - \rho_0)\bar{E}}{3\rho_{б.р.}(1-2\mu)} , \quad (12)$$

где ρ_0 – плотность промывочной жидкости на устье скважины; $\rho_{б.р.}$ – плотность промывочного раствора в условиях забоя скважины; ρ_n – плотность пористого песчаника.

Таким образом, при заданных значениях физических параметров промывочной жидкости и пористой породы скорость струи, необходимая для гидромеханического разрушения забоя скважины, может быть определена на основании совместного решения вышеуказанных формул:

$$v = \frac{\rho_{б.р.} - \rho_0}{3\rho_{p,t}^2(1-2\mu)}\cdot\frac{E_{ж}\cdot E_n}{E_{ж}(1-m)+mE_n}\text{x}$$

$$\text{x}\sqrt{\frac{(1+\mu)(1-2\mu)}{\bar{E}(1-\mu)+(1-\mu^2)(1-2\mu)(am+b)}} \quad (13)$$

Для качественной оценки различных факторов на механическую скорость бурения при условии обеспечения гидромониторного эффекта по формуле (13) выполнены расчеты, которые проиллюстрированы на рис.1.

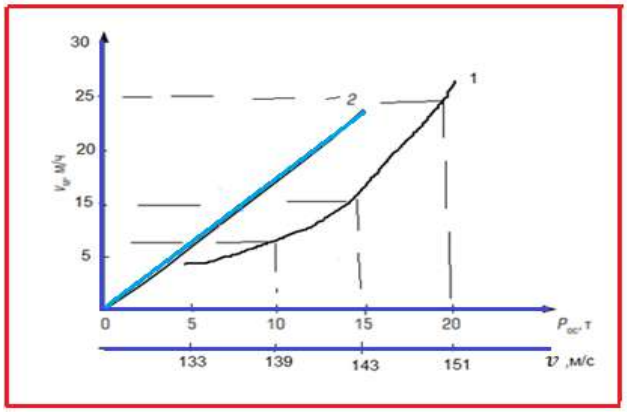


Рис.1. Зависимость механической скорости бурения от скорости струи (1) и осевой нагрузки (2)

Кривые на рис. 1 построены с использованием следующих исходных данных:

$P_{ос}$=5,10,15 и 20 т
$P_{б.р.}$ =1890;1850;1820;1800 кг/м^3
ρ_o =1860;1820;1790;1770 кг/м^3
a= 2.87·10^9 Н/м^2 ; $в$= 2.39·10^{10} Н/м^2 ; m=0.30.

Как показывает обзор исследований, посвященных моделированию процесса бурения скважин и принятию решений, разрешение проблемы сводится к построению различных, как детерминированных, так и статистических моделей, а в последнее время и нечетких моделей. Большая роль отводится в последние годы геомеханическому моделированию, и в данном случае основным сдерживающим фактором в применении существующих методик и методических подходов является недостаточное использование возможностей комплексной информации, получаемой в результате геофизических и геолого-технологических исследований в процессе бурения. Применение современных методов при обработке данных и анализе информации позволит повысить качество информации и принимаемых решений.

Применяемое в работах (Efendiyev et al., 2024; Efendiyev et al., 2021; Efendiyev et al., 2019) геомеханическое моделирование дает возможность провести сравнительный анализ изменений свойств горных пород и скорости проходки, выделить однородные интервалы по свойствам горных пород и буримости в целом, проследить за интервалами возможных осложнений и т.д. Таким образом, развитие современных технических средств и технологий для информационного обеспечения процесса бурения скважин и их широкое внедрение допускают повышение качества получаемой информации и требуют ее соответствующего анализа. Оперативная информация, получаемая в процессе бурения, позволяющая производить геомеханическое моделирование, имеет большое значение при бурении скважин, особенно в малоизученных регионах со сложными горно-геологическими и экологическими условиями.

Применение вероятностных методов и нечеткой логики, позволяя производить в оперативном порядке прогнозирование свойств пород, слагающих разрез скважины, и выделение однородных интервалов по комплексу признаков, сыграло большую роль при проектировании строительства скважин. В опубликованных работах предложена расчетная схема для оценки буримости горных пород, связанной с их свойствами, прогнозируемыми по результатам комплексного каротажа в процессе бурения. По результатам геофизических и геолого-технологических исследований в процессе бурения скважин показаны способы построения уточненной литологической колонки. Предложенные с применением вышеизложенных методов усовершенствованные методика и методические подходы могут быть рекомендованы для анализа данных при бурении, уточнения литологии и границ отдельных типов горных пород, что играет важную роль при принятии решений по выбору технологических параметров бурения скважин.

Заключение

Таким образом, на основе совокупности представленных данных можно сделать вывод, что при изменении давления в порах пород заключенная в них жидкость сжимается, при этом происходит гидравлический удар, в результате чего стенки пор, расширяясь, хрупко разрушаются. При расчетах в результате взаимодействия высоконапорной струи промывочной жидкости в забое скважины с пористыми породами происходит гидромеханическое разрушение забоя. В условиях забоя скважины следует учитывать объемную упругость пористой среды, заполненной жидкостью.

В целом, анализ накопленного опыта моделирования процессов взаимодействия породоразрушающего инструмента с породой показал недостаточность проработки вопросов изучения механизма воздействия инструмента на породу. В связи с этим выполнены сравнительные расчеты по различным выражениям, выявлены актуальные проблемы, на которых необходимо сосредоточить внимание в дальнейших исследованиях. В частности, показана необходимость учета упругих характеристик горных пород при расчете скорости струи при гидромеханическом разрушении.

REFERENCES

Brown DF, Cuddy SJ, Garmendia Doval AB et al (2000) The prediction of permeability in oil-bearing strata using genetic algorithms. Paper presented at the Third IASTED International Conference Artificial Intelligence and Soft Computing, Banff, Alberta, Canada, 24–26 July 2000

Efendiyev G, Isayev R, Piriverdiyev I (2021) Decision-making while drilling wells based on the results of modeling the characteristics of rocks using probabilistic-statistical methods and fuzzy logic. Journal of Physics: Conference Series, 1828(1):012016. https://doi.org/1088/1742-6596/1828/1/012016

Efendiyev GM, Karazhanova MK, Piriverdiyev IA et al (2024) Assessment of the characteristics of the geological section of wells based on probabilistic-fuzzy analysis of complex geophysical and geological-technological information. SOCAR Proceedings, 3:3–8. https://doi.org/10.5510/OGP2024030098

Efendiyev GM, Mammadov PZ, Piriverdiyev IA (2019) Modeling and evaluation of rock properties based on integrated logging while drilling with the use of statistical methods and fuzzy logic. Paper presented at the 10th International Conference on Theory

and Applications of Soft Computing, Computing with Words and Perceptions, ICSCCW, Prague, 27-28 August 2019, Advances in Intelligent Systems and Computing (AISC), 1095:503–511

Efendiyev GM, Mammadov PZ, Piriverdiyev IA et al (2017) Selection of the best combination of bit types and technological parameters during drilling, taking into account uncertainty. Paper presented at the 9th International Conference on Theory and Application of Soft Computing, Computing with Words and Perception, ICSCCW, Budapest, 22-23 August 2017, Procedia Computer Science, 120:67–74. http://dx.doi.org/10.1016/j.procs.2017.11.211

Fedorenko PI (2008) Geometric forecasting of qualitative characteristics of ferruginous quartzites of Kryvbas. Collection of scientific works of the AGN of Ukraine, Ukrrudprom, Mekhanobrchermet. Krivoy Rog, Ukraine, p 75–79 (in Russian)

Gavrilenko YuN, Ermakova VN (2004) Man-made consequences of coal mine closure in Ukraine. Monograph. Nord-press, Donetsk, p 631 (in Russian)

Ibrahimov RS, Bahshaliyeva Sh, Ibrahimov Z (2022) Analysis of the hydraulic characteristics of flushing fluid when gas enters wells drilled from semi-submersible. Nafta-Gaz, 06/2022 (in Polish)

Kozyrev SP, Shalnev KK (1970) Relaxation hypothesis of the mechanism of collision of a liquid and a solid body. Doc. Academy of Sciences of the USSR, 192(3):552–554 (in Russian)

Kyazimov EA, Islamov HM (2023) Development of effective compositions of drilling fluids for improving the quality of well drilling in the Caspian Basin of Kazakhstan. SOCAR Proceedings, 1:19–25. http://dx.doi.org/10.5510/OGP20230100800

Loitsyansky LG (2003) Mechanics of liquid and gas. Textbook for universities, 7th edn. Drofa, Moscow, p 840 (in Russian)

Maxwell DC (2012) Works on Kinetic Theory. Collection of Scientific Papers [Electronic resource]: electronic edition, Binom. Lab. of Knowledge, Moscow, p 406 (in Russian)

Milne-Thomson LM (1964) Theoretical hydrodynamics. Mir, Moscow, p 656 (in Russian)

Rabotnov YuN (1979) Mechanics of a deformable solid body. Science, Moscow, p 743

Sadovenko IA (1991) Synthesis of numerical models in solving problems of control of the geofiltration state of a rock mass. Gorny Zhurnal 12:19–22 (in Russian)

Sadovenko IA, Inkin AV (2015) Modeling of hydrogeothermal fields during underground combustion of coal seams. Geotechnical mechanics 120:161-171 (in Russian)

Sedov LI (1980) Continuum Mechanics. vol 2, Science, Moscow, p 568.

Simonov VV, Vyskrebtsov VG (1990) Operation of a roller bit and their improvement. Nedra, Moscow, p 224 (in Russian)

Spivak AI, Popov AN (1986) Destruction of rocks during well drilling. Nedra, Moscow, p 208 (in Russian)

Stepanova GYu (1983) Introduction to fluid dynamics. Mir, Moscow, p 760 (in Russian)

Sudakov AK (2020) Hydroaeromechanics in Drilling: Textbook. Dnipro Polytechnic National Technical University, Dnipro, Ukraine, p 204 (in Russian)

МОДЕЛИРОВАНИЕ РАБОТЫ ПОРОДОРАЗРУШАЮЩЕГО ИНСТРУМЕНТА ДЛЯ БУРЕНИЯ СКВАЖИН

Ибрагимов Р.С.*, Бахшалиева Ш.О.

Азербайджанский Государственный Университет Нефти и Промышленности, Азербайджан

AZ1101, Баку, просп. Азадлыг, 34

**Автор, ответственный за переписку*: *rafiq.ibrahimov@yahoo.com*

Резюме. В статье рассмотрены результаты исследования процесса бурения, при котором возникает давление в скважине под воздействием высокого напора струи, вытекающей из насадок долота. Напор струи в скважине по своей природе является пульсирующим. В породе, где действует горное давление, возникает напряжение, в результате чего происходит усталость породы. Опыты показали, что релаксационный период, когда жидкость сохраняет свойства твердого тела, измеряется миллионными долями секунды, а период растекания длится в сотни раз дольше. Причем период релаксации весьма трудно обнаружить в опытах. При неизменной осевой нагрузке и скорости вращения механическая скорость проходки с увеличением расхода жидкости возрастает. В статье указано, что при заданных значениях физических параметров промывочной жидкости и породы скорость струи, необходимая для гидромеханического разрушения забоя скважины, может быть определена на основании применения эмпирической формулы. Таким образом, в статье показано, что из-за резкого изменения давления в породах на забое жидкость сжимается, происходит гидравлический удар, в результате чего стенки пор, расширяясь, подвергаются хрупкому разрушению. Этот процесс происходит при достижении критического значения растягивающего напряжения. При расчетах в результате взаимодействия высоконапорной струи промывочной жидкости в забое скважины с породами происходит гидромеханическое разрушение забоя. В условиях забоя скважины следует учесть объемную упругость пористой среды, заполненной жидкостью. В целом, анализ накопленного опыта моделирования процессов взаимодействия породоразрушающего инструмента с породой показал недостаточность проработки вопросов изучения механизма воздействия инструмента на породу. В статье показана необходимость учета упругих характеристик горных пород при расчете скорости струи при гидромеханическом разрушении.

Ключевые слова: *проходка, скважина, гидромониторные долота, горное давление, плотность жидкости, промывочная жидкость*

QUYULARIN QAZILMASI ÜÇÜN SÜXURDAĞIDICI ALƏTİN İŞİNİN MODELLƏŞDİRİLMƏSİ

İbrahimov R.S.*, Baxşəliyeva Ş.O.
Azərbaycan Dövlət Neft və Sənaye Universiteti, Azərbaycan
AZ1101 Bakı, Azadlıq prospekti, 34
**Yazışmalara məsul:rafiq.ibrahimov@yahoo.com*

Xülasə. Məqalədə göstərilir ki, qazma prosessinin tədqiqinin nəticələri olaraq hidromonitor baltanın keçmələrindən çıxan axının yüksək təzyiqli şırnağının təsiri altında süxurlarda pulsasiyalı dağılma baş verir. Dağ təzyiqinə məruz qalan süxurda gərginlik yaranır və nəticədə süxurlarda yorğunluğu yaranır. Təcrübələr göstərmişdir ki, məhlulun bərk cismin xüsusiyyətlərini saxladığı relaksasiya dövrü saniyənin milyonda biri ilə ölçülür, yayılma müddəti isə yüzlərlə dəfə uzun çəkir. Üstəlik, təcrübələrdə relaksasiya dövrünü aşkar etmək çox çətindir. Daimi baltaya verilən oxboyu yükdə və alətin fırlanma sürətində, maye axınının artması ilə baltanın mexaniki sürəti artır. Məqalədə göstərilir ki, yuma mayesinin və məsaməli süxurun fiziki parametrlərinin verilmiş qiymətləri üçün quyudibinin hidromexaniki dağıdılması üçün tələb olunan reaktiv sürət empirik formulanın tətbiqi əsasında müəyyən edilə bilər. Beləliklə, məqalədə göstərilir ki süxurun məsamələrində təzyiqin kəskin dəyişməsi nəticəsində quyudibindəki maye sıxılır, hidravlik zərbə baş verir, nəticədə genişlənən məsamə divarları kövrək şəkildə dağılır. Bu proses dartılma gərginliyinin kritik qiymətinə çatdıqda baş verir. Hesablamalarda quyudibində olan yüksək təzyiqli axan mayenin məsaməli süxurlarla qarşılıqlı təsiri nəticəsində süxurda hidromexaniki dağılması baş verir və quyudibi şəraitində süxurlarda maye ilə doldurulmuş məsaməli mühitin həcm elastikliyini nəzərə almaq lazımdır. Ümumiyyətlə, süxurdağıdıcı alətlə süxur arasında qarşılıqlı təsir proseslərinin modelləşdirilməsi üzrə toplanmış təcrübənin təhlili göstərdi ki, alətin süxura təsir mexanizminin öyrənilməsi məsələləri kifayət qədər işlənməmişdir. Bununla bağlı müxtəlif ifadələrdən istifadə etməklə müqayisəli hesablamalar aparılmış, gələcək tədqiqatlarda diqqət mərkəzində saxlanılmalı olan cari problemlər müəyyən edilmişdir. Məqalədə süxurun hidromexaniki dağılması zamanı məhlulun axın sürətinin hesablanmasında süxurların elastik xüsusiyyətlərinin nəzərə alınmasının zəruriliyi göstərilir.

Açar sözlər*: qazma keçidi, quyu, hidromonitor balta, dağ təzyiqi, məhlulun sıxlığı, yuyucu maye*

ANAS Transactions Earth Sciences 2 / 2025

http://www.journalesgia.com

MÜNDƏRİCAT

Babazadə V.M., Abdullayeva Ş.F., Novruzova S.R., Vəliyev A.Ə., İbrahimov C.R. – Mərkəzi Qafqazın Azərbaycan seqmentində filiz yataqlarının yerləşməsindəki regional struktur nəzarət: uzun müddət inkişaf edən dislokasiyaların tədqiqi rolu 3-13

Eppelbaum L., Katz Yu., Qədirov F., Ben-Avraham Z. – Aralıq dənizinin cənub-şərqinin allokton okean qabığının mənbələri harada əmələ gəlmişdir? 14-28

Karşıyev O.A., Evseeva G.B., Tokareva K.M., Kudaşeva L.R., Rabbimkulov S.A. – Çarcou mərhələsinin şimal-qərb hissəsindəki Yura karbonat formasiyasının kollektor süxurlarının geoloji quruluşu və petrofiziki xüsusiyyətləri 29-40

Zeynalov Q.Ə. – Cənubi Xəzər və Kür hövzələrində Məhsuldar Qat çöküntülərində kalsit sementlərinin paylanması və onların kollektor süxurlarına təsiri 41-53

Qalkin S.V., Kolychev I.Y., Savitsky Y.V., Şumilov A.V., Qurbanov V.Ş., Abbasova Q.Q. – Kern/karotajın kompleks petrofiziki məlumatlarına görə kollektorların bitumlaşmasının və islanmasının müəyyən edilməsi imkanları 54-63

Əliyev N.A., Rəsulov M.A., Cəlalov G.İ., Sinsoisal B., Xanbabayeva M.X. – Fraktal mühitdə mayenin müstəvi-radial hərəkət prosesini təsvir edən kəsr tərtibli differensial məsələnin ikinci növ Fredholm inteqral tənliyinə gətirilməsi 64-72

Həsənov Ə.B., Ramazanova N.A., Bayramov K.T. – Neftli süxurların mexaniki xüsusiyyətləri və quyudibi zonasının dayanıqlığı 73-78

Hadıyeva A.S., Bisembayeva K.T., Mamalov Y.N., Sabirbayeva G.S. – Neft laylarına polimer və su-qaz təsirinin kompleks üsulunun effektivliyinin tədqiqi 79-88

Cahyadi A., Aji T.N., Haryono E., Widiyastuti M., Agniy R.F., Naufal M., Setiawan N., Fatoni G., Pratama A.D., Riyanto I.A., Fatchurohman H. – Qununqsevu karst regionunda (Indoneziya) süni izləmə üsulu ilə tədqiq edilmiş allogen sularla qidalanan çayların yeraltı axın xüsusiyyətləri 89-97

Sultanov B.N., Qədirli F.R., Hacıyeva G.N. – Xəzər dənizinin səviyyə tərəddüdünün Abşeron yarımadasının sahil zonasındakı yeraltı sulara təsirinin qiymətləndirilməsi və ekolojı problemlər.... 98-105

Salamov Ə.M., Səfərov R.T., Zamanova A.H., Əhmədova E.V., Qəhrəmanov M.R. – Abşeron yarımadasının Yanardağ sahəsində ekzogen geoloji proseslərin inkişafının şaquli elektrik zondlama üsulu ilə tədqiqi (Azərbaycan) 106-113

İbrahimov R.S., Baxşəliyeva Ş.O. – Quyuların qazılması üçün süxurdağıdıcı alətin işinin model-ləşdirilməsi 114-119

CONTENTS

Babazadeh V.M., Abdullayeva Sh.F., Novruzova S.R., Valiyev A.A., Ibrahimov J.R. – Regional structural control on ore deposits location in the Central Caucasus Segment of Azerbaijan: an investigation of the role of tectonic dislocations 3-13

Eppelbaum L., Katz Y., Kadirov F., Ben-Avraham Z. – Where did the initial sources of the allochthonous oceanic crust in the Southern Easternmost Mediterranean originate? 14-28

Karshiyev O.A., Evseeva G.B., Tokareva K.M., Kudasheva L.R., Rabbimkulov S.A. – Geological structure and petrophysical features of collector rocks of the Jurassic carbonate formation in the northwestern part of the Chardzhou step 29-40

Zeynalov G.A. – Distribution of calcite cements and their influence on reservoirs in the Productive Series of the South Caspian and Kur Basins 41-53

Galkin S.V., Kolychev I.J., Savitsky Y.V., Shumilov A.V., Gurbanov V.Sh., Abbasova G.G. – Possibilities for detecting reservoir wettability and bituminisation based on integrated petrophysical core and well-logging data 54-63

Aliyev N.A., Rasulov M.A., Jalalov G.I., Sinsoysal B., Xanbabayeva M.H. – Reduction of the fractional differential model of flat-radial fluid flow in a fractal medium to a second-kind Fredholm equation 64-72

Hasanov A.B., Ramazanova N.A., Bayramov K.T. – Mechanical properties of oil-bearing rocks and stability of the bottom hole zone 73-78

Hadiyeva A.S., Bissembayeva K.T., Mamalov E.N., Sabyrbayeva G.S. – Research on the effectiveness of the combined method of polymer and water-gas impact on oil reservoirs 79-88

Cahyadi A., Adji T.N., Haryono E., Widyastuti M., Agniy R.F., Naufal M., Setiawan N., Fathoni H., Pratama A.D., Riyanto I.A., Fatchurohman H. – Characterization of underground river passages controlled by allogenic recharge: insights from an artificial tracer test in the Gunungsewu Karst Area, Indonesia 89-97

Sultanov B.N., Gadirly F.R., Hajiyeva G.N. – Impact assessment of Caspian Sea level variations on groundwater in the Absheron coastal zone and associated ecological problems 98-105

Salamov A.M., Safarov R.T., Zamanova A.H., Ahmadova E.V., Gahramanov M.R. – Assessment of exogenic geological process dynamics in the Yanardag area of Absheron peninsula (Azerbaijan) based on vertical electrical sounding data 106-113

Ibrahimov R.S., Bakshaliyeva Sh.O. – Modeling the operation of a rock-destructing tool for well drilling 114-119

ОГЛАВЛЕНИЕ

Баба-заде В.М., Абдуллаева Ш.Ф., Новрузова С.Р., Велиев А.А., Ибрагимов Д.Р. – Региональный структурный контроль размещения рудных месторождений в Азербайджанском сегменте Центрального Кавказа: исследование роли длительно развивающихся тектонических дислокаций 3-13

Эппельбаум Л., Кац Ю., Кадиров Ф., Бен-Аврахам Ц. – Где были сформированы источники аллохтонной океанической коры южной части Восточного Средиземноморья? 14-28

Каршиев О.А., Евсеева Г.Б., Токарева К.М., Кудашева Л.Р., Раббимкулов С.А. – Геологическое строение и петрофизические особенности пород-коллекторов карбонатной формации юры в северо-западной части Чарджоуской ступени 29-40

Зейналов Г.А. – Распределение кальцитовых цементов и их влияние на резервуары в продуктивной толще Южно-Каспийского и Куринского бассейнов 41-53

Галкин С.В., Колычев И.Ю., Савицкий Ю.В., Шумилов А.В., Гурбанов В.Ш., Аббасова Г.Г. – Возможности обнаружения смачиваемости и битумизации коллекторов по комплексным петрофизическим данным керна/каротажа 54-63

Алиев Н.А., Расулов М.А., Джалалов Г.И., Синсойсал Б., Ханбабаева М.Х. – Сведение задачи дробного дифференциального уравнения, описывающего процесс плоскорадиального движения жидкости во фрактальной среде, к интегральному уравнению Фредгольма второго рода 64-72

Гасанов А.Б., Рамазанова Н.А., Байрамов К.Т. – Механические свойства нефтеносных пород и устойчивость призабойной зоны скважин 73-78

Хадиева А.С., Бисембаева К.Т., Мамалов Е.Н., Сабырбаева Г.С. – Исследование эффективности комплексного метода полимерного и водогазового воздействия на нефтяные пласты 79-88

Кахиади А., Аджи Т.Н., Харьоно Э., Видьястути М., Агний Р.Ф., Науфал М., Сетиаван Н., Фатони Г., Пратама А.Д., Рийанто И.А., Фатчурохман Г. – Особенности подземного стока рек с аллогенными водами, выявленные методом искусственного трассирования в карстовом регионе Гунунгсеву (Индонезия) 89-97

Султанов Б.Н., Кадирли Ф.Р., Гаджиева Г.Н. – Оценка воздействия колебаний уровня Каспийского моря на подземные воды прибрежной зоны Абшеронского полуострова и экологические проблемы 98-105

Саламов А.М., Сафаров Р.Т., Заманова А.Г., Ахмедова Э.В., Кахраманов М.Р. – Исследование развития экзогенных геологических процессов вертикальным электрическим зондированием на площади Янардаг Абшеронского полуострова (Азербайджан) 106-113

Ибрагимов Р.С., Бахшалиева Ш.О. – Моделирование работы породоразрушающего инструмента для бурения скважин 114-119